THE UNIVERSITY of EDINBURGH

This thesis has been submitted in fulfilment of the requirements for a postgraduate degree (e.g. PhD, MPhil, DClinPsychol) at the University of Edinburgh. Please note the following terms and conditions of use:

- This work is protected by copyright and other intellectual property rights, which are retained by the thesis author, unless otherwise stated.
- A copy can be downloaded for personal non-commercial research or study, without prior permission or charge.
- This thesis cannot be reproduced or quoted extensively from without first obtaining permission in writing from the author.
- The content must not be changed in any way or sold commercially in any format or medium without the formal permission of the author.
- When referring to this work, full bibliographic details including the author, title, awarding institution and date of the thesis must be given.

Mixtures of proteins and protein-stabilised droplets: rheology of emulsions and emulsion gels

Marion Roullet

Doctor of Philosophy
The University of Edinburgh
2019

Abstract

The soft materials formed from emulsions stabilised by proteins, like yogurt, are referred to as emulsion gels. This designation is however not precise enough to reflect the variety of composition of these materials. Indeed, during emulsification not all the proteins in solution adsorb at the interface and the emulsion is thus a mixture of protein-stabilised droplets and unadsorbed proteins. The composition of this mixture affects the viscosity of the emulsions and the texture of the emulsion gels.

The objective of this thesis is to study the rheological properties of protein-stabilised emulsions and the gels they form considering the full range of their composition. A first step has been to characterise separately the purified suspensions of protein-stabilised droplets, and of suspensions of pure proteins and their gelation. These components have then been combined, resulting in emulsions and emulsion gels of well-characterised compositions, thus allowing a rigorous approach to the rheology of these systems.

The viscosity of purified suspensions of proteins and of protein-stabilised droplets has been studied. It was found that these systems are conveniently studied in the framework developed for soft colloidal suspensions, for which the viscosity scales with the volume fraction. The properties of the droplet and protein suspensions have then been used to model the behaviour of their mixtures. The viscosity models for the two types of pure suspensions have facilitated the development of a semi-empirical model that relates the viscosity of protein-stabilised emulsions to their composition.

The gelation of the pure suspensions has then been characterised. Indeed, at low pH, proteins can aggregate and also form gels, either of protein molecules in solution or of protein-covered droplets. The rheological properties of these fractal networks were found to depend on their volume fraction, in good correspondence with previous studies on colloidal gels. Protein gels and droplet gels display very similar mechanical properties when the scaling by the volume fraction is used to describe their concentration.

These results have then been used to characterise the rheological properties of emulsion gels over a wide range of compositions. The choice of parameters is important and it was shown that using the total volume fraction and the ratio of volume fractions of the components, rather than the individual volume fractions, makes it possible to change paradigm for these systems, from droplet-filled protein gels to composite gels. Using this approach it was demonstrated that the rheological properties of pure protein gels, emulsion gels and pure droplet gels vary continuously with their composition.

Finally, the influence of the size of droplets has been briefly studied. Larger droplets were produced and the rheological properties of the droplet suspensions and droplet gels were compared with the results for smaller droplets and for proteins. It appeared that the increase in size only causes minor changes in the rheological behaviour of the emulsion and emulsion gel, and the variation with the volume fraction is consistent with the other types of samples.

Lay summary

In this thesis, I study the physics of yoghurt to get a better understanding of ice cream. The link between physics, ice cream and yoghurt may seem tenuous, and can be described as such since it lies in a milk protein that is one thousand times smaller than the thickness of a hair. Milk proteins have an outstanding ability to organise and arrange the matter at a very tiny scale, so they are fundamental to form what physicists call the *microstructure*. And without microstructure, many food products would be far from mouth-watering. Ice cream for example would just be some ice cubes and chunks of flavoured fat floating in sweetened water.

The amazing property of milk protein is that it forms many types of microstructures, naturally or with a bit of help. In milk, it goes around the surface of tiny droplets of fat, so that fat and water can mix better than in a mixture of just olive oil and vinegar, and form what is called an *emulsion*. If milk is slowly acidified, all the proteins stick together to form a network, and yoghurt is obtained, that physicists describe as an *emulsion gel*.

In this thesis, I study the texture of the gel formed by a model milk. This model milk is just a mixture of oil droplets with proteins in water. And I study how the squishiness of the gel formed depends on the amount of fat and protein. It is like comparing yoghurt made from full fat, semi skimmed and skimmed milk. I also look at how the small proteins and oil droplets are organised together to form the microstructure. And more importantly, I try to understand the relationship between the amount of fat and proteins, the texture and the microstructure.

The final application of my work is not only yoghurt but also ice cream. Ice cream is a more complex dairy product, but understanding the role of the milk protein in the microstructure and texture of yoghurt can help do the same in ice cream. It is then possible to improve the recipes by optimising the amounts of fat, or of protein, or even replace those by more eco-friendly vegetal proteins.

Declaration

I declare that this thesis was composed by myself, that the work contained herein is my own except where explicitly stated otherwise in the text, and that this work has not been submitted for any other degree or professional qualification except as specified.

Parts of this work have been published in [1].

(*Marion Roullet, 2019*)

Acknowledgements

Although only my name appears in the front page, quite a few people have been involved in the making of this thesis, and without their help it would never have been completed.

My thanks go first and foremost to my supervisors, Bill Frith and Paul Clegg. It is safe to say that, without them, this work would have never got very far. The scientific guidance and the continued support of Bill have been invaluable in the last three years, and the most compelling results in this thesis derived from his ideas. I am also thankful to Bill and Paul for supporting my involvement in outreach, even when it was obviously distracting me from my thesis, as this has been a very welcome escape route at times. Finally, the reader can join me in thanking them for patiently proof-reading this manuscript and correcting the countless mistakes, since this thesis would otherwise have been filled with unintended Frenglish.

The wise reader will notice that experimental results make up the most of this thesis, and these could not have been obtained without the kind help of my colleagues. Many thanks go to Alison Russell for patiently teaching me the ropes of confocal microscopy, to John Royer for helping me with the rheo-imaging setup, and to Andrew Schofield for preparing a massive batch of particles for some experiments that unfortunately didn't make it to this thesis. Regarding the rheo-imaging results, Mattia and Mélanie deserve acknowledgements as well, for their incredible smuggling of my samples after I forgot them on my way to Edinburgh. I would also like to thank Damiano Rossetti, George Marinov, Peter Schuetz, Felix Oppong and Julian Bent for their advice.

I am also grateful to those who made these years of doctoral studies more enjoyable, especially to Paschalia for the numerous ice cream breaks and to Célia for fuelling science with delicious sweets. And finally *merci beaucoup* to my family for their constant encouragements, especially at the times of putting on paper the final words of this thesis.

Contents

Abstract i

Lay summary iii

Declaration v

Acknowledgements vii

Contents ix

List of Figures xvii

List of Tables xxxiii

1 Introduction and thesis outline 1

- 1.1 Introduction 1
- 1.2 Choosing the right paradigms 3
- 1.3 Thesis outline 4

2 Background 7

- 2.1 An introduction to shear rheology 7
  - 2.1.1 Rotational shear rheology 8
  - 2.1.2 Oscillatory shear rheology 10

2.2 Some soft matter systems and their rheological properties 11

2.2.1 Colloidal suspensions: hard and soft particles 11

2.2.2 Emulsions 17

2.2.3 Gels 20

2.2.4 Emulsion Gels 24

2.3 Structure and functional properties of proteins 26

2.3.1 Structure of proteins 26

2.3.2 Proteins as emulsifiers 27

2.3.3 Proteins as gelling agents 29

2.4 An example protein: sodium caseinate 30

2.4.1 Nature and structure of sodium caseinate 30

2.4.2 Sodium caseinate-stabilised emulsions 32

2.4.3 Sodium caseinate gels 33

3 Preparation of the protein and emulsion samples 37

3.1 Materials 37

3.1.1 Protein: Sodium caseinate 37

3.1.2 Oils: Glyceryl-tri-octanoate and tetradecane 38

3.1.3 Gelation agent: Glucono-delta lactone 39

3.2 Preparation of the protein samples 39

3.3 Preparation of the protein-stabilised droplets 41

3.3.1 Emulsification techniques 41

3.3.2 Preparation of the protein-stabilised emulsions 44

3.3.3 Purification of the droplets 45

3.4 Preparation of the mixtures of proteins and droplets 50

3.4.1 Preparation protocol 50

3.4.2 Composition of the mixtures 50

3.5 Acid-induced gelation of proteins... 52

3.6 Conclusion 55

4 Characterisation of sodium caseinate and droplet dispersions 57

4.1 Introduction 57

4.2 Materials & Methods 58

4.2.1 Techniques for the determination of protein concentration... 58

4.2.2 Techniques for particle size analysis 60

4.3 Concentration measurements in protein solutions 65

4.3.1 Absorbance to estimate protein loss during purification 65

4.3.2 Refractometry to measure the protein concentration after preparation 67

4.4 Separation of the droplets from the emulsion and characterisation.. 68

4.4.1 Formation of a transparent layer during centrifugation 69

4.4.2 Concentration of droplets and density of dense suspension after centrifugation 74

4.4.3 Surface coverage of droplets after emulsification............... 75

4.4.4 Composition of the droplets 76

4.5 Size of proteins and droplets.. 76

4.5.1 Size distributions of droplets by Static and Dynamic Light Scattering... 77

4.5.2 Size distribution of proteins by Field Flow Fractionation..... 78

4.6 Conclusion 81

5 Viscosity of protein suspensions and protein-stabilised droplets 83

5.1 Introduction 84

5.2 Materials & Methods 85

5.2.1 Preparation of the samples 85

5.2.2 Rotational rheology 85

5.3 Viscosity of suspensions in the semi-dilute regime: determination of the volume fraction 86

5.3.1 Estimation of the volume fraction using the intrinsic viscosity 88

5.3.2 Estimation of the volume fraction using Batchelor model 90

5.3.3 Discussion of the scaling by the effective volume fraction 92

5.4 Viscosity behaviour of pure suspensions of droplets and proteins in the concentrated regime 96

5.4.1 Modelling the viscosity behaviours of colloidal suspensions 96

5.5 Viscosity of mixtures: contributions of the pure components 101

5.5.1 Semi-empirical predictive model for the viscosity of mixtures 104

5.5.2 Use of the semi-predictive model to estimate the composition of emulsions 108

5.6 Flow curves and shear-thinning behaviour 111

5.6.1 Model for the description of shear thinning 113

5.6.2 Comparison of the shear thinning behaviour of different suspensions 113

5.7 Conclusion 117

6 Protein gels and protein-stabilised droplet gels: gelation, microstructure and rheology 119

6.1 Introduction 120

6.2 Materials & Methods 122

6.2.1 Preparation of the sols 122

6.2.2 Gelation 122

6.2.3 Oscillatory Rheometry 123

6.2.4 Laser scanning confocal microscopy 124

6.2.5 Rheo-imaging 127

6.2.6 Image analysis 128

6.3 Formation of protein and droplet gels: kinetics of gelation 130

6.3.1 Gelation and microstructure coarsening 131

6.3.2 Development of mechanical properties 139

6.3.3 After gelation: is there an end point? 142

6.4 Micro-structure of gels: colloidal species and volume fraction 143

6.5 Rheology of gels: comparison of droplet gels and protein gels 146

6.5.1 Linear viscoelasticity of gels 147

6.5.2 Frequency dependence of gels 152

6.5.3 Strain dependence of gels 156

6.5.4 Irreversible fracture of gels 161

6.6 Conclusion 163

7 Gelation and rheology of gels of mixtures of proteins and droplets 165

7.1 Introduction 166

7.2 Materials & Methods 167

7.2.1 Rheo-imaging 167

7.3 Gelation of emulsion gels: a rheo-imaging study 168

7.4 Description of gels of mixtures: a change of the composition parameters for a new framework ... 171

7.5 Rheology of gels of mixtures ... 172

7.5.1 Viscoelastic properties: decoupling of total volume fraction and composition ... 172

7.5.2 Frequency dependence of emulsion gels ... 177

7.6 Change in paradigm for the description of emulsion gels ... 179

7.6.1 Classical approach: emulsion gels as a filled matrix ... 179

7.6.2 New approach: intermediate behaviour of gels of mixtures .. 182

7.6.3 Changing framework for the study of emulsion gels ... 183

7.7 Conclusion ... 185

8 Influence of the droplet size on the rheology of droplet emulsions and gels 187

8.1 Introduction ... 188

8.2 Materials & Methods ... 189

8.2.1 Preparation of the large droplets ... 189

8.2.2 Rheological measurements ... 189

8.3 Characterisation of the large droplets ... 189

8.3.1 Concentration of the droplet suspensions ... 190

8.3.2 Size distributions of the large droplets ... 190

8.3.3 Increasing the size of the droplets changes their structure ... 191

8.4 Influence of the droplet size on the viscosity of suspensions ... 192

8.4.1 Estimation of the volume fraction ... 192

8.4.2 Viscosity model for suspensions of large droplets ... 193

8.4.3 Non-Newtonian suspensions and shear-thinning ... 196

8.4.4 Conclusion on the effect of droplet size on the rheological behaviour of suspensions of droplets ... 198

8.5 Influence of the droplet size on the rheology of emulsion gels ... 199

8.5.1 Linear viscoelasticity of the droplet gels ... 200

8.5.2 Frequency dependence of the droplet gels ... 202

8.5.3 Strain dependence and non-linear viscoelasticity ... 204

8.5.4 Summary of the effect of the droplet size on the rheological behaviour of emulsion gels ... 206

8.6 Conclusion ... 208

9 Conclusion and outlook 211

A Error propagation theory 213

Bibliography 215

List of Figures

(1.1) Illustration of the variety of the compositions of emulsion gels. The arrow represents the ratio of un-adsorbed proteins over the total amount of proteins in the gel. 3

(2.1) Illustration of a rotational rheology test: the tool with the top plate is in continuous rotation, while the bottom plate is fixed. Reproduced from Ref. [2]. 8

(2.2) Typical flow curves (left) and viscosity curves (right) for three types of liquids: Newtonian (line, blue), shear thickening (dotted line, red) and shear thinning (dashed line, green). 9

(2.3) Typical oscillatory rheology measurement in the linear regime: sinusoidal shear deformation $\gamma = \gamma_0 \ \sin(2\pi f t)$ (red), and resulting stress $\sigma = \sigma_0 \ \sin(2\pi f(t - \delta t))$ (green), where γ_0 and σ_0 are the amplitudes of the strain and stress signals, f is their frequency, and δt is the time shift between strain and stress. 10

(2.4) Cartoons of the soft matter systems studied in this thesis. From left to right: suspension of soft colloids, emulsion, (soft) colloidal gel and emulsion gel. 12

(2.5) Illustrations of soft particles (a) Cartoons of polymeric coil, star polymer, microgel, emulsion, and hard sphere. The arrow points to the direction of enhanced elasticity and transition from soft to hard repulsive pair interaction potential. Reproduced from Ref. [3]. (b) Two-colour superresolution microscopy of densely packed microgels showing compression, deformation and partial interpenetration. Scale bar 500 nm. Reproduced from Ref. [4]. . . 16

(2.6) Dependence of the zero-shear viscosity (normalized to the solvent viscosity) of various colloidal systems on the effective volume fraction. The dashed line is the best fit of hard sphere data to the Quemada model [5] (Equation 2.4). The low-shear viscosity data of star polymer data are well represented by a double exponential function (dotted line). Reproduced from Ref. [3]. 18

(2.7) Emulsion instability processes, reproduced from Ref. [6]. 19

(2.8) Structure of a low-concentration DLCA gel obtained by computer simulation, reproduced from Ref. [7]. 21

(2.9) Principle of small-deformation oscillatory rheology (a) and typical dynamical viscoelastic properties upon gelation (b): storage modulus G', loss modulus G'', and loss tangent tan δ. Reproduced from Ref. [8]. 23

(2.10) Schematic structures of (a) an emulsion-filled particle gel, (b) a particle-stabilised emulsion gel. Reproduced from Ref. [9]. 24

(2.11) Effects of active (circles) and inactive fillers (squares) on the storage modulus. The logarithm of G'/G'_m where G'_m is the modulus of the gel matrix is plotted against the oil volume fraction ϕ. Reproduced from Ref. [9]. 26

(2.12) Microstructure of an acid-induced sodium caseinate gel after 140 min from the start of the acidification. The image is 100 µm across. Reproduced from Ref. [10]. 34

(2.13) Evolution of properties of an acid-induced caseinate gel with a slow acidification: (A) pH decreases over time. The horizontal line indicates the isoelectric pH of caseins. (B) Corresponding evolution of the fraction of free caseins x_{free}. (C) Evolution of the elastic modulus G'. (D) Evolution of pore size ξ measured by confocal microscopy. Reproduced from Ref. [11]. 36

(3.1) Chemical structure of glyceryl trioctanoate. 39

(3.2) Chemical structure of glucono-δ lactone. 39

(3.3) Several stages of the preparation of a sodium caseinate solution. (a) After dispersion of the protein powder; (b) after centrifugation at 40 000 × g for 4 h, the impurities are separated from the solution: fat globules on the top (dotted green arrow) and unidentified sediment at the bottom (dashed blue arrow); (c) after filtration through a 0.45 µm membrane. 40

(3.4) Bench top Silverson L4R mixer/emulsifier, and close-up on rotor-stator element. 42

(3.5) Bench top Microfluidizer (Microfluidics Inc.) mixer/emulsifier, and close-up on the path of circulation of the sample. The yellow arrows indicate the compressed air flow while the blue arrows indicate the sample flow. 44

(3.6) Pre-emulsion of oil in sodium caseinate solution, (a) after mixing with a rotor-stator, and (b) after 4 h. The dotted yellow frame indicates the presence of foam, while the dashed blue frame highlights the creaming of the oil droplets. 45

(3.7) Fixed angle rotor for ultracentrifuge, with an illustration of the separation of a sample with particles (in blue) less dense than the suspending medium. Adapted from Ref. [12]. 46

(3.8) Several stages of the preparation of small protein-stabilised droplets (a) after 3 passes through the microfluidiser and (b) after ultracentrifugation at $234\,800 \times g$ for 16 h that leads to the fractionation of the emulsion into a cream of jammed droplets, a subnatant and a small protein sediment. 47

(3.9) Typical size distributions of the emulsion before centrifugation (dashed line) and of the droplets after separation by centrifugation and redispersion in water (dotted line). The particle sizings were performed using Static Light Scattering (Mastersizer) on only one sample, but are representative of the results obtained for all samples. 49

(3.10) Composition, in effective volume fractions $\phi_{eff,drop}$ defined in Chapter 5, of suspensions of sodium caseinate (squares, navy), sodium-caseinate stabilised droplets (circles, cyan), and of mixtures (triangles, colour-coded as a function of χ_{prot} defined in Equation 3.1) studied in Chapter 5. The compositional parameters of the mixture samples are listed in Table 3.2. 52

(3.11) Acidification of suspensions containing equal amounts of glucono δ-lactone at 50 °C. The blue line denotes a suspension of $45\,\mathrm{mg}\cdot\mathrm{mL}^{-1}$ sodium caseinate, while the orange line is deionised water. Both suspensions have an initial pH of 6.7, but the steep initial decrease in pH upon mixing with glucono δ-lactone powder could not be measured. 54

(4.1) Typical SLS setup, reproduced from Ref. [13] 61

(4.2) Separation principle of Flow Field Fractionation (FFF) technique. Image courtesy of PostNova [14]. 64

(4.3) Estimation of the concentration of 5.0 %(wt) protein suspensions after purification following different protocols (circles): centrifuged at 60 000 × g only, centrifuged and filtered using a 0.45 µm membrane, centrifuged and filtered using a 0.2 µm membrane, filtered using a 0.45 µm membrane only, and filtered using a 0.45 µm membrane and then centrifuged at 60 000 × g. The absorbance was measured for solutions diluted 80 times, but the concentration of the mother solutions is shown here on the x-axis. The calibration curve (squares) was obtained using suspensions of non purified protein, and performing a linear fit. 66

(4.4) Concentration ($g \cdot mL^{-1}$) of suspensions of sodium caseinate calculated via refractometry as a function of their weight fraction as estimated during preparation. The dotted line denotes a linear fit of equation $y = 0.88 \times x$. 68

(4.5) Heterogeneous supernatant after ultra-centrifugation of sodium caseinate-stabilised o/w emulsion. (a) Two distinct layers of cream: (yellow dots) a white layer at the top, and (green dashes) a transparent layer at the bottom. Below, the interface with the subnatant is visible by a turbid rim containing oil droplets. (b) A small amount of the transparent layer is exhibited on a spatula. (c) The transparent layer has a blue hue when illuminated from the side, and (d) an orange hue when the light shines through it. 69

(4.6) Transition of the optical properties in the heterogeneous supernatant after ultra-centrifugation of sodium caseinate-stabilised o/w emulsion. Cyan dashes: the transition between the white and the transparent layer is observed from accross the tube and a blue hue is observed. Red dots: looking closer at the transition from the side of the tube, the full visible spectrum can be seen. The yellow frames and colour gradients are indicated as guides for the eye. . . 71

(4.7) Size distributions of protein-stabilised droplets after centrifugation, as presented in Figure 4.5: the lower transparent layer was collected separately and the size distribution of the droplets it contains (dotted line, in blue) is compared to the droplets in the entire plug (dashed line, in orange). 72

(4.8) Size distributions of protein-stabilised droplets (same droplets at two different concentrations) measured by Dynamic Light Scattering (dot line, red) and by Static Light Scattering (dash dot line, orange). Mean sizes (volume mean diameters D_{43}): Mastersizer (130 ± 63) nm Zetasizer (221 ± 98) nm. 77

(4.9) Elution profile of sodium caseinate using Flow Field Fractionation. This data was provided by PostNova Analytics Ltd. SLS and DLS setups are placed inline and allow to measure the concentration (from the intensity of the SLS), gyration radius R_g (from the scattering profile of the SLS), and hydrodynamic radius R_g (from the temporal fluctuations of the DLS). 79

(4.10) Size distributions of sodium caseinate as prepared by the method described in Section3.2. The sample was fractionated by Asymetric Flow Field Flow Fractionation (kindly performed by PostNova Analytics Ltd), and the sizes were measured online by Dynamic Light Scattering (dot line, red) and by Multi Angle Light Scattering (dash dot line, orange).The inset is a zoom of the small fraction of proteins that makes bigger aggregates. 80

(5.1) Rheology setup: stress-controlled MCR 502 (Anton Paar), Couette geometry and temperature-controlling Peltier cell. 86

(5.2) Flow curves of sodium caseinate-stabilised droplets (top, circles) and sodium caseinate suspensions (bottom, squares) at several concentrations. These curves are the average of 3 measurements, and the error bars indicate the reproducibility. For the shear thinning samples, only the zero-shear viscosity η_0 is considered, as indicated by the shaded area. A more thorough study of their behaviour is presented in Section 5.6. 87

(5.3) Relative viscosity of sodium caseinate suspensions (squares, navy blue) and sodium caseinate-stabilised droplets (circles, cyan) as a function of the concentration. The lines denote Batchelor model for hard spheres in the semi-dilute regime, Equation 2.3. The error bars represent the standard error upon averaging the viscosity plateau for the three measurements. 88

(5.4) Specific viscosity $\left(\frac{\eta_0}{\eta_s} - 1\right)/c$ of sodium caseinate suspensions (squares, navy blue) and sodium caseinate-stabilised droplets (circles, cyan) as a function of the concentration. The line denotes a linear fit. 89

(5.5) Cartoon of a protein-stabilised droplet where R_c and R_{c+s} are the radii of, respectively, the oil core and the droplet (including the soft shell of adsorbed proteins). 92

(5.6) Relative zero-shear viscosity of sodium caseinate-stabilised droplets (circles, cyan) as a function of the effective volume fraction. The red dashed line denotes Quemada equation for hard spheres (Equation 2.4) with $\phi_m = 0.79$. 97

(5.7) Relative viscosity of sodium caseinate suspensions (squares, navy) as a function of the effective volume fraction. The red dashed line denotes the modified Quemada equation, Equation 5.9, the values for n and ϕ_m are listed in Table 5.1. 99

(5.8) Flow curves of mixtures of sodium caseinate-stabilised droplets and sodium caseinate at several concentrations. These curves are the average of 3 measurements, and the error bars indicate the reproducibility. For the shear thinning samples, only the zero-shear viscosity η_0 is considered, as indicated by the shaded area. A more thorough study of their behaviour is presented in Section 5.6.102

(5.9) Relative zero-shear viscosities η_0/η_s of suspensions of sodium caseinate suspensions (squares, navy), sodium-caseinate stabilised droplets (circles, cyan), and of mixtures (triangles, colour-coded as a function of χ_{prot} defined in Equation 5.10) as a function of the effective volume fraction ϕ_{eff}. 103

(5.10)Development of a semi-empirical model to predict the viscosity of protein-stabilised emulsions. The un-adsorbed proteins increase the viscosity of the continuous phase as a function of their volume fraction in the interstices between droplets ϕ^i_{prot} 104

(5.11)Calculated relative contributions of the continuous phase and of the dispersed phase alone to the viscosity of caseinate-stabilised emulsions. (a) Relative viscosity of the continuous phase containing un-adsorbed sodium caseinate aggregates. It is estimated by calculating, for each composition, the volume fraction of protein in the interstices between the droplets ϕ^i_{prot}. Then the relative viscosity of a suspension of protein at this volume fraction $\eta_{r,prot}\left(\phi^i_{prot}\right)$ is calculated. (b) Relative viscosity of sodium caseinate-stabilised droplets $\eta_{r,drop}\left(\phi_{drop}\right)$, calculated from the composition of each mixture. For the two graphs, the colour coding indicates the compositional index of the mixtures $\chi_{prot} = \phi_{eff,prot}/\left(\phi_{eff,prot} + \phi_{eff,drop}\right)$. The error bars are calculated using the error propagation theory (see Appendix A), and only displayed if larger than the symbol size. 106

(5.12)Predicted relative viscosity of mixture suspensions $\eta^p_{r,mix}$, calculated with Equation 5.12, as a function of the measured viscosity $\eta^m_{r,mix}$ from Figure 5.9. Each point is a mixture of different composition, as listed in Table 3.2, where the colour indicates the value of the compositional index χ_{prot} defined at Equation 5.10. The straight line represents $\eta^p_{r,mix} = \eta^m_{r,mix}$, and a regression analysis gives an adjusted R^2 of 0.988. The error bars are calculated using the error propagation theory (see Appendix A). 107

(5.13) Reversal of semi-predictive model for the viscosity of protein-stabilised emulsions. The measurement of the emulsion viscosity $\eta_{r,mix}$ makes possible the calculation of the volume fraction of un-adsorbed proteins $\phi_{eff,prot}$, given that the volume fraction of droplets $\phi_{eff,drop}$ is known from the preparation protocol. 109

(5.14) Flow curves of shear-thinning samples, fitted using Equation 2.7. The relative viscosity η/η_s is plotted as a function of the shear stress σ. Left (squares): Concentrated suspensions of sodium caseinate at effective volume fractions $\phi_{eff,prot}$ of 0.93, 1.03, 1.05, 1.12 and 1.33. Right (circles): Concentrated suspensions of pure sodium caseinate-stabilised oil droplets at effective volume fractions $\phi_{eff,drop}$ of 0.63, 0.68, 0.80 and 0.83. For clarity, only 1/3 of datapoints are displayed for each curve. 111

(5.15) Flow curves of shear-thinning emulsions, fitted using Equation 2.7. The relative viscosity η/η_s is plotted as a function of the shear stress σ. Concentrated mixtures of caseinate-stabilised droplets and un-adsorbed sodium caseinate in suspension (triangles, colour indicates the value of the compositional index χ_{prot} defined at Equation 5.10). The compositions of the samples are listed in Table 5.2. For clarity, only 1/3 of datapoints are displayed for each curve. 112

(5.16) Shear thinning behaviour of concentrated suspension of sodium caseinate (squares, navy), sodium-caseinate stabilised droplets (circles, cyan), and of mixtures of both (triangles, colour-coded by the value of χ_{prot}) as characterised by the critical shear stress for shear-thinning. (a) Critical shear stress σ_c as a function of the zero-shear relative viscosity η_0/η_s for several concentrated suspensions. σ_c and η_0 were estimated by fitting the flow curves in Figure 5.14 and 5.15 with Equation 2.7. (b) Reduced critical shear stress $\sigma_{r,c}$ 5.14 as a function of the zero-shear relative viscosity η_0/η_s. The error bars indicate the uncertainty of the fitting parameters, and the lines are indicated as guide for the eye. 115

(6.1) Illustration of the measuring sequence for the oscillatory rheometry of the emulsion gels, detailed in the Methods part. Frequency (open squares) and strain amplitude (filled triangles) of the oscillatory shear vary with time in the 4 steps of the measurement. At the time $t = 0\,\text{s}$, the glucono δ-lactone was added to the sols. . 124

(6.2) Illustration of laser scanning confocal microscopy: (a) Setup of the confocal microscope used in this study (LSM 780 with inverted Axio observer, Zeiss), (b) Principal light pathways in confocal microscopy (reproduced from Ref. [15]). 125

(6.3) Molecular structure of Bodipy 493/503 126

(6.4) Experimental setup for rheo-imaging. Assembly of a rheometer (MCR 502, Anton Paar) and a fast-imaging confocal microscope (DMI8-CS, Leica). The cartoon represents the measurement zone: the sample is deposited between a circular glass slide and a rheometer tool, here a plate geometry (PP25, smooth). 127

(6.5) Protocol for the Fast Fourier Transform of a micrograph. The image is multiplied by a Hanning window of the same size before the FFT is calculated. The spectrum $I(q)$ is obtained using the plugin Radial Profile to perform a radial average of the Fourier transform. 129

(6.6) Illustration of the quantifications of the gel microstructure and extraction of the parameters from the Fast Fourier Transform analysis. The decrease of the structure factor $S(q)$ (left) and FFT spectrum $I(q)$ (right) is first fitted by a power law, linear in double logarithmic scale. Its intersection with the plateau defines the critical spatial frequency q_c. The distance between the plateau at low and high frequency (red arrow) marks the peak height. 130

(6.7) Confocal micrographs of acid-induced gelation of a suspension of sodium caseinate ($\phi_{eff,prot} = 9.8\,\%$) at room temperature, and emergence of viscoelasticity. Sodium caseinate is labelled by adding Rhodamine B in the suspension before gelation. Each frame is taken at 10 µm above the glass slide and at different stages of gelation, and is numbered from top to bottom and left to right: (1) $t = t_0 = 11 \times 10^3\,\mathrm{s}$ after addition of glucono δ-lactone. , (2) $t = t_0 + 1620\,\mathrm{s}$, (3) $t = t_0 + 1845\,\mathrm{s}$, (4) $t = t_0 + 1980\,\mathrm{s}$, (5) $t = t_0 + 2205\,\mathrm{s}$, (6) $t = t_0 + 2430\,\mathrm{s}$, (7) $t = t_0 + 2700\,\mathrm{s}$, (8) $t = t_0 + 3600\,\mathrm{s}$. The length of the scale bar represents 30 µm. The storage (G', solid line) and loss (G", dashed line) corresponding to the micrographs are indicated on the gelation plot (red stars). . . 132

(6.8) Confocal micrographs of acid-induced gelation of a suspension of caseinate-stabilised nanosized oil droplets ($\phi_{eff,drop} = 9.0\,\%$) at room temperature, and emergence of viscoelasticity. Sodium caseinate is labelled using Rhodamine B, and oil using Bodipy 493/503, both were added in the suspension before gelation. Each frame is taken at 10 µm above the glass slide and at different stages of gelation, and is numbered from top to bottom and left to right: (1) $t = t_0 = 9.4 \times 10^3\,\mathrm{s}$ after addition of glucono δ-lactone, (2) $t = t_0{+}420\,\mathrm{s}$, (3) $t = t_0{+}600\,\mathrm{s}$, (4) $t = t_0{+}840\,\mathrm{s}$, (5) $t = t_0{+}1020\,\mathrm{s}$, (6) $t = t_0 + 1200\,\mathrm{s}$, (7) $t = t_0 + 1380\,\mathrm{s}$, (8) $t = t_0 + 2700\,\mathrm{s}$. The length of the scale bar represents 30 µm. The storage (G', solid line) and loss (G", dashed line) corresponding to the micrographs are indicated on the gelation plot (red stars). 135

(6.9) Fast Fourier Transform analysis of the confocal micrographs of gelation of a suspension of sodium caseinate (left, $\phi_{eff,prot} = 9.8\,\%$, presented in Figure 6.7) of a suspension of caseinate-stabilised droplets (right, $\phi_{eff,drop} = 9.0\,\%$, presented in Figure 6.8). (a) Structure factors $S(q)$ of each micrograph are plotted versus the spatial frequency q. (b) Characteristic lengthscales L_C (top) and peak heights (bottom) extracted from the structure factors $S(q)$ are plotted versus the gelation time t. 137

(6.10) Comparison between acid-induced gelation behaviour of protein suspensions ($\phi_{eff,prot} = 53\,\%$ sodium caseinate, in navy blue) and protein stabilised droplets ($\phi_{eff,drop} = 53\,\%$ caseinate-stabilised oil droplets, in cyan) at 35 °C. Storage (G', continuous line) and loss (G'', dotted line) moduli were averaged on the existing data, and the coloured area represents the error after averaging. The inset represents the variation of the phase angle δ after gelation. All are plotted as function of the shifted time $t' = t - t_{gel}$. Small-oscillatory measurements at 1 Hz. 140

(6.11) Gelation times t_{gel} of protein (squares, navy blue) and droplet (circles, cyan) suspensions, at 35 °C, after addition of glucono δ-lactone, as a function of the volume fraction ϕ_{eff}. The error bars represent the standard deviation of data for each sample. Each gel is prepared using a fixed gdl:protein ratio, as decribed in Chapter 3. 141

(6.12) Micrographs (100 µm × 100 µm) of aged acid-induced gels formed from suspensions of: (top) sodium caseinate, and of (bottom) caseinate-stabilised droplets, at different volume fractions ϕ_{eff}. The scale bars are 30 µm long. The graph presents the characteristic lengthscale L_C of the gels, as a function of the volume fraction ϕ_{eff}, for caseinate gels (squares, navy blue) and caseinate-stabilised droplet gels (circles, cyan). For each point, L_C was obtained by performing a FFT of one micrograph and extracting the position of the peak in the spectrum $I(q)$, as described in Figure 6.5. The inaccuracy of this determination is indicated by the error bar. When two points are presented for one concentration, they correspond to different micrographs of similar samples. 145

(6.13) Storage (G', (a)) and loss (G'', (b)) moduli at 1 Hz of protein-stabilised droplet gels (circles, cyan) and of protein gels (squares, navy blue) as functions of the effective volume fraction of the gel (scaling derived in Section 5.3.2). A fit (Equation 6.1) of each type of system was performed and the model (parameters listed in Table 6.2) as well as the 95 % confidence band are displayed on each graph. The horizontal error bars arise from error propagation upon calculation of the volume fraction, while the vertical error bars are smaller than the data points, so not diplayed here. 148

(6.14) Comparison of the frequency dependence for protein gels (sodium caseinate: $\phi_{eff} = 53\,\%$, in navy blue) and droplet gels (caseinate-stabilised oil droplets: $\phi_{eff} = 53\,\%$, in cyan). Storage modulus G' and loss modulus G'' are represented as functions of the angular frequency ω. G' was fitted with a power law for both types of samples, and the fitting parameters can be found in Table 6.3. . . 152

(6.15) Comparison of frequency dependence for protein gels (squares, navy blue) and protein stabilised droplets (circles, cyan): power-law exponent β, obtained by fitting $G' = f(\omega)$ with Equation 6.14, as a function of the effective volume fraction ϕ_{eff}. 154

(6.16) Variation of the phase angle with the angular frequency ω for droplet gels at several effective volume fractions $\phi_{eff,drop}$. The behaviour of one protein gel ($\phi_{eff,prot} = 31\,\%$, squares, in navy blue) is presented to illustrate the absence of variations in this type of samples. 155

(6.17) Oscillatory strain sweep of protein ($\phi_{eff,prot} = 9.8\,\%$, squares, navy blue) and protein-stabilised droplet ($\phi_{eff,drop} = 9.0\,\%$, circles, in cyan) gels. Normalised storage modulus G'/G'_0 of the gels as a function of (a) the shear strain amplitude γ (in %), and (b) the shear stress amplitude σ (in Pa). The changes in regime are described by the critical and maximum strain (γ_c and γ_m) in (a), as well as critical and maximum stress (σ_c and σ_m) in (b), and their determination illustrated for the protein gel by the dashed and dotted lines. Beyond γ_m and σ_m, the samples fracture irreversibly so the measurement is not reliable. Each curve is an average of 3 measurements, after normalisation by the storage modulus in linear regime G'_0. The error bars represent the standard error upon averaging. 157

(6.18) Parameters for the strain dependence of protein gels (navy blue) and protein-stabilised droplet gels (cyan). (a) Critical strain γ_c and maximum strain γ_m, and (b) Critical stress σ_c and maximum stress σ_m (Pa) as a function of the effective volume fraction ϕ_{eff} in protein and in droplets. The parameters are extracted as illustrated in Figure after averaging the curves for 3 measurements of gels prepared in a similar fashion. The error bars represent the accuracy of this procedure. 158

(6.19) Storage modulus G' normalised by its value in the linear regime G'_0 as a function of the oscillatory strain amplitude γ normalised by its value at the onset of the non-linear regime γ_c.(a) Sodium caseinate-stabilised droplet gels at several volume fractions ϕ , (b) Sodium caseinate gels at several volume fractions ϕ. Each curve is the average of 3 measurements, but for clarity the error bars are not represented here. 160

(6.20) Recovery of protein gels (navy blue) and protein-stabilised droplet gels (cyan) after application of large-amplitude oscillatory shear. The storage modulus G' (Pa) measured by small-amplitude oscillations is represented as a function of time t (s), starting immediately after shearing the sample. The storage modulus in linear regime G'_0 and the drop upon fracture for protein gels and droplets gels are represented by the sets of horizontal lines and arrows. (a) Recovery of gels at low concentration: protein gel at $\phi_{eff} \approx 9\,\%$ and droplet gel at $\phi_{eff} \approx 9.8\,\%$. (b) Recovery of gels at high concentration: protein gel and droplet gel at $\phi_{eff} \approx 53\,\%$. 162

(7.1) Confocal micrographs of the acid-induced gelation of a suspension containing sodium caseinate ($\phi_{eff,prot} = 7.6\,\%$) and caseinate-stabilised droplets ($\phi_{eff,drop} = 4.3\,\%$) at room temperature, and emergence of viscoelasticity. Sodium caseinate and oil are labelled by adding Rhodamine B (red) and Bodipy 493/503 (green) in the suspension before gelation. Each frame is taken at 10 µm above the glass slide and at different stages of gelation, and is numbered from top to bottom and left to right: (1) $t = t_0 = 10.4 \times 10^3$ s after addition of glucono δ-lactone, (2) $t = t_0 + 180$ s, (3) $t = t_0 + 300$ s, (4) $t = t_0 + 360$ s, (5) $t = t_0 + 420$ s, (6) $t = t_0 + 540$ s, (7) $t = t_0 + 720$ s, (8) $t = t_0 + 1620$ s. The length of the scale bar represents 30 µm. The storage (G', solid line) and loss (G", dashed line) corresponding to the micrographs are indicated on the gelation plot (red stars). 169

(7.2) Fast Fourier Transform analysis of the confocal micrographs of gelation of a suspension of sodium caseinate and of caseinate-stabilised droplets (presented in Figure 7.1). (Left) Structure factors $S(q)$ of each micrograph are plotted versus the spatial frequency q. (Right) Characteristic lengthscales L_C (top) and peak heights (bottom) extracted from the structure factors $S(q)$ are plotted versus the gelation time t. 170

(7.3) From emulsions in suspensions to emulsion gels: a change of variables for the description of mixtures. Emulsion gels are better described by their total volume fraction $\phi_{eff,prot} + \phi_{eff,drop}$ (coded by the size of symbols), and by the ratio of droplets over the total volume fraction $\phi_{eff,drop}/(\phi_{eff,prot} + \phi_{eff,drop})$ (colour-coded as introduced in Chapter 5). 173

(7.4) Storage (G', (a)) and loss (G'', (b)) moduli at 1 Hz of protein-stabilised droplet gels (circles, cyan), of protein gels (squares, navy blue), and of gels of mixtures (diamonds, colour-coded), as functions of the effective volume fraction of the gel (respectively $\phi_{eff,drop}$, $\phi_{eff,prot}$ and $\phi_{eff,prot} + \phi_{eff,drop}$, scaling derived in Section 5.3.2). A fit (Equation 6.1) was performed for each system and the model (parameters listed in Table 6.2) as well as the 95 % confidence band are displayed on each graph. The horizontal error bars arise from error propagation upon calculation of the volume fraction, while the vertical error bars are smaller than the data points, so not diplayed here. 175

(7.5) Storage modulus normalised by the effect of the volume fraction $G'^{\,exp}_{mixture}/G'^{\,model}_{protein}(\phi_{protein} + \phi_{droplet})$ as a function of the relative amount of the composition $\phi_{eff,drop}/(\phi_{eff,prot} + \phi_{eff,drop})$. The size of the data points indicates the total volume fraction $\phi_{eff,tot} = \phi_{eff,drop} + \phi_{eff,prot}$. This graph represents the same samples of gels of mixtures than shown in Figure 7.4. 176

(7.6) Comparison of frequency dependence for gels of mixtures (diamonds, colour-coded), of protein stabilised droplets (circles, in cyan) and of protein (squares, in dark blue): power-law exponent β, obtained by fitting $G' = f(\omega)$ with Equation 6.14, as a function of the ratio $\phi_{eff,drop}/(\phi_{eff,prot} + \phi_{eff,drop})$. The size of the data points indicates the total volume fraction $\phi_{eff,tot} = \phi_{eff,drop} + \phi_{eff,prot}$. The shaded area is a guide for the eye. 178

(7.7) Reinforcement of a protein gel upon addition of droplets $G'^{\,exp}_{mixture}/G'^{\,model}_{protein}(\phi_{protein})$ (top, from left to right), and of a droplet gel upon addition of proteins $G'^{\,exp}_{mixture}/G'^{\,model}_{droplet}(\phi_{droplet})$ (bottom, from right to left) as a function of the relative amount of droplet added $\phi_{eff,drop}/(\phi_{eff,prot}+\phi_{eff,drop})$. $\phi = x\%$ indicates samples of miscellaneous concentrations. The two graphs represent the same samples of gels of mixtures, as shown in Figure 7.4, but differ by the arbitrary role of the components: the proteins form the matrix in the top graph while they are the fillers in the bottom graph, and vice-versa for the droplets. 181

(7.8) From droplet-filled protein gel matrix to composite gel: changing paradigm for the study of protein-stabilised emulsion gels. The cartoon on the left is inspired from the existing literature on emulsion gels and present emulsion gels as a matrix of protein gel (lines) containing droplets that act as fillers [16]. Motivated by the heterogeneous structure of the emulsion gel (centre, confocal microscopy image, scale bar 10 µm, oil dyed in yellow and proteins in blue), a novel approach was developed. The cartoon on the right represents the new paradigm, in which emulsion gels are envisioned as composite colloidal gels with an intermediate behaviour between pure protein gels and pure droplet gels. 184

(8.1) Size distributions of the droplets prepared using a microfluidiser (blue, as presented in Chapter 4) and a homogeniser (purple). The volume-weighted distributions were measured using a Mastersizer (dash-dot line) and a Zetasizer (DLS, short-dashed line). 191

(8.2) Flow curves of sodium caseinate-stabilised droplets ($R_h = (450 \pm 815)$ nm) at several concentrations. These curves are the average of 3 measurements, and the error bars indicate the reproducibility. For the shear thinning samples, only the zero-shear viscosity η_0 is considered, as indicated by the shaded area. A more thorough study of their behaviour is presented in Section 8.4.3. 193

(8.3) Relative viscosity of sodium caseinate-stabilised droplets of radii $R_h = (110 \pm 49)$ nm (circles, cyan, as presented in Chapter 6) and $R_h = (450 \pm 815)$ nm (triangles, purple) as a function of the concentration. The lines denote Batchelor model for hard spheres in the dilute regime, Equation 2.3. The error bars represent the standard error upon averaging the viscosity plateau for the three measurements. 194

(8.4) Relative viscosity of sodium caseinate-stabilised large droplets ($R_h = (450 \pm 815)\,\text{nm}$, triangles, purple) and small droplets ($R_h = (110 \pm 49)\,\text{nm}$, circles, cyan, as presented in Chapter 5) as a function of the effective volume fraction ϕ_{eff}. The dashed lines denote Quemada equation for hard spheres, Equation 2.4 for large droplets ($R_h = (450 \pm 815)\,\text{nm}$, purple, with $\phi_m = 75\,\%$) and small droplets ($R_h = (110 \pm 49)\,\text{nm}$, purple, with $\phi_m = 79\,\%$, as presented in Chapter 5). 195

(8.5) Flow curves of shear-thinning samples, fitted using Equation 2.7. The relative viscosity η/η_s is plotted as a function of the shear stress σ. Left (circles): Concentrated suspensions of pure small oil droplets ($R_h = (110 \pm 49)\,\text{nm}$) at effective volume fractions $\phi_{eff,drop}$ of 0.63, 0.68, 0.80 and 0.83, from Figure 5.14. Right (triangles): Concentrated suspensions of pure large oil droplets ($R_h = (450 \pm 815)\,\text{nm}$) at effective volume fractions $\phi_{eff,large\ drop}$ of 0.51, 0.67 and 0.75. 196

(8.6) Shear thinning behaviour of concentrated suspensions of sodium-caseinate stabilised droplets of different sizes: $R_h = (110 \pm 49)\,\text{nm}$ (circles, cyan) and $R_h = (450 \pm 815)\,\text{nm}$ (triangles, purple), and of sodium caseinate (squares, navy). (a) Critical shear stress σ_c as a function of the zero-shear relative viscosity η_0/η_s for several concentrated suspensions. σ_c and η_0 were estimated by fitting the flow curves flow curves in Figure 5.14 and 8.5 with Equation 2.7. (b) Reduced critical shear stress $\sigma_{r,c}$, calculated using Equation 5.14, as a function of the zero-shear relative viscosity η_0/η_s. The error bars indicate the uncertainty of the fitting parameters, and the lines are indicated as guide for the eye. The data for the small droplet and the protein suspensions are from Figure 5.16. 198

(8.7) Storage (G', (a)) and loss (G'', (b)) moduli at 1 Hz of protein gels (square, navy blue, from Chapter 6) and of gels of protein-stabilised droplet of radii $R_h = (110 \pm 49)\,\text{nm}$ (circle, cyan, from Chapter 6) and $R_h = (450 \pm 815)\,\text{nm}$ (triangle, purple) as functions of the effective volume fraction of the gel. A fit of each type of system was performed using Equation 6.1, and the models (with the parameters listed in Table 8.2) as well as the 95 % confidence bands are displayed on each graph. 201

(8.8) Comparison of the frequency dependence of a gel of small droplets ($R_h = (110 \pm 49)\,\text{nm}$, $\phi_{eff} = 53\,\%$, in cyan), a gel of large droplets ($R_h = (450 \pm 815)\,\text{nm}$, $\phi_{eff} = 51\,\%$, in purple), and a protein gel ($\phi_{eff} = 53\,\%$, in navy blue). Storage modulus G' and loss modulus G'' are represented as functions of the angular frequency ω. G' was fitted with a power law for both types of samples. 203

(8.9) Modelling of the frequency dependence of gels of small droplets ($R_h = (110 \pm 49)\,\mathrm{nm}$, circles, in cyan), gels of large droplets ($R_h = (450 \pm 815)\,\mathrm{nm}$, triangles, in purple), and protein gels (squares, in navy blue): power-law exponent β, obtained by fitting $G' = f(\omega)$ with Equation 6.14, as a function of the effective volume fraction ϕ_{eff}. 204

(8.10) Storage modulus G' normalised by its value in the linear regime G'_0 as a function of the oscillatory strain amplitude γ normalised by its value at the onset of the non-linear regime γ_c: Sodium caseinate-stabilised large droplet gels ($R_h = (450 \pm 815)\,\mathrm{nm}$) at several effective volume fractions ϕ_{eff}. 205

(8.11) Strain hardening of gels of small droplets ($R_h = (110 \pm 49)\,\mathrm{nm}$, circles, in cyan), gels of large droplets ($R_h = (450 \pm 815)\,\mathrm{nm}$,triangles, in purple), and protein gels (squares, in navy blue). Storage modulus G' normalised by its value in the linear regime G'_0 as a function of the oscillatory strain amplitude γ normalised by its value at the onset of the non-linear regime γ_c for: (a) Gels of low volume fraction ($\phi_{eff} \approx 10\,\%$), and (b) gels of high volume fraction ($\phi_{eff} \approx 50\,\%$). 207

List of Tables

(3.1) Composition of the batch of sodium caseinate used in this study. The chemical analysis was performed by the manufacturer (Friesland Campina). 38

(3.2) Composition of the mixture samples made of sodium caseinate (proteins) and sodium caseinate-stabilised droplets (droplets) . . . 53

(5.1) Parameters for the modified Quemada model for soft colloids, Equation 5.9, applied to sodium caseinate suspensions 100

(5.2) Composition of the concentrated emulsions (mixtures of protein-stabilised droplets and un-adsorbed proteins) that present a shear-thinning behaviour, and whose flow curves are displayed in Figure 5.15. ϕ_{eff} indicates the effective volume fractions calculated with Equation 5.4. 112

(6.1) Experimental details for the rheo-imaging of protein and droplet gels 128

(6.2) Parameters for Equation 6.1 to fit viscoelasticity of gels at 1 Hz displayed in Figure 6.13 149

(6.3) Frequency dependence of gels: parameters for Equation 6.3 to fit the viscoelasticity of gels displayed in Figure 6.14 153

(7.1) Experimental details for the rheo-imaging of emulsion gels. 168

(8.1) Summary table: Influence of the size of droplets on the rheological properties of droplet suspensions 199

(8.2) Parameters used to fit the viscoelasticity of gels at 1 Hz displayed in Figure 8.7 with Equation 6.1. 202

(8.3) Parameters for normalising the strain dependence displayed in Figure 8.10 206

(8.4) Summary table: Influence of the size of droplets on the rheological properties of droplet gels 208

Chapter 1

Introduction and thesis outline

> What matters more than the [paradigm] you choose to use is to realise that you have one in the first place, because then you have the power to question and change it.
>
> Doughnut economics,
> KATE RAWORTH

1.1 Introduction

Food proteins are often only seen as an efficient contribution to nutritional intake; however their functional properties are also important for the formation of complex structures in food products. It is this structural aspect of these biological systems that caught the interest of physicists, leading to a growing activity, over the last three decades [17], within the broader framework of soft matter science.

This subfield of condensed matter science focuses on the physico chemical study of materials whose softness arises from the weak interactions within them, which allow a responsiveness to perturbations of the order of the thermal energy. As food is meant to be masticated, most food products fall in the category of soft materials [18]. Although most of them have a complex structure, some are well described as simple emulsions (*e.g.* milk, mayonnaise), gels (*e.g.* jam, jelly) or emulsion gels (*e.g.* yoghurt, cheese). All these examples derive their structures from the functional properties of proteins or of biological polymers called polysaccharides.

An emulsion is formed by the dispersion of one liquid into another, with which it is immiscible, in the form of microscopic or colloidal droplets [19]. As it is energetically unstable, the use of an emulsifier is necessary: because it decreases the interfacial energy, it adsorbs at the interface and stabilises the droplets against coalescence by a combination of electrostatic and steric repulsion.

A gel on the other hand can be described as a continuous three-dimensional network, the pores of which are filled with a fluid, water in the case of hydrogels. When the gel arises from the aggregation of colloidal elements, it is called a colloidal gel [20]. Its structure, the properties of the building blocks, and the interactions between those determine its properties.

An interesting property of proteins is their ability to both stabilise emulsions [21] and form gels [22]. In this way, they also offer the possibility to form emulsion gels. Among the food proteins, one of the best at forming emulsions and gels is a milk protein, casein [23], which has been widely studied and is commonly used in industry. An everyday-life example of a casein emulsion gel is yoghurt: native oil droplets from milk are embedded in a matrix of casein gel [9].

During emulsification not all the proteins in solution adsorb at the interface, it is thus important to take into account the ratio between adsorbed and suspended proteins in solution before gelation, as illustrated in Figure 1.1. If this ratio is low, i.e. most of the protein is suspended, the gelled system can be seen as a matrix of protein gel with the oil droplets acting as fillers. At a higher ratio the emulsion gel is more of a composite formed of both a protein and a droplet network.

The objective here is to study in detail the protein-stabilised emulsions and the gels they form considering the full range of their composition. Rheological and microscopic approaches are combined to characterise the behaviour of the sols and gels, in order to develop an understanding of how the droplets and proteins contribute to the overall properties.

Importantly, in this work, the term *emulsion* implies that the system is a mixture of droplets and proteins. A protein-stabilised emulsion differs thus from a suspension of protein-stabilised droplets by the presence of un-adsorbed proteins

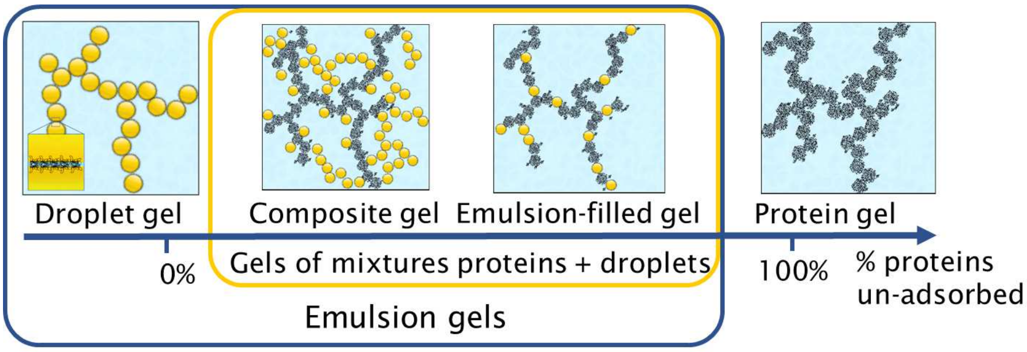

Figure 1.1 *Illustration of the variety of the compositions of emulsion gels. The arrow represents the ratio of un-adsorbed proteins over the total amount of proteins in the gel.*

in the suspending medium.

1.2 Choosing the right paradigms

In this thesis, a bridge between food science and soft matter physics is built in order to develop a thorough understanding of the relationship between composition, microstructure, and rheological properties of casein emulsions and gels. Indeed, these systems have traditionally been studied using a food science approach, where the complexity of a system is reduced by fixing all the parameters but one, and the changes in properties are subsequently assessed. This approach is however limited by the possible interdependence of several parameters, leading to conclusions that can only apply to the system studied rather than being generalised. To overcome these limitations, a soft matter physics approach is used instead, where complex systems are described by idealised models that can be studied using a set of laws and equations.

A key part of this study of emulsions and emulsion gels is thus the choice of paradigms and models to frame both the study and the systems. Indeed, from this choice derive all the results and discussions throughout this thesis, that make the link between previous food science studies of caseins and the literature in soft matter physics. Because the paradigms chosen represent an essential bias of the outputs of this thesis, they are made explicit here.

First, proteins, and more specifically caseins, are complex biological macromolecules, so a model is required for physicists to study them. Here, the framework of soft colloids, developed in the last two decades, is used. It is thus possible to draw on the knowledge of soft colloids to give a set of rules for the discussion of the behaviour of casein in suspension. Notably, this framework can also be used for protein-stabilised droplets, as they can be modelled by particles with a hard core and a soft shell. By extension, the gels formed by caseins and casein-stabilised droplets can be studied in the framework of colloidal gels.

Furthermore, an essential assumption of this study is that protein-stabilised emulsions and emulsion gels are mixtures of proteins and droplets. Because the focus is placed on the influence of the composition on the properties of this system, a strategy to identify the contributions of the components on the mixture is developed here. The systems of pure components are thus first studied, and they are then combined to form mixtures of controlled compositions. The properties of the mixtures, either gelled or not, are subsequently compared to the properties of the pure components. The framework chosen to describe the composition of these mixtures must take into account the specificity of each system. By consequence, the study of emulsions and that of emulsion gels of controlled composition require a different paradigm that reflects their physical state, either liquid suspension or solid fractal network.

Eventually, the results for casein-stabilised emulsions and emulsion gels correspond well with the existing literature on soft colloidal suspensions and colloidal gels. This confirms that the paradigms and models chosen to describe these systems are relevant, and that the theory is robust enough to be applied to complex biological soft matter systems. In addition, the strategy chosen to study suspensions of a mixture of proteins and droplets appears successful in providing a semi-empirical predictive model of their viscosity. This case study of mixtures is promising and it would be interesting to explore its application to other mixtures, as it may set fundamental basis for the formulation of industrial products.

1.3 Thesis outline

As stated previously, in this thesis I investigate the contributions of un-adsorbed proteins and protein-stabilised droplets to the rheology of emulsions, and to the microstructure and rheological properties of emulsion gels. Before discussing the results, I present the relevant literature in Chapter 2. The models used in soft matter physics are first introduced, and then more details are provided about the use of proteins, and more specifically casein, to stabilise emulsions and form gels.

Furthermore, the strategy used to study these systems requires the preparation of suspensions and gels of pure proteins and of pure droplets. Some protocols were thus developed specifically for the preparation of these samples, and are described in Chapter 3.

The concentrations and particle size distributions of the prepared samples of proteins and droplets were subsequently measured as described in Chapter 4. This characterisation allows the precise determination of the composition of the samples, and is also essential to the interpretation of the rheological results.

The viscosity of protein-stabilised emulsions could then be investigated in Chapter 5. This was performed by characterising the pure suspensions of proteins and of droplets separately, before analysing mixtures of controlled composition. A semi-empirical model could be derived that predicts the viscosity of an emulsion from its composition. Most of the results presented in this chapter have been published [1].

The focus was later shifted to emulsion gels. In Chapter 6, I study extensively the gels formed by pure suspensions of proteins and of droplets. Their gelation, microstructure and rheological properties are investigated as functions of the concentration.

In Chapter 7, these components were then combined, resulting in protein-droplet gels, or emulsion gels, of well-characterised compositions, thus allowing a rigorous approach to these systems. Through the dependence on composition of the rheological properties of emulsion gels, a change of paradigm is discussed for these systems, from droplet-filled matrix to composite networks.

Finally, the influence of the droplet size on the previous results derived for emulsions and emulsion gels is studied in Chapter 8, by investigating the droplet suspensions and the droplet gels like in Chapters 5 and 6 at a larger droplet size.

Chapter 2

Background

Throughout this thesis, I draw on a substantial body of work in the fields of soft matter physics and food science. In this chapter, I give an overview of the relevant background literature.

I first give a brief introduction to rheology, both as a scientific field and as an experimental technique of characterisation. Rheology is discussed at length in this thesis and is relevant to the main results in Chapters 5, 6, 7 and 8.

I then present some soft matter systems together with some key features of their rheological behaviour. Colloidal suspensions and emulsions will be discussed most in Chapter 5 and 8, and gels, prepared using suspensions of both colloidal particles and emulsion droplets, will be the focus of Chapters 6, 7 and 8.

Finally, I present the literature relevant to the specific systems studied in this thesis. To that aim, I detail the properties of proteins as emulsifiers and gelling agents, before presenting the protein chosen in this study as a case study, namely sodium caseinate.

2.1 An introduction to shear rheology

Rheology can be defined as the field of study of the flow of fluids, and by extension the response to stress of soft materials [24]. The flow behaviour of materials is particularly relevant for many applications, for example in the industries of food & drinks, cosmetics and paints. In these cases, it is desirable to reach some well-defined mechanical properties for the production and the use of the products.

The term *rheology* can also be used to describe the experimental determination of the rheological behaviour of soft materials, although it is rigorously called *rheometry*. In this manuscript, rheology is used for both the theoretical study of the properties of liquids and soft materials, and the experimental measurements of those same properties, more specifically those related to the shearing of these systems.

Shear rheology measurements are performed by applying a shear strain or stress to the samples and measuring the resulting internal stress or strain, respectively. The strain-stress dependence provides some information on the properties of the material [8]. Depending on the nature, dynamics, and amplitude of the deformation applied, a wide range of properties of the material of interest can be measured.

Here we describe the two major types of shear rheological measurements, namely rotational and oscillatory. In Section 2.2, a few systems on which rheology can be used will then be presented, as well as some of their rheological properties .

2.1.1 Rotational shear rheology

When the main focus of the study is to determine the flow behaviour of a liquid or a soft solid, rotational rheology is a key technique [24]. In a typical test, the sample is deposited between two plates, a stationary lower plate and a moving upper plate, as illustrated in Figure 2.1. During the test, the upper plate is rotated continuously, and thus a continuous shear is applied to the sample.

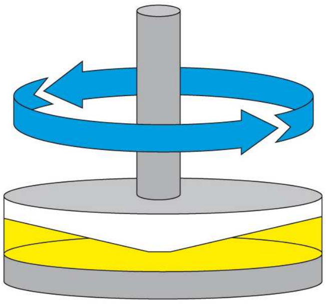

Figure 2.1 *Illustration of a rotational rheology test: the tool with the top plate is in continuous rotation, while the bottom plate is fixed. Reproduced from Ref. [2].*

Any fluid or soft material presents a resistance to be put in motion, so the sample applies a torque to the moving plate, and this torque is measured and converted into shear stress σ by the instrument. The ratio of this shear stress with the shear rate $\dot{\gamma}$, *i.e.* the speed at which the material is sheared, is, by definition, the viscosity η of the sample:

$$\eta = \frac{\sigma}{\dot{\gamma}} \tag{2.1}$$

For soft solids, this viscosity may only be defined when the structure of the material breaks down and allows it to flow. This transition occurs at the yield point, and the critical shear stress is called the yield stress σ_y.

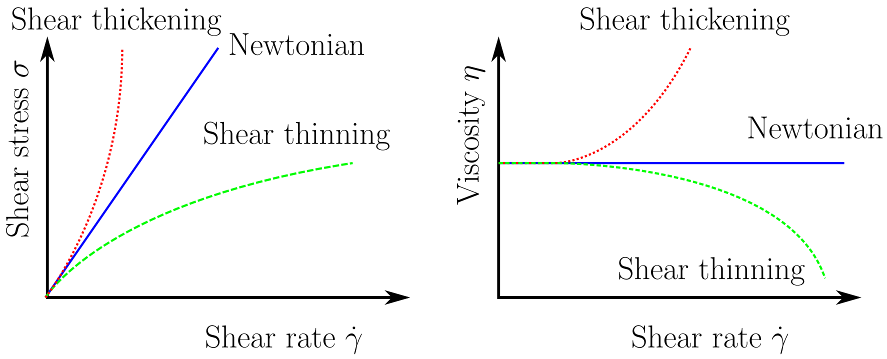

Figure 2.2 *Typical flow curves (left) and viscosity curves (right) for three types of liquids: Newtonian (line, blue), shear thickening (dotted line, red) and shear thinning (dashed line, green).*

The viscosity of a liquid or solid after yielding is often measured over a range of shear rate, and the resulting curves $\sigma(\dot{\gamma})$ and $\eta(\dot{\gamma})$ are termed *flow curve* and *viscosity curve*, respectively. Some typical behaviours for these curves are shown in Figure 2.2.

For the most simple liquids, the viscosity does not depend on the shear rate, and these liquids are said to be *Newtonian*. For many systems like paint or shampoo, the viscosity decreases upon shear, and so they display *shear thinning*. Finally, concentrated suspensions of some particles, like corn starch, become more viscous at high shear, and are said to be *shear thickening* liquids.

Rotational rheology is thus adapted to measure the flow behaviour and viscosity of liquids and soft solids. For determining other mechanical properties of soft materials, one can use oscillatory rheology.

2.1.2 Oscillatory shear rheology

Oscillatory rheology is another technique that can be used to characterise soft materials. The applied deformation here is a sinusoidal shear signal $\gamma = \gamma_0 \sin(2\pi ft)$, and the resulting stress is proportional to the strain in the linear regime, by definition. So, in the linear regime, the stress signal is also sinusoidal and can be written $\sigma = \sigma_0 \sin(2\pi f(t-\delta t))$, where γ_0 and σ_0 are the amplitudes of the strain and stress signals, f is their frequency, and δt is the time shift between strain and stress [24]. These two sinusoids are represented in Figure 2.3.

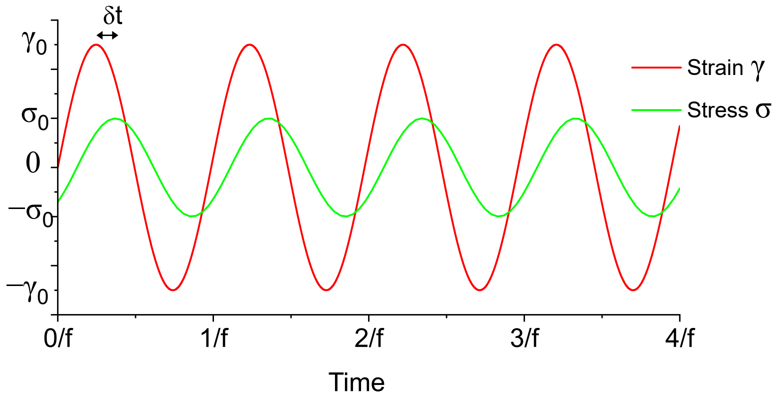

Figure 2.3 *Typical oscillatory rheology measurement in the linear regime: sinusoidal shear deformation* $\gamma = \gamma_0 \sin(2\pi ft)$ *(red), and resulting stress* $\sigma = \sigma_0 \sin(2\pi f(t-\delta t))$ *(green), where* γ_0 *and* σ_0 *are the amplitudes of the strain and stress signals,* f *is their frequency, and* δt *is the time shift between strain and stress.*

The shift between the two sinusoids can be expressed as the phase angle $\delta = 2\pi f\delta t$, that can be physically interpreted as the viscoelastic character of the sample. Indeed, for a purely elastic Hookean solid $\delta = 0$ and for a purely viscous Newtonian liquid $\delta = \pi/2$, while materials with both viscous and elastic components display an intermediate phase shift $0 < \delta < \pi/2$.

Furthermore, the ratio between the applied strain wave and the measured stress wave can be expressed by the complex shear modulus G^* (of absolute value $|G^*| = \gamma_0/\sigma_0$ and of argument $\arg(G^*) = \delta$). For viscoelastic materials, it can be useful to decompose G^* as follows:

- The elastic component, called storage modulus $G' = Re(G^*) = \gamma_0/\sigma_0 \cos(\delta)$.
- The viscous component, called loss modulus $G'' = Im(G^*) = \gamma_0/\sigma_0 \sin(\delta)$.

It can be noted that the phase angle δ is linked to the elastic and viscous moduli via $\tan\delta = G''/G'$. These parameters are the typical results of small-oscillation dynamic rheology measurements, for which the deformations are small enough not to disrupt the structure of the material, and that is thus performed in the linear regime.

In addition, the viscoelasticity of materials is often studied over a wide range of amplitudes and frequencies of the shear signal. Indeed, the frequency dependency of the shear modulus provides informations about the dynamics of the sample of interest. Increasing the amplitude of the deformation also makes it possible to probe the non-linear regime, in which the structure of the material is affected, and a high deformation may lead to the yielding of the material.

Rheology is thus a wide field of study at the interface between physics and materials engineering. Rheological measurements are a widely used tool by scientists and technologists alike.

2.2 Some soft matter systems and their rheological properties

Soft matter is a class of materials that can be easily deformed by stresses of the same order of magnitude as thermal fluctuations [25]. This property arises mostly from the presence of a *mesostructure* in these systems, which is to say that these systems are structured at a scale much larger than the atomic scale, but much smaller than the macroscopic scale of the material.

Here, the soft matter systems studied in this thesis, as illustrated in Figure 2.4, are presented, along with some of their rheological properties.

2.2.1 Colloidal suspensions: hard and soft particles

If small enough solid particles, typically below 1 µm, are dispersed in a liquid they form an heterogeneous solution called a *colloidal suspension* [26]. Inks and blood are only a few examples of colloidal suspensions, as these are ubiquitous, either man-made or naturally occurring.

A practical difficulty when dealing with colloidal suspensions is to stabilise the

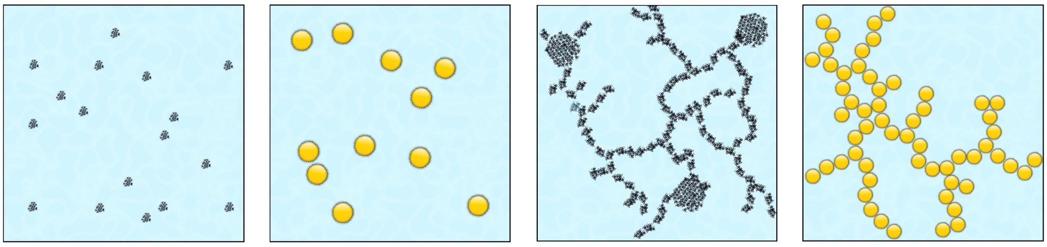

Figure 2.4 *Cartoons of the soft matter systems studied in this thesis. From left to right: suspension of soft colloids, emulsion, (soft) colloidal gel and emulsion gel.*

particles so that they do not aggregate, because extensive aggregation can lead to the phase separation of the suspension. A model case of stable particles are the so-called *hard spheres*. Hard spheres present the simplest possible interactions between particles: two particles do not interact together when they are apart, but when there is contact, they apply an infinite repulsion to each other.

Although it is an ideal model of colloidal particles, and as such difficult to achieve experimentally, the concept of hard spheres is a convenient tool for the development of a theory on the rheology of colloidal suspensions.

Viscosity of hard sphere suspensions

The viscosity of hard sphere suspensions has been the focus of many studies in the last century [27]. Models have been developed to express the viscosity as a function of the volume fraction, but their ranges of validity vary and they are more or less empirical. Here, only the models that will be used in the following chapters are quickly presented.

First, as shown in the typical flow curves of Figure 2.2, some liquids present non-linear variations of the shear-stress as a function of the shear rate $\dot{\gamma}$, so the viscosity of a suspension may vary in a given range of shear rates. In order to compare a similar physical quantity for different fluids, it is thus necessary to narrow the study to the linear regime at low shear, in which the viscosity is constant. The viscosity at this low-shear plateau is called *zero-shear viscosity* η_0, and is used here to compare suspensions at different concentrations.

When there are only a few particles in the suspending liquid, the suspension is said to be in the *dilute regime*, that can arbitrarily be defined by a volume fraction of particles $\phi \leq 5\,\%$. In this regime, Einstein found that the viscosity can be calculated by considering the flow field around each particle to be independent and he derived the equation [28]:

$$\frac{\eta_0}{\eta_s} = 1 + 2.5\phi \tag{2.2}$$

Where the zero-shear viscosity of the suspension η_0 is normalised by the viscosity of the suspending liquid η_s.

Batchelor then expanded this model for suspensions with $\phi \leq 15\,\%$, in the regime called *semi-dilute*, by taking into account the hydrodynamic interactions between particles. He thus developed a model for the viscosity of a monodisperse hard sphere suspension in the semi-dilute regime [29]:

$$\frac{\eta_0}{\eta_s} = 1 + 2.5\phi + 6.2\phi^2 \tag{2.3}$$

For more concentrated suspensions, the crowding of the particles increases the complexity of the hydrodynamics of the medium. A number of models have been developed [27, 30–33], and here the equation devised by Quemada is selected [5] because of its mathematical simplicity. The Quemada equation for the viscosity of a concentrated monodisperse hard sphere suspension reads:

$$\frac{\eta_0}{\eta_s} = \left(1 - \frac{\phi}{\phi_m}\right)^{-2} \tag{2.4}$$

Where the parameter ϕ_m is the maximum volume fraction at which the viscosity of the suspension diverges:

$$\lim_{\phi \to \phi_m} \frac{\eta_0}{\eta_s} = \infty \tag{2.5}$$

These equations are a convenient tool when studying the viscosity of hard sphere suspensions because they make it possible to model the behaviour with a very limited number of parameters. However, they rely on several limiting assumptions, including the monodispersity of the suspensions, *i.e.* the fact that all the particles have the same size. In practice, colloidal suspensions are often polydisperse, so models need to be adjusted.

Concentrated colloidal suspensions: Shear thinning

Suspensions of colloidal hard spheres become non-Newtonian at high concentrations, since the viscosity becomes dependent on the shear applied, as shown in Figure 2.2. When a colloidal suspension is sheared faster than the timescale of its structural relaxation, the flow field is thought to enhance the relaxation and induce some microstructural order [34], and the viscosity consequently decreases with the applied shear rate (or shear stress in a stress-controlled rheometer) [26]. This phenomenon is called shear thinning, and is commonly observed for colloidal suspensions [35, 36].

Models of this behaviour have been derived in previous studies. In a seminal work from Cross [37], the decrease in viscosity is assumed to be driven by the kinetics of formation and breakages of linkages between particles under the effect of shear. The following model is then derived to describe the viscosity η as a function of shear rate $\dot{\gamma}$ based on the kinetics of multiplet formation:

$$\frac{\eta}{\eta_s} = \eta_\infty + \frac{\eta_0 - \eta_\infty}{1 + \alpha \dot{\gamma}^n} \tag{2.6}$$

Where η_0 and η_∞ are the relative viscosities in the two limiting regimes of respectively zero-shear and infinite shear, and α is a kinetic parameter given by the ratio between the kinetic rate of breakage of bonds by shear over the formation of bonds by Brownian motion. Finally, n is here empirically $n = 2/3$ in order to fit the experimental data. However, in a later work, the same author notes that n can be a parameter indicative of polydispersity on a wider range of experimental data, and is related to the molecular weights for polymeric systems [38].

Because it is thought that the driving physical parameter for shear-thinning phenomena is the shear stress σ rather than the shear rate $\dot{\gamma}$ [39], Equation 2.6 can be adapted [40]:

$$\frac{\eta}{\eta_s} = \eta_\infty + \frac{\eta_0 - \eta_\infty}{1 + (\sigma/\sigma_c)^m} \tag{2.7}$$

Where σ_c indicates the shear stress required for the shear-thinning to occur, and the exponent m describes the sharpness of the change in regime between η_0 and η_∞.

In this study, the expression of shear thinning as a function for the shear stress will be favoured to describe the behaviour of the suspensions of interest.

Viscosity of mixtures and effect of polydispersity

It is not uncommon for particles to have a significantly large size distribution, depending on the nature of the particles and on their synthesis. Mixtures of colloidal particles are another example of polydisperse suspensions, and they also require an adjustment of the viscosity models.

One way to take into account the polydispersity of a suspension seems to be the modification of the maximum packing fraction. In a recent study, it was shown that the maximum volume fraction ϕ_m of a polydisperse suspension of hard spheres can be accurately predicted using simple geometrical arguments [41]. This approach is based on a previous analytical and simulation study where the authors find a simple numerical algorithm to estimate the random close packing fraction ϕ_{rcp} based on the size distribution of the hard sphere suspension [42]. A freeware based on the algorithm, `spherepack1d`, is available online [43], and it has been used to successfully estimate the maximum volume fraction ϕ_m of multiple hard-sphere suspensions [41].

Some studies have focused on the specific topic of the viscosity of mixtures [44]. This is a particularly relevant issue for the formulation of many industrial products, as they often are complex mixtures for which the fine tuning of the rheological properties is essential, and this is an outstanding problem for formulation in industry. A few complex models have been developed to predict the viscosity of suspensions of pluri-modal particles [45, 46]. When the components of the mixture have different viscosity behaviours, the viscosity models for describing them are even more complex [47].

Beyond hard spheres: the rheology of soft colloids

In this section, we have focused so far on the hard sphere model for colloidal particles. This model, although simple, describes accurately some colloidal systems, but it appears insufficient for some others. In some cases, the notion of the softness of the particle has to be introduced, and thus requires the adjustment of the rheological models.

From a theoretical point of view, particles, colloidal or not, can be described as soft if they have the ability to change size and shape at high concentration [3], as illustrated in Figure 2.5. Such a definition covers a striking variety of systems, including gel microparticles [48, 49], microgels [50–52], star polymers [53, 54], block co-polymer micelles [55] and even more complex particles, like fruit purees [56].

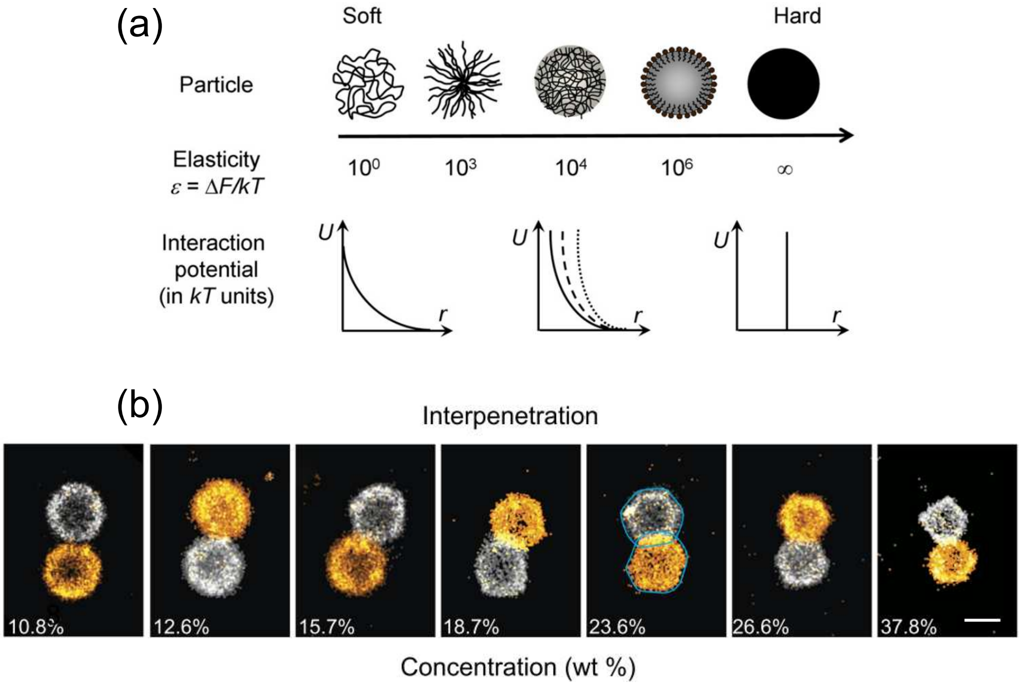
(a)
Soft
Hard
Particle
Elasticity
$\varepsilon = \Delta F/kT$
10^0
10^3
10^4
10^6
∞
Interaction potential (in kT units)
U
r
U
r
U
r
(b)
Interpenetration
10.8%
12.6%
15.7%
18.7%
23.6%
26.6%
37.8%
Concentration (wt %)

Figure 2.5 *Illustrations of soft particles (a) Cartoons of polymeric coil, star polymer, microgel, emulsion, and hard sphere. The arrow points to the direction of enhanced elasticity and transition from soft to hard repulsive pair interaction potential. Reproduced from Ref. [3].*
(b) Two-colour superresolution microscopy of densely packed microgels showing compression, deformation and partial interpenetration. Scale bar 500 nm. *Reproduced from Ref. [4].*

In the last two decades, these complex particles have attracted a lot of interest because of their rich rheological behaviours [3]. Indeed, the variety of soft particles leads to a wide range of phase diagrams, and, in particular, the glasses they form by jamming at high concentrations have been widely studied [52, 57, 58]. In addition, the softness of these particles may depend on many environmental parameters, including temperature [59], pH [51, 60], and ionic strength [61]. The ability of easily changing the properties of the soft particles makes it possible to fine-tune their rheology, which is of both theoretical and practical interest.

Because they can deform and deswell at high concentration [4, 62], one major challenge to modelling the behaviour of such soft particles is the availability of a well-defined volume fraction ϕ for the suspensions. Indeed, in contrast with hard spheres, the volume filled by soft particles is a function of their concentration so it cannot be calculated simply with experimental parameters. In addition, for nanometer-sized soft particles, this volume fraction also cannot be easily determined by imaging the suspension.

To overcome the challenge of defining the volume fraction of soft colloids, a common approach is to use an effective volume fraction ϕ_{eff} proportional to the concentration c, $\phi_{eff} = k_0 \times c$, where k_0 is a constant indicating the voluminosity of the soft particle of interest, usually determined in the dilute or semi-dilute regime. Such a definition for ϕ_{eff} does not take into account the deformation or shrinking of the particle at high concentrations, so high values of volume fraction ($\phi_{eff} > 1$) can be reached.

A range of tools are available to determine the voluminosity of particles in the dilute or semi-dilute regime. k_0 can thus be estimated using, for example, osmometry [63], light scattering [64] or viscosimetry [51, 53, 59, 65]. The latter approach is preferred in this study, and relies on the modelling of the relative zero-shear viscosity η_0/η_s behaviour of the pure suspensions in the semi-dilute regime using a hard sphere law, such as Equation 2.3. The underlying assumption is that the softness of the particles is negligible when they are sufficiently diluted, and so they behave in a very similar fashion to hard spheres.

At high concentration, however, this assumption is not valid since the soft particles may undergo significant compression, deformation and interpenetration, as shown in Figure 2.5 (b). The rheological models thus have to be adapted to describe the viscosity of soft colloidal suspensions, and this has been done for star polymers [66].

In addition to the high effective volume fraction ϕ_{eff} reached by the suspensions of soft colloidal particles, these systems also differ from the hard sphere model in their viscosity behaviour. Indeed, as can be seen in Figure 2.6, the divergence of the viscosity depends on the type of soft colloidal particles, and is not accurately represented by Equation 2.4 as the asymptote at high volume fraction is oblique rather than vertical.

2.2.2 Emulsions

Emulsions are yet another type of colloid, in which a liquid phase is dispersed into another liquid with which it is immiscible. In many respects, an emulsion

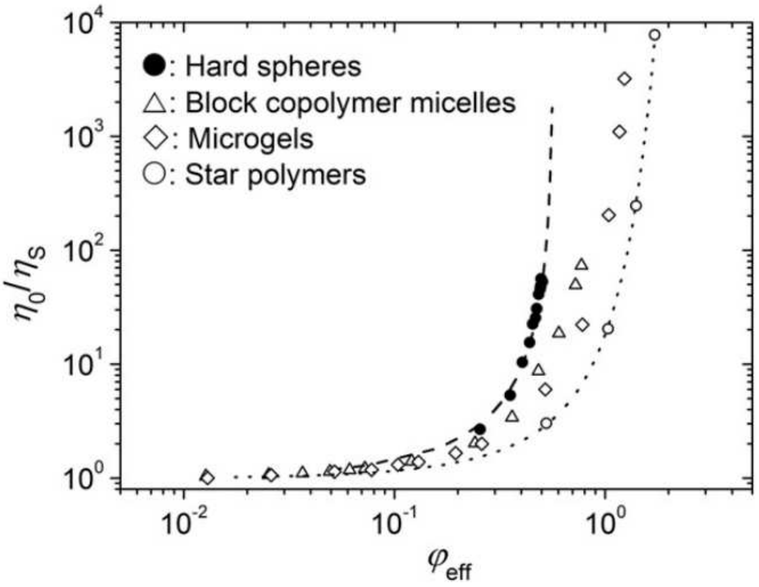

Figure 2.6 *Dependence of the zero-shear viscosity (normalized to the solvent viscosity) of various colloidal systems on the effective volume fraction. The dashed line is the best fit of hard sphere data to the Quemada model [5] (Equation 2.4). The low-shear viscosity data of star polymer data are well represented by a double exponential function (dotted line). Reproduced from Ref. [3].*

can also be seen as a suspension of droplets, and many of the notions presented in the previous section thus apply to their study, but the liquid nature of the particles and the presence of a liquid-liquid interface set them apart from the model of hard sphere suspensions [67].

One interesting aspect of emulsions is their formation, that is achieved by mixing the two phases. The equilibrium state of a system made of two immiscible liquids is two macroscopic layers with a plane interface to minimise the free energy, in that case the main contribution is the interfacial energy. Upon disruption of the two phases, *e.g.* by mechanical stirring, the interfacial area and consequently interfacial energy are minimised by the formation of spherical droplets [68].

However, this emulsion is not a stable state, and if the disruption is interrupted, it will quickly revert to its initial state through several instability processes [6], as presented in Figure 2.7. The use of surface-active species is thus required to reduce the interfacial energy and slow down the breaking of the emulsion in order to obtain a durable suspension of spherical droplets. Emulsions are thus only kinetically stable but, thanks to the advances in emulsion technology, the shelf-life of commercial emulsions can reach several years, if they are properly engineered.

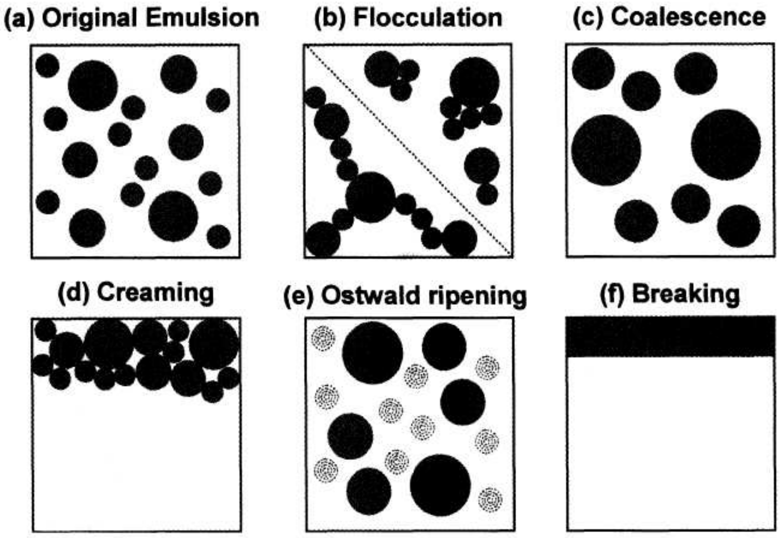

Figure 2.7 *Emulsion instability processes, reproduced from Ref. [6].*

In addition, the mechanical properties of the droplets depend on the protocol used to prepare the emulsion. Indeed, emulsion droplets have an internal pressure, called the *Laplace pressure* ΔP, arising from the interfacial tension between the two liquids γ and that can be expressed:

$$\Delta P = \gamma(1/R_1 + 1/R_2) \tag{2.8}$$

where R_1 and R_2 are the principal radii of curvature of the droplet, with $R_1 = R_2$ for spherical droplets. Thus the rigidity of the droplets arising from this pressure difference decreases with the droplet size, but increases with the interfacial tension, which depends on the nature of the two phases and of the surface-active component. Large droplets can thus be deformed by sufficiently high shear stresses, while small droplets may act similarly to solid particles, depending on their interfacial tension γ, during a rheological measurement.

Because many industrial products such as mayonnaise, shampoo, and ice cream involve emulsions either during their fabrication or as the final product, it is important to understand the rheological properties of these colloidal systems. The viscosity behaviour of emulsions has been studied as a function of several parameters. The polydispersity, and more specifically the presence of a fraction of small droplets was found to decrease the viscosity of an emulsion with respect to a monodisperse emulsion at the same volume fraction [69]. The droplet size was also shown to influence the shear thinning of concentrated droplet suspensions [70]. Finally, at even higher concentrations, it was observed that concentrated droplets form glasses that are very similar to those formed by soft particles, and where the rheology is governed by the properties of the thin film between the droplets [71].

Emulsions are thus similar to colloidal suspensions, but under certain circumstances the droplets behave as soft colloidal particles. In this thesis, this approach will be used, as it offers a convenient framework for the study of emulsions, and more specifically protein-stabilised emulsions.

2.2.3 Gels

Gels are a common example of soft materials, although there is an increasing interest in creating tougher gels [72, 73]. They differ from colloidal suspensions and emulsions by the presence of a characteristic microstructure. In fact, the IUPAC definition of a gel focuses on this aspect, by describing it as a *“Nonfluid colloidal network or polymer network that is expanded throughout its whole volume by a fluid”* [74]. This definition is however the structural description at a macroscopic scale of systems that can be very different both in composition and in mesostructure.

In general, materials are thought of as gels when they are formed by cross-linked macromolecular chains, either covalently or by physical bonds. However another way to form the continuous three dimensional network defining a gel is by slow aggregation of colloidal particles, to enable the formation of a space filling network [75].

A major difference between these two types of gels is the origin of their elasticity. Particle gels are enthalpic in the sense that any deformation of the material causes changes in interparticle interactions and elasticity arises from the consequent increase in enthalpy. This is fundamentally very different from the elasticity of polymer gels which results from a decrease in possible conformations for the chain and thus in entropy upon deformation. The mechanical properties of both types of gels are thus rather different: a typical colloidal gel is stiff and brittle, and breaks under a lower strain than a polymer gel (*i.e.* shorter linear viscoelastic region) [76]. Even for colloidal gels, a wide variety of structures and mechanical properties can be obtained depending on the range and stength of particle-particle interactions [77] and on the morphology of the particles [75].

Here, we will focus on colloidal gels formed in presence of a strong short-range attraction. In that case, the particles irreversibly stick to each other upon contact, and the gelation route is diffusion limited cluster aggregation, abbreviated *DLCA* [20].

Gelation of colloidal gels by diffusion-limited cluster aggregation (DLCA)

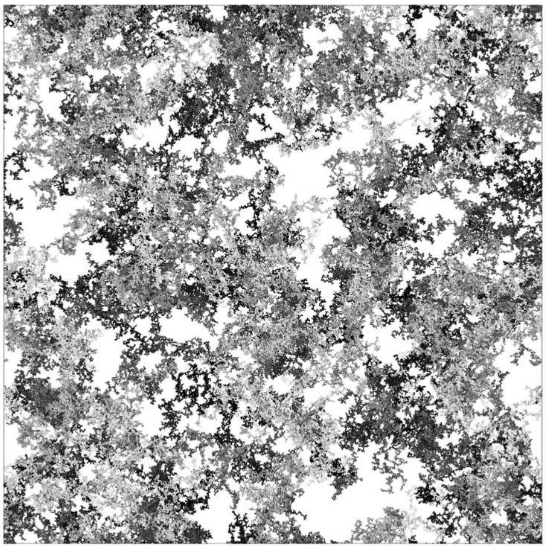

Figure 2.8 *Structure of a low-concentration DLCA gel obtained by computer simulation, reproduced from Ref. [7].*

During gelation, the attractive particles form fractal clusters, which means that over a certain range of length scales their structure is scale invariant. These clusters grow as the particles diffuse, until they occupy all the space and the particles are trapped in a continuous network. An example of fractal structure obtained by DLCA is shown in Figure 2.8.

Based on this mechanism, a theoretical description of fractal particle gels can be developed [76, 78, 79]. To quantify the density of the structure of these gels, an important parameter is the fractal dimension D_f of the clusters. The fractal dimension links the number of particles N_d, each of a radius a, in an aggregate with the average radius of the aggregate R:

$$N_d \sim (R/a)^{D_f} \tag{2.9}$$

The fractal dimension D_f thus scales the volume fraction of particles in a floc ϕ_a, compared to the close packing of particles:

$$\phi_a \sim (R/a)^{D_f - 3} \tag{2.10}$$

In the case of particle gels, D_f has a predicted value around 2, with small variations depending on the stickiness of the particles and the reversibility of flocculation [78]. Indeed, clusters are denser, *i.e.* D_f is higher, when the particles have a lower probability of forming a bond upon contact.

Furthermore, as aggregation increases, the gelation of a particle suspension can be described as the progressive growth of some flocs until they occupy all the space available. This means that gelation occurs when the flocs reach a volume fraction ϕ_a equal to the volume fraction of particles in the system ϕ [78]. Combined with Equation 2.10, this gives a critical radius of flocs for gelation R_c (although in practice these radii are rather ill-defined):

$$R_c = a\phi^{1/(D_f - 3)} \tag{2.11}$$

This expression emphasises the importance of the concentration of particles, and allows the calculation of the fractal dimension of gels from microscopic observation. The experimental values thus obtained are in general somewhat higher than the theoretical prediction, around 2.3. The size of pores can also be measured on micrographs to roughly quantify how coarse the structure is [10]. The structure of a gel is an important aspect to determine and describe as it will drive its permeability and mechanical properties [76].

Rheology of colloidal gels

Oscillatory rheology can be used to study the gelation and the mechanical properties of the gels [22]. Indeed, by applying small-amplitudes (*i.e.* in the linear regime of strain) oscillations, one can probe the structure without disrupting it.

The application of this technique to measure the progressive development of moduli during gelation is illustrated in Figure 2.9. The transition liquid (sol) - solid (gel) is often described by the gel point, at which the elastic component G' overtakes the viscous component G''.

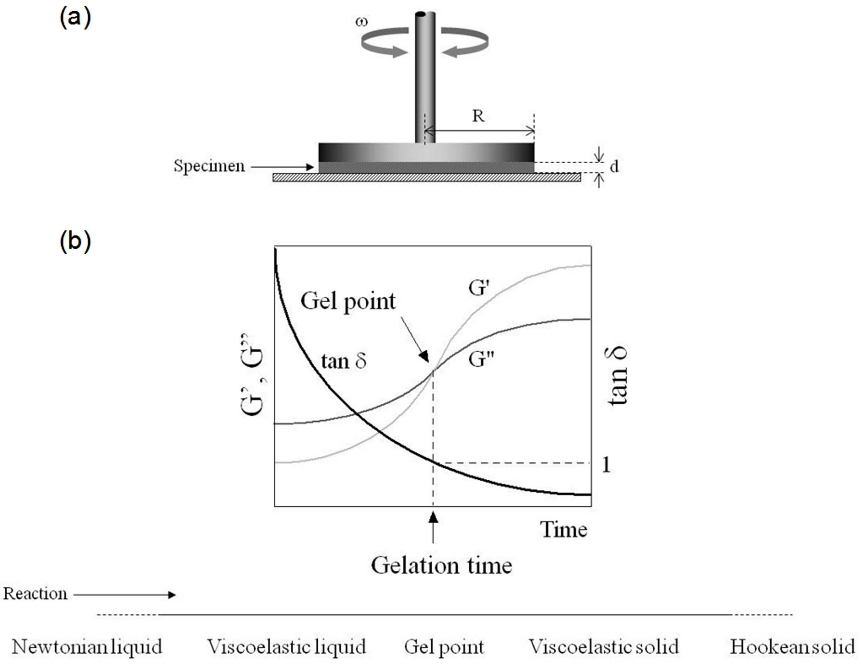
(a)
ω
R
Specimen
d
(b)
Gel point
G'
tan δ
G"
G', G"
tan δ
1
Time
Gelation time
Reaction
Newtonian liquid
Viscoelastic liquid
Gel point
Viscoelastic solid
Hookean solid

Figure 2.9 *Principle of small-deformation oscillatory rheology (a) and typical dynamical viscoelastic properties upon gelation (b): storage modulus G', loss modulus G'', and loss tangent tan δ. Reproduced from Ref. [8].*

The storage modulus can be related to the fractal dimension D_f by considering the number of particles N making up the stress-bearing "backbone" in one cluster of size R_c. This number scales as $N \sim R_c^{D_b}$, where D_b is defined as the bond dimension and $D_b \simeq 1.1$ for DLCA gels [20]. By using this to calculate the bending force constant, it is found that the storage modulus G' of a DLCA gel scales as:

$$G' \sim \phi^{\frac{3+D_b}{3-D_f}} \tag{2.12}$$

The storage modulus of a DLCA gel thus varies with the volume fraction ϕ of particles following a power law of exponent $(3 + D_b) \,/\, (3 - D_f)$. This behaviour has been experimentally observed for colloidal gels [80].

Notably, 3D numerical simulation is a very suitable approach to study colloidal gels as these systems are made of a large number of particles with tailored interparticle interactions. Simulation makes it possible to reproduce the structure of real particle gels, and once a simulated gel has been generated, properties like shear modulus can be calculated and compared with experiments [81, 82]. In this field, theory, experiments and simulation go together remarkably well and provide a coherent insight into particle gels [77, 83].

An example of a computational rheology study of colloidal gels is a recent work on the yielding of model gels. It was found that at low concentration, the gels present strain stiffening, *i.e.* their elasticity increases upon high shear [84]. Using simulations of the topology of the gel networks , it was found that this behaviour could be related to stretching and reorientation of the gel branches. It is thus very dependent on the structure of the network, and hence on the volume fraction of the gel. The sparser the gel, the more structural heterogeneities make possible the redistribution of the stress before failure of the material, while denser gels are more homogeneous and thus lead to a quicker breaking of bonds in the absence of reorganisation of the network.

2.2.4 Emulsion Gels

Because emulsions are suspensions of droplets, one can imagine that colloidal gels can also be built using oil droplets instead of solid particles. This type of gel would thus be obtained upon destabilisation of an emulsion, either by reducing the inter-droplets repulsive interactions, or by adding non-adsorbed polymers or small colloids, in which case the mechanism is called depletion flocculation [85] and will not be discussed here.

The viscoelastic soft solid obtained from the gelation of an emulsion is called an emulsion gel. However, this convenient name designates several structures, each with their specific properties. In Reference [9], the author makes a useful distinction between the particle-stabilised emulsion gels, and the emulsion-filled particle gel, as illustrated in Figure 2.10. The structural difference between the two materials is the nature of the primary structural units.

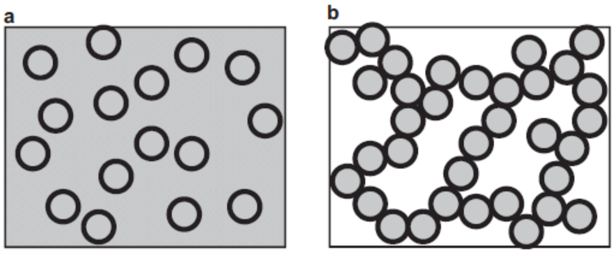

Figure 2.10 *Schematic structures of (a) an emulsion-filled particle gel, (b) a particle-stabilised emulsion gel. Reproduced from Ref. [9].*

First, for the particle-stabilised emulsion gel in Figure 2.10 (b), the individual oil droplets together with their stabilising coating are seen as particles, which become sticky upon destabilisation. The main differences with the colloidal gels described in the previous section are that, in an emulsion gel, the interface of the constitutive particles may flow, and the particles can be deformable as their elasticity arises both from Laplace pressure in the droplet and from the rigidity of the adsorbed layer [9]. This may be similar to a situation where soft particles, such as star polymers or microgels, are used to form gels.

On the other hand, the emulsion-filled particle gel shown in Figure 2.10 (a) can be studied using a polymer engineering approach, where the oil droplets act as fillers in a rubbery matrix. From a fundamental point of view, a filled gel is of interest as it combines both interfacial and bulk behaviour of the constitutive elements. The reinforcement of rubbers by particles has been widely studied and the basic principles it relies on can be a good starting point for describing the rheology of emulsion-filled particle gels. If the oil droplets are considered to be perfectly rigid, and uniformly dispersed in an incompressible matrix with a shear modulus of G_m, then the overall shear modulus G can be written [86]:

$$G/G_m = 1 + \frac{2.5\phi}{(1 - 2\phi)} \tag{2.13}$$

This simple model however needs to be refined as the assumptions are too restrictive to describe correctly deformable fillers like oil droplets which may flocculate and consequently be dispersed in a very inhomogeneous way [9].

Another very important parameter for the emulsion-filled particle gel is the chemical interaction between the filler (*i.e.* the droplets) and the matrix. Indeed, a distinction has to be made between droplets which can interact with the matrix, called *active*, *reactive* or *bound* fillers; and non-interacting particles, also called *inactive* or *unbound*. Active fillers bind to the network and thus contribute to its strength: the storage modulus of the filled gel increases with the increase of volume fraction of active filler. On the other hand, passive fillers are a disruption to the network, and as such weaken the gel [16, 87]. This is illustrated in Figure 2.11.

It is worth noting that real systems lie in between these two extremes [9], and an extensive exploration of the role of the matrix in a gel, from a system with 0% unadsorbed particles (emulsion particle gel) to one with 100% unadsorbed particles (particle gel) has not been carried out yet.

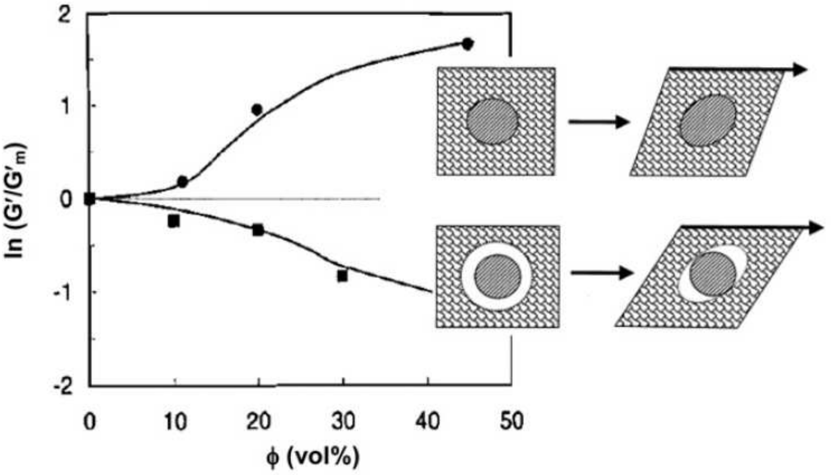

Figure 2.11 *Effects of active (circles) and inactive fillers (squares) on the storage modulus. The logarithm of G'/G'_m where G'_m is the modulus of the gel matrix is plotted against the oil volume fraction ϕ. Reproduced from Ref. [9].*

2.3 Structure and functional properties of proteins

2.3.1 Structure of proteins

Proteins are biological macromolecules that perform a broad variety of functions in cells. Their building blocks, also called *residues*, are amino acids, which contain an amine, a carboxylic acid group and a different side chain for each of the 20 amino acid. These residues are linked together with peptide bonds that have a covalent character. As the amino acids contain both anionic and cationic groups, the proteins present a charge highly dependent on the pH, which reaches zero at the so-called *isoelectric point* pI. The amino acids are also more or less hydrophilic depending on their side chain, and this gives the amphiphilic character of the proteins [88].

The sequence of amino acids determines the primary structure of the protein, but a structure exists at three other possible levels. Depending on the sequence, repetitive local patterns can also be formed by hydrogen bonding, called *secondary structures*. They are typically α-helix, β-sheets and turns [89]. These structures then combine together to reach a conformation minimising the free energy of the protein: this is the tertiary structure in which the hydrophobic parts are buried inside the molecule [90]. A protein with a tertiary structure is also called *folded*. In some cases, several subunits can assemble together in a quaternary structure, it is the case for *e.g.* of haemoglobin.

The stability of the tertiary structure is very important for the biological functionality of the protein but it can be challenged by different conditions of temperature, pH and ionic strength. An increase in the temperature causes the weakening of stabilising ionic and hydrogen bonding, while the pH sets the charge of the protein and thus the electrostatic interactions, and finally an increasing ionic strength which diminishes the electrical double layer and consequently the electrostatic interactions [91]. The loss of structure is called denaturation or unfolding, and is in theory reversible under proper conditions [89] and for relatively small proteins or domains. Indeed, proteins are known to be dynamic and to oscillate between several conformations. In practice however, an irreversibility of unfolding is often observed.

Depending on the situation, a protein can physically be described in soft condensed matter either as a polyelctrolyte (random-coil proteins), as a charged colloidal sphere (globular protein), or as an intermediate form (*e.g.* molten globular state) [92].

Besides their crucial functions in most biological mechanisms, proteins are a key ingredient in food products, not only for their nutritional value but also for their outstanding ability to stabilise emulsions and form gels.

2.3.2 Proteins as emulsifiers

Proteins can be good emulsifiers [93], but only if they fulfil several conditions:

1. Water-solubility: occurs when the electrostatic repulsive forces are higher than the hydrophobic attractive interactions. Consequently, proteins are in general insoluble around their isoelectric pH [91].

2. Flexible backbone, dependent on the primary structure of a protein. It is necessary so the protein can unfold and presents its hydrophobic parts to the oil phase, which is entropically favourable.

3. Sufficient *surface* hydrophobicity, which can be rather different from molecular hydrophobicity determined by the nature of residues. The

amphiphilic character of the protein is implied by the first point.

The ability of a protein to stabilise an emulsion is linked to its molecular size [88]: smaller proteins diffuse faster so they are quicker to adsorb at interfaces during emulsification, while larger molecules will be better anchored. The protein's conformation and so the availability of its hydrophobic parts also plays a role in the kinetics and thermodynamics of adsorption.

After adsorption, proteins stabilise an oil droplet by both steric and electrostatic repulsion. The molecular size is therefore important here as large proteins will make a thick stabilising layer. This mechanism of stabilisation also takes advantage of the fact that a high surface charge in a continuous phase of low ionic strength is an asset for a protein used as emulsifier [21].

In terms of adsorbed interfacial layer, protein-stabilised emulsions are more complex than classical surfactant-stabilised emulsions [94]. First, proteins may unfold and change their conformation upon adsorption [95] , and the structure of the layer they form and the adsorption strength is very dependent on the nature and the structure of the protein [96]. It is also possible for some proteins to adsorb as multilayer structures [97], with irreversible bonding of the first layer and a reversible bonding of the other layers. In addition, the composition of the interfacial layer can be heterogeneous [93, 98], either with respect to the nature of the proteins when several sorts of proteins are present, as often happens with commercial proteins; or with respect to the conformational states of one protein [94].

Despite this complexity of the adsorbed layer of proteins, it is generally agreed that the adsorption can be considered as irreversible, as the desorption of proteins is negligible upon dilution [94]. Indeed, proteins have a greater adsorption energy than low molecular weight surfactants because they adsorb with several segments of their structure. At sufficient concentration a saturated monolayer can thus be reached at the oil-water interface [99].

Finally, regarding the rheology of concentrated emulsions, it has been shown that, at a given droplet size, protein-stabilised emulsions exhibit a much higher bulk elastic modulus than surfactant-stabilised emulsions, as well as higher moduli in interfacial shear rheology. Both parameters may be related, and it has been hypothesised that this discrepancy in mechanical properties may be due to the attractive short-range interaction in protein systems, as compared to the repulsive interaction in the case of surfactants [100].

2.3.3 Proteins as gelling agents

Upon destabilisation, a protein unfolds, its hydrophobic domains are no longer buried inside its structure and so they are available for intermolecular association. The unfolding is followed by the association or aggregation of proteins. Under suitable conditions, a continuous 3D network is formed and a protein hydrogel is obtained.

Gelation of proteins

As for the emulsification properties, the structure of proteins plays an important role in gelation: not only does the protein need to be somehow “sticky” under certain conditions, but it also helps if it is flexible enough for a facile unfolding [22]. The interactions that enable the proteins to attract each other are a complex combination that have not been fully elucidated yet, although some models have been developed that make possible the estimation of the interparticle potential [92]. For many proteins, the knowledge of the interactions at play during gelation is thus still mostly empirical.

Several stimuli can be used to destabilise the folded proteins and their nature is important to the final properties of the gel. First, heat can induce the unfolding of some proteins and the resulting aggregation, for *e.g.* of whey proteins or of egg-yolk proteins. The increase of temperature enhances hydrophobic bonding interactions but breaks hydrogen bonds, while the surface charge of the protein remains essentially the same. A similar gelation process is the so-called *cold-gelation*, where the increase of temperature is only used to irreversibly unfold the protein followed by cooling, and the gelation then occurs upon addition of salt. Another very common technique is acid-induced gelation. In contrast to heat-set gelation, the change is in the overall charge density, modifying the balance between electrostatic repulsion and van der Waals attraction. The most common proteins used for these gels are caseins, and a well known application of casein gelation is the production of yoghurt. Finally, the application of a high pressure can also lead to the unfolding of proteins and subsequent gelation, although the pressure-sensitivity of different protein types varies widely [92].

Properties of protein gels

Van Vliet showed that protein gels can be described as fractal systems [78]. The colloidal particles acting as building blocks may be the primary proteins or, more usually, larger elements. This is due to rolling and rearrangements between fractal clusters that occurs until all the building blocks are sufficiently bonded to each other. These temperature-dependent rearrangements lead to a change of structures from a fine stranded to a coarser gel. This can have various consequences for the properties of the gel, such as a lower fracture strain and an *a priori* lower modulus.

In the case of the emulsion-filled gels described in Figure 2.11, the fact that proteins are used makes the filler effect less straightforward. Indeed, it was shown that proteins may adsorb on filler particles (*i.e.* oil droplets), and thus not be available for bulk-phase gelation. The main difference with a particle system is that the proteins can still adsorb after the emulsification to form multilayers. Thus, at a sufficiently low concentration of protein (*ie* for a sufficiently weak gel) and of filler, a decrease in gel strength is observed upon addition of fillers [101]. This is an opposite effect to the usual reinforcing of the gel by active fillers.

2.4 An example protein: sodium caseinate

This study focuses on a specific protein used both as emulsifier and as gelling agent. For its wide use in industry and its availability, sodium caseinate was chosen, which is derived from the caseins in milk. Caseins are the most common proteins in cow's milk. They have attracted a lot of attention for the last 40 years, mainly because of their widespread use as food ingredients in numerous commercial products (processed cheese, ice-cream, coffee whiteners, cream liqueur, etc). Here, their structure is described briefly and the current state of the art concerning the emulsifying and gelling properties of sodium caseinate is presented.

2.4.1 Nature and structure of sodium caseinate

It is interesting to consider the structure of caseins as it plays an important part in their functionality. There are four major native proteins forming the caseins,

α_{s1}- , α_{s2}- , β- and κ-casein. They are all present in a single native casein micelle with a mass ratio of roughly 4:1:4:1. They have been sequenced and their primary structure reveals that there are relatively hydrophobic and contain largely separate domains for their hydrophobic and hydrophilic clusters. They show little or no secondary and tertiary structure, so caseins are traditionally seen as random coils [102], although some authors consider that the presence of some secondary structure fits better with a molten globular state, a sort of intermediate state between folded and unfolded [103].

Much has been written for more than three decades about the exact structure of the casein micelles, but it is still a subject under discussion [104, 105]. There is agreement on the fact that it is a self-assembled structure of around 100 nm containing a certain amount of calcium phosphate. However, there is still a controversy on a model that could describe accurately the structure of the micelle: early models describe casein as an ensemble of colloidal submicelles glued together with calcium phosphate clusters, but it has been criticised and several others have been suggested. De Kruif & Holt consider the micelle as a sort of microgel particle formed of unfolded casein chains cross-linked by calcium phosphate nanoclusters [106]. Horne proposes that caseins are more like block-copolymers that self-assemble together, with internal gel-like structure [107]. To sum up, an individual casein micelle is made of self-assembled sub-units. A sub-unit has a diameter estimated at $\approx 20\,\mathrm{nm}$, and there is no agreement as to whether is best described as a polyectrolyte [92], a colloidal particle (globular), or as a molten globule [103]. In any case, the structure formed is swollen by water and hence casein has a high voluminosity, of around $10\,\mathrm{mL} \cdot \mathrm{mg}^{-1}$, which is pH- and ionic strength- dependent [65].

Sodium caseinate is produced by reducing the pH of skimmed milk while heating, to precipitate the caseins and dissolve the calcium. The precipitated caseins are separated by filtration and washed to remove remaining calcium. The caseins are then redissolved by neutralising with sodium hydroxide, and dried by roll- or spray-drying. Other types of caseinates can be produced by varying the alkali used during production. In the case of sodium caseinate, the protein is negatively charged, increasing its solubility in water, with sodium acting as counter-ion. Significant variations of properties between sodium caseinates were found [108] depending on the manufacturing process and even between batches.

The structure of sodium caseinate itself in water is not straightforward as several studies hint at its self-assembly. Indeed, it has been established that sodium caseinate is not present as monomers in suspension, but rather in naturally-occurring small aggregates [109]. These aggregates seem to present a non-spherical conformation [63, 105, 109]. There is no consensus on their detailed structure, as some studies mention linear macromolecules [63] while others see more similarity to star-like polymers [110]. These varied hypotheses may arise from the fact that the association was demonstrated to be highly dependent on protein concentration, pH and ionic strength [110–112]. In any case, it is generally admitted that the naturally-occurring caseinate aggregates are elongated and their diameter is estimated to be around 20 nm [63, 105, 109]. Some larger aggregates can also form in the presence of residual traces of calcium or oil from the original milk, however these only represent a small fraction of the protein [108].

This overview of the structure of sodium caseinate in water shows that the study of its emulsification and gelation properties has to be carried out with great caution. Despite the necessary use of physical models to describe the emulsions and gels formed by sodium caseinate, the underlying complexity of the system needs to be kept in mind.

2.4.2 Sodium caseinate-stabilised emulsions

Sodium caseinate at interfaces

The two main components of sodium caseinate, namely α_{s1}- and β-caseins, demonstrate flexible enough backbones and sufficient hydrophobicity to be, in theory, good emulsifiers. In the form of sodium caseinate they also have an improved solubility in water [93]. In practice, they are indeed excellent at stabilising emulsions [96, 113, 114]. It was shown that for caseins a saturated monolayer can be reached at the oil-water interface [99] at low protein concentration, *i.e.* around $1 \times 10^{-3}\%$(wt) [115].

Because of the differences in structures of these two caseins, there is competitive adsorption at the interface and hence the film composition varies with time [93]. This dynamic nature of casein adsorption is due to the progressive unfolding of the proteins and the burying of the hydrophobic domains at the interface [116]. In practice, both proteins will be considered to be adsorbed in varying proportions, and that their stabilisation performance is not affected by the ageing of the emulsion.

The structure of an adsorbed layer of caseinate is very likely to be a multilayer at high enough concentration, as described previously [117]. An interesting insight on the structure of the interfacial layer was provided by studying thin films containing caseinate: a stepwise decrease of thickness was observed as the liquid was gradually removed, which can be explained by a layered submicellar structure inside the film [97].

Influence of adsorbed and un-adsorbed caseinate on the stability of the emulsion

A critical parameter when making emulsions is the amount of emulsifier that has to be added for a good stabilisation. It was shown indeed that if not enough proteins are present during emulsification, the stability of the emulsion is compromised by irreversible bridging flocculation, as the interface is not saturated [85, 118].

On the other hand, when the emulsion is produced with the right proportion of emulsifier with respect to the dispersed phase, a stable emulsion can be obtained. In that case, sodium caseinate-stabilised droplets present a high interfacial shear elasticity, so they can be seen as droplets coated by a solid shell [119]. This case is ideal for the stability of the emulsion, but there is no agreement on the ratio of caseinate required, as the surface coverage depends on many parameters [117].

Finally, the stability of the emulsion is reduced by creaming if an excess of protein is used. Indeed, in that case, there is a significant amount of un-adsorbed caseinate in the continuous phase, and depletion flocculation occurs between the droplets [85, 113, 118].

2.4.3 Sodium caseinate gels

Formation of caseinate gels

Sodium caseinate is charged negatively at neutral pH, and electrostatic repulsion is an important condition for the stability of both sodium caseinate naturally occurring aggregates and sodium caseinate-stabilised droplets [23]. However, as the suspending medium is acidified, the charge at the surface of the protein decreases, and at the isoelectric point the average surface charge reaches zero. The decrease in repulsion leads to the association or aggregation of the proteins. Despite being well-known, this phenomenon is not completely elucidated as the combination of attractive interactions in play is complex in these biological systems [92].

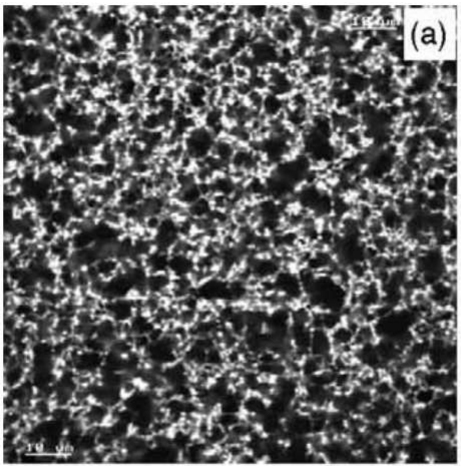

Figure 2.12 *Microstructure of an acid-induced sodium caseinate gel after* 140 min *from the start of the acidification. The image is* 100 µm *across. Reproduced from Ref. [10].*

Furthermore, if the acidification is slow and rather homogeneous, the aggregation of sodium caseinate can lead to the formation of a space-filling gel [22], as illustrated in Figure 2.12. The kinetics of the gelation, as well as the final gel properties, depend on extrinsic factors[22] such as final pH [120], volume fraction [121], ionic strength [111] or incubation temperature [122].

Properties of caseinate gels

Caseinate gels are relatively well-known and several studies have been carried out to understand their rheology [120, 122–124], microrheology [125], and microstructure [10], along with the effect of several molecules often found in the commercial casein gels [23].

In particular, the final pH was identified as an important parameter for the properties of acid-induced gels. A maximum in the gel moduli was found for a pH between 4 and 5, which corresponds to the isoelectric point of caseins (pH ≈ 4.6). Above this range, the decrease in electrostatic interactions is not sufficient to form a strong gel, while below it, the medium is over-acidified and the proteins become charged positively, so the electrostatic interactions weaken the gel [120], as can be seen in Figure 2.13 (C). This weakening is believed to be related to the release of free caseinate particles in the solvent below the isoelectric point [11], as illustrated in Figure 2.13 (B). The microstructure of the gel is also affected by the final pH and the kinetics of gelation, as illustrated by the decrease in pore size at lower pH in Figure 2.13 (D).

Furthermore, the acidification rate is also critical for the gel. Indeed, it was observed that the steady-state mechanical properties are deeply affected by a quick decrease in pH. A fast acidification produces a gel with a lower fracturing stress and lower compressive Young's modulus compared to gels formed with a slower process. The capacity to retain water is also affected and is lower at higher acidification rate [126].

In addition, the key rheological features of the caseinate gels have been determined. Similarly to colloidal gels, caseinate gels present a power-law dependence of the viscoelasticity with the volume fraction [79, 121], that can be attributed to their fractal nature, as demonstrated by imaging of their microstructure [78, 120]. In addition, the frequency dependence of the gels was also found to be satisfyingly fitted by a power-law [79, 120, 127] . Finally, the gels that undergo high shear display an irreversible and brittle fracture, which has also been studied from a fundamental perspective [124, 128].

Finally, fractal gels can also be formed by acidifying sodium-caseinate stabilised emulsions [120, 129]. For these emulsion gels, the nature of the interactions at play during gelation is the same as for caseinate gels, as the droplets become attractive at the isoelectric point of the protein. Because caseinate assemblies and caseinate-stabilised droplets differ by their nature, structure and size, it is interesting to investigate the similarities and differences between caseinate gels and caseinate-stabilised emulsion gels. Although a preliminary study drawing this comparison has been performed [120], a thorough investigation is still lacking.

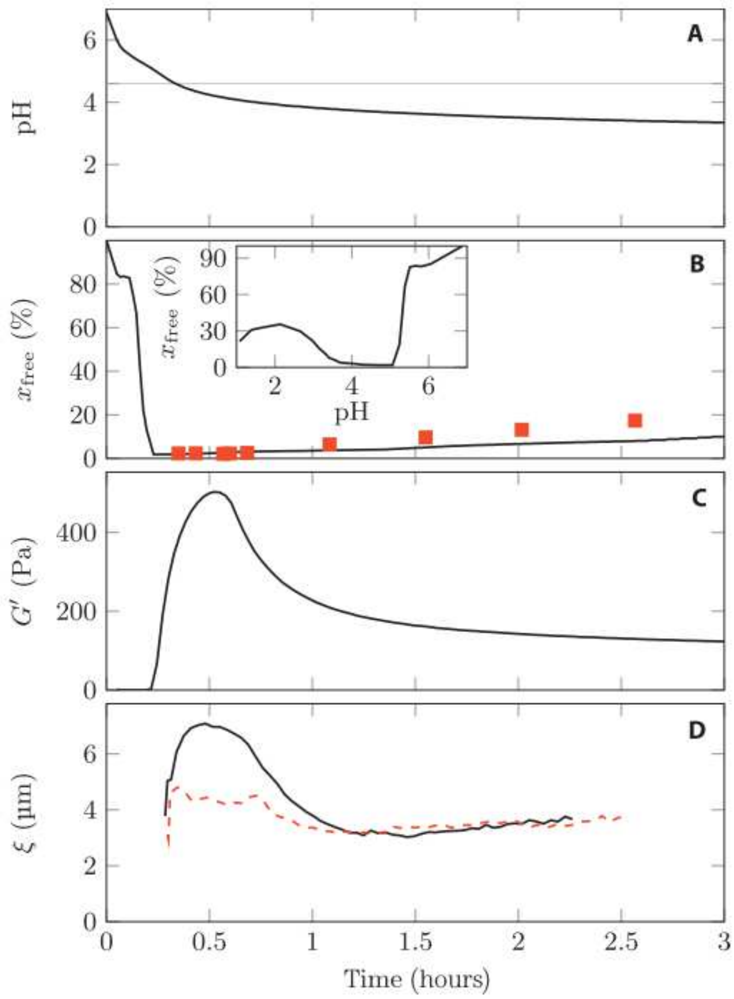

Figure 2.13 *Evolution of properties of an acid-induced caseinate gel with a slow acidification: (A) pH decreases over time. The horizontal line indicates the isoelectric pH of caseins. (B) Corresponding evolution of the fraction of free caseins* x_{free}*. (C) Evolution of the elastic modulus* G'*. (D) Evolution of pore size* ξ *measured by confocal microscopy. Reproduced from Ref. [11].*

Chapter 3

Preparation of the protein and emulsion samples

In this chapter, I describe the materials and the preparation protocols used to make the samples that are investigated in this study. I also give the technical details of the methods employed for this purpose. The characterisation techniques however will be presented in the chapters where the corresponding results are given.

3.1 Materials

3.1.1 Protein: Sodium caseinate

Because of its excellent ability to stabilise emulsions, sodium caseinate (Excellion S grade, spray-dried, graciously provided by DMV, Friesland Campina, Netherlands), a modified milk protein, was used in this study of protein-stabilised emulsions.

The properties of sodium caseinate vary between manufacturers, and even from batch to batch of the same manufacturer [109]. To prevent any reproducibility issues, all the sodium caseinate used for the experiments of this thesis came from the same batch of protein stored as a powder in airtight containers at room temperature.

Table 3.1 *Composition of the batch of sodium caseinate used in this study. The chemical analysis was performed by the manufacturer (Friesland Campina).*

Characteristic	Concentration in %(wt)
Protein	90
Moisture	5.5
Calcium	1.0
Sodium	1.4
Fat droplets and impurities	2.1

The composition for the sodium caseinate used here is shown in Table 3.1, as given by the analysis certificate provided by the manufacturer. In addition to the protein, moisture and mineral content, there are some residual fat droplets from milk, as well as some other organic and inorganic impurities, which were not quantified in the analysis certificate.

Although sodium caseinate is widely used in the literature, by itself or as an emulsifier, there are important variations in the way it is prepared [10, 98, 104, 117, 118, 120, 127]. The protocol developed to prepare and purify sodium caseinate in this study is described in the following section.

3.1.2 Oils: Glyceryl-tri-octanoate and tetradecane

When dealing with emulsions, it is important to select an oil that corresponds to the experimental requirements. Indeed, there are large variations of composition and physical chemical properties between linear alkanes, of very simple chemical structure, and vegetable oils, of complex chemical composition.

To make the study of protein-stabilised emulsions relevant to the food industry, it is sensible to use a triglyceride close to the commercial ingredients. However, food-grade vegetable oils often contain low amounts of mono- and diglycerides. These molecules are surface-active and are thus in competition with sodium caseinate to adsorb at the oil/water interface [130]. To prevent this effect, the use of a pure triglyceride gives a good compromise between a model and a real-life system.

In all the protein-stabilised emulsions studied in Chapters 4, 5, 6, 7 and 8, glyceryl trioctanoate (also called tricaprylin, Sigma Aldrich, $\geq 99\,\%$, written GTO in the following) was used. Its structure is presented in Figure 3.1. GTO is liquid at room temperature, and is saturated and therefore chemically stable. One of the advantages of GTO is its relatively high density, that allows for a slow creaming of the emulsion. Indeed, its density is $\rho_{GTO} = 0.956\,\mathrm{g} \cdot \mathrm{mL}^{-1}$ at 20 °C [131].

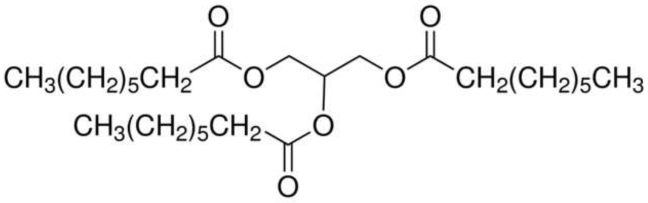

Figure 3.1 *Chemical structure of glyceryl trioctanoate.*

3.1.3 Gelation agent: Glucono-delta lactone

In Chapters 6 and 7, gels of protein and protein-stabilised emulsions are made by decreasing the pH. The slow decrease in pH is performed by using glucono-δ lactone (Roquette), the structure of which is shown in Figure 3.2.

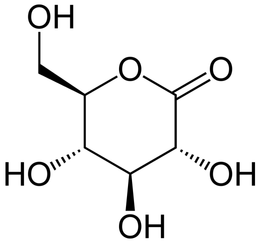

Figure 3.2 *Chemical structure of glucono-δ lactone.*

Glucono-δ lactone is a cyclic ester of D-gluconic acid that is widely used in the food industry, for example for manufacturing cheese or tofu. Its use as a gelling agent is detailed at a later stage in this chapter.

3.2 Preparation of the protein samples

Sodium caseinate was suspended in deionised water at $5 - 9\%$ (wt), by mixing thoroughly with a magnetic stirrer for 16 h at room temperature. The resulting suspension was hazy as shown in Figure 3.3 (a).

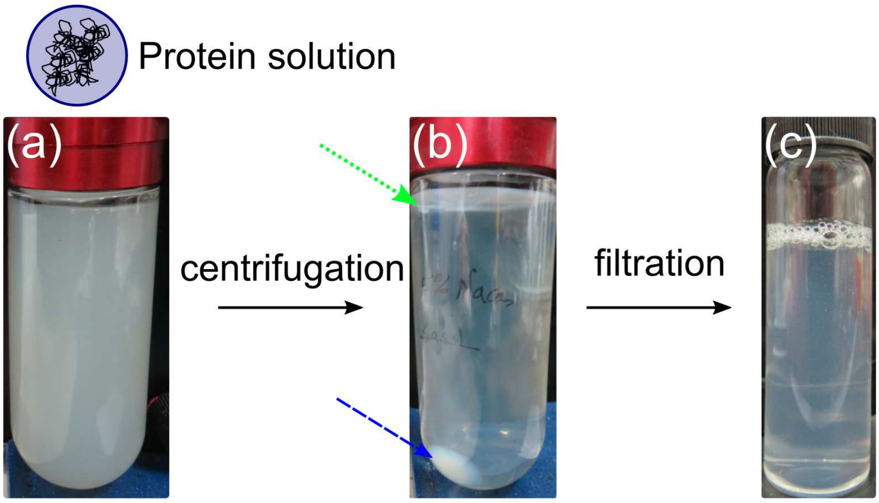

Figure 3.3 *Several stages of the preparation of a sodium caseinate solution. (a) After dispersion of the protein powder; (b) after centrifugation at* 40 000 × g *for* 4 h*, the impurities are separated from the solution: fat globules on the top (dotted green arrow) and unidentified sediment at the bottom (dashed blue arrow); (c) after filtration through a* 0.45 µm *membrane.*

To remove the impurities, a cleaning step was required in the preparation of the protein suspensions. Separation by centrifugation and by filtration were the two main techniques used to purify the suspensions. Several protocols involving different centrifugation speeds and time lengths, as well as different membranes, were tested and assessed, as detailed in Chapter 4. The protocol described below is the one that offered the best compromise between elimination of large protein aggregates/ impurities and loss of proteins.

The turbid suspension obtained after complete dispersion was first centrifuged at 40 000×g (Evolution RC, Sorvall with rotor SA 600, Sorvall and clear 50 mL tubes, Beckmann) for 4 h at 21 °C. Subsequently, the supernatant, made of residual fat contamination, and the sediment were separated from the suspension, that was now clearer, as can be seen in Figure 3.3 (b). The solution was then filtered using a 50 mL stirred ultra-filtration cell (Micon, Millipore) with a 0.45 µm membrane (Sartolon Polyamid, Sartorius). A clear protein solution was thus obtained, as can be seen in Figure 3.3 (c). In order to avoid spoilage of the protein solution 0.05% of the biocide ProClin 50 (Sigma Aldrich), a commercial 2-Methyl-4-isothiazolin-3-one solution, was added. The pH and size distribution of the protein sample were measured before and after the addition of ProClin to ensure that no major changes occurred to the protein. As will be seen in Chapter 4, this purified protein suspension is at the concentration of 45 mg · mL^{-1} because of protein loss.

Protein suspensions at a wide range of concentrations were then prepared from the stock suspension at 45 mg · mL^{-1}, made following the previous protocol. This stock suspension was thus either diluted, by adding deionised water, or concentrated, using a rotative evaporator (Rotavapor R-210, Buchi), to the suitable concentration. Mild conditions were used for the evaporation of the excess water to avoid changing the structure of the proteins: the water bath was set at 40 °C and a vacuum of 45 mbar was used. The concentration of all the suspensions after purification was estimated by refractometry, using a refractometer RM 50 (Mettler Toledo), LED at 589.3 nm and a refractive index increment of $dn/dc = (0.1888 \pm 0.0033)\,\mathrm{mL \cdot g^{-1}}$ [132] (*cf* page 59 for more details).

Size analysis by Flow Field Fractionation (graciously performed by PostNova Analytics Ltd) showed that the resulting suspensions of sodium caseinate were made of small aggregates of a hydrodynamic radius of 11 nm at 96 %, while the remaining 4 % form larger aggregates with a wide range of sizes (hydrodynamic radii from 40 nm to 120 nm). More details and further characterisation of the sodium caseinate suspensions are provided in Chapter 4.

3.3 Preparation of the protein-stabilised droplets

The protein-stabilised droplets were prepared by emulsifying glyceryl trioctanoate in the protein suspension described previously. A wide range of techniques are available to make emulsions, and two were selected to prepare the emulsions of interest. In this section, the techniques are first detailed, and then the preparation protocol for the emulsions used here is presented.

3.3.1 Emulsification techniques

Emulsification relies on the breaking down of droplets of a liquid into smaller droplets, while dispersed in a phase with which the liquid is immiscible. The presence of a surface-active component is critical to decrease the surface tension, both to make emulsification easier and to stabilise the droplets formed. In this study, proteins were used to stabilise the emulsions of interests. Several techniques are suitable for this process, and below are described the ones used to prepare the samples for this study.

Rotor stator

A commonly-used type of emulsifier is the rotor-stator. In this study, a Silverson L4R is used to coarsely emulsify the oil in the protein suspensions. The apparatus is illustrated in Figure 3.4. This bench top model is adapted to prepare samples of around 150 mL to 600 mL. The shear rate can be adjusted using the control box.

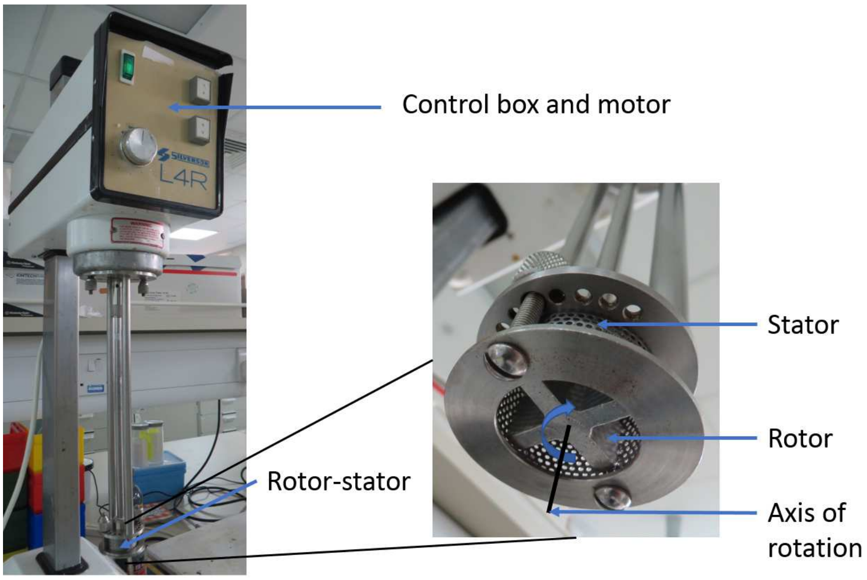

Figure 3.4 *Bench top Silverson L4R mixer/emulsifier, and close-up on rotor-stator element.*

The emulsification process is based on the use of high shear rates applied to the fluids in the gap between the rotating part (rotor) and the stationary part (stator). The stator used here is a grid punched with circular holes of around 1 mm radius.

Rotor-stators have the advantage of being easy to use and with a readily adjustable shear rate. But, in some situations, high-pressure homogenisers are favoured for the emulsification of samples.

High-pressure homogenisers

High-pressure homogenisers are not based on rotating parts, instead their driving force is, as hinted by their name, the application of high pressure to the fluids pushed through a channel, and a sudden depressurisation. The exact principles of dispersion vary between the different models of homogenisers, but in general they present the advantage of being continuous processes and more energy-efficient than rotor stators. In addition, smaller sizes of droplets can be achieved because these equipments generate larger energy densities in the liquids and because of higher levels of extensional flow, driven by turbulence.

Microfluidiser

Microfluidizer is a range of homogenisers commercialised by Microfluidics Inc. The bench top model used to produce the fine protein-stabilised emulsions used in Chapters 5, 6 and 7 is shown in Figure 3.5. The sample is powered at high pressure in the channel using the pump. It then reaches the interaction chamber, which is where most of the dispersion occurs. Although the details of the interaction chamber geometry are not communicated by the manufacturer, it is based on a Y shape: the channel separates into two smaller channels of around 100 µm of diameter. The two microfluidic channels then converge into a small chamber, where the divided streams recombine, causing high impact and high extensional flow.

This technique allows for the formation of finer and more monodisperse emulsions than rotor-stators or most other homogenisers.

Homogeniser

In addition to the droplets prepared using the Microfluidizer and used mostly in this thesis, larger droplets were prepared, as detailed in Chapter 8. Because the change of input pressure in the Microfluidizer only led to a widening of the droplet size distribution, but not to an increase of the average droplet size, the use of another model of homogeniser was required.

To produce larger droplets, a bench top high-pressure homogeniser (APV 1000, single piston, IKA) was used. It relies on the decompression of the liquid from high to ambient pressure to induce the break-up of droplets by turbulence and cavitation. The high pressure is built up with a piston pump and released in a controlled way via the adjustable gap of the homogenising valve.

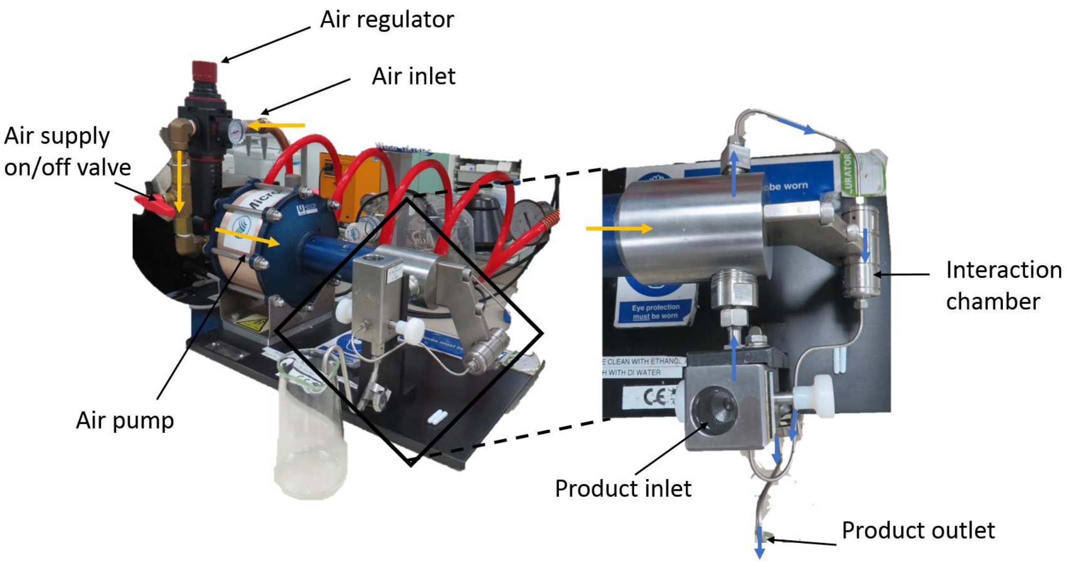

Figure 3.5 *Bench top Microfluidizer (Microfluidics Inc.) mixer/emulsifier, and close-up on the path of circulation of the sample. The yellow arrows indicate the compressed air flow while the blue arrows indicate the sample flow.*

3.3.2 Preparation of the protein-stabilised emulsions

As outlined above, the emulsification was performed in two steps to produce relatively monodisperse protein-stabilised droplets.

First, a pre-emulsion was prepared using the Silverson L4R rotor-stator shown in Figure 3.4. It was obtained by mixing a $45\,\mathrm{mg\cdot mL^{-1}}$ sodium caseinate solution (prepared as detailed previously) at low speed and adding progressively glyceryl trioctanoate up to a water:oil weight ratio 4:1. After all the oil was added, the rotor-stator was set at maximum speed (≈ 8000 rpm) and the oil was emulsified for 5 min. Because of energy dissipation, the temperature rose from around 15 °C to around 40 °C during the process. As can be observed on Figure 3.6 (a), there was also significant foaming. This pre-emulsion was then stored at room temperature for 4 h to decrease its temperature and the amount of foam, as the presence of air in the microfluidiser may damage its constituents. As can be observed on Figure 3.6 (b), creaming occurs quickly in the pre-emulsion, which is due to the relatively large droplet size ($\approx 14\,\mu$m).

The second step was dependent on the size of droplets required, as the model of homogeniser was different for the small droplets, used mostly in this thesis, and for the larger droplets, presented in Chapter 8.

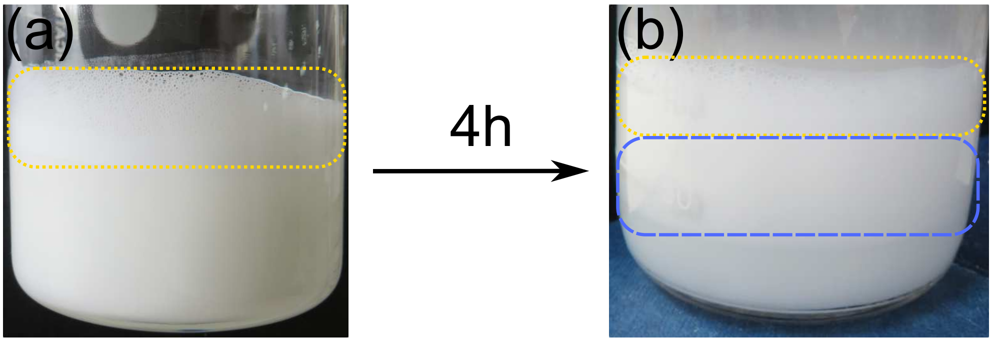

Figure 3.6 *Pre-emulsion of oil in sodium caseinate solution, (a) after mixing with a rotor-stator, and (b) after* 4 h. *The dotted yellow frame indicates the presence of foam, while the dashed blue frame highlights the creaming of the oil droplets.*

Emulsification of the small droplets

After 4 h ageing, the pre-emulsion was passed through the Microfluidizer (Microfluidics Inc.) with an input pressure of 5 bar three times consecutively, which is amplified to ≈ 1000 bar by the microfluidizer. After 3 passes, a stationary regime was reached where the size of droplets could not be reduced any further. The sodium caseinate-stabilised emulsion prepared according to this protocol has an average droplet radius of ≈ 110 nm, so the use of the microfluidiser allowed for the reduction of droplet size of 2 orders of magnitude (as measured using a Mastersizer). The droplet size distribution will be presented in Chapter 4.

Emulsification of the larger droplets

For larger droplet sizes, the pre-emulsion was passed through the High Pressure Homogeniser (single piston HPH 2000, IKA) using a pressure of 200 bar six times consecutively. The resulting emulsion presents an average droplet radius of ≈ 160 nm, and is more polydisperse than the emulsion obtained using the Microfluidizer.

3.3.3 Purification of the droplets

A main motivation for this study is to distinguish the contributions of the unadsorbed proteins from the contributions of the droplets in the rheological and microstructural behaviour of suspensions and gels of protein-stabilised emulsions. It is thus important to separate the protein-stabilised droplets from any unadsorbed proteins in suspension. To this end, the different components of the emulsion are separated by centrifugation.

Separation by centrifugation relies on the use of centrifugal force to separate particular elements in suspension according to their discrepancy in buoyancy. Particles denser than the suspending medium, like proteins, will sink and sediment to the bottom of the centrifuge tube while particles lighter than the continuous phase will move up. The centrifugal force arises from the angular rotation of a rotor, in which the centrifuge tubes are placed. The direction of the force is radially outward from the axis of rotation.

Centrifuge rotors are one of two types. In fixed-angle rotors, tubes are held at an angle to the rotation axis. In this case, the layering of the components occurs with an angle to the tube wall, as illustrated in Figure 3.7. In swinging bucket rotors, the tubes have the freedom to rotate and align as the centrifugal force is applied, and the resulting layering of components is horizontal.

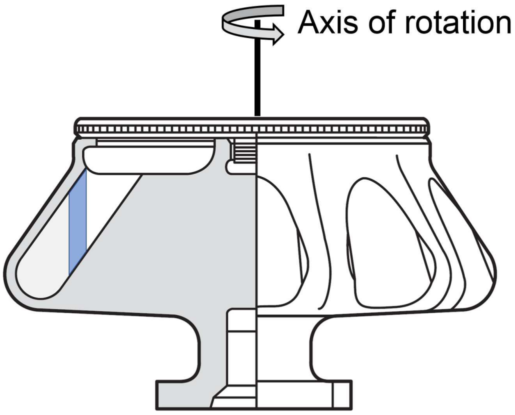

Figure 3.7 *Fixed angle rotor for ultracentrifuge, with an illustration of the separation of a sample with particles (in blue) less dense than the suspending medium. Adapted from Ref. [12].*

The most important parameter in a separation protocol using centrifugation is the centrifugal force, expressed in units of gravity $\times g$, that can be related to the rotation speed, expressed in revolutions per minute (rpm), using the geometrical features of the rotor.

The protein-coated droplets prepared in this study are covered with a layer of proteins, denser than water, so their mean density is an average between the density of the oil and of the protein coating and is dependent on the size of the droplets. To perform the separation of the small droplets (radius $\simeq 110\,\mathrm{nm}$ to $\approx 160\,\mathrm{nm}$), a very high angular speed is thus required. Consequently, a common laboratory centrifuge is not sufficient, and an ultracentrifuge that can reach speeds of 70 000 rpm is required. In this study, the model used was a Sorvall Discovery 90 SE (Thermo Scientific). Among the available rotors, the fixed angle 45 Ti type (Beckmann Coulter) was selected because it offers a good compromise between maximum rotation speed (45 000 rpm) and volume capacity of the tubes (here bottles of 70 mL are used).

The separation of the protein-stabilised droplets was achieved by centrifuging the microfluidised emulsion described in the previous section at 45 000 rpm, which corresponds to a centrifugal force of $234\,800 \times g$ for 16 h at 21 °C. The acceleration and deceleration speed can be set on the equipment, so the deceleration speed was set to a low value to avoid disturbing the separated sample.

This speed was adapted for the production of larger droplets using the homogeniser. Indeed, the creaming speed varies as the inverse of the size of the droplets. In addition, the buoyancy force varies as R^3 so care was taken that the centrifugation process did not apply an excessive force on the droplets causing their destabilisation. The centrifuge speed was thus decreased to 24 600 rpm, which corresponds to a centrifugal force of $70\,000 \times g$.

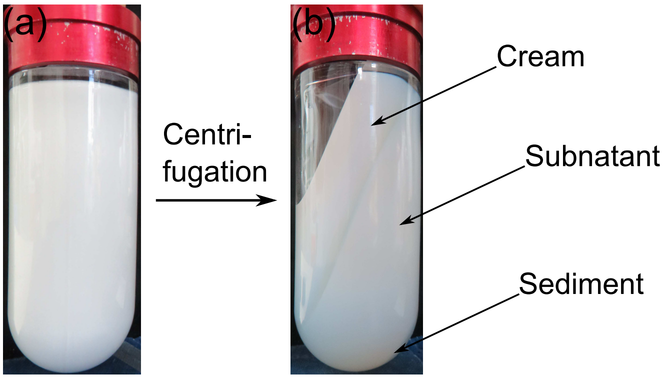

Figure 3.8 *Several stages of the preparation of small protein-stabilised droplets (a) after 3 passes through the microfluidiser and (b) after ultracentrifugation at* $234\,800 \times g$ *for* 16 h *that leads to the fractionation of the emulsion into a cream of jammed droplets, a subnatant and a small protein sediment.*

After the centrifugation run, 3 main fractions could be observed, as illustrated in Figure 3.8 (b):

- At the top, a solid layer was made of jammed droplets. Visually, the layer was not homogeneous but rather formed of a stiff opaque layer on the top and a softer transparent layer. This inhomogeneity will be discussed in Chapter 4.

- In the middle, the liquid phase formed the biggest part of the sample. It was less turbid than before centrifugation, but there was still a significant turbidity that could not be attributed only to the proteins. It was thus concluded that some of the protein-stabilised droplets were still in suspension.
- At the bottom, a solid and sticky layer formed the sediment . It was presumably made of the larger assemblies of sodium caseinate present in suspension, as presented in Section 4.5.2.

After separation, the different fractions were collected individually. First, the liquid subnatant was removed, by piercing through the top layer using a syringe and a needle, and discarded. Then, the fraction of interest, the top layer, was carefully scraped out of the tube and collected in a glass bottle. Finally, the sediment was scraped and discarded. The paste of jammed droplets was homogenised by mixing with a spatula and kept as a stock of protein-stabilised droplets. The concentration of this stock was estimated by drying a known volume of the paste, and weighting the resulting dry matter, which yielded a concentration of $(0.519 \pm 0.008)\,\mathrm{g \cdot mL^{-1}}$ for the jammed droplets. Further characterisations of the fractions obtained during the separation by centrifugation are detailed in Chapter 4.

The suspensions of pure droplets were then prepared by diluting the stock paste at the required concentrations (from $8\,\mathrm{mg \cdot mL^{-1}}$ to $0.384\,\mathrm{g \cdot mL^{-1}}$) with de-ionised water. To re-disperse the droplets, the paste of jammed droplets was first roughly homogenised with a spatula in the vial, and then gently mixed using a magnetic stirrer. The mixing time required to obtain a homogeneous sample ranged from 1 to 30 min, as for higher concentrations it becomes increasingly difficult to mix the sample.

The resulting suspensions are considered in this study to be exclusively made of protein-stabilised droplets, without any unadsorbed proteins. This assumption relies on the low concentration of suspending medium in the paste of concentrated droplets. Furthermore the concentration in unadsorbed proteins may be lower in this medium than in the subnatant because of the depletion force between droplets arising from the presence of the unadsorbed proteins during centrifugation. This protocol was thus initially estimated to be sufficient for performing the purification of the emulsion. With hindsight, a more thorough purification could have been achieved by rinsing the droplets in de-ionised water and separating them again from the suspending medium, and possibly repeating these steps two or three times.

The size distribution of the resulting pure suspensions of protein-stabilised droplets was measured to ensure that the droplets did not suffer major changes in size during the purification process due to coalescence or irreversible flocculation, as can be seen on Figure 3.9.

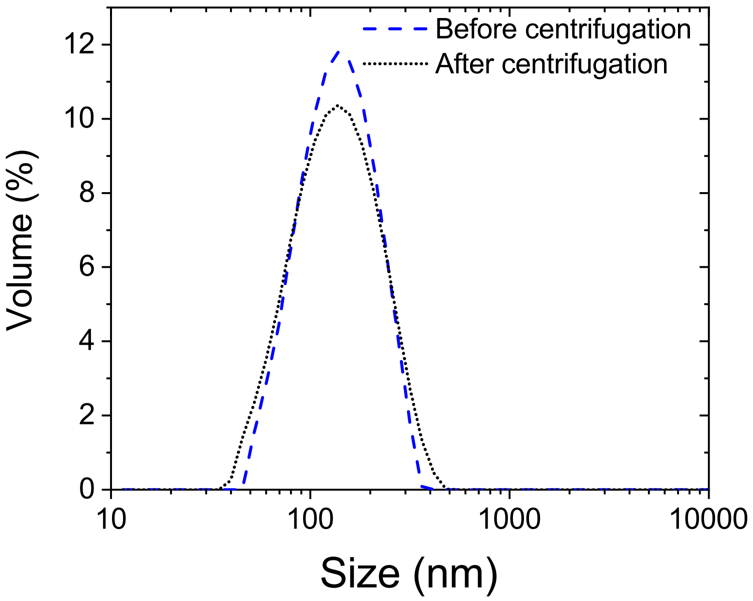

Figure 3.9 *Typical size distributions of the emulsion before centrifugation (dashed line) and of the droplets after separation by centrifugation and redispersion in water (dotted line). The particle sizings were performed using Static Light Scattering (Mastersizer) on only one sample, but are representative of the results obtained for all samples.*

Only minor differences were observed in the size distribution of the droplets before and after purification. The absence of a shift towards the bigger sizes of droplets show that coalescence or irreversible flocculation is negligible, demonstrating the sturdiness of sodium caseinate-stabilised droplets.

The droplets thus produced were used to study the rheological behaviour of protein-stabilised emulsions, as well as the properties and microstructure of the gels they form. To this aim, the droplets can be mixed with protein suspensions to produce mixtures of controlled composition.

3.4 Preparation of the mixtures of proteins and droplets

Sodium-caseinate emulsions of well-characterised compositions were prepared by mixing precise amounts of the protein suspension and of the paste of purified droplets. A wide range of compositions of mixtures was explored. In the following, the terms mixture and emulsion will be used without distinction to indicate the samples prepared in this section (as opposed to a standard emulsion where the amount of un-adsorbed protein is uncontrolled).

3.4.1 Preparation protocol

To prepare emulsions with a controlled amount of proteins in suspension, the paste of purified droplets at $(0.519 \pm 0.008)\,\mathrm{g \cdot mL^{-1}}$ was re-suspended in a protein suspension. The protein suspension was prepared as described previously at $45\,\mathrm{mg \cdot mL^{-1}}$ and diluted to the desired concentration. As for the suspensions of pure droplets, the paste was first roughly homogenised with a spatula in the vial, and then gently mixed using a magnetic stirrer. The mixing time required to obtain a visibly homogeneous sample ranged from 5 min to 2 h. The re-dispersion required longer stirring times at high concentration of droplets and at high concentration of proteins. At a given droplet concentration, significantly more stirring was required to disperse the droplets in a protein suspension than in water.

3.4.2 Composition of the mixtures

One of the main interests in this study is to determine the contribution of un-adsorbed proteins in protein-stabilised emulsions and emulsion gels. In order to achieve this, it is important to study the full range of what is described as an emulsion, and thus to vary the contents of droplets and un-adsorbed proteins, both in terms of total concentration and also relative to the other component.

It is useful to think about protein-stabilised emulsions as ternary mixtures, made of water and of two sorts of colloidal particles: droplets and protein aggregates. Their composition can be described using the concentration or volume fraction of each component in the total suspension. In addition, it is convenient to characterise the mixtures using the ratio of its different components, χ_{prot}, defined as:

$$\chi_{prot} = \frac{\phi_{eff,prot}}{\phi_{eff,prot} + \phi_{eff,drop}} \tag{3.1}$$

Where $\phi_{eff,prot}$ and $\phi_{eff,drop}$ designate the effective volume fractions respectively of the protein and of the droplets, which will be expressed as functions of the concentrations in Chapter 5.

Hence, χ_{prot} describes the relative fraction of protein in the emulsion compared to the droplets, where the amounts of each component are expressed as volume fractions. Thus, $\chi_{prot} = 1$ for samples containing only proteins, $\chi_{prot} = 0$ for samples containing only protein-stabilised droplets, and $\chi_{prot} = 0.5$ for mixtures containing an equal volume fraction of proteins and protein-stabilised droplets.

The mixture samples prepared to explore the range of composition of protein-stabilised emulsions can conveniently be displayed on a ternary diagram. Figure 3.10 illustrates the samples prepared to study the viscosity of such systems, as described in Chapter 5. The samples used in Chapter 7 are the samples of mixtures at intermediate concentrations. Indeed, dilute samples would not form a gel while it would be difficult to homogeneously decrease the pH in the samples at high concentration because of their viscosity.

Table 3.2 gives the composition of all the mixture samples displayed on Figure 3.10 and used in Chapter 5. The concentrations were calculated from the dilution of the stocks of pure proteins and pure droplets, while volume fractions were calculated from the concentrations as detailed in Chapter 5.

The description of the mixtures and the consequent choice of parameters is not impartial for the interpretation of the influence of the composition on the properties of the emulsions and gels. This will be discussed more in detail in Chapter 7.

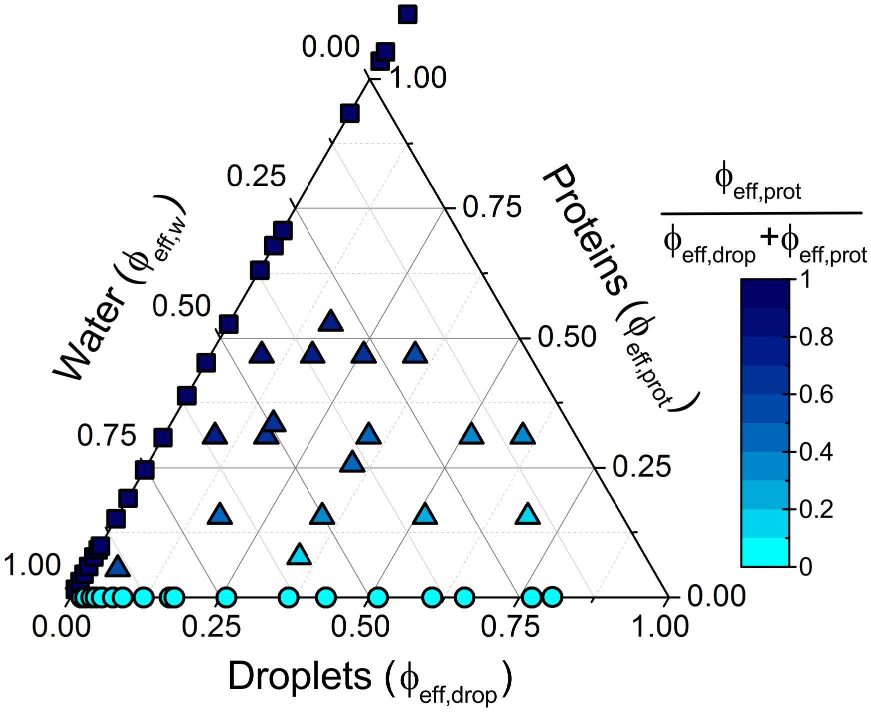

Figure 3.10 *Composition, in effective volume fractions* $\phi_{eff,drop}$ *defined in Chapter 5, of suspensions of sodium caseinate (squares, navy), sodium-caseinate stabilised droplets (circles, cyan), and of mixtures (triangles, colour-coded as a function of* χ_{prot} *defined in Equation 3.1) studied in Chapter 5. The compositional parameters of the mixture samples are listed in Table 3.2.*

3.5 Acid-induced gelation of proteins

In Chapters 6 and 7, protein and protein-stabilised emulsion gels are prepared and their rheological and microstructural properties are investigated. The gelation is based on a slow decrease in pH in protein suspensions and emulsions. Indeed, an abrupt destabilisation of the protein caused by the addition of a strong acid would lead to inhomogeneous gels or even aggregation without formation of a network.

Slow acidification of aqueous solutions

The slow acidifier used in this study is glucono δ-lactone, the structure of which is presented in Figure 3.2. When added to water, this molecule progressively and partially hydrolyses to gluconic acid. The hydrolysis rate is dependent on several

Table 3.2 *Composition of the mixture samples made of sodium caseinate (proteins) and sodium caseinate-stabilised droplets (droplets)*

Concentrations ($\mathrm{mg \cdot mL^{-1}}$)		Volume fractions		Ratio proteins/droplets
Proteins	Droplets	Proteins	Droplets	χ_{prot}
6.4	25	0.054	0.053	0.50
34	27	0.29	0.057	0.83
18	42	0.15	0.092	0.63
54	42	0.46	0.092	0.83
36	43	0.31	0.092	0.77
13	50	0.11	0.11	0.51
38	80	0.33	0.173	0.65
62	82	0.53	0.18	0.75
18	84	0.15	0.18	0.46
22	84	0.19	0.18	0.51
36	84	0.31	0.18	0.63
54	85	0.46	0.18	0.72
54	1.3×10^2	0.46	0.27	0.63
18	1.7×10^2	0.15	0.36	0.30
36	1.7×10^2	0.31	0.36	0.46
54	1.7×10^2	0.46	0.36	0.56
9.0	1.7×10^2	0.076	0.38	0.17
30	1.8×10^2	0.26	0.38	0.40
18	2.5×10^2	0.15	0.54	0.22
36	2.5×10^2	0.31	0.54	0.36
7.9	2.7×10^2	0.068	0.57	0.10
36	2.9×10^2	0.31	0.63	0.32
17	3.3×10^2	0.14	0.71	0.17

parameters.

First, the temperature affects the hydrolysis rate. Indeed, an increase in temperature leads to a quicker hydrolysis of glucono δ-lactone [133], while the final pH stays constant at fixed amount of acidifier.

In addition, the ratio glucono δ-lactone:protein also plays a role in the kinetics of hydrolysis and final pH. In the presence of sodium caseinate, the chemical equilibrium between glucono δ-lactone and gluconic acid is not simple, and the protein suspension acts as a buffer. This buffer effect leads to a slower and less extensive acidification by glucono δ-lactone of caseinate suspensions than in water, as can be observed in Figure 3.11.

The hydrolysis rate being highly dependent on the medium, the amount of glucono δ-lactone had to be adjusted here for each type of sample to obtain

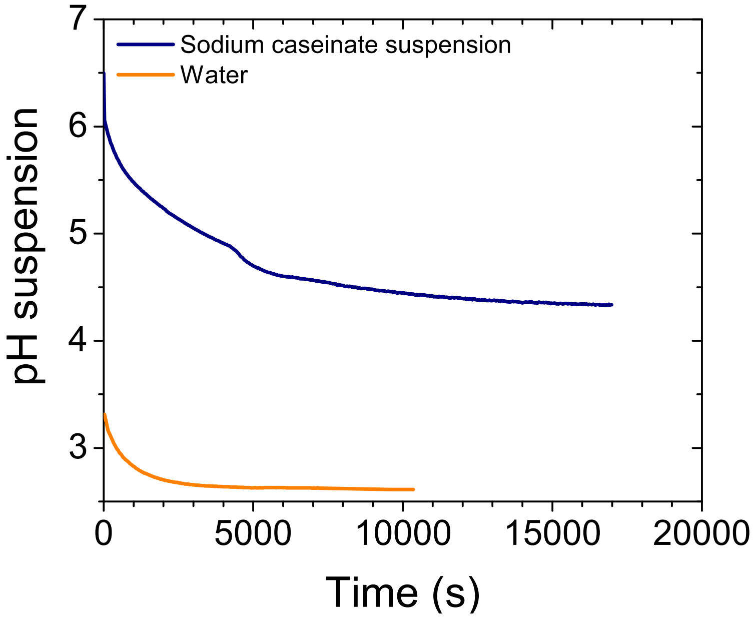

Figure 3.11 *Acidification of suspensions containing equal amounts of glucono δ-lactone at* 50 °C. *The blue line denotes a suspension of* $45\,\mathrm{mg\cdot mL^{-1}}$ *sodium caseinate, while the orange line is deionised water. Both suspensions have an initial pH of 6.7, but the steep initial decrease in pH upon mixing with glucono δ-lactone powder could not be measured.*

the same pH decrease in different systems. In addition, it has been shown that the properties of the final gel are dependent on the ratio glucono δ-lactone:protein [126], so the ratio was fixed for a given type of sample.

Thus, for suspensions of pure proteins, pure droplets and for mixtures, the ratio glucono δ-lactone:protein required to reach a final pH between 4.5 and 5 was found and kept constant over the range of concentrations used. The kinetics of acidification, however, are still dependent on the composition of the samples.

Protocol for the gelation of the samples

To perform the gelation of the suspensions prepared as detailed in this chapter, the powder of glucono δ-lactone was first quickly dissolved in one or two droplets of deionised water. This liquid was then immediately mixed with the solution of interest and placed directly either in the rheometer cup or in the observation cell for confocal microscopy, in order to ensure that the gelation occurs in-situ and the gel is not modified by the loading of the samples on the characterisation equipment.

The ratios glucono δ-lactone:protein and glucono δ-lactone:droplet were found by scanning the range of ratios at given concentration of proteins and/or droplets, and by measuring the final pH. For sodium caseinate suspensions, the weight ratio was found to be $\frac{glucono\ \delta-lactone}{protein} = 0.185$.

For caseinate-stabilised droplets, the weight ratio used was $\frac{glucono\ \delta-lactone}{droplet} = 0.075$. Although this ratio was found empirically, it can be related to the ratio glucono δ-lactone:protein if the layer of adsorbed protein is assumed to represent 13 % of the weight of the droplets, as will be detailed in Chapter 4. In this case, it is found that $\frac{glucono\ \delta-lactone}{protein} = 0.58$ for droplet suspensions. The discrepancy with the value for protein suspensions probably originates from the differences in configuration between the two colloidal systems, as part of the protein may be buried inside the self-forming sodium caseinate aggregates, while the protein is probably unfolded at the surface of the oil droplet, thus requiring more acidifier to reach the same pH.

For mixtures of proteins and droplets, the amount of glucono δ-lactone was calculated appropriately for the protein and droplet contents of each sample. The final pH was kept between 4.5 and 5.0 as in this range of pH, caseinate is at its isoelectric point and thus forms strong gels [120].

The gelation was performed at 35 °C in order to accelerate the phase transition. Indeed, over long time scales, adverse phenomena such as bacterial growth or creaming may occur in the samples, despite the use of biocide and the low difference in density between droplets and continuous phase. Following this protocol, the gelation of the suspensions takes between 30 min and 2 h , depending on the type of sample and concentration. This will be discussed more in detail in Chapter 6.

3.6 Conclusion

In this chapter, the preparation protocols were described for making suspensions containing proteins, droplets or a mixture of the two components with a finely controlled composition. Sodium caseinate suspensions were purified in order to remove the residual oil droplets and ill-characterised aggregates. In addition, the protein-stabilised oil droplets were separated from the unadsorbed proteins using centrifugation. The latter protocol represents one of the original aspects of the work presented in this thesis, as it makes it possible to characterise the influence of the composition on the rheological properties of emulsions and emulsion gels.

Chapter 4

Characterisation of sodium caseinate and droplet dispersions

In this chapter, I characterise the dispersions of sodium caseinate and of sodium caseinate-stabilised droplets prepared in Chapter 3.

I first estimate the concentration of protein solutions after purification. Refractometry is used to measure the concentration of protein without the need of a calibration curve.

Then, I discuss the peculiar optical heterogeneity of the dense paste of protein-stabilised droplets during the purification step of the preparation of pure droplets. The nature of this heterogeneity is explored and a qualitative explanation is proposed.

Finally, I measure the size distributions of proteins and droplets using several techniques. Light scattering allows the characterisation of the protein-stabilised droplets, while the proteins require a preliminary fractionation by size, performed using a flow field fractionation technique.

4.1 Introduction

For understanding the rheological behaviour of emulsions and emulsion gel, the characterisation of their components, namely unadsorbed protein and protein-stabilised droplets is essential. In this thesis, the influence of the composition on the rheology of suspensions and gels is discussed. It is thus necessary to describe precisely this composition in the samples prepared.

For this reason, suspensions of pure sodium caseinate and pure caseinate-stabilised droplets were prepared as described in Chapter 3. In this chapter, their concentration in colloidal species is determined using different methods.

Furthermore, the size distribution of colloidal species play a role in the viscosity of their suspensions [41]. It is thus important to characterise the size of the proteins and droplets used here.

The size of naturally-occurring aggregates of sodium caseinate has been the focus of many studies [63, 105, 109], but it has been shown to depend on environmental parameters, such as the manufacturing process and the calcium content. In order to have an accurate size distribution for the exact batch of protein used in this study, it is thus sensible to measure it.

In addition, the size distribution of an emulsion depends on the emulsification techniques, and the nature of the oil and the emulsifier. In this study, the high-pressure homogeniser used allows the production of small and relatively monodisperse protein-stabilised droplets, as measured here using light scattering techniques.

4.2 Materials & Methods

The preparation of samples is fully described in Chapter 3. I will focus here on describing the experimental techniques used to characterise the suspensions of sodium caseinate and of caseinate-stabilised droplets.

4.2.1 Techniques for the determination of protein concentration

It is interesting to evaluate the amount of proteins that adsorb at the oil/water interface during emulsification and compare it to the total amount of proteins. To achieve this, a precise measurement of the concentration in sodium caseinate needs to be performed. Several techniques are possible to carry out this measurement, but their scope of application varies.

Protein concentration by absorbance

An easy estimation of the protein content can be achieved by measuring the UV-vis absorbance of a protein solution at a wavelength of 280 nm using a spectrometer [134]. Indeed, the tyrosine and tryptophan residues of a protein backbone absorb light at this wavelength.

Light absorbance can be described accurately by the Beer-Lambert law:

$$log\left(\frac{I_0}{I}\right) = \epsilon l c \tag{4.1}$$

Where I_0 is the intensity of the incident light beam, I is the intensity of the light after going through the sample, ϵ is the molar absorptivity coefficient (in cm^{-1}), l is the light path length and c is the concentration of the solution (here, the weight ratio).

As can be seen in Equation 4.1, there is a linear relationship between the absorbance $log(I_0/I)$ and the protein concentration c, making it possible, in theory, to determine the protein content in dilute suspensions with a simple calibration curve.

Nonetheless, this technique presents some drawbacks. A minor limitation is the dependence on the micro-environment of the absorbing residues (*i.e.* pH, ionic strength, aggregation, unfolding). More importantly, this technique cannot be used if light scattering competes with light absorbance. Thus, it is not possible to use it to determine the protein concentration in turbid protein-stabilised emulsions.

Protein concentration by refractometry

The refractive index of a suspension can give an indication of its concentration, provided that the refractive index increment dn/dc is known for the component in suspension. Indeed, the concentration c (in $\mathrm{g} \cdot \mathrm{mL}^{-1}$) can then be determined using the simple proportional law:

$$c = \frac{n_{sample} - n_{solvent}}{dn/dc} \tag{4.2}$$

Where n_{sample} and $n_{solvent}$ are the refractive indexes of the sample and the solvent, respectively.

The derivative of the refractive index with the concentration, dn/dc, is notoriously hard to determine experimentally. Values from the literature are commonly used and in the specific case of proteins, the long-held assumption that all the proteins have a similar refractive index increment dn/dc, close to $(0.1888 \pm 0.0033)\,\mathrm{mL \cdot g^{-1}}$ is generally applied [135].

Recent studies have challenged the validity of this assumption, but they also showed that intrinsically disordered proteins were part of the proteins for which the assumption holds [132]. β-casein display some disordered regions [136], it is thus assumed here that sodium caseinate belongs to this category. Therefore, in this study, the refractive index increment of sodium caseinate is estimated to be $dn/dc = (0.1888 \pm 0.0033)\,\mathrm{mL \cdot g^{-1}}$.

The refractometer used here to estimate the concentration of sodium caseinate suspensions is a RM 50 (Mettler Toledo), and has a precision of 5 digits. The measurement is based on the illumination of the sample using an LED of wavelength 589.3 nm, and the optical determination of the total reflection angle using a CCD chip.

Here, the samples of sodium caseinate were simply added on the top of the measuring prism, and the measurement was performed at room temperature (25 °C).

In common with other optical techniques, such as the absorbance presented previously, refractometry cannot be used for samples that scatter light. It can therefore only be used on samples of pure sodium caseinate, and not on samples containing residual fat droplets.

4.2.2 Techniques for particle size analysis

The size of colloidal particles, and more specifically the size distribution, is a parameter that plays an important role in determining rheological properties. In this study, a few techniques were used to determine the sizes of sodium caseinate naturally-occurring aggregates and sodium-caseinate stabilised droplets.

When particles are hit by a beam of light, the light intensity in the incident direction is decreased as the particles interact with the electromagnetic wave. The light is thus scattered in other directions by the particles. This light scattering phenomenon depends on several parameters, such as the particle size, the wavelength of the light beam and the concentration of the particles. It can therefore be used to estimate the size of particles in suspensions. Amongst the techniques utilising this phenomenon, Static Light Scattering (SLS) and Dynamic Light Scattering (DLS) are commonly used to characterise colloidal species.

Static Light Scattering

Static Light Scattering (SLS) uses the variation of scattered light intensity with the angle to the incident beam to determine some properties of the scattering particles. The typical setup for SLS is illustrated in Figure 4.1.

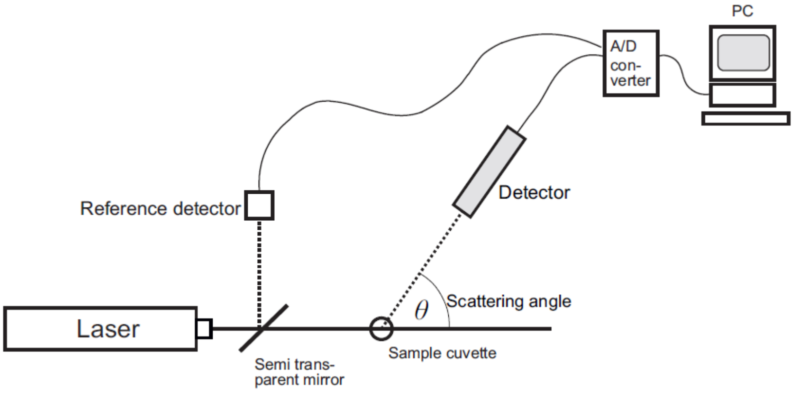

Figure 4.1 *Typical SLS setup, reproduced from Ref. [13]*

During a SLS measurement, the scattered intensity is measured at a wide range of scattering angles θ, as represented in Figure 4.1. Because of the dynamic aspect of light scattering, the measurement at each angle is usually averaged over a short period of time (around 1 s). The intensity versus angle is then fitted by a model to obtain information on the scattering particles.

In this study, a commercial apparatus for SLS (Mastersizer, Malvern Panalytical) was used. This automatised setup allows quick measurement of the particle size distribution. A few drops of samples are added to the dispersion chamber containing deionised water, and the diluted sample is then pumped in the measurement area, where it is illuminated by a laser beam. The intensity of the scattered light is then measured by detectors placed at several angles, for red light and blue light.

The instrument software then uses the variation in intensity of the scattered light with the measurement angle to calculate the size distribution of the particles contained in the sample. In this case, the radius obtained is an optical cross-section, rather than the radius of gyration that can be determined with a classical SLS setup.

The size measurements for the protein solutions and droplet suspensions were performed as follows. The sample was added in the dispersion chamber in a large enough amount to reach an obscuration level between 10 % and 20 %. This quantity depends on the refractive index and size of the particles used, as well their concentrations, but was in general in the range of 0.2 mL to 2 mL. The size distribution was calculated using Mie theory with the following refractive indexes as parameters:

- For the droplets, the refractive index for glyceryl-trioctanoate was used, *i.e.* $n_{oil} = 1.458$
- For the proteins, the refractive index for casein was used, *i.e.* $n_{protein} = 1.420$

For both type of particles, an absorption factor of 0.001 was used.

Dynamic Light Scattering

The other common light scattering method for determining some properties of colloidal particles is Dynamic Light Scattering (DLS). In this technique, the scattered intensity is not as important as its fluctuation in time. Indeed, when doing DLS, the fluctuations of the intensity of scattered light is used to estimate the speed of diffusion of the colloidal particles. The diffusion coefficient can then be used to calculate the size of the particles from Stokes-Einstein equation of diffusion.

An essential assumption to relate the typical fluctuation time of the scattering intensity with the diffusion of the particles is that a given ray of light is scattered only once in the sample before going out of the cuvette. This means that the samples used need to be very dilute to limit as much as possible multiple scattering.

The size obtained from the analysis of DLS data is called the hydrodynamic radius R_h, because it is based on the diffusion properties of the particles. This size is in general larger than the optical cross-section obtained using the Mastersizer as it takes into account some additional properties of the particle, such as the surface charge and the "hairy" corona of soft colloids, rather than only the difference in refractive index for the optical cross-section.

In this study, a commercial apparatus of DLS (Zetasizer Nano ZS, Malvern Panalytical) was used. It is set up so that the backscattered light intensity is measured, *i.e.* the light scattered at 173 deg from the incident beam. This setting is meant to limit multiple scattering as the light does not go through the entire thickness of the sample.

The samples were first diluted down to concentrations around 0.1%(wt) for the droplets and around 1%(wt) for the proteins. The cell (a folded capillary cell, model DTS 1070) was then carefully filled with the diluted samples to avoid trapping air bubbles that may disrupt the measurement. The full cell was inserted in the measuring chamber and the DLS measurement was performed automatically by the apparatus at 25 °C. The size of the particles was then estimated from the fluctuations of the scattered light using the same optical properties of the proteins and droplets than for the SLS measurements.

For both SLS and DLS, a major disadvantage is the lack of accuracy of light scattering measurements for polydisperse samples. Indeed, in both cases there is a large bias towards larger colloidal particles, as they scatter much more than smaller particles. Thus, light scattering is not a reliable technique to measure the size distribution in a polydisperse system containing both large and small particles, as it overestimates significantly the relative amount of large particles.

Flow Field Fractionation

To overcome the limitation of light scattering for polydisperse suspensions, it is possible to separate the particles by size before performing size measurements. This separation can be achieved using the Flow Field Fractionation (FFF) technique.

The separation principle of this technique is illustrated in Figure 4.2.

The FFF technique is based on the hydrodynamic separation of particles in a

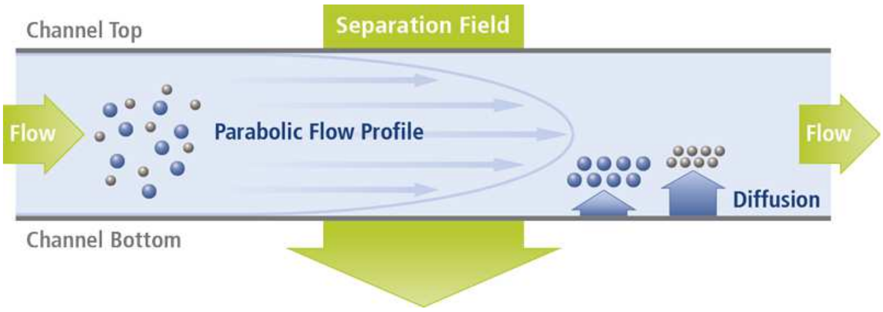

Figure 4.2 *Separation principle of Flow Field Fractionation (FFF) technique. Image courtesy of PostNova [14].*

parabolic flow profile. The migration of particles in different regions of this laminar flow can be achieved using various separation fields. Indeed, electric, thermal or centrifugal fields are a few examples of possibilities to separate the particles perpendicularly to the flow by using their distribution in charge, size or density.

Here the asymmetric flow FFF technique was used. The separation is based on the initial focusing of particles by a cross-flow, that pushes the bigger particles further towards the membrane placed on the porous channel bottom, while the smaller particles stay towards the centre of the channel.

As can be seen on Figure 4.2, after the initial focusing in the centre of the channel, the particles go through the channel and are separated by their difference of speed in the flow profile. Thus the small particles will be eluted first, and the bigger particles will require a longer elution time. The elution profile is thus a function of the size distributions of the particles.

The size of the different fractions of particles can finally be measured in-line using a wide range of techniques with increased accuracy. Indeed, each size measurement is made on a fairly monodisperse sample. The modularity of the setup enables the comparison of the result of different light scattering techniques, here Dynamic Light Scattering (DLS) and MALS (Multi Angle Light Scattering).

An additional advantage of the technique is that the use of hydrodynamics to separate the fractions allows measurement of the sample “as it is”, without any need of further filtration, which is the limitation of common fractionation techniques like Size Exclusion Chromatography. It is thus well adapted to quantify the sizes of commercial grades of proteins, that may contain large impurities.

The size measurement of a 5 %(wt) sodium caseinate suspension, prepared as detailed in Chapter 3, using an asymmetric flow FFF setup was kindly performed by PostNova Ltd. The channel used had a thickness of 350 µm and a NovARC 10 kDa membrane was used to prevent contamination of the perpendiculr channel that allows the cross-flow. The sample was eluted at a flow rate of $0.5\,\mathrm{mL} \cdot \mathrm{min}^{-1}$ using a phosphate buffer at $pH = 7.4$. After separation, a series of 4 detectors was used: UV absorbance, refractive index, DLS and SLS.

4.3 Concentration measurements in protein solutions

The protein used in this study is a commercial grade of sodium caseinate. As it is often the case for commercial food grades of ingredients, our batch of sodium caseinate is not pure, as can be seen on the manufacturer specifications presented in Table 3.1. The weight fraction of protein therefore differs from the amount of powder used for the preparation of the samples. There may also be an additional decrease in concentration of protein during the purification process detailed in Chapter 3, in which the insoluble fractions of proteins are removed. It is thus important to be able to measure the protein concentration in the final samples of sodium caseinate suspensions.

Several techniques can be used to measure the concentration of protein of suspensions. Suspensions could be dried to measure their solid content, but the precision of this technique decreases at low concentration. Biuret test and Kjeldahl digestion are other available options that have not been explored in this work.

4.3.1 Absorbance to estimate protein loss during purification

Absorbance measurements were used to characterise the decrease in protein content due to the purification process, in order to refine the preparation protocol of sodium caseinate. A calibration curve was first obtained by diluting a non-purified sample of 5.0 %(wt) powder of sodium caseinate and measuring the absorbance at a range of dilutions from 50 times to 200 times. A linear fit of this data makes it possible to derive a proportional law $log(I_0/I) = \alpha \times c + \beta$, where $\alpha = 0.096$ and $\beta = 0.075$.

The concentration of protein suspensions, initially prepared at 5.0 %(wt) of commercial protein powder, after different purification protocols could thus be estimated, by diluting the suspensions 80 times and by measuring the absorbance of the diluted suspensions. The results, together with the calibration curve, are displayed in Figure 4.3.

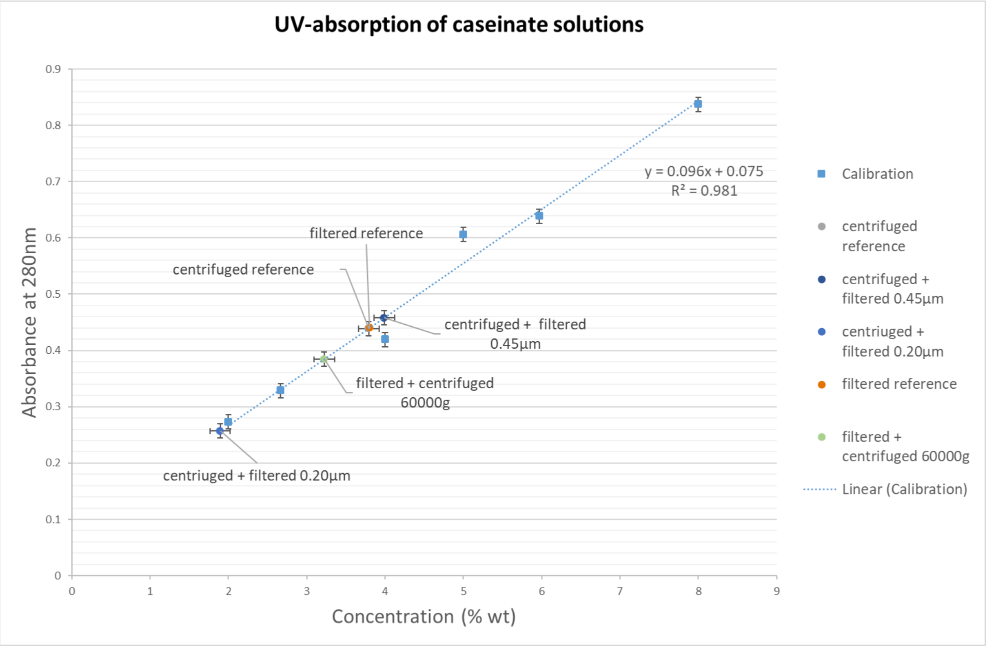

Figure 4.3 *Estimation of the concentration of* 5.0 %*(wt) protein suspensions after purification following different protocols (circles): centrifuged at* 60 000×*g only, centrifuged and filtered using a* 0.45 µm *membrane, centrifuged and filtered using a* 0.2 µm *membrane, filtered using a* 0.45 µm *membrane only, and filtered using a* 0.45 µm *membrane and then centrifuged at* 60 000 × *g. The absorbance was measured for solutions diluted 80 times, but the concentration of the mother solutions is shown here on the* x*-axis. The calibration curve (squares) was obtained using suspensions of non purified protein, and performing a linear fit.*

Together with a visual estimation of the turbidity, and with the experimental practicality, these results were used to determine the most relevant purification protocol. Therefore, because of the low decrease in protein content and the transparency of the final purified protein suspension, it was decided to first centrifuge at 60 000×g the protein solution and then filter it through a membrane with a pore size of 0.45 µm.

This protocol applied to the preparation of a solution with a protein powder content of 5 %(wt) yielded a caseinate concentration of 4 %(wt) after purification. Because the protein powder contains 90 %(wt) protein, a caseinate concentration closer to 4.5 %(wt) would have been expected. The nature of the protein removed in the process is unclear, but it is thought that large caseinate aggregates are present in solution and they sediment during centrifugation.

This preparation protocol leads to a significantly higher decrease in concentration than in previous studies. Indeed, in one study, a purification process using a similar centrifugation and filtration through a membrane with a pore size of only 0.22 µm caused a decrease of only 5 % of the initial concentration [110]. This discrepancy may be related to the variation in protein aggregation state in commercial caseinate, associated with the calcium content of the different batches [108].

The concentrations estimated here however do not take into account the moisture and residues in the commercial powder, and are thus only rough approximations. In order to measure the concentration without relying on calibration curves, that can be affected by the choice of the standard and its turbidity, the refractometry technique was preferred.

4.3.2 Refractometry to measure the protein concentration after preparation

To measure the concentrations of the protein solutions after the preparation protocol has been completed, their refractive index n was measured. By using Equation 4.2, with $dn/dc = (0.189 \pm 0.003)\,\mathrm{mL} \cdot \mathrm{g}^{-1}$, the concentration in $\mathrm{g} \cdot \mathrm{mL}^{-1}$ could by calculated from n.

This concentration could be compared with the estimated weight fraction obtained by the absorbance measurement. These results are presented on Figure 4.4.

The concentration in $\mathrm{g} \cdot \mathrm{mL}^{-1}$ appears proportional to the estimated weight fraction with a constant of variation of $0.88\,\mathrm{mL} \cdot \mathrm{g}^{-1}$. This constant is not equal to the protein content in the commercial powder of sodium caseinate because the units are different, but the figures are in good agreement, considering that the concentration in $\mathrm{g} \cdot \mathrm{mL}^{-1}$ takes into account the progressive increase of density as the protein solution becomes more concentrated.

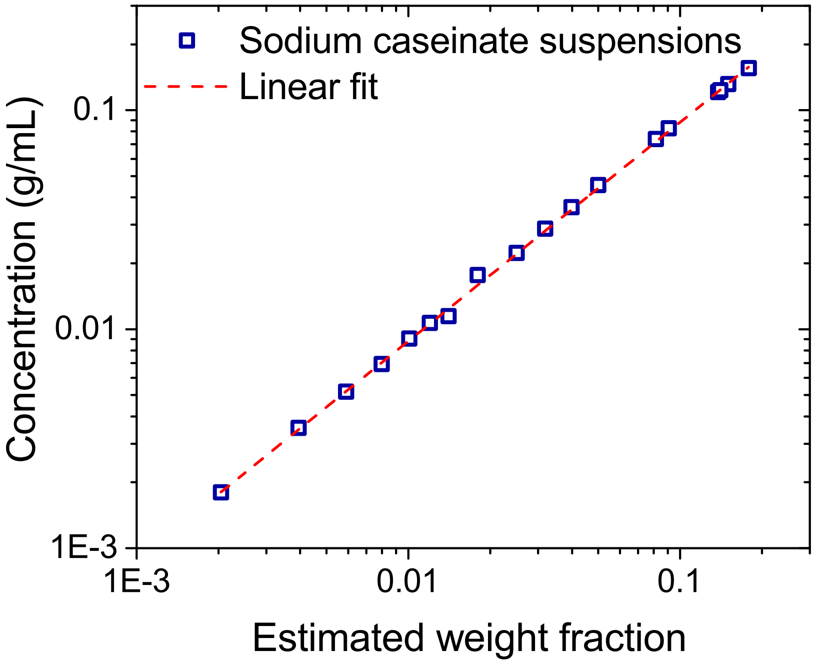

Figure 4.4 *Concentration* ($\mathrm{g \cdot mL^{-1}}$) *of suspensions of sodium caseinate calculated via refractometry as a function of their weight fraction as estimated during preparation. The dotted line denotes a linear fit of equation* $y = 0.88 \times x$.

4.4 Separation of the droplets from the emulsion and characterisation

The preparation protocol for pure dispersions of protein-stabilised droplets includes the separation by centrifugation of the droplets, as detailed in Chapter 3. During the centrifugation, performed at very high speed (corresponding to a force of $2.3 \times 10^5 \times g$) over 16 h, the droplets migrate to the top of the sample.

The appearance of the obtained cream, or dense paste of droplets, is unusual and is described here. In addition, its concentration in droplets and density are estimated. Finally, the surface coverage of the droplets is briefly discussed.

4.4.1 Formation of a transparent layer during centrifugation

At the end of the centrifugation, the formation of an unusual transparent layer of cream was observed, below the expected white cream layer of concentrated droplets. Here we detail the observation of this phenomenon, the characterisation of the two layers, and we provide some qualitative clues as to why this may happen.

Observation

This layered formation in the dense droplets after centrifugation is shown in Figure 4.5. The layer that displays some transparency also displays some change in colour as a function of the illumination angle. Indeed, it appears blue when looking at the scattered light, and red when looking at the incident light.

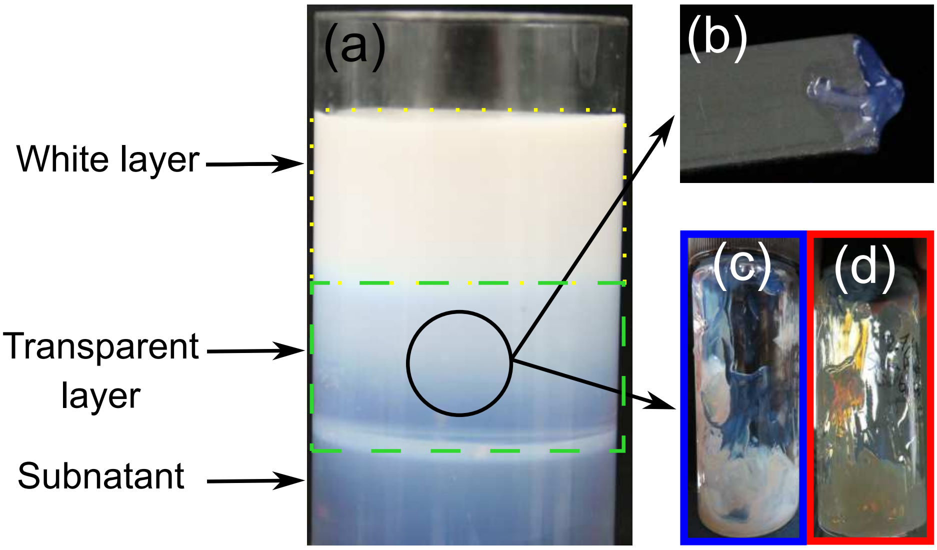

Figure 4.5 *Heterogeneous supernatant after ultra-centrifugation of sodium caseinate-stabilised o/w emulsion.*
(a) Two distinct layers of cream: (yellow dots) a white layer at the top, and (green dashes) a transparent layer at the bottom. Below, the interface with the subnatant is visible by a turbid rim containing oil droplets. (b) A small amount of the transparent layer is exhibited on a spatula. (c) The transparent layer has a blue hue when illuminated from the side, and (d) an orange hue when the light shines through it.

This behaviour is a signature of the Rayleigh scattering occurring in the dense layer of droplets. Indeed the shorter wavelengths corresponding to the blue light are completely scattered away from the incident angle, leaving only the longer wavelengths corresponding to the red light. The same scattering pattern is observed when the protein-stabilised droplets in the transparent paste are in dilute dispersion.

A similar Rayleigh scattering has been observed for droplets of radius around 100 nm [137]. In this intermediate optical regime, the optical properties of these droplets are dependent on their refractive index and concentration. The striking observation here is the sharp transition between a transparent layer and a white layer, where multiple scattering dominates.

A closer observation of this transition in another geometry of centrifuge tube is presented in Figure 4.6. As can be seen, a faint blue hue is visible at the transition between white and transparent layer. When observed from the side of the tube, the full visible spectrum can even be seen at this transition.

The investigation of these interesting optical properties of the dense paste of protein-stabilised droplets is made difficult by experimental limitations. Indeed, the perfect separation of the transparent layer from the turbid layer proved to be challenging.

However, a rough separation of the two extreme layers of the supernatant plug after centrifugation could be performed. This was achieved by scraping the bottom surface for the clear soft transparent layer and the top surface for the hard turbid layer. Notably, most of the supernatant was in between these two phases. Although this technique lacks precision, it allowed characterisation of the two layers, in order to understand their difference in optical properties.

Characterisation

The two different pastes of emulsion droplets thus obtained by scraping the two sides of the supernatant plug after centrifugation were analysed. Because light scattering depends on the size and concentrations of particles in both pastes, the characterisation was focused on these two aspects.

First, the concentration of droplets was determined by measuring the moisture content of the pastes. The two samples were dried in the oven at 70 °C with a vacuum of 800 mbar for 24 h, and the moisture content was then calculated as the weight loss upon drying.

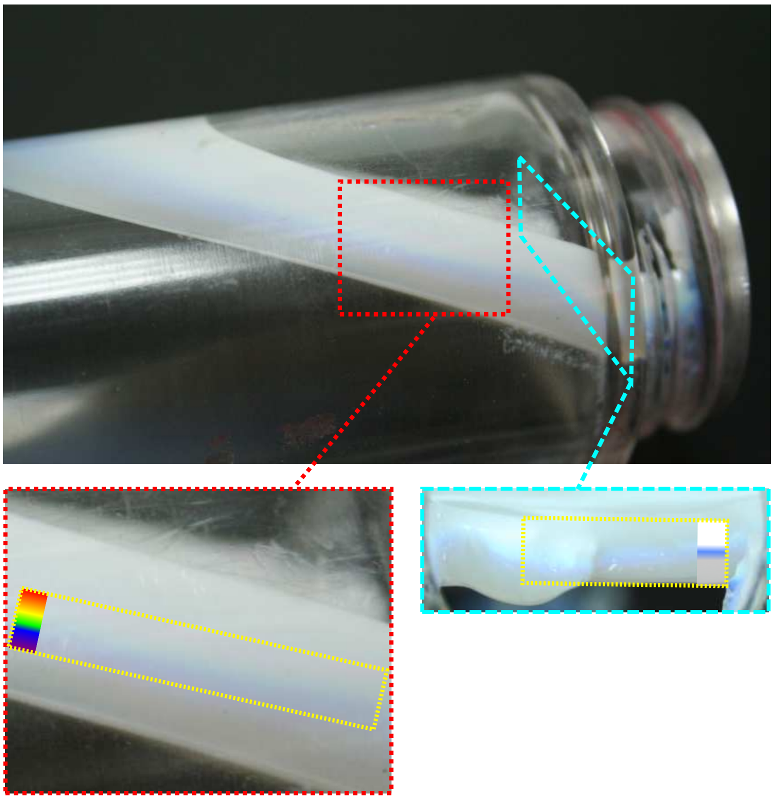

Figure 4.6 *Transition of the optical properties in the heterogeneous supernatant after ultra-centrifugation of sodium caseinate-stabilised o/w emulsion.*
Cyan dashes: the transition between the white and the transparent layer is observed from accross the tube and a blue hue is observed.
Red dots: looking closer at the transition from the side of the tube, the full visible spectrum can be seen.
The yellow frames and colour gradients are indicated as guides for the eye.

It appeared that the water content differs significantly in the two layers of the supernatant. Indeed, the upper hard turbid layer contains 30 % (wt) water, while the water content of the lower soft transparent layer is 42 % (wt). This seems to indicate that the concentration of droplets is not the main driver to the discrepancy in optical properties. Indeed, at a fixed particle size, there is more scattering at higher concentration of particles.

The size distributions of the soft transparent layer was also measured using the commercial SLS apparatus Mastersizer, and compared to the size distribution of all the droplets. These results are presented in Figure 4.7.

As can be seen, the transparent layer presents a narrower size distribution, and

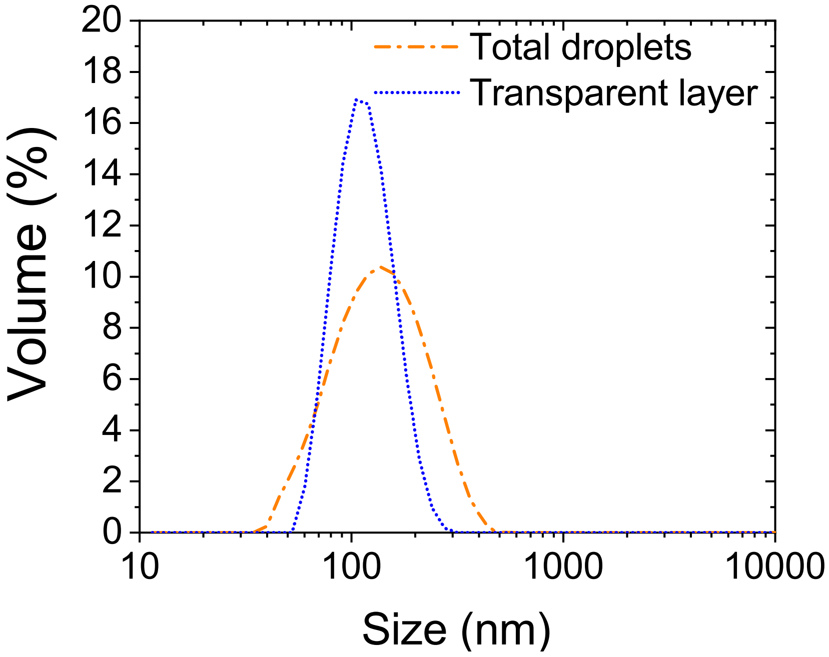

Figure 4.7 *Size distributions of protein-stabilised droplets after centrifugation, as presented in Figure 4.5: the lower transparent layer was collected separately and the size distribution of the droplets it contains (dotted line, in blue) is compared to the droplets in the entire plug (dashed line, in orange).*

is centred over smaller droplet sizes, than all the droplets. This is expected as the centrifugal force varies with the radius of the particles, and thus allows a fractionation by size to a certain extent [138].

Possible explanation

It is possible to qualitatively explain these differences by considering the distinct optical regimes of the two layers, in relation to the concentration and size of the scattering elements. It is interesting to look at the changes in light scattering of colloidal suspensions as the concentration in particles increases.

First, at low concentration of droplets, every droplet scatters in an uncorrelated fashion with respect to the others, and the scattering coefficient is the sum of the coefficients for each particle. This is the approximation of independent scattering. But upon increasing the volume fraction of droplets, the system ceases to be described by this approximation. Collective effects then occur and there is interference between the light rays.

If the concentration is subsequently further increased, the interference between scattered electromagnetic waves becomes completely destructive and the scattered light reaches zero. In terms of the path for the electromagnetic wave, this means that the scattering mean path (*i.e.* the distance covered by the photons between two scattering events) becomes greater than the typical length scale of the medium (here the diameter of the centrifuge tube) [139]. In this regime, the medium is said to be optically homogeneous and appears transparent. An increase in concentration can thus lead to a transition in the optical properties of a medium from opaque to transparent. This is similar to the increased transparency that has been observed for nanoemulsions at high concentration [137].

This transition is however dependent on other parameters that influence light scattering, such as the refractive index and size of the scatterers. It is thus possible that the discrepancy in size between the particles in the transparent layer and the opaque layer leads the optical homogenisation of the dense emulsion at different concentrations. In that case, the opaque layer, despite being at a higher concentration, scatters completely the incident light; while the transparent layer is optically homogeneous and the scattered light is annihilated by destructive interference of the electromagnetic waves.

Because of the number of parameters involved in the phenomenon of light scattering, this simple phenomenological approach would require some qualitative analysis to be validated. A more thorough experimental investigation, using more accurate optical techniques such as neutron scattering, would also be required to reach a better understanding of the differences in optical properties of the two layers of dense droplets, as has been done for surfactant-stabilised dense nanoemulsions [137, 140].

In the rest of this study, the plug of dense droplets was mixed with a spatula so that the optical and mechanical properties of the paste were uniform. In that case, a white opaque paste was obtained.

4.4.2 Concentration of droplets and density of dense suspension after centrifugation

After centrifugation, the plug of concentrated droplets displayed in Figures 4.5 and 4.6 was mixed to give a stock of dense droplets. This stock could then be redispersed in water or in a protein-suspension, without sign of irreversible bridging flocculation or coalescence, to form emulsions of controlled compositions.

The concentration of this paste was estimated by drying it and measuring the weight loss, assuming that it indicates the moisture content. More precisely, the paste was diluted in a controlled manner, by a weight factor a, to obtain a liquid, the density ρ_{dilute} of which was measured using a densitometer (DMA 35, Anton Paar). A small amount of diluted sample, of known mass m_{dilute}, was then deposited in 3 glass vials and dried in the oven at 70 °C with a vacuum of 800 mbar for 24 h. After 24 h the dry matter mass m_{dry} was stabilised and subsequently measured.

The concentration of the stock solution (c_{stock} in $\mathrm{g \cdot mL^{-1}}$) could thus be calculated with the equation:

$$c_{stock} = a \times \rho_{dilute} \times \frac{m_{dry}}{m_{dilute}} \tag{4.3}$$

It was subsequently found that the stock of protein-stabilised droplets formed using the microfluidiser, as described in Chapter 3 is at the concentration of $c_{stock} = (0.52 \pm 0.01)\,\mathrm{g \cdot mL^{-1}}$. This indirect determination of the concentration of droplets is less accurate than the refractometry measurements performed to estimate the concentration of protein solutions. This error is then propagated when emulsions of different compositions are prepared.

In order to calculate the concentration of the emulsions after dilution by addition of a known mass of solvent, the density of the stock of droplets was also determined. This was estimated by weighting a plastic vial of 7 mL filled with the paste. The filling was performed progressively and the vial was tapped after each addition of paste to avoid entrapped air bubbles within the vial.

The actual volume of such vial was independently measured to be 8.06 mL, which yielded a density of the droplet stock of $\rho_{stock} = 0.987\,\mathrm{g \cdot mL^{-1}}$. This value has to be compared with the density of the oil used $\rho_{stock} > \rho_{oil} = 0.956\,\mathrm{g \cdot mL^{-1}}$.

The density value thus takes into account the concentration of droplets and the presence of adsorbed sodium caseinate at their interface.

The concentration in droplet c_{drop} (in $\mathrm{g \cdot mL^{-1}}$) of the emulsions prepared using this stock, either suspensions of pure droplets or mixtures, could then be estimated using this characterisation of the droplet stock. For each sample, it was calculated to be:

$$c_{drop} = c_{stock} \frac{\frac{m_{stock}}{\rho_{stock}}}{\frac{m_{stock}}{\rho_{stock}} + \frac{m_{solvent}}{\rho_{solvent}}} \tag{4.4}$$

4.4.3 Surface coverage of droplets after emulsification

It is difficult to estimate the amount of protein adsorbed at the oil/water interface after emulsification. The surface coverage of the adsorbed layer is in general determined by separating the oil droplets from the emulsion and then measuring the concentration of protein still in solution; the subtraction of this quantity from the total protein content gives an estimation of the protein concentration at the interface [117].

Here, there are practical difficulties in performing this technique. Indeed, after ultracentrifugation of the emulsion, a small fraction of droplets, presumably at the lower end of the size distribution, is either not separated or easily resuspended in solution when the liquid subnatant and solid supernatant are collected. As a consequence, after removal of the droplets, the protein suspension still contains oil droplets that scatter light and make it turbid, thus ruling out optical techniques for measuring the protein concentration.

We can therefore make the assumption that the surface coverage here is similar to the one measured for similar sodium caseinate-stabilised emulsions in the literature. The surface coverage is assumed to be around $3.0\,\mathrm{mg \cdot m^{-2}}$ [98, 117, 118]. It has to be noted however that the surface coverage was found to be dependent on the protein concentration, and is probably modified by the nature of the oil and the curvature of the very small droplets, so this is an approximate value.

In Chapter 5, an indirect method for estimating the amount of unadsorbed droplets, and thus the surface coverage, from the study of the viscosity of the emulsions will be discussed.

4.4.4 Composition of the droplets

The protein-stabilised droplets can be represented as core-shell particles with an oil core and a soft shell of adsorbed proteins, as will be discussed in Chapter 5. The relative contribution of each component to the weight of a single droplet can be estimated. Indeed, the weight of protein adsorbed to the droplets can be calculated using the surface coverage and the size of the droplets and compared to the total weight of droplets in the emulsion.

The total surface of the droplets S_{tot} in the emulsion can be written:

$$S_{tot} = \frac{3 \times m_{oil}}{\rho_{oil} \times R_{drop}}$$

where m_{oil} is the mass of oil in the emulsion, ρ_{oil} is the density of the oil used and R_{drop} is the radius of the oil core. For 1 kg of emulsion prepared as described in Chapter 3 and for a droplet size of $R_{opt} = 65\,\text{nm}$, as will be presented in the next section, a total surface of $S_{tot} = 9.6 \times 10^3\,\text{m}^2$ is found.

The weight of adsorbed proteins $m_{adsorbed\ prot}$ can then be calculated by multiplying the total surface with the surface coverage, and for 1 kg of emulsion $m_{adsorbed\ prot} = 29\,\text{g}$ is obtained.

Finally, the weight fraction of oil in the droplets $[oil]_{droplet} = m_{oil}/m_{droplet} = m_{oil}/(m_{oil} + m_{adsorbed\ prot})$ can be derived. Using the previous calculations, it is estimated that $[oil]_{droplet} = 0.87$, ie 87 % of the weight of the droplets comes from their oil content, while the adsorbed proteins account for the remaining 13 % of the weight. This is why the density of the droplets is higher than the oil density, making the separation of the droplets by centrifugation more difficult, as discussed in Chapter 3.

4.5 Size of proteins and droplets

An important parameter when studying colloidal systems is the size of the particles of the dispersed phase. The size distributions were determined for both the protein-stabilised droplets and the naturally-occurring protein aggregates.

4.5.1 Size distributions of droplets by Static and Dynamic Light Scattering

After centrifugation, the dense paste of concentrated droplets were redispersed in water to make pure droplet suspensions. Because the droplets were thus separated from the unadsorbed proteins, the characterisation of their size could be performed more precisely than before centrifugation, when they are in mixtures.

Light scattering techniques were used to measure the size of the protein-stabilised droplets prepared as described in Chapter 3. The size distributions thus measured using both DLS and SLS are displayed in Figure 4.8.

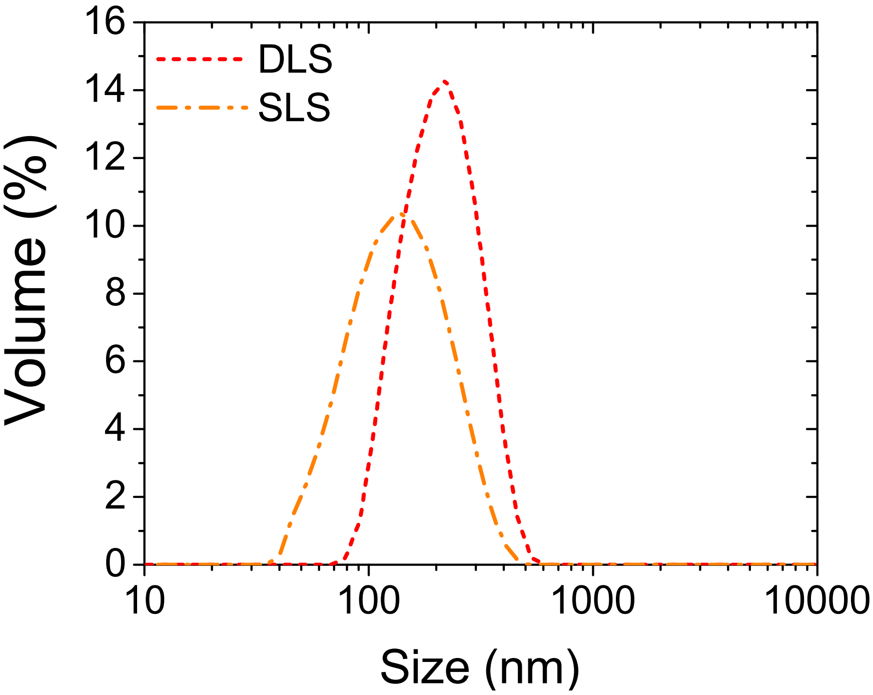

Figure 4.8 *Size distributions of protein-stabilised droplets (same droplets at two different concentrations) measured by Dynamic Light Scattering (dot line, red) and by Static Light Scattering (dash dot line, orange). Mean sizes (volume mean diameters D_{43}): Mastersizer* (130 ± 63) nm *Zetasizer* (221 ± 98) nm.

As can be seen, the results given by SLS and DLS differ slightly. Indeed, the two distributions do not correspond because of the different definitions for the particle size in each case. The DLS measurement provides the hydrodynamic size D_h, while the size measured by SLS represents the optical cross-section D_{opt} of the droplets. The hydrodynamic size D_h takes into account the adsorbed layer of proteins around the oil and its influence on the diffusion properties of the droplet, while D_{opt} is only given by the scattering of the oil core of the droplet. Thus the size distribution given by DLS is shifted towards larger sizes with respect to the one obtained by SLS.

For both definitions of the particle size, the distribution can be described by the volume mean diameter D_{43} and its standard deviation, that are obtained by averaging the size distribution. Here we find that for the hydrodynamic size measured by DLS $D_{h,43} = (221 \pm 98)\,\mathrm{nm}$, and for the optical cross-section measured by SLS $D_{opt,43} = (130 \pm 63)\,\mathrm{nm}$. The difference in average size can be seen as an indication of the hydrodynamic thickness of the adsorbed layer of proteins. This point will be discussed more in details in Chapter 5.

As each size distribution corresponds to a different definition of the size of colloidal particles, both will be used for different physical considerations in the next chapters. Indeed, the rheological properties of colloidal suspensions and gels are influenced by the hydrodynamic size D_h; while the surface coverage is determined by the size of the oil core that can be estimated using the optical cross-section D_{opt}.

It has to be noted that the protocol used for the emulsification may produce very small droplets (around 50 nm), as has been observed in previous studies [141]. In that case, these small droplets would not be readily observable because of the scattering of larger droplets, but would contribute to the rheological properties of the droplet suspensions at high concentrations. This will be discussed in Chapter 5.

4.5.2 Size distribution of proteins by Field Flow Fractionation

The commercial DLS setup Zetasizer was not successful in determining the size distribution of sodium caseinate as the presence of large aggregates (around 100 nm) meant that it was not possible to measure the expected smaller naturally occurring structures (around 20 nm) [63, 105, 110]. A preliminary fractionation by size of the protein solution was thus required. A common technique for this separation is Size Exclusion Chromatography [109], but Field Flow Fractionation was favoured here as it does not require the sample to be filtered before separation.

This technique provides the variation of concentration in the eluant using the intensity given by light scattering at any point in time. In addition it gives the variation of the hydrodynamic radius R_h and radius of gyration R_g as a function of the elution time. These results are displayed in Figure 4.9. They have to be integrated to give the distribution of concentration over the range of sizes.

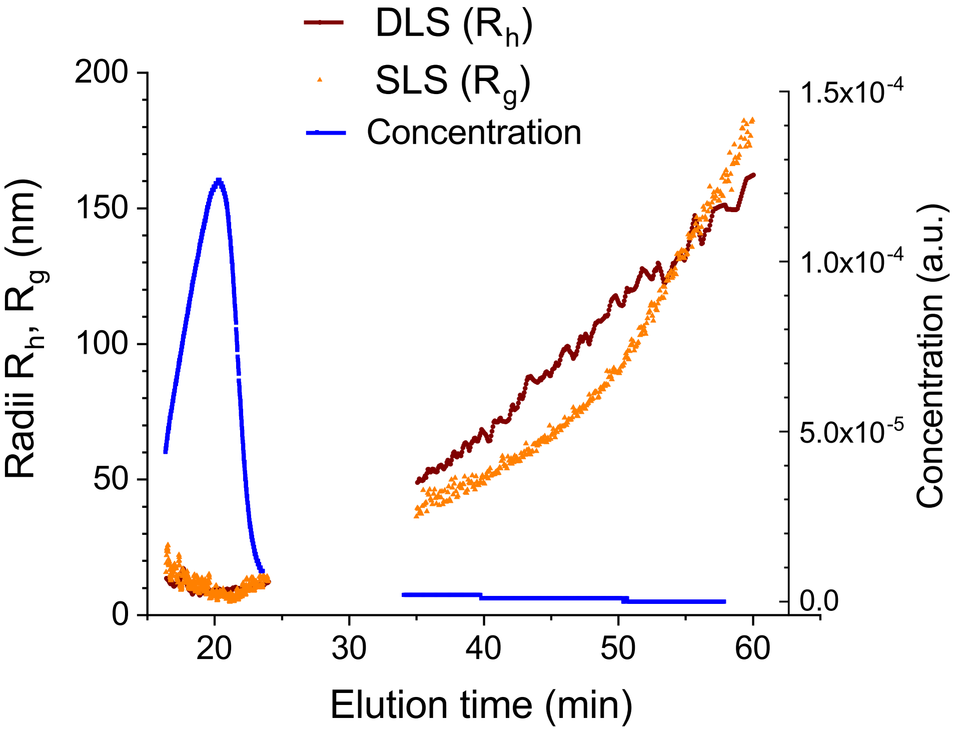

Figure 4.9 *Elution profile of sodium caseinate using Flow Field Fractionation. This data was provided by PostNova Analytics Ltd. SLS and DLS setups are placed inline and allow to measure the concentration (from the intensity of the SLS), gyration radius R_g (from the scattering profile of the SLS), and hydrodynamic radius R_g (from the temporal fluctuations of the DLS).*

This was performed for both radii following the same protocol. First, the positions of the bins for the size distribution were determined, using a logarithmic distribution: $R[j] = 10^{log(R)+x*j}$ where x is the bin size and j is the bin number. Then, for each data point of the curve the bin j to which the size R belongs was identified. Finally, for each j, the concentrations of all the protein aggregates of which the measured size belonged to the bin j were summed and normalised to obtain the size distribution.

The method described here for the calculation of size distributions was applied to the sizes measured both with Zetasizer (R_h) and with MALS (R_g). The resulting size distributions using a bin size of $x = 0.01$ (in log scale) are displayed on Figure 4.10.

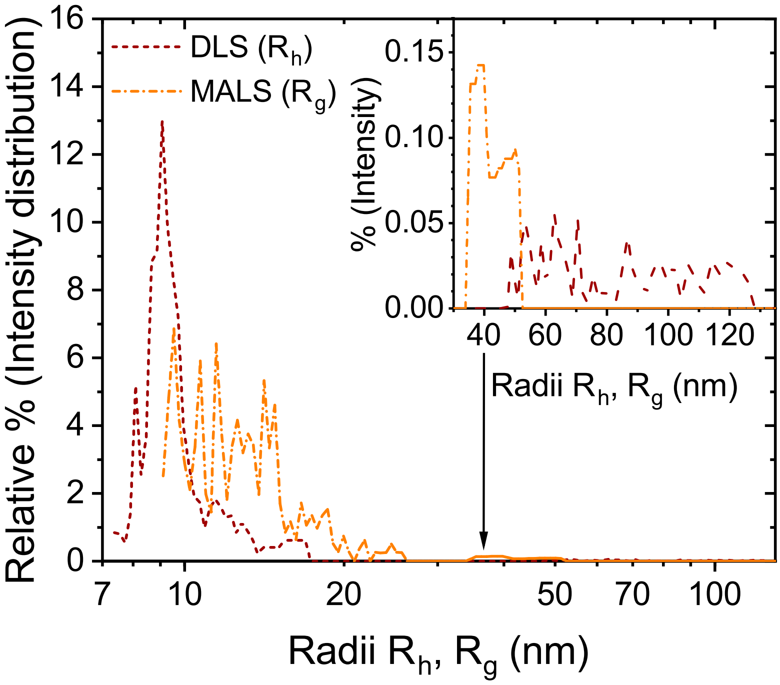

Figure 4.10 *Size distributions of sodium caseinate as prepared by the method described in Section3.2. The sample was fractionated by Asymetric Flow Field Flow Fractionation (kindly performed by PostNova Analytics Ltd), and the sizes were measured online by Dynamic Light Scattering (dot line, red) and by Multi Angle Light Scattering (dash dot line, orange).The inset is a zoom of the small fraction of proteins that makes bigger aggregates.*

As can be seen, the resulting suspensions of sodium caseinate are composed of small aggregates of a hydrodynamic radius of 11 nm at 96 %, while the remaining 4 % formed larger aggregates with a wide range of sizes (hydrodynamic radii from 40 nm to 120 nm). It is also interesting to note that the fractions of caseinate corresponding to the two regions do not have the same R_g/R_h, indicating that their structures and shapes may be different. In the first region, the hydrodynamic radius is smaller than the gyration radius, which is an indication of the elongated shape of the smaller aggregates, in good correspondence with previous studies [105, 109]. In the second region, by contrast, the aggregates have a size ratio similar to hard spheres, for which $R_g/R_h = 0.78$, so the larger aggregates are likely to be spherical.

This technique is believed to provide a more accurate image of the size distributions in sodium caseinate. Indeed, it does offer the ability to measure the sizes of each fraction independently, thus avoiding the overestimation of the bigger elements, a common problem in light scattering techniques.

Light scattering techniques were thus used to estimate the size distributions of both protein aggregates, after size fractionation by FFF, and protein-stabilised oil droplets. The sizes of the two colloidal species differ by an order of magnitude, as the droplets display an average hydrodynamic radius $R_{h,drop} = 110\,\mathrm{nm}$ while for the proteins $R_{h,prot} = 10\,\mathrm{nm}$.

4.6 Conclusion

In this chapter, the characterisation of the proteins and protein-stabilised droplets used in the next chapters was performed. The set of results obtained here will be exploited in various ways.

The concentration of the protein suspensions and of the droplet stocks will be used to prepare emulsions of precise compositions. We will see in Chapter 5 that the volume fraction is a more relevant parameter to discuss the rheological properties of suspensions and gels, so the concentration is used for the preparation of the samples, but their composition is then scaled by the volume fraction for the discussion of the results.

The average size of proteins and droplets will be used in Chapter 5 to make the parallel between the flow curves of the two types of suspension, and to justify the colloidal approach to sodium caseinate.

The size distributions of proteins and droplets will be used to analyse the viscosity behaviour of concentrated suspensions in Chapter 5. Indeed, the random close-packing of colloidal species at high concentration is influenced by their polydispersity [41, 42].

The most intriguing observation of this chapter is probably the optical heterogeneity of the dense paste of droplets obtained after ultra-centrifugation of the emulsion. Here, we suggest that this phenomenon may arise from the difference in size and concentration along the subnatant plug. This qualitative explanation could benefit from a more thorough investigation of the sample using more advanced techniques such as neutron scattering. As detailed in Chapter 3, the fractions of the paste corresponding to different optical regimes were mixed before preparing the droplet suspensions, so the droplets will only be regarded as polydisperse, and the aspect of the paste will not be dealt with in more details in the next chapters.

Chapter 5

Viscosity of protein suspensions and protein-stabilised droplets

In this chapter I study the viscosity of suspensions of varying compositions, prepared as described in Chapter 3. Gels of these suspensions will then be discussed in Chapters 6 and 7. Examining the properties of the sols is thus the first step to develop a better understanding of the emulsion gel systems.

Here I first examine the semi-dilute regime of pure suspensions of sodium caseinate and of sodium caseinate-stabilised oil droplets. An expression for the effective volume fraction can be deduced as a function of the concentration in colloidal particles. This is a necessary step to be able to draw comparisons between suspensions and gels of proteins and of droplets.

I then model the behaviour of the viscosity of each suspension as a function of the volume fraction using a model from a previous study [5] for the droplets, as well as an empirically modified version for the proteins. Mixtures containing both sodium caseinate-stabilised droplets and unadsorbed sodium caseinate in various amounts are then prepared.

I subsequently combine the descriptive models of the viscosity of the pure suspensions to develop a semi-empirical model that predicts the viscosity of the mixtures as a function of their composition. This model provides good predictions of the viscosity of sodium caseinate-stabilised emulsions or helps identifying their composition, depending on which parameter is known.

Finally, I look at the most concentrated samples of suspensions of pure proteins, droplets and of mixtures. Those do not behave as Newtonian liquids, but exhibit a decrease in the viscosity with the shear rate, called shear thinning. The characterisation of this behaviour also helps the understanding of the structure and interactions of the colloidal suspensions.

5.1 Introduction

Many food products such as mayonnaise, ice cream, and cheese involve protein-stabilised emulsions either during their fabrication or as the final product. Because of their ability to strongly adsorb at oil/water interfaces and to stabilise oil droplets by steric and electrostatic repulsion, water-soluble proteins are widely used as efficient emulsifiers in food products. It has been shown that proteins do not completely adsorb at the interface, and that a residual fraction of protein is suspended in the continuous phase after emulsification [98, 117]. Protein-stabilised emulsions are thus mixtures of protein-stabilised droplets and suspended proteins. Understanding the contributions of these two components to the properties of the final emulsion remains a challenge.

Sodium caseinate is used here to stabilise emulsions because of its outstanding properties as an emulsifier, as discussed in Chapter 2. It has been established that sodium caseinate is not present as a monomer in suspension, but rather in naturally-occurring small aggregates that have been characterised as elongated and their size estimated to be around 20 nm, both in the literature [63, 105, 109] and in the results presented in Chapter 4. The viscosity behaviour of sodium caseinate in suspension as a function of concentration shows similarities with hard-sphere suspensions at relatively low concentrations. But at higher concentrations, over $c > 130\,\mathrm{g} \cdot \mathrm{L}^{-1}$, the viscosity continues to increase with a power-law rather than diverging [63, 110] as would be expected for a hard sphere suspension [27]. This behaviour is not dissimilar to that of the soft colloidal particles [3] presented in Chapter 2. In this chapter, the rheology of protein suspensions is thus examined within the framework of soft colloidal particles.

Similarly, the droplets in protein-stabilised emulsions can be considered as colloidal particles with some degree of softness, because of their external shell of adsorbed proteins [119]. Modelling proteins and protein-coated droplets in this way ignores protein-specific elements [142, 143], but it provides a convenient theoretical framework to separate and discuss the contributions of both suspended sodium caseinate and the droplets to the viscosity of emulsions using a unifying approach for the two components.

The aim of this chapter is to present a predictive model of the viscosity of protein-stabilised emulsions, that takes into account the presence and behaviour of both the protein stabilised droplets and the unadsorbed protein. A first step is to characterise separately the flow behaviour and viscosity of suspensions of purified protein-stabilised droplets, and of protein suspensions over a wide range of concentrations. This also allows a critical assessment of the soft colloidal approach. These components are then combined to form mixtures of well-characterised composition and their viscosity is compared to a semi-empirical model. Finally, the shear thinning behaviour of some samples is discussed as it confirms the apparent colloidal nature of the components of the emulsions and protein suspensions.

5.2 Materials & Methods

5.2.1 Preparation of the samples

Suspensions of pure sodium caseinate (protein suspensions), pure sodium caseinate-stabilised droplets (droplet suspensions), and mixtures of sodium caseinate and sodium caseinate-stabilised droplets were prepared at a wide range of concentrations, as described in Chapter 3.

5.2.2 Rotational rheology

Rotational rheology measurements were performed using a stress-controlled MCR 502 rheometer (Anton Paar) and a Couette geometry (smooth bob and cup CC17, inner radius 16.66 mm, outer radius 18.08 mm yielding a 1.42 mm tool gap, gap length 25 mm) at 25 °C, the setup used here is displayed in Figure 5.1. For each sample, three measurements are performed and averaged to obtain the flow curve. The values of viscosity on the plateau at low shear are averaged to determine the zero-shear viscosity. Viscosity measurements were performed at different concentrations for protein suspensions, protein-stabilised droplet suspensions, and

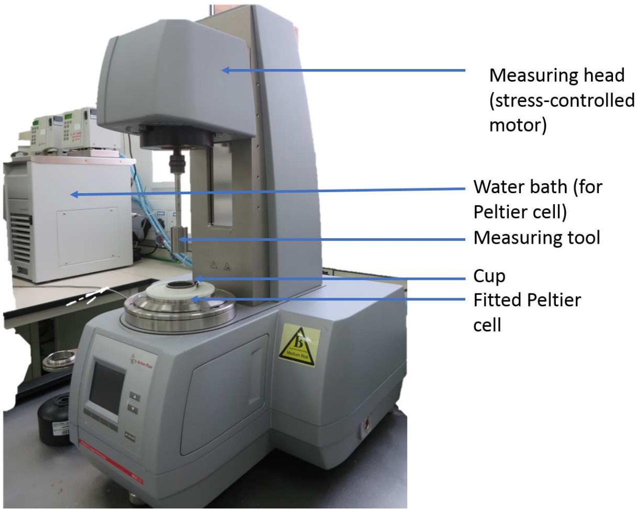
Measuring head (stress-controlled motor)
Water bath (for Peltier cell)
Measuring tool
Cup
Fitted Peltier cell

Figure 5.1 *Rheology setup: stress-controlled MCR 502 (Anton Paar), Couette geometry and temperature-controlling Peltier cell.*

mixtures.

5.3 Viscosity of suspensions in the semi-dilute regime: determination of the volume fraction

The mass concentration (in $\mathrm{g \cdot mL^{-1}}$) is a sufficient parameter to describe the composition in the case of one suspension, but only the use of the volume fraction of the suspended particles allows meaningful comparisons between protein assemblies and droplets. In the framework of soft colloids, the effective volume fraction ϕ_{eff} of a colloidal suspension can be determined by modelling the viscosity in the semi-dilute regime.

Flow curves $\eta(\dot{\gamma})$ describe the dynamic viscosity behaviour η of a sample at various shear rates $\dot{\gamma}$ at 25 °C. Flow curves for suspensions of proteins and droplets are shown in Figure5.2.

As can be seen, for most samples, the rheological behaviour is Newtonian, and the viscosity is thus averaged. The most concentrated samples present some shear thinning behaviour. In that case, the viscosity value at the plateau at low shear of these flow curves indicates the zero-shear viscosity η_0, and this value is used to calculate the relative zero-shear viscosity η_0/η_s, where η_s is the solvent viscosity (in this study $\eta_s = (8.7 \pm 0.3) \times 10^{-4}\,\mathrm{Pa \cdot s}$ for deionised water).

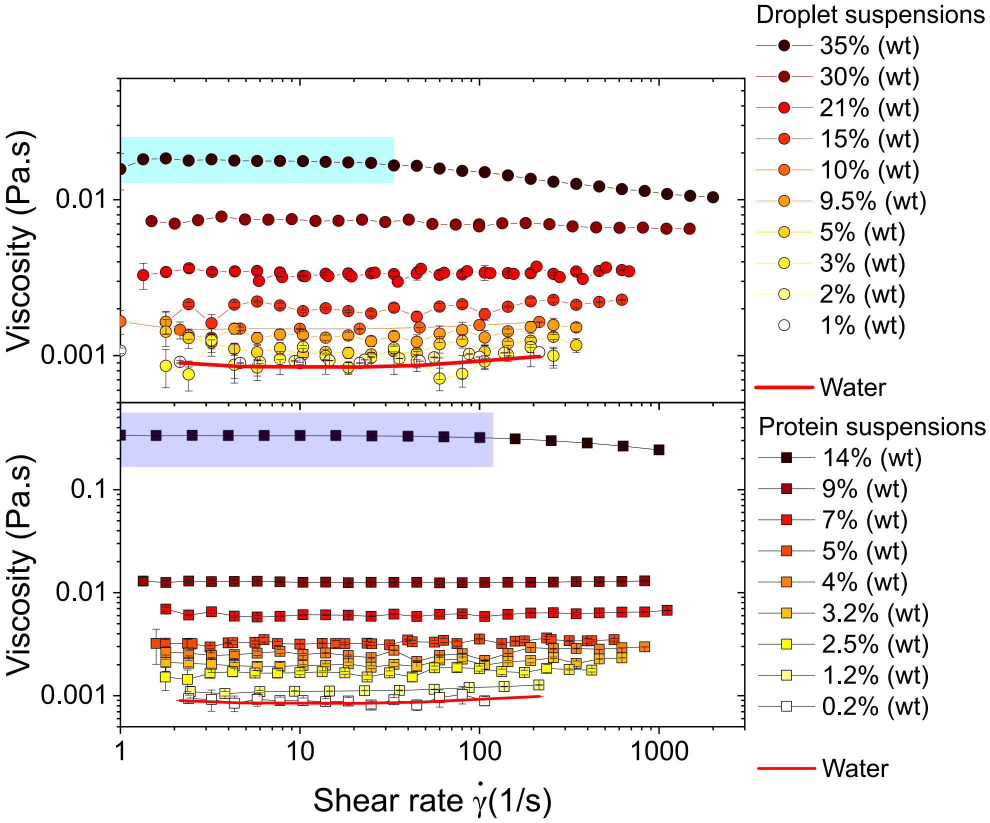

Figure 5.2 *Flow curves of sodium caseinate-stabilised droplets (top, circles) and sodium caseinate suspensions (bottom, squares) at several concentrations. These curves are the average of 3 measurements, and the error bars indicate the reproducibility. For the shear thinning samples, only the zero-shear viscosity* η_0 *is considered, as indicated by the shaded area. A more thorough study of their behaviour is presented in Section 5.6.*

The relative zero-shear viscosities of semi-dilute samples are displayed in Figure 5.3 as a function of the mass concentration in protein or droplets. As can be observed, protein suspensions reach a higher viscosity at a lower weight fraction than droplet suspensions. This is because the protein is highly hydrated and swollen, and so occupies a greater volume per unit mass than do the droplets, where the main contributor to the occupied volume is the oil core.

Some studies on sodium caseinate [65] used semi-empirical hydrodynamic models to determine the voluminosity of proteins but in this work sodium caseinate is assumed to be a non-interacting hard sphere in the semi-dilute regime, as in more recent studies [105, 110]. Consequently, two methods for the determination of volume fraction of hard-sphere suspensions can be used.

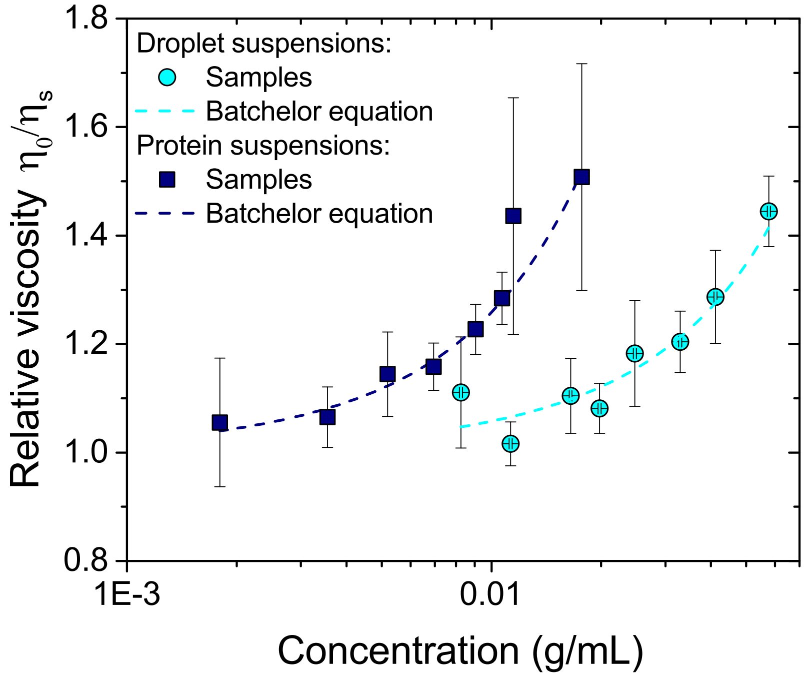

Figure 5.3 *Relative viscosity of sodium caseinate suspensions (squares, navy blue) and sodium caseinate-stabilised droplets (circles, cyan) as a function of the concentration. The lines denote Batchelor model for hard spheres in the semi-dilute regime, Equation 2.3. The error bars represent the standard error upon averaging the viscosity plateau for the three measurements.*

5.3.1 Estimation of the volume fraction using the intrinsic viscosity

The intrinsic viscosity $[\eta]$ is defined as the limit of the specific viscosity $\left(\frac{\eta_0}{\eta_s} - 1\right)/c$ at low concentration:

$$[\eta] = \lim_{c \to 0} \frac{\frac{\eta_0}{\eta_s} - 1}{c} \tag{5.1}$$

This definition comes from the study of non-charged long-chain polymers by Huggins [144], where the following expression was derived for the specific viscosity of polymer solutions at low concentration:

$$\frac{\frac{\eta_0}{\eta_s} - 1}{c} = [\eta] + k_H[\eta]^2 c \tag{5.2}$$

where k_H is the Huggins constant, and where low concentration was empirically defined by suspensions for which $\eta_0/\eta_s \leq 2$. Although Equation 5.1 was originally derived for polymers, it has been empirically shown that it can also be applied in a colloidal framework. It is thus assumed to be valid for pure suspensions of proteins and of protein-stabilised droplets.

Importantly, however, Equation 5.1 is not valid for polyelectrolyte suspensions, for which a divergence to infinity of the specific viscosity has been observed at very low concentrations [145]. Sodium caseinate in suspension is charged, but, as it can be observed in Figure 5.4, does not display such unusual behaviour. This peculiarity is possibly due to the presence of mineral salts acting as counter-ions and screening the protein charges. As a result, Equation 5.1 is considered here to be valid for the two types of colloidal suspensions studied.

$[\eta]$ can thus be determined graphically by plotting the specific viscosity as a function of the concentration $\left(\frac{\eta_0}{\eta_s} - 1\right)/c = f(c)$.

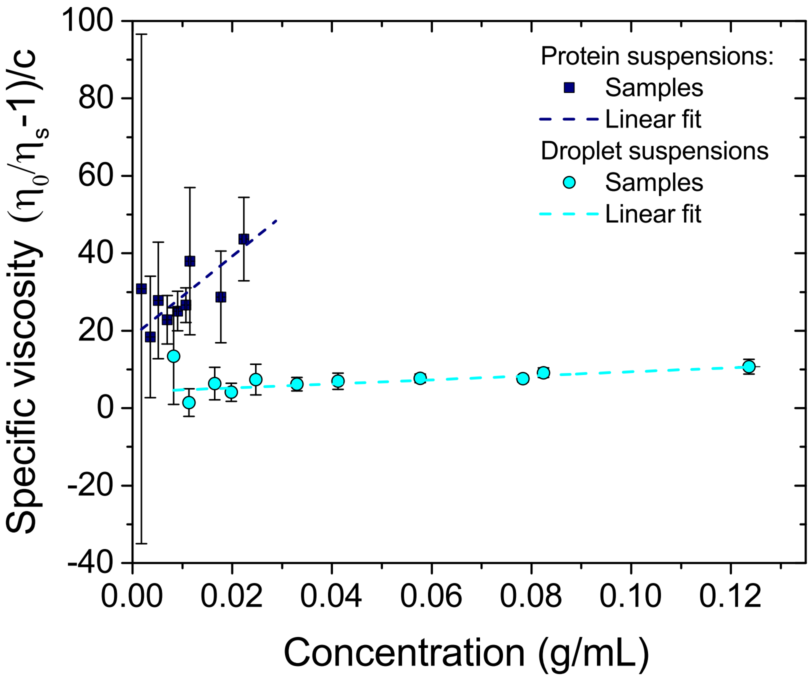

Figure 5.4 *Specific viscosity* $\left(\frac{\eta_0}{\eta_s} - 1\right)/c$ *of sodium caseinate suspensions (squares, navy blue) and sodium caseinate-stabilised droplets (circles, cyan) as a function of the concentration. The line denotes a linear fit.*

By applying a linear fit to Figure 5.4, it is found for sodium caseinate suspensions: $[\eta]_{prot} = (18 \pm 37)\,\mathrm{mL} \cdot \mathrm{g}^{-1}$. Apart from the size of the error bars, that is discussed below, this result is in good agreement with a previous work on sodium caseinate where $[\eta]_{prot} = 16\,\mathrm{mL}\cdot\mathrm{g}^{-1}$ [110]. Similarly, the same protocol applied to the specific viscosity of the droplets gives $[\eta]_{drop} = (4.1 \pm 0.8)\,\mathrm{mL}\cdot\mathrm{g}^{-1}$.

The value of the intrinsic viscosity $[\eta]$ of a type of suspension can then be used to estimate the effective volume fraction ϕ_{eff}. Indeed, the following equation relating ϕ_{eff} with the concentration c can be written [146]:

$$\phi_{eff} = \frac{[\eta]}{2.5}c \tag{5.3}$$

The underlying assumption when Equation 5.3 is applied to sodium caseinate suspensions is that the naturally occurring aggregates are spherical. This is an approximation as some studies found the aggregates to be elongated to some extent [63, 105], and their exact structure is still under discussion.

When the effective volume fraction $\phi_{eff,prot}$ is an estimation of the space filled by particles considered as spheres, the expression $\phi_{eff,prot} = \frac{[\eta]_{prot}}{2.5} \times c = 7.4 \pm 1.5 \times c$ is found. Similarly, for a suspension of spherical protein-stabilised droplets, $\phi_{eff,drop} = 1.7 \pm 0.3 \times c$.

Finally, the estimation of the volume fractions determined with this method seem to lack precision. Indeed, the definition of the intrinsic viscosity implies a divergence to infinity of the error bars at low concentrations, which in turn limits the accuracy of the estimation of the intrinsic viscosity. The problem here is thus that the method for fitting the data lacks precision. In the following section, another form of Equation 5.2 is used, that makes possible a more accurate fitting protocol.

5.3.2 Estimation of the volume fraction using Batchelor model

The previous section presented a method to estimate the volume fraction using viscosity measurements of colloidal suspensions at different concentrations through the determination of the intrinsic viscosity $[\eta]$. However, this method showed a lack of precision. Another analysis of the same data can be carried out that instead of calculating the specific viscosity of colloidal suspensions, uses the relative viscosity to estimate the effective volume fraction. The viscosity behaviour of each type of suspension as a function of the volume fraction ϕ in the semi-dilute regime can be described by a theoretical model such as Batchelor's equation [29]:

$$\frac{\eta_0}{\eta_s} = 1 + 2.5\phi_{eff} + 6.2\phi_{eff}^2 \tag{2.3}$$

This involves assuming that the particles in the suspension of interest do not have specific interparticle interactions in this regime, and can be accurately described as hard spheres.

In addition, as a first approximation, the effective volume fraction ϕ_{eff} of soft particles in suspension is assumed to be proportional to the weight concentration c:

$$\phi_{eff} = k_0 \times c \tag{5.4}$$

Where k_0 is a constant expressed in $\mathrm{mL \cdot g^{-1}}$. This equation is combined with Equation 2.3 in order to obtain an expression for the viscosity as a function of the concentration. When applied to experimental viscosity values for suspensions of protein or droplets at concentrations in the semi-dilute regime, such an expression allows estimation of k_0. The effective volume fraction ϕ_{eff} of the suspensions can then be calculated using Equation 5.4.

When fitted to the viscosity data for pure sodium caseinate suspensions and pure emulsions, as described above, Equation 2.3 gave satisfactory fits as shown in Figure 5.3. The resulting values for k_0 were, for protein suspensions, $k_{0,prot} = (8.5 \pm 0.2)\,\mathrm{mL \cdot g^{-1}}$, and for droplet suspensions the constant was found to be $k_{0,drop} = (2.2 \pm 0.1)\,\mathrm{mL \cdot g^{-1}}$.

The protein result is in reasonable agreement with previous results, for which derivations of the volume fraction using the intrinsic viscosity gave $\phi_{eff,prot} = 6.4 \times c$ [110] and $\phi_{eff,prot} = (6.5 \pm 0.5) \times c$ [105], while osmometry measurements (at a higher temperature) gave $\phi_{eff,prot} = 4.47 \times c$ [63]. For droplet suspensions, if the droplets were purely made of a hard oil core, their voluminosity would be $1/\rho_{oil} = 1.05\,\mathrm{mL \cdot g^{-1}}$. The higher value observed can be attributed to the layer of adsorbed proteins at the surface of the droplets. This is an indication that the nano-sized droplets can be modelled as core-shell particles, as discussed below.

These results are in good agreement with the results obtained using the intrinsic viscosity, with an increased precision. This section thus illustrated another possible interpretation of the viscosity data to determine the volume fraction from the value of the weight concentration, and the results are judged more satisfactory. The intrinsic viscosity is thus not used in the rest of this study, and the values for the effective volume fraction all derive from the application of Batchelor equation to the viscosities of semi-dilute suspensions.

5.3.3 Discussion of the scaling by the effective volume fraction

The effective volume fraction derived previously is an essential result in this thesis, as this scaling of the concentration will be used to describe samples of suspensions and gels throughout the following chapters. Because of its importance here, it is interesting to discuss the implications of this scaling.

In the previous calculation of the effective volume fraction of protein-coated droplets, estimated in Equation 5.4 as $\phi_{eff} = k_0 \times c$ with $k_{0,drop} = (2.2 \pm 0.1)\,\mathrm{mL} \cdot \mathrm{g}^{-1}$, droplets were considered as hard colloidal particles without consideration for the details of their structure. The value of the parameter $k_{0,drop}$ obtained is thus an indication of the volume occupied by the droplets relative to their weight and is different from the inverse of the density of the oil core. Because the protein-stabilised droplets are complex colloidal particles, it is possible to refine the physical interpretation of $k_{0,drop}$ by using the framework of core-shell particles.

Protein-stabilised droplets as core-shell particles

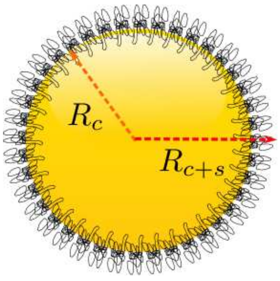

Figure 5.5 *Cartoon of a protein-stabilised droplet where R_c and R_{c+s} are the radii of, respectively, the oil core and the droplet (including the soft shell of adsorbed proteins).*

The structural inhomogeneities of protein-stabilised droplets can be accounted for by representing the droplets as core-shell particles, as illustrated in Figure 5.5. Indeed, at the size of droplets considered, the internal Laplace pressure arising from the surface energy of the droplets is around $\Delta P = 2\gamma/R \approxeq 3.1\,\mathrm{kPa}$, if the surface tension is considered to be around $\gamma = 0.1\,\mathrm{mN}\cdot\mathrm{m}^{-1}$ [119]. The oil core of the particle is thus not easily deformable, and the layer of adsorbed sodium caseinate can reasonably be assumed to be softer because of the nature of the proteins [63].

The viscosity of droplet suspensions in the semi-dilute regime can thus be interpreted in line with previous studies on core-shell latex particles. In this framework, the effective volume of oil droplets $\phi_{eff,drop}$ can be expressed [59]:

$$\phi_{eff,drop} = \left(\frac{R_{c+s}}{R_c}\right)^3 \phi_c \tag{5.5}$$

where ϕ_c is the volume fraction occupied by the oil core in the suspension, R_c and R_{c+s} are the radii of, respectively, the oil core and the droplet (including the soft shell of adsorbed proteins) as represented on Figure 5.5.

Moreover, ϕ_c can be written:

$$\phi_c = \frac{V_{oil}}{V_{total}} = \frac{m_{oil}/\rho_{oil}}{V_{total}} \tag{5.6}$$

Where ρ_{oil} is the density of the oil used to produce the emulsion droplets.

The weight fraction of oil in the droplets $[oil]_{droplet} = m_{oil}/m_{droplet} = m_{oil}/(m_{oil} + m_{adsorbedprot})$, as presented in Chapter 4, can be introduced in Equation 5.6. Equation 5.6 then becomes:

$$\phi_c = \frac{[oil]_{droplet} \times m_{droplet}/\rho_{oil}}{V_{total}} = \frac{[oil]_{droplet}}{\rho_{oil}} c_{droplet} \tag{5.7}$$

By combining Equations 5.5, 5.7 and 5.4, it is thus possible to link $k_{0,drop}$ with R_{c+s}/R_c:

$$\left(\frac{R_{c+s}}{R_c}\right)^3 = \frac{\rho_{oil} . k_{0,drop}}{[oil]_{droplet}} \tag{5.8}$$

As estimated in Chapter 4, $[oil]_{droplet} = 0.87$, so using $k_{0,drop} = (2.2 \pm 0.1)\,\mathrm{mL}\cdot\mathrm{g}^{-1}$, $R_{c+s}/R_c = 1.3$ is found. This value thus indicates that the shell, *i.e.* the layer of adsorbed droplets, has an effective thickness of around 30 % the size of the oil core.

This estimation is entirely based on the hydrodynamic properties of the droplets, on which the adsorbed layer appears to have a significant influence. To have a more precise characterisation of the droplets as core-shell colloidal particles, this value can be discussed in the light of the size measurements presented on page 77.

Core-shell particles and interpretation of the colloidal sizes

To assess the validity of the core-shell model for protein-stabilised droplets, it is appropriate to compare the value for the ratio R_{c+s}/R_c with droplet sizes measured with light scattering techniques in Chapter 4. Each technique probes a slightly different parameter of the droplets, so the following considerations are not completely physically accurate, but provide ground for discussion.

To start with, R_c can be estimated from SLS measurement of the purified emulsion. Indeed, because of the discrepancy of refractive index, the oil core is the part of the droplet which has the biggest contribution to the scattering of a light beam shone through the droplet suspension. More precisely, this measurement gives an estimation of the optical radius of the oil core, so $R_{Mastersizer} = R_{opt,c} = 65\,\mathrm{nm}$. By putting this size in Equation 5.8, $R_{opt,c+s} = 84\,\mathrm{nm}$ is obtained, which is an estimation of the radius of the entire droplet, including the protein shell. The adsorbed protein can therefore be estimated to form a 19 nm layer around the droplet. Sodium caseinate being charged, this value has to be seen as an effective value of a size which combines hydrodynamic and optical properties. This result is in good correspondence with the hydrodynamically thick layers formed by adsorption of pure β-casein at a water/polystyrene interface, for which the thickness was estimated to be 16 nm [147]. It is also in good agreement with the measured thickness of a thin film of sodium caseinate in air [148]. In that case, the double layer of adsorbed caseinate is around 30 nm thick.

In addition, this result can be compared with the mean size measured by Dynamic Light Scattering (DLS). Indeed, in DLS the hydrodynamic radius is estimated, based on the Stokes-Einstein relationship of diffusion. One would expect the protein shell of the droplets to play a role in its hydrodynamic properties, and it is thus relevant to compare the calculated $R_{opt,c+s}$ with the measured $R_{h,DLS}$. Dynamic Light Scattering performed on a suspension of droplets gives a mean size (volume averaged) of $R_{Zetasizer} \simeq R_{h,c+s} = 110\,\mathrm{nm}$. This value is higher than the estimated $R_{opt,c+s} = 84\,\mathrm{nm}$, probably because DLS is entirely based on the hydrodynamic properties of the droplets, and it takes fully into account the polyelectrolyte and the soft nature of the adsorbed protein layer, to which an optical technique like the one used by the Mastersizer is less sensitive.

To conclude, two different methods for the estimation of the volume fraction ϕ_{eff} of semi-dilute suspensions from the viscosity behaviour were presented, and the results obtained discussed. It was noted that the method using Batchelor equation provided a more accurate estimation, consequently it will be the option retained in the following.

The concept of volume fraction is very important for the rheological properties of soft materials, and the estimations obtained offer thus the possibility of considering non-trivial suspensions, such as those studied here, in the strong theoretical framework developed over the last half-century for colloidal suspensions of hard and soft particles, and gels in the following chapters.

To this aim, the definition of the effective volume fraction presented in Equation 5.4 will be extended to the full range of concentrations studied in this work. This assumption implies that each colloidal particle occupies the same volume, at all concentration, as it does in the semi-dilute regime, where its interactions with its neighbours are limited to hydrodynamic effects. In other words, it is assumed that there are no changes in voluminosity or interpenetration with increasing concentration.

It is well-known however that colloidal particles softer than hard spheres will present one or the other of these effects [3]. The definition of the effective volume fraction is thus a working hypothesis, and it has to be kept in mind that this parameter may not indicate the "true" volume fraction. This is illustrated by the high values reached by the effective volume fraction ($\phi_{eff} > 1$) as will be discussed later. Nonetheless, the benefits of using the effective volume fraction to scale the rheological properties are major and are presented in what follows.

5.4 Viscosity behaviour of pure suspensions of droplets and proteins in the concentrated regime

Using the scaling for the effective volume fraction ϕ_{eff} derived in the semi-dilute regime (Equation 5.4) facilitates plotting the viscosity behaviour as a function of volume fraction for suspensions of either protein-stabilised droplets or of proteins over the whole range of concentrations. These can then be compared to each other and to the results obtained for other suspensions of hard or of soft colloids.

5.4.1 Modelling the viscosity behaviours of colloidal suspensions

In order to compare quantitatively the behaviours of the two types of colloidal suspensions studied here, it is relevant to use descriptive models. As presented in Chapter 2, there is a rich collection of empirical, semi-empirical or theoretical models that describe the viscosity of colloidal suspensions. These models include hypotheses on the nature and the properties of the particles, so more than one model will have to be used here. Indeed, as noted before, the naturally-occurring sodium caseinate aggregates that form the protein suspensions differ significantly from the sodium caseinate-stabilised droplets. In the following, suitable empirical relations are selected to describe the viscosity behaviour of droplet and protein suspensions. They are then applied to the experimental data, and their accuracy is discussed.

Suspensions of protein-stabilised droplets are similar to hard spheres

The viscosity of protein-stabilised droplet suspensions is displayed in Figure 5.6. A sharp divergence is observed at high volume fraction and this behaviour is typical of hard-sphere suspensions [35]. It is thus interesting to use one of the laws derived for such systems to model the viscosity behaviour of droplet suspensions.

Amongst the multiple models for the viscosity of hard-sphere suspensions that have been derived over time, the empirical relation developed by Quemada [5] is

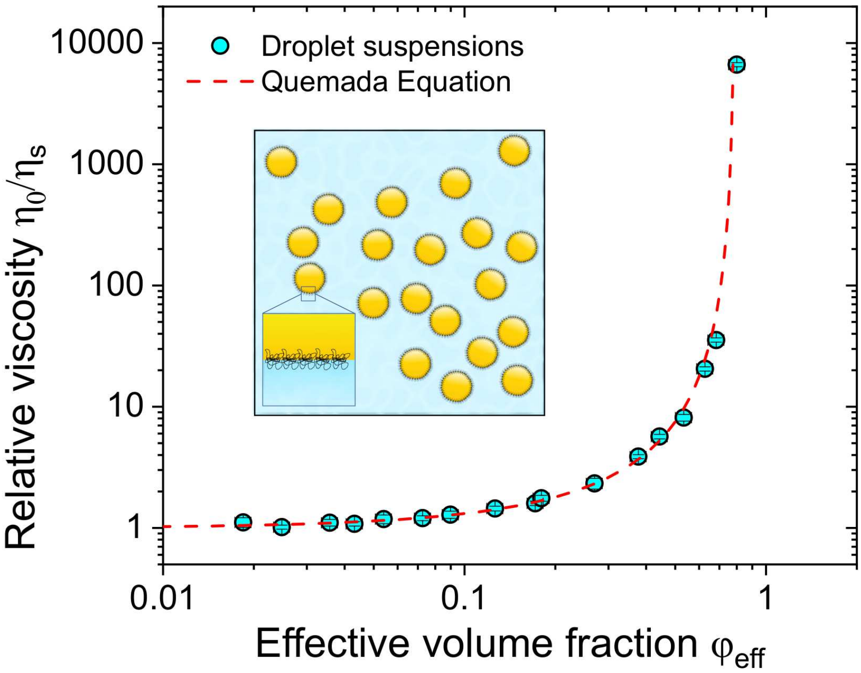

Figure 5.6 *Relative zero-shear viscosity of sodium caseinate-stabilised droplets (circles, cyan) as a function of the effective volume fraction. The red dashed line denotes Quemada equation for hard spheres (Equation 2.4) with* $\phi_m = 0.79$.

used in this work, as presented in Chapter 2:

$$\frac{\eta_0}{\eta_s} = \left(1 - \frac{\phi}{\phi_m}\right)^{-2} \tag{2.4}$$

Where the parameter ϕ_m is the maximum volume fraction at which the viscosity of the suspension diverges, as can be seen in Equation 2.5.

The Quemada model fits remarkably well to the experimental data of the relative viscosity η_0/η_s of suspensions of droplets when ϕ is approximated by the effective volume fraction ϕ_{eff}. The value for the maximum volume fraction is found to be $\phi_m = 0.79 \pm 0.02$. Despite the similar behaviour of viscosity between droplet suspensions and hard-sphere suspensions, the maximum volume fraction found here is considerably higher than the theoretical value of $\phi_m = \phi_{rcp} = 0.64$ for randomly close-packed hard spheres.

A possible explanation for this discrepancy is the polydispersity of the droplet suspension. Indeed, random close-packing is highly affected by the size distribution of the particles, as smaller particles can fill the gaps between bigger particles. As presented in Chapter 2, the maximum volume fraction of a polydisperse suspension of hard spheres can be accurately estimated from the size distribution of the particles [41, 42].

Here, the size distributions of the protein-stabilised droplets measured with both the Mastersizer and the Zetasizer, as presented in Chapter 4, can be used with the `spherepack1d` freeware [43] to obtain a numerically estimated random close-packing volume fraction ϕ_{rcp}. For both size distributions, it is thus found that $\phi_{rcp} = 0.68$. Although this is a higher maximum volume fraction than for a monodisperse hard-sphere suspension, it is still considerably lower than the experimental value, $\phi_m = 0.79$.

A closer look at the variations of ϕ_{rcp} with the polydispersity reveals that such a high random close-packing fraction can be achieved numerically, but only if a significant fraction of droplets, of radius two times smaller than the average radius, is added to the distributions obtained by light scattering mentioned here. The hypothesis of the presence of small droplets, undetectable without fractionation of the suspension prior to the size measurement by light scattering, is supported by the observation of such droplets upon fractionation of a very similar emulsion in a previous study [141].

It is also possible that other mechanisms than the polydispersity come into play at high volume fraction of droplets. Although it would be hard to quantify, it is likely that the soft layer of adsorbed proteins may undergo some changes at high volume fraction, such as deswelling or interpenetration.

Protein suspensions: adaptation of the hard-sphere model for soft colloids

Naturally-occurring aggregates of sodium caseinate differ from protein-stabilised droplets because of their swollen structure. The viscosity behaviour of the suspensions they form is displayed in Figure 5.7. At high concentrations, the divergence of their viscosity is not as sharp as for the suspensions of droplets. This result is in agreement with previous studies of sodium caseinate, in which suspensions at higher concentrations were studied [63, 110, 149]. In these works, it was shown that the viscosity does not diverge but follows a power law $\eta_0/\eta_s \propto (\phi_{eff,prot})^{12}$.

Because the behaviour displayed by sodium caseinate resembles that of core-

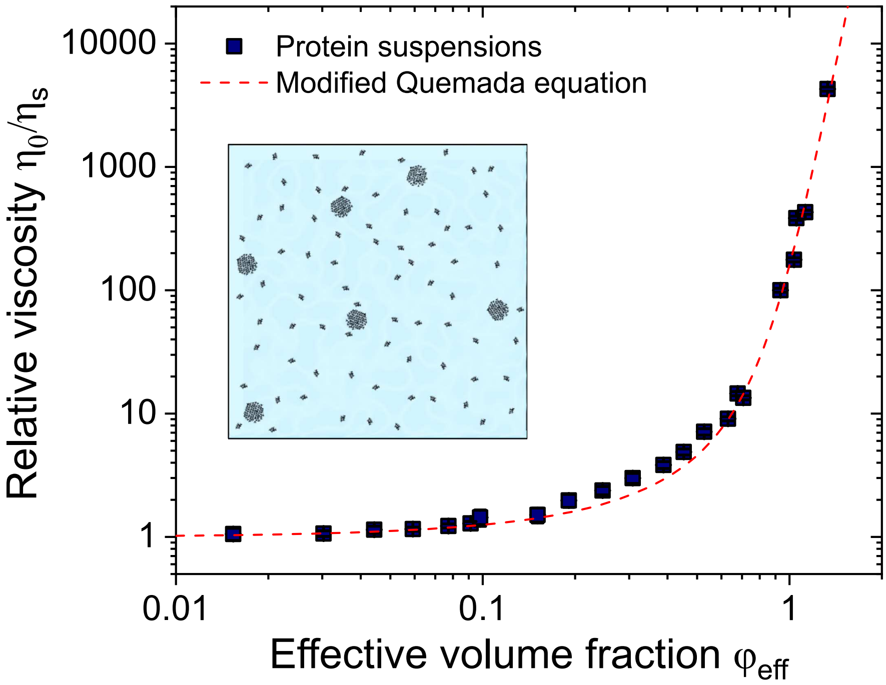

Figure 5.7 *Relative viscosity of sodium caseinate suspensions (squares, navy) as a function of the effective volume fraction. The red dashed line denotes the modified Quemada equation, Equation 5.9, the values for n and ϕ_m are listed in Table 5.1.*

shell microgels [51] and soft spherical brushes [64], a soft colloid framework, as presented in Chapter 2, seems suitable for the study of these suspensions.

A general feature of the viscosity behaviour of soft colloidal suspensions is the oblique asymptote at high concentrations. Indeed, because when particles are added, the volume occupied by each particle decreases, by de-swelling or interpenetration, the strong viscosity divergence of hard-sphere suspensions is absent for soft colloids. To describe the behaviour of such suspensions, it is thus required to modify the existing models to take into account this distinctive limit at high concentrations while retaining their expression at lower concentrations.

An empirical modification that fulfils the previous criteria is the substitution of the maximum volume fraction ϕ_m by a ϕ-dependent parameter ϕ_m^* that can be expressed, for example, $\phi_m^* = ({\phi_m}^n + \phi^n)^{1/n}$.

As a result, a modified version of Equation 2.4 can be derived, that takes into account the softness of the particles via a concentration-dependent maximum volume fraction ϕ_m^*. This semi-empirical viscosity model is expressed:

$$\frac{\eta_0}{\eta_s} = \left(1 - \frac{\phi}{\phi_m^*}\right)^{-2} \tag{5.9}$$

Where:

$$\phi_m^* = \phi_m \left(1 + \left(\frac{\phi}{\phi_m}\right)^n\right)^{1/n}$$

The addition of the exponent n as parameter expresses the discrepancy from the hard-sphere model. The smaller n, the lower the volume fraction ϕ at which ϕ_m^* diverges from ϕ_m, and the less sharp the divergence in viscosity.

The model in Equation 5.9 was applied to fit the experimental data displayed in Figure 5.7, and the resulting fitting parameters are listed in Table 5.1.

Table 5.1 *Parameters for the modified Quemada model for soft colloids, Equation 5.9, applied to sodium caseinate suspensions*

Parameter	Value	Standard Error
ϕ_m	0.93	0.02
n	6.1	0.4

The use of these parameters gives a correct description of the viscosity behaviour of sodium caseinate in the range of concentrations used here. In addition, this semi-empirical model also satisfactorily describes the viscosity of sodium caseinate suspensions at higher concentration from Ref. [63, 110]. It is to note that the inflexion of viscosity is slightly sharper for the model than for the experimental data.

Using this model, $\phi_m = 0.93 \pm 0.02$, while for monodisperse hard spheres the expected value would be of 0.64. Whilst it is not clear that ϕ_m in our model should be consistent with the packing of hard-spheres, such high values have also been obtained for other soft colloidal systems, such as microgels [52, 61] or star polymers [150]. This is mainly because the effective volume fraction ϕ_{eff} is an ambiguous parameter for soft colloids that does not necessarily describe the actual volume fraction occupied by the particles [3]. It is indeed likely that osmotic deswelling of the charged protein aggregates occurs at high concentrations, due to the increase of concentration of counter-ions in the solution, leading to a high effective volume fraction.

The power-law towards which the relative viscosity η_0/η_s described by Equation 5.9 tends at high concentration (ie $\phi > \phi_m$) can be calculated by developing

ϕ_m^*. Indeed, at high concentration ϕ_m^* converges towards $\phi \times \left(1 + \frac{1}{n} \times \left(\frac{\phi_m}{\phi}\right)^n\right)$, so η_0/η_s converges towards $\left(1 + n\left(\frac{(\phi_{eff})}{\phi_m}\right)^n\right)^2 \propto (\phi_{eff,prot})^{2n}$. Using the value in Table 5.1, the relative viscosity of sodium caseinate suspensions is found to follow the power law $\eta_0/\eta_s \propto (\phi_{eff,prot})^{12.3 \pm 0.8}$. This value is in good agreement with the literature where $\eta_0/\eta_s \propto (\phi_{eff,prot})^{12}$ in the concentrated regime [63, 110, 149].

Applications of the models

Models have thus been found for both suspensions of sodium caseinate and of caseinate-stabilised droplets. This makes it possible to estimate the viscosity of a suspension of known concentration. These models form the basis of a semi-empirical model to predict the viscosity of mixtures of proteins and droplets, such as emulsions. The development of this model will be presented in the next section.

5.5 Viscosity of mixtures: contributions of the pure components

Emulsifying oil in a protein suspension is a common processing step in the food industry. Regardless of the protein concentration, not all the proteins will adsorb on the oil/water interface during the emulsification, and protein-stabilised emulsions are thus mixtures of protein-stabilised droplets and un-adsorbed proteins [98, 117]. After having studied separately the components of protein-stabilised emulsions, the next logical step is thus to prepare mixtures of well-characterised composition by combining purified droplets and protein suspensions.

The preparation protocol of these mixtures as well as the list of their composition can be found in Chapter 3. In the following, the suspensions of mixtures are presented using their total effective volume fraction $\phi_{eff,tot}$ with $\phi_{eff,tot} = \phi_{eff,prot} + \phi_{eff,drop}$, as well as the relative percentage of protein in the emulsion compared to the droplets χ_{prot}:

$$\chi_{prot} = \frac{\phi_{eff,prot}}{\phi_{eff,prot} + \phi_{eff,drop}} \tag{5.10}$$

Notably, no phase separation is observed in the emulsion samples at the timescale of the experiments. Despite sodium caseinate-stabilised emulsions being notoriously prone to depletion induced-flocculation [85, 113, 118] caused by the presence of unadsorbed sodium caseinate [117], the emulsions prepared here present a rheological behaviour that differs from those of flocculated samples. Indeed, most of the mixtures of this study are Newtonian fluids, as shown in Figure 5.8. In addition, the comparison of the non-Newtonian behaviour of the most concentrated samples prepared here, as can be found in the next section, with the flow curves of emulsions in which depletion flocculation is occurring in Ref. [118] shows clear differences. Concentrated mixture samples display a clear zero-shear viscosity plateau and present shear-thinning at shear stresses one order of magnitude higher than equivalent flocculated samples, as will be shown in Section 5.6.

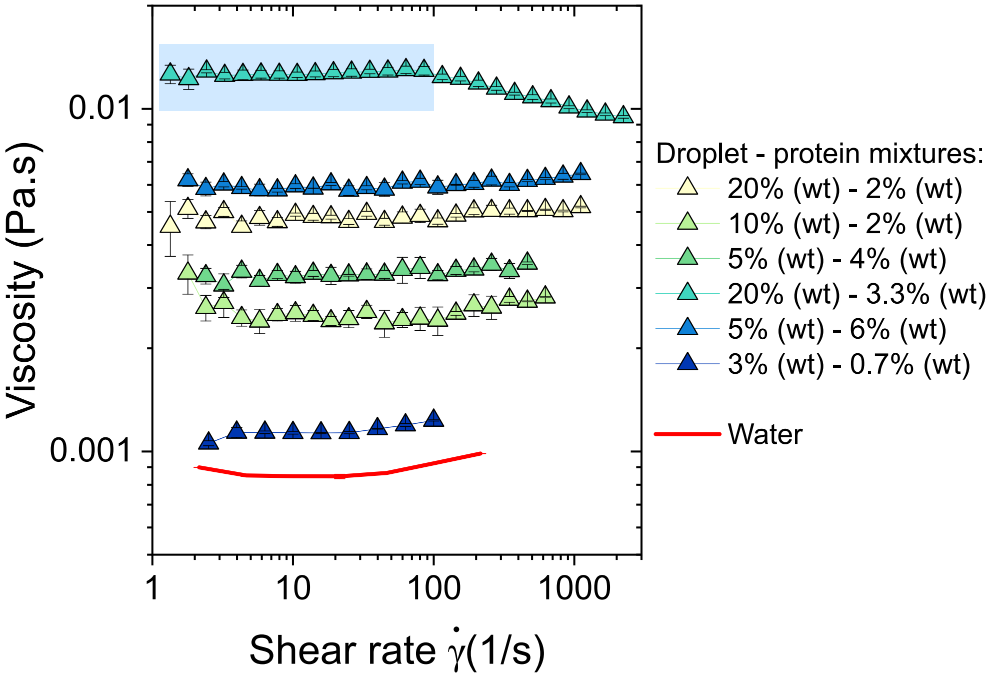

Figure 5.8 *Flow curves of mixtures of sodium caseinate-stabilised droplets and sodium caseinate at several concentrations. These curves are the average of 3 measurements, and the error bars indicate the reproducibility. For the shear thinning samples, only the zero-shear viscosity* η_0 *is considered, as indicated by the shaded area. A more thorough study of their behaviour is presented in Section 5.6.*

The weak depletion interaction probably arises here from a combination of the small size of the droplets and the reduced calcium concentration in the samples. Indeed, depletion flocculation has been exploited to obtain monodisperse emulsions in a similar system, in which caseinate-stabilised droplets of radius 180 nm were separated from the emulsion by the depletion-induced creaming of larger droplets [119], following a depletion crystallisation scheme [151]. This shows that droplets of radius below 180 nm like those studied here are less prone to depletion-induced flocculation. In addition, the purification protocol used here to clean the protein may change the concentration of calcium, a common impurity in commercial sodium caseinate that has been shown to play an important role in the stability of caseinate-stabilised emulsions [152].

The viscosity of the mixtures containing both proteins and protein-stabilised droplets was measured as for the pure suspensions and these values are represented in Figure 5.9.

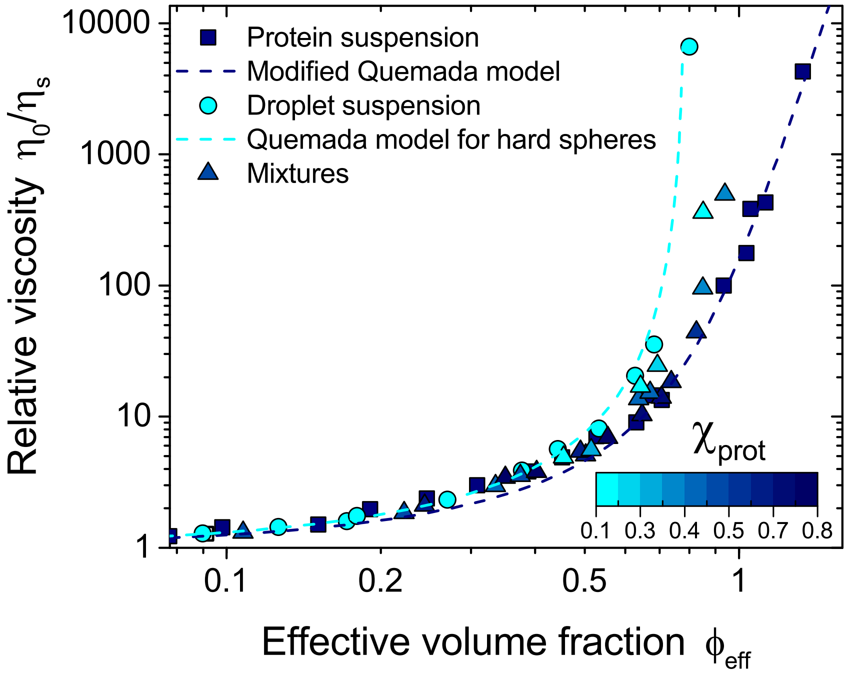

Figure 5.9 *Relative zero-shear viscosities η_0/η_s of suspensions of sodium caseinate suspensions (squares, navy), sodium-caseinate stabilised droplets (circles, cyan), and of mixtures (triangles, colour-coded as a function of χ_{prot} defined in Equation 5.10) as a function of the effective volume fraction ϕ_{eff}.*

The emulsions display viscosities below the viscosity of pure droplets at a given volume fraction, and either above or below the viscosity of pure proteins depending on their compositional index χ_{prot}. The knowledge and models acquired for the suspensions of proteins and droplets in the previous sections can be used to develop a semi-empirical model to describe the viscosity of mixtures.

5.5.1 Semi-empirical predictive model for the viscosity of mixtures

Models have been developed previously to predict the viscosity of suspensions of pluri-modal particles, for example in Ref. [46, 47]. However these models add unnecessary mathematical complexity without managing to accurately describe our experimental results.

Instead, a simple and useful approach is to consider that each component of the mixture is independent from the other, as in the early model for pluri-modal suspensions described in [153]. In this case, the protein suspension acts as a viscous suspending medium for the droplets, whose viscosity behaviour was previously characterised and modelled by Equation 2.4. Because the viscosity behaviour of the protein suspension is also known, it can be combined with the droplet behaviour to determine the viscosity of the mixture. This approach is illustrated on Figure 5.10.

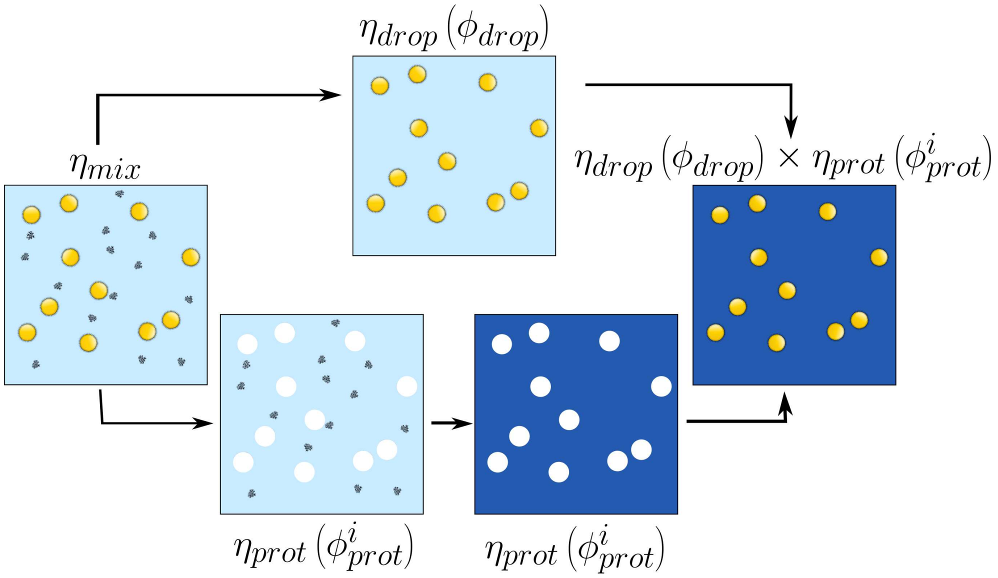
$\eta_{drop}\left(\phi_{drop}\right)$
η_{mix}
$\eta_{drop}\left(\phi_{drop}\right) \times \eta_{prot}\left(\phi^i_{prot}\right)$
$\eta_{prot}\left(\phi^i_{prot}\right)$
$\eta_{prot}\left(\phi^i_{prot}\right)$

Figure 5.10 *Development of a semi-empirical model to predict the viscosity of protein-stabilised emulsions. The un-adsorbed proteins increase the viscosity of the continuous phase as a function of their volume fraction in the interstices between droplets* ϕ^i_{prot}

Combination of viscosities of pure proteins and droplets

Considering the suspending media alone first, it is useful to consider the protein content of the aqueous phase in the interstices between the droplets, ϕ^i_{prot}:

$$\phi^i_{prot} = \frac{V_{prot}}{V_{prot} + V_{water}} = \frac{\phi_{prot}}{\phi_{prot} + \phi_{water}} = \frac{\phi_{prot}}{1 - \phi_{droplet}} \tag{5.11}$$

Where it is approximated that $\phi_{prot} \simeq \phi_{eff,prot} = k_{0,prot} \times c_{prot}$ and $\phi_{droplet} \simeq \phi_{eff,drop} = k_{0,drop} \times c_{drop}$, as in Equation 5.4, with $k_{0,prot}$ and $k_{0,drop}$ determined at Section 5.3.2 using the Batchelor equation on semi-dilute suspensions of pure proteins and pure droplets. The accuracy of this approximation will be discussed later.

In addition, the study of the pure suspensions of protein-stabilised droplets and of proteins makes it possible to model the viscosity behaviour of both suspensions:

- The relative viscosity of a suspension of protein-stabilised droplets $\eta_{r,drop}(\phi)$ is described by Equation 2.4 with the parameter $\phi_m = 0.79 \pm 0.02$ (Quemada model for hard spheres [5])
- The relative viscosity of a suspension of sodium caseinate $\eta_{r,prot}(\phi)$ is described by Equation 5.9 with the parameters listed in Table 5.1 (modified Quemada model)

In that framework, if there are no specific interactions between the droplets and the proteins, the predicted relative viscosity of the mixture $\eta^p_{r,mix}$ can be expressed by:

$$\eta^p_{r,mix}(\phi_{eff,prot}, \phi_{eff,drop}) = \eta_{r,prot}\left(\phi^i_{prot}\right) \times \eta_{r,drop}\left(\phi_{eff,drop}\right) \tag{5.12}$$

The separation of the contributions of the two components thus makes their calculation possible using only the models developed for the pure suspensions and a corrected volume fraction of the protein in the continuous phase ϕ^i_{prot}.

Application of the semi-predictive model to protein-stabilised emulsions

The contributions of protein-stabilised droplets and of un-adsorbed proteins to the viscosity of the mixtures are displayed in Figure 5.11.

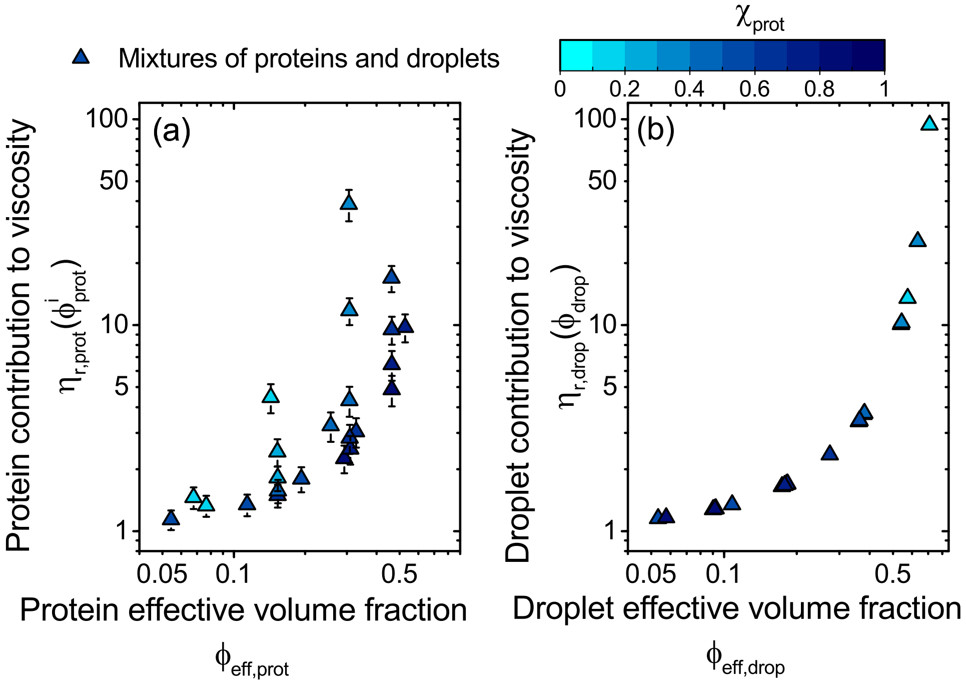

Figure 5.11 *Calculated relative contributions of the continuous phase and of the dispersed phase alone to the viscosity of caseinate-stabilised emulsions.*

(a) Relative viscosity of the continuous phase containing unadsorbed sodium caseinate aggregates. It is estimated by calculating, for each composition, the volume fraction of protein in the interstices between the droplets ϕ^i_{prot}*. Then the relative viscosity of a suspension of protein at this volume fraction* $\eta_{r,prot}\left(\phi^i_{prot}\right)$ *is calculated.*

(b) Relative viscosity of sodium caseinate-stabilised droplets $\eta_{r,drop}\left(\phi_{drop}\right)$*, calculated from the composition of each mixture.*

For the two graphs, the colour coding indicates the compositional index of the mixtures $\chi_{prot} = \phi_{eff,prot}/\left(\phi_{eff,prot} + \phi_{eff,drop}\right)$*. The error bars are calculated using the error propagation theory (see Appendix A), and only displayed if larger than the symbol size.*

The values of the relative viscosity calculated for each mixture sample using Equation 5.12, and the contributions shown in Figure 5.11, can then be compared to the experimentally measured relative viscosity $\eta^{m}_{r,mix}$, as displayed in Figure 5.12.

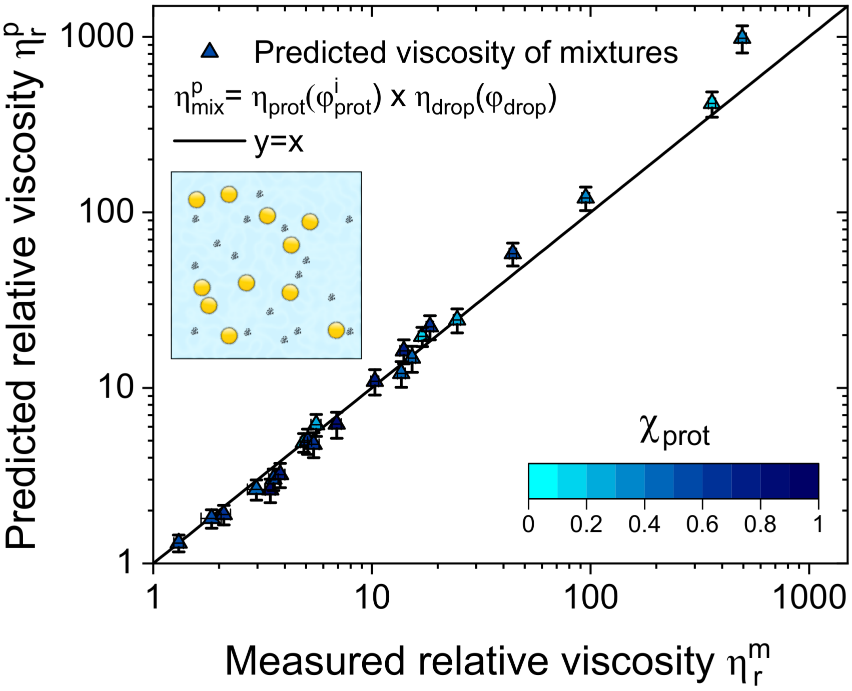

Figure 5.12 *Predicted relative viscosity of mixture suspensions* $\eta^{p}_{r,mix}$*, calculated with Equation 5.12, as a function of the measured viscosity* $\eta^{m}_{r,mix}$ *from Figure 5.9. Each point is a mixture of different composition, as listed in Table 3.2, where the colour indicates the value of the compositional index* χ_{prot} *defined at Equation 5.10. The straight line represents* $\eta^{p}_{r,mix} = \eta^{m}_{r,mix}$*, and a regression analysis gives an adjusted* R^2 *of* 0.988*. The error bars are calculated using the error propagation theory (see Appendix A).*

Despite the simplicity of this model, it provides a reasonably accurate prediction of the viscosity of protein-stabilised emulsions. This result seems to indicate that there are no specific interactions between the proteins and the droplets, neither at a molecular scale between un-adsorbed and adsorbed proteins, nor at a bigger length scale where depletion interactions could occur. This is likely to be related to the small size of the droplets in this specific system, and increasing the droplet size may result in a decreased accuracy of this simple model. The influence of the droplet size on the viscosity behaviour of emulsions will be described in Chapter 8.

A few limitations in the development of the model can account for the variations of accuracy of the model. First, at moderate viscosity ($\eta_r < 10$), the slight discrepancy between predicted and measured viscosity of the samples with a high χ_{prot} is probably a reflection of the modest underestimation of the viscosity of protein suspensions for $0.2 < \phi_{eff} < 0.7$ (corresponding to $2 < \eta_{prot}/\eta_s < 10$) by Equation 5.9.

Then, at higher concentrations, the effective volume fraction approximation may break down. Indeed, as observed previously for pure suspensions, ϕ_{eff} can reach high values and may not correspond exactly to the volume fraction actually occupied by the particles, especially in the case of $\phi_{eff,prot}$. A natural consequence is that the relationship $\phi_{eff,prot} + \phi_{eff,drop} + \phi_{eff,water} = 1$ may not be verified, leading to an overestimation of ϕ^i_{prot} when calculated by Equation 5.11. It should be noted that the lack of unifying definition of the volume fraction for soft colloids is a particularly relevant challenge when dealing with mixtures. A way to address this problem could be to take one of the viscosity behaviours of the two components as a reference, and map the volume fraction of the other component to follow this reference viscosity [47], but it would considerably increase the complexity of the model.

In conclusion of this section, the preliminary study of the individual components of a mixture allows for the prediction of the viscosity of mixtures of these components with reasonable accuracy, providing that the composition of the mixtures is known.

5.5.2 Use of the semi-predictive model to estimate the composition of emulsions

A common challenge when producing protein-stabilised emulsions is to estimate the amount of proteins adsorbed at the interface as opposed to the proteins suspended in the aqueous phase. A typical technique to measure the adsorbed proteins is to separate the aqueous phase from the droplets by centrifugation and measure the concentration of proteins in the two separated phases [98, 117].

However, for the substantially small droplets used in this study, it is extremely difficult to obtain a satisfactory separation, as shown in Figure 3.8. In addition, even for bigger droplets, the separation process makes the characterisation cumbersome for practical applications such as on production lines. A technique that could make possible to measure the composition of the emulsion quickly would thus be extremely valuable.

Here the semi-empirical model developed in the previous section is reversed to estimate the amount of proteins in suspension after emulsification. It is argued that, after calibration of the model, this estimation can be achieved with a simple viscosity measurement, that can be performed on-line in advanced industrial processing lines. The calculation process is illustrated in Figure 5.13.

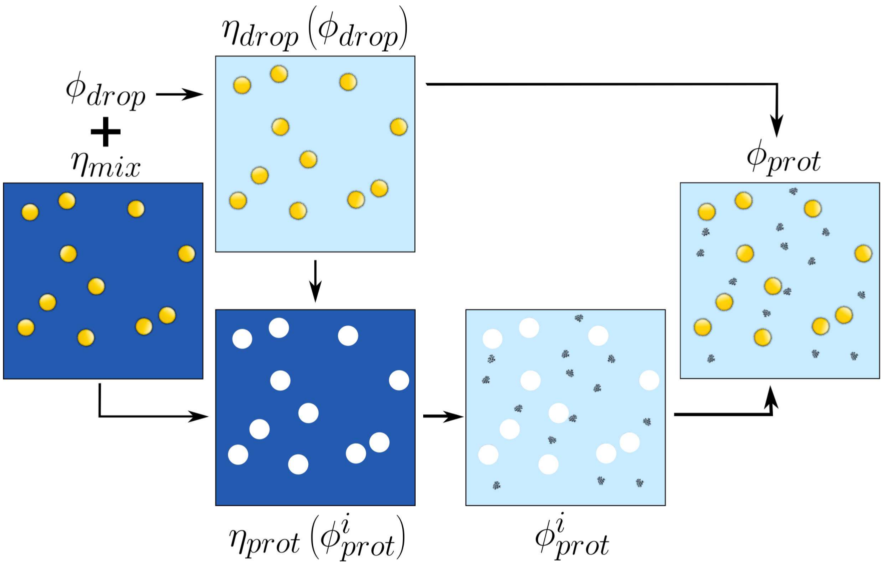
$\eta_{drop}\left(\phi_{drop}\right)$
ϕ_{drop}
+
η_{mix}
ϕ_{prot}
$\eta_{prot}\left(\phi^{i}_{prot}\right)$
ϕ^{i}_{prot}

Figure 5.13 *Reversal of semi-predictive model for the viscosity of protein-stabilised emulsions. The measurement of the emulsion viscosity* $\eta_{r,mix}$ *makes possible the calculation of the volume fraction of un-adsorbed proteins* $\phi_{eff,prot}$*, given that the volume fraction of droplets* $\phi_{eff,drop}$ *is known from the preparation protocol.*

To assess the accuracy of the suggested method, a case in point is the emulsion used to prepare the sodium caseinate droplets in this study after microfluidisation. It is composed of 20% (wt) oil and 4.0% (wt) sodium caseinate, and its relative viscosity was measured to be $\eta^{m}_{r,mix} = 10$.

The first step is to calculate the contribution of the oil droplets to the viscosity of the mixture, in order to isolate the protein contribution. A 20 % (wt) content in oil corresponds to $\phi_{eff,drop} = 0.40$, so $\eta_{r,drop} = \left(1 - \phi_{eff,drop}/\phi_m\right)^{-2} = 4.1$.

It is then possible, using the Equation 5.12, to calculate the viscosity of the continuous phase $\eta_{r,prot}\left(\phi^{i}_{prot}\right) = \eta^{m}_{r,mix}/\eta_{r,drop} = 2.4$, assumed to arise from the presence of un-adsorbed proteins. In order to estimate the volume fraction of proteins in the interstices ϕ^i_{prot}, the equation below has to be solved:

$$\left(1 + \left(\frac{\phi_{eff,prot,m}}{\phi^i_{prot}}\right)^n\right)^{-1/n} = 1 - \frac{1}{\sqrt{\eta_{r,prot}}} \tag{5.13}$$

Finally, numerically solving Equation 5.13 with the values for n and ϕ_m from Table 5.1 gives $\phi^i_{prot} = 0.33 \pm 0.06$. This result corresponds to a volume fraction of un-adsorbed proteins in the overall emulsion $\phi_{eff,prot} = \phi^i_{prot}(1 - \phi_{eff,drop}) = 0.20 \pm 0.04$, or expressed as a concentration in the emulsion: $c = (23 \pm 5)\,\mathrm{mg \cdot mL^{-1}}$. This has to be compared with the initial concentration of $45\,\mathrm{mg \cdot mL^{-1}}$ in proteins before emulsification. Thus, only half of the amount of proteins adsorb at the interface, while the other half is still in suspension. The validity of this result is difficult to assess experimentally, because the presence of small oil droplets in the subnatant after ultracentrifugation of the emulsion prevents the use of optical techniques for the determination of the protein concentration, as discussed in Chapter 4.

This result can be converted into a surface coverage to be compared with studies on sodium caseinate-stabilised emulsions using micron-sized droplets. As presented in Chapter 4, it is estimated that 1 kg of emulsion containing 20 % (wt) of oil, and with a droplet size of $R_{opt,c} = 65\,\mathrm{nm}$ presents a surface area of oil of $9.6 \times 10^3\,\mathrm{m^2}$. Furthermore, the reversal of the semi-predictive model yielded that $(22 \pm 5)\,\mathrm{g}$ of sodium caseinate is adsorbed at the interfaces. Thus, the surface coverage found here is $(2.3 \pm 0.5)\,\mathrm{mg \cdot m^{-2}}$. This result is in good correspondence with studies on similar emulsions at larger droplet sizes, in which a surface coverage of around $3.0\,\mathrm{mg \cdot m^{-2}}$ was found upon emulsification with a protein excess [98, 117, 118]. This plausible surface coverage thus provides a validation for the use of the measurement of the viscosity as a tool to estimate the amount of unadsorbed proteins present in the emulsions studied here.

The semi-empirical model for the viscosity of emulsions developed in this section, once calibrated, can thus be used not only as a predictive tool for mixtures of droplets and proteins of known composition, but also as a method to estimate the amount of adsorbed proteins without the need for further separation of the components. This extension of the model to industrial applications would however require further validation, as some practical complications may emerge from the time-dependence of these systems over longer times. Indeed, variations in the aggregation state of the protein, Ostwald ripening or depletion-induced flocculation may occur. The reliability of the calibration also relies on the repeatability of the emulsification, which may be reduced by the variations of composition of different batches of sodium caseinate.

5.6 Flow curves and shear-thinning behaviour

Concentrated suspensions of colloidal particles may display non-Newtonian behaviours, as presented in Chapter 2. More specifically, shear thinning, *i.e.* a decrease of the viscosity at high shear rates, is commonly observed for hard sphere suspensions at high concentrations [26, 35, 36]. In this study, concentrated suspensions of protein-stabilised droplets, of proteins and in mixtures of proteins and droplets, also display shear thinning, as it can be observed in Figure 5.14 and 5.15.

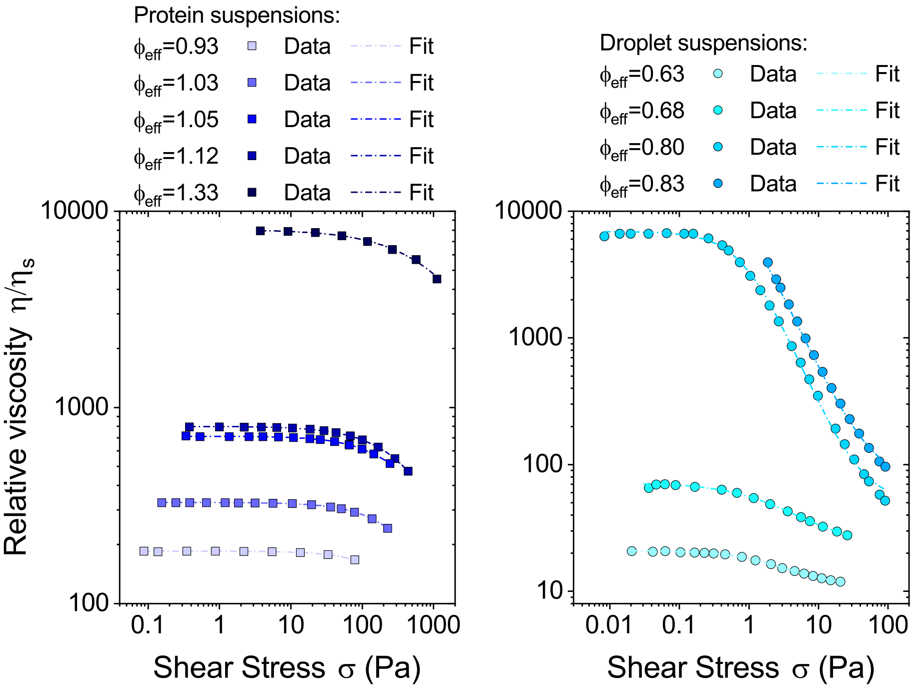

Figure 5.14 *Flow curves of shear-thinning samples, fitted using Equation 2.7. The relative viscosity* η/η_s *is plotted as a function of the shear stress* σ*.*
Left (squares): Concentrated suspensions of sodium caseinate at effective volume fractions $\phi_{eff,prot}$ *of* 0.93, 1.03, 1.05, 1.12 *and* 1.33.
Right (circles): Concentrated suspensions of pure sodium caseinate-stabilised oil droplets at effective volume fractions $\phi_{eff,drop}$ *of* 0.63, 0.68, 0.80 *and* 0.83.
For clarity, only 1/3 *of datapoints are displayed for each curve.*

Table 5.2 *Composition of the concentrated emulsions (mixtures of protein-stabilised droplets and un-adsorbed proteins) that present a shear-thinning behaviour, and whose flow curves are displayed in Figure 5.15.* ϕ_{eff} *indicates the effective volume fractions calculated with Equation 5.4.*

Droplets ($\phi_{eff,drop}$)	Proteins ($\phi_{eff,prot}$)	Total ($\phi_{eff,tot}$)	χ_{prot} (Eq 5.10)
0.64	0.30	0.94	0.32
0.73	0.15	0.88	0.17
0.37	0.46	0.83	0.55
0.58	0.10	0.68	0.14

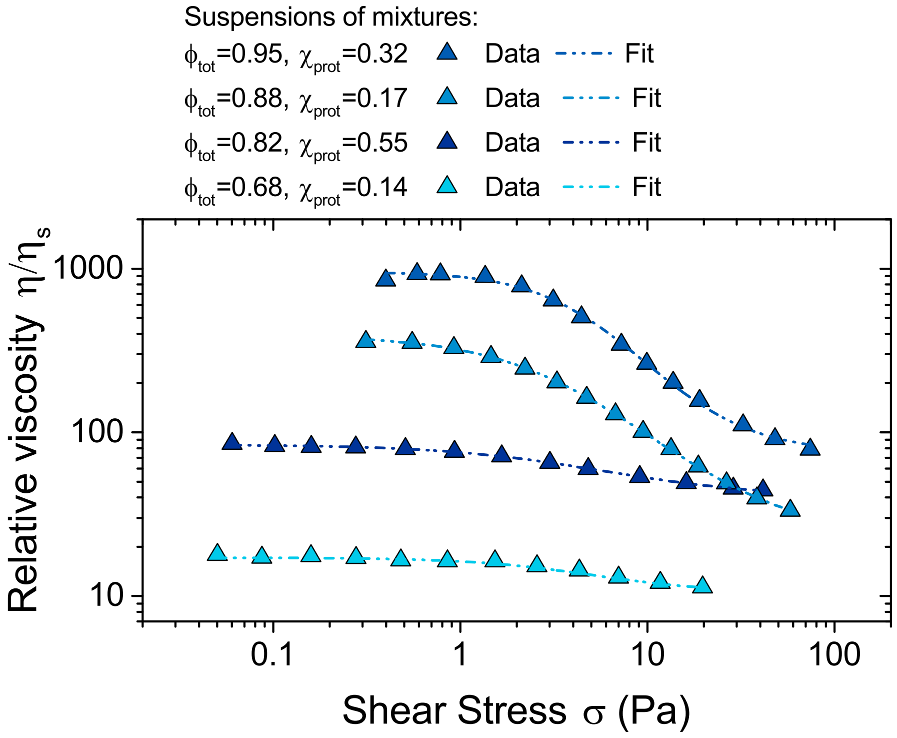

Figure 5.15 *Flow curves of shear-thinning emulsions, fitted using Equation 2.7. The relative viscosity* η/η_s *is plotted as a function of the shear stress* σ*.*
Concentrated mixtures of caseinate-stabilised droplets and un-adsorbed sodium caseinate in suspension (triangles, colour indicates the value of the compositional index χ_{prot} *defined at Equation 5.10). The compositions of the samples are listed in Table 5.2.*
For clarity, only 1/3 *of datapoints are displayed for each curve.*

5.6.1 Model for the description of shear thinning

As detailed in Chapter 2, the change of the relative viscosity $\frac{\eta}{\eta_s}$ with the shear stress σ upon shear thinning can be modelled by the expression [40]:

$$\frac{\eta}{\eta_s} = \eta_\infty + \frac{\eta_0 - \eta_\infty}{1 + (\sigma/\sigma_c)^m} \tag{2.7}$$

Where η_0 and η_∞ are the relative viscosities in the two limiting regimes of respectively zero-shear and infinite shear, σ_c indicates the shear stress required for the shear-thinning to occur, and m is an experimental parameter.

As can be seen in Figure 5.14 and 5.15, Equation 2.7 describes correctly the flow curves of the samples studied here over their range of concentrations. In addition, the fitting of the flow curves allows for the extraction of parameters that make possible a qualitative comparisons of the suspensions, in their diversity of colloidal particles and of volume fractions.

5.6.2 Comparison of the shear thinning behaviour of different suspensions

A first qualitative analysis of Figure 5.14 shows that the onset of shear thinning behaviour occurs at different volume fractions for the two types of suspensions. Indeed, droplet suspensions are Newtonian up to $\phi_{eff,drop} = 0.55$ and start displaying shear thinning for samples at $\phi_{eff,drop} \geq 0.63$, while protein suspensions are essentially Newtonian up to $\phi_{eff,prot} = 1$. Moreover, in terms of zero-shear viscosity, protein suspensions start shear-thinning at relative viscosities ($\sim$ 200) that are one order of magnitude higher than for droplet suspensions ($\sim$ 20). This discrepancy probably arises from the difference in softness between protein aggregates and droplets. Indeed, as discussed previously, suspensions of pure proteins and of pure droplets display different viscosities at the same volume fraction in very concentrated regime, and protein aggregates can reach higher effective volume fractions.

In addition, the mixtures of protein-stabilised droplets and of proteins also display shear thinning, as can be seen in Figure 5.15 and Table 5.2. Here the onset appears closer to the droplet systems as $\phi_{eff,prot} + \phi_{eff,drop} \geq 0.68$ for the least concentrated shear-thinning sample. However, the appearance and the extent of shear thinning are also dependent of the composition of the mixtures as indicated by χ_{prot}, defined in Equation 5.10.

A more refined analysis can be performed by using the quantitative parameters extracted by fitting Equation 2.7 to the flow curves (Figure 5.14 and 5.15). The zero-shear relative viscosity was detailed in the previous sections for a wider range of concentrations, and the infinite shear viscosity could not be determined precisely. For all samples, the exponent m is between 0.8 and 1.6, with no identifiable trend among different types of suspensions or within the concentration range of each sample. The focus here will thus be on the study of the critical shear stress σ_c. This parameter could be determined visually, but it is believed that the fitting protocol allows a more reproducible estimation of σ_c.

Discrepancy in critical shear stress: size matters

The critical shear stress σ_c for each suspension of pure protein aggregates, pure protein-stabilised droplets and mixture of droplets and un-adsorbed proteins is presented in the top part of Figure 5.16.

As can be observed in Figure 5.16, protein suspensions require a much higher stress to display shear-thinning than droplet suspensions. Indeed, σ_c is two orders of magnitudes higher in the case of protein aggregates. However, because the shear applied is in competition with the size-dependent Brownian motion, the difference in particle size for the two systems needs to be accounted for.

A more meaningful comparison can thus be achieved by using a reduced critical shear stress $\sigma_{r,c}$ [31] defined as:

$$\sigma_{r,c} = \frac{\sigma_{r,c} R^3}{kT} \tag{5.14}$$

Where R is the radius of the colloidal particle, k is the Boltzmann constant ($k = 1.38 \times 10^{-23}\,\mathrm{J \cdot K^{-1}}$) and T is the temperature of the suspension (here $T = 298\,\mathrm{K}$). Such a dimensionless critical stress is the equivalent of a Péclet number, in that it weights the effect of shear against diffusion caused by Brownian motion.

The values of $\sigma_{r,c}$ are subsequently calculated, for the shear-thinning samples presented here, using $R_{drop} \equiv R_{h,drop} = 110\,\mathrm{nm}$ and $R_{prot} \equiv R_{h,prot} = 10\,\mathrm{nm}$. For all samples, the reduced critical shear stress $\sigma_{r,c}$ is displayed in Figure 5.16 (b).

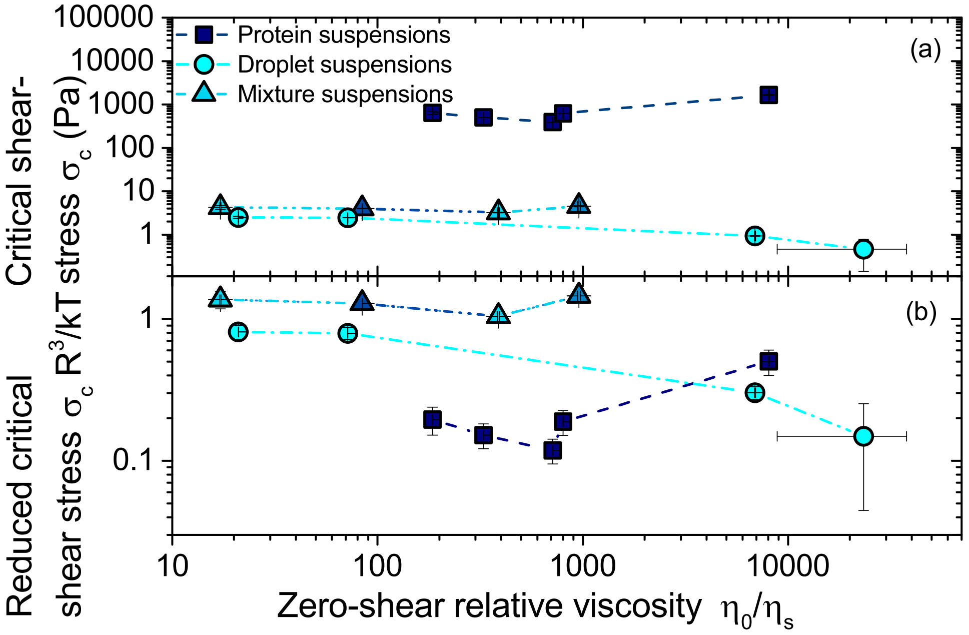

Figure 5.16 *Shear thinning behaviour of concentrated suspension of sodium caseinate (squares, navy), sodium-caseinate stabilised droplets (circles, cyan), and of mixtures of both (triangles, colour-coded by the value of χ_{prot}) as characterised by the critical shear stress for shear-thinning.*
(a) Critical shear stress σ_c as a function of the zero-shear relative viscosity η_0/η_s for several concentrated suspensions. σ_c and η_0 were estimated by fitting the flow curves in Figure 5.14 and 5.15 with Equation 2.7.
(b) Reduced critical shear stress $\sigma_{r,c}$ 5.14 as a function of the zero-shear relative viscosity η_0/η_s. The error bars indicate the uncertainty of the fitting parameters, and the lines are indicated as guide for the eye.

A first observation is that the discrepancy between droplet suspensions and protein suspensions mostly fades away when the reduced critical shear-stress is used, confirming that the main difference between both systems is the size of the particles and that there are no differences in interparticle interactions at high concentrations, notably no further extensive aggregation of sodium caseinate. Shear thinning is thus another aspect of the rheology of sodium caseinate that shows a definitive colloidal rather than polymeric behaviour.

In addition, there seems to be a decrease in the critical shear-stress with volume fraction for droplet suspensions while no trend can be identified for the protein suspensions. This may correspond to the two regimes of critical shear stress observed in Reference [35] as a function of the volume fraction for hard spheres: $\sigma_{r,c}$ first increases up to $\phi = 0.5$ and then decreases. This change in critical stress with concentration might be attributed to a decrease in volume occupied by particles at high volume fraction.

Bimodal mixtures of proteins and droplets and critical shear stress

Because of the differences in nature and sizes of the components in the mixtures, it is more difficult to interpret the behaviour of shear-thinning samples. In addition, the emulsions presented here vary significantly in composition, as underlined in Table 5.2, making it challenging to compare the mixtures to the pure samples of droplets and proteins.

Interestingly, the critical shear stress σ_c for the mixture samples is close to the one found for the droplet suspensions, so as a first approximation the droplet size is used to calculate the reduced critical shear stress $\sigma_{r,c}$, ie $R_{mix} \equiv R_{h,drop} = 110\,\mathrm{nm}$. As can be observed in Figure 5.16 (b), the resulting $\sigma_{r,c}$ are only slightly larger than the values obtained for droplet suspensions.

This result seems to indicate that the shear thinning behaviour of mixtures in this range of shear stresses is dominated by the bigger particles, here the protein-stabilised droplets. It is in theory possible that the system displays a double shear thinning and that at higher shear stress, not reached experimentally here, a second shear thinning regime due to the proteins would occur.

The characterisation of more concentrated samples of mixtures would be required to weight the relative effects of the total volume fraction $\phi_{eff,tot}$ and of the composition χ_{prot} on the shear thinning behaviour of such suspensions. In particular, it would be interesting to see either mixtures containing more proteins, *i.e.* with a greater χ_{prot}, would have behaviours closer to suspensions of pure proteins or if even a relatively small amount of droplets is enough to dominate the shear thinning.

5.7 Conclusion

Here, the first step in characterising protein-stabilised emulsion gels as a function of its components is described. Indeed, the study of the sols is an important source of information for characterising the systems. First, knowing the viscosity of semi-dilute systems allows the estimation of an effective volume fraction, which is a necessary step to study both suspensions and gels with different compositions. In addition, the study of the viscosity of concentrated suspensions demonstrated the relevance of a colloidal framework to study protein-stabilised emulsions and the limits of the model hard sphere system for their descriptions. This study also made it possible to draw specific conclusions on suspensions of pure sodium caseinate, caseinate-stabilised droplets and mixtures of the two components.

About protein suspensions first, it is interesting to note that previous studies have attempted to compare the rheological properties of sodium caseinate to those of a suspension of hard spheres, and found that agreement at high concentrations is poor [63, 110]. As a result it was concluded that a colloidal model is inadequate to describe the observed behaviour. Here I argue that this is mainly due to the choice of hard spheres as colloidal reference, and I show that using the framework developed for soft colloidal particles [3], helps toward a better description of the viscosity behaviour of the protein dispersions. Although this approach neglects the additional layer of complexity due to the biological nature of the sodium caseinate , such as inhomogeneous charge distribution and dynamic aggregation [142, 143], it gives a satisfactory model that can be used to build a better description of protein-stabilised emulsions. This approach will thus be used to characterise the gels formed by these systems in Chapters 6 and 7. Interestingly, the soft colloidal approach can also be successfully applied to the rheology of non-colloidal food particles, such as fruit purees [56].

In addition, the viscosity behaviour of the nano-sized droplets appeared to be very similar to the hard sphere model. In Chapter 6 the similarity of the protein-stabilised droplets with colloidal hard spheres will also be applied to droplet gels.

The main discrepancy for suspensions of droplets is the high effective volume fraction at which the viscosity diverges, which may be due to the size distribution of droplets or arise from the softness of the layer of adsorbed proteins. This will be further investigated by studying the viscosity of suspensions containing larger droplets in Chapter 8, for which the softness is modified as the internal pressure and the influence of the soft layer of proteins are decreased.

Finally, examining protein-stabilised emulsions as ternary mixtures of water, unadsorbed proteins and droplets has allowed the development a semi-empirical model for their viscosity. The contributions of each component to the overall viscosity of the emulsions being quantified by the analysis of the properties of the pure suspensions of droplets or proteins. It should be noted, however, that the droplet size is likely to be critical to the validity of the model, as it is expected that flocculation of droplets will occur for larger droplets [85, 113, 118, 119]. This is due to the depletion interaction generated by the proteins in the mixture, which is not taken into account in the present model.

In the next chapters, gels rather than suspensions will be studied. A similar approach of the mixtures will be used, so the pure gels of proteins and droplets will first be studied separately in Chapter 6 and then the contributions of each component in the properties of the emulsion gels made of both proteins and droplets will be investigated in Chapter 7. Because the elasticity of these networks arise from different mechanisms than the viscosity of colloidal suspensions, I will show that the combination of the results from pure gels of proteins and droplets is more complex than presented here.

Chapter 6

Protein gels and protein-stabilised droplet gels: gelation, microstructure and rheology

In this Chapter, I present the gels made from the suspensions studied in Chapter 5, and prepared as described in Chapter 3. The study of gels of pure proteins and of pure droplets highlights the similarities and differences of such systems, setting the foundations for the characterisation of emulsion gels, seen as mixtures of droplet and protein gels, that will be presented in Chapter 7.

First, I study the acid-induced gelation of protein and droplet suspensions. This sol-gel transition is characterised using rheo-imaging and rheometry techniques. I find that for the two types of samples, the gelation is very similar to the formation of colloidal gels by aggregation of particles into clusters and percolation into a space-filling network.

Then, I use confocal microscopy to characterise protein and droplet gels formed at several volume fractions. Their microstructure is also in agreement with the theory on colloidal gels, and the features can be quantified using Fast Fourier Transform analysis.

Finally, I present a range of rheological properties of the gels and their variation with volume fraction. The scaling by volume fraction indicates that protein gels and droplet gels are more similar than was believed. Some minor variations, such as the frequency dependence, are consistent over the range of volume fractions studied and thus enable the discrimination between the two types of gels.

6.1 Introduction

Emulsion and protein gels form the basis of many food products, such as yoghurt, soft cheese or tofu, where the acidification of a vegetable or animal milk leads to the formation of a soft solid via aggregation of proteins and fat droplets. This ancient process has been used for more than 1000 years in traditional cooking, but a deep understanding of the mechanisms of the physical transformation occurring in these systems only came in the recent decades with the study of colloidal gels [17]. While much effort has been spent in correlating the structure formation and the gel properties with the interparticle interactions [77], there are still many challenges for a full understanding of colloidal gels, both in terms of fundamental science and of specific applications.

Colloidal gels differ from polymer gels by their fractal, rather than fine-stranded, microstructure and the enthalpic, rather than entropic, origin of their elasticity. However, within the family of colloidal gels, several sub-categories can be identified, depending on the route to gelation [20, 77]. Here, we focus on gels formed by diffusion-limited cluster aggregation (DLCA gels). In these systems, particles present a short-range attraction, and thus stick immediately to each other upon contact. This leads to the aggregation of particles into clusters, that ultimately form a space-spanning network that gives rise to viscoelastic properties. The gels formed are fractal gels [78] and their mechanical properties can be linked to their fractal microstructures, as it will be discussed later. This theoretical framework can be applied not only to model attractive hard spheres, but also to protein and emulsion gels, and in particular to casein systems.

Sodium caseinate is charged negatively at neutral pH, but as the suspending medium is acidified, the charge at the surface of the protein decreases, and at the isoelectric point the average surface charge reaches zero. The decrease in electrostatic repulsion leads to the aggregation of proteins that, if slow and rather homogeneous, leads to the formation of a gel [22, 120–122, 126]. As demonstrated in Chapter 5, the colloidal framework is a convenient model to study sodium caseinate suspensions, and it is extended here to caseinate gels.

Casein and caseinate gels have attracted a sustained interest in the past 3 decades, and some key features have been identified. First, a power-law dependence of the viscoelasticity of acid casein gels on concentration, using both native casein and sodium caseinate, was observed in previous studies [79, 121], and was attributed to the fractal nature of this type of protein gels, as demonstrated by imaging of their microstructure [78, 120]. Interestingly, native casein can also form depletion gels, for which a similar scaling of the elastic modulus with the volume fraction may exist, although it is unclear if G' presents an exponential or a power law-dependence with the volume fraction [154]. In addition, the frequency dependence of the gels has been characterised [79, 120, 127] . Finally, the brittle fracture of casein gels has also been studied from a fundamental perspective [124, 128].

Emulsion gels have also been studied in the past and compared to protein gels [23, 120, 129], but never have the protein-stabilised droplets been separated from the un-adsorbed proteins with which they are mixed in suspension. The present study is motivated by an improved understanding of the contributions of each component in emulsion gels, hence the need to characterise gels made of pure droplets stabilised by a layer of adsorbed caseinates.

The comparison here is thus to be drawn between gels made of proteins suspended in solution and systems where proteins are adsorbed at the interface of nano-sized droplets, as characterised in Chapter 4. In addition to the relevance of droplet gels to food products like yogurt, this comparison also yields fundamental questions on the nature of fractal gels. Indeed, the inter-particle interactions are the same and arise from the destabilisation of sodium caseinate, but the particles differ in their size, nature and softness.

The approach used for such a comparison is the study of gels at a wide range of concentrations for each system. To identify intrinsic differences between droplet gels and protein gels, it is indeed essential to contrast the behaviours of the parameters with the composition of the systems, rather than comparing individual samples. The concept of the effective volume fraction of colloidal suspensions introduced in Chapter 5 is instrumental to tackle this challenge and is thus extended here to the gel systems. Therefore, the microstructure and several aspects of the rheology of protein and droplet gels are studied over a range of volume fractions to examine the similarity of gels involving similar interactions but different constitutive particles. The results obtained will also build the foundations for the following study of emulsion gels seen as mixtures, detailed in Chapter 7.

After the preparation of the samples, rheo-imaging, confocal microscopy and oscillatory rheometry were used to characterise the gels of different compositions. It has been shown that the gelation of sodium caseinate and the gel properties depend on extrinsic factors [22], such as final pH [120], volume fraction [121], or incubation temperature [122]. To reduce the number of variables, some of these factors were arbitrarily set here:

- Wherever possible, the temperature was fixed at 35 °C for a reasonably fast gelation. This choice may affect other aspects of gelation such as cluster and network formation [121].
- The final pH was fixed by the amount of acidifier used, as described in Chapter 3. Small variations have however been observed with such a technique upon change of concentration of protein [122, 126], but the final pH was kept between 4 and 5, a range that ensures formation of the strongest gels [120].

Here, we first consider the dynamical process of gelation. The gels are then studied in their metastable state, which in the absence of equilibrium is considered to be an arrested state. In both cases, we use information on the microstructure, obtained by confocal microscopy, and on the mechanical properties, obtained by rheometry, to draw comparisons between the behaviours of protein and droplet gels.

6.2 Materials & Methods

6.2.1 Preparation of the sols

Suspensions of pure sodium caseinate, pure sodium caseinate-stabilised droplets and of mixtures of both components were prepared as described in Chapter 3. They were then used as sols for the preparation of acid-induced gels.

6.2.2 Gelation

The decrease in pH required for the gelation of the sols to occur was caused by the slow hydrolysis of glucono δ-lactone (Roquette), as described in Chapter 3. For the rheometry, the sols containing glucono δ-lactone were placed in the rheometer cup just after preparation, and the measurements were started immediately. For the microstructural characterisation, the sols were first mixed with the fluorescent dyes, then with glucono δ-lactone and placed in CoverWell imaging chambers (diameter 20 mm, thickness 1.7 mm, Grace Bio-Labs). The chambers were filled and sealed with a glass cover slide, then incubated at 35 °C before imaging.

6.2.3 Oscillatory Rheometry

Oscillatory rheology measurements were performed using a stress-controlled MCR 502 rheometer (Anton Paar) and a Couette geometry (17 mm radius profiled bob and cup CC17-P6, inner radius 16.66 mm, outer radius 18.08 mm yielding a 1.42 mm tool gap, gap length 25 mm, serration width 1.5 mm, serration depth 0.5 mm). To avoid slip at the wall during shearing, profiled bob and cup were selected as measurement tools. The temperature was set by a Peltier cell at 35 °C during the entire measurement sequence. To prevent evaporation, a thin layer of silicon oil of low viscosity (10 cSt) was deposited on the surface of the sample before starting the measurement.

As represented in Figure 6.1,the measurements consisted in 4 steps:

1. Small-amplitude oscillations to follow the development of viscoelasticity with time during gelation. The measurement is arbitrary long (9000 sec), so depending on the gelation time the ageing of the gel is different from one sample to the other in the following steps. The signal was kept constant over this step, and the multiwave mode was activated to simultaneously measure the gelation behaviour at several frequencies. The shear signal was thus the superposition of sinusoids of amplitude $\gamma_0 = 0.5\,\%$ at the frequencies 0.2 Hz, 0.6 Hz, 1 Hz, 2 Hz, 5 Hz, 10 Hz (maximum amplitude: $\gamma_0 = 4.0\,\%$).

2. Frequency sweep to measure the frequency dependence of the moduli for the newly formed gel: with the multiwave mode still activated, the frequency was logarithmically increased ($f = 0.005 \ldots 50\,\mathrm{Hz}$ for the base frequency) at fixed amplitude ($\gamma_0 = 4\,\%$). The multiwave mode allows to obtain more data points without slowing the measurement down.

3. Dynamic strain sweep to measure the range of the linear regime and the onset of non-linearity: the amplitude of the deformation was logarithmically

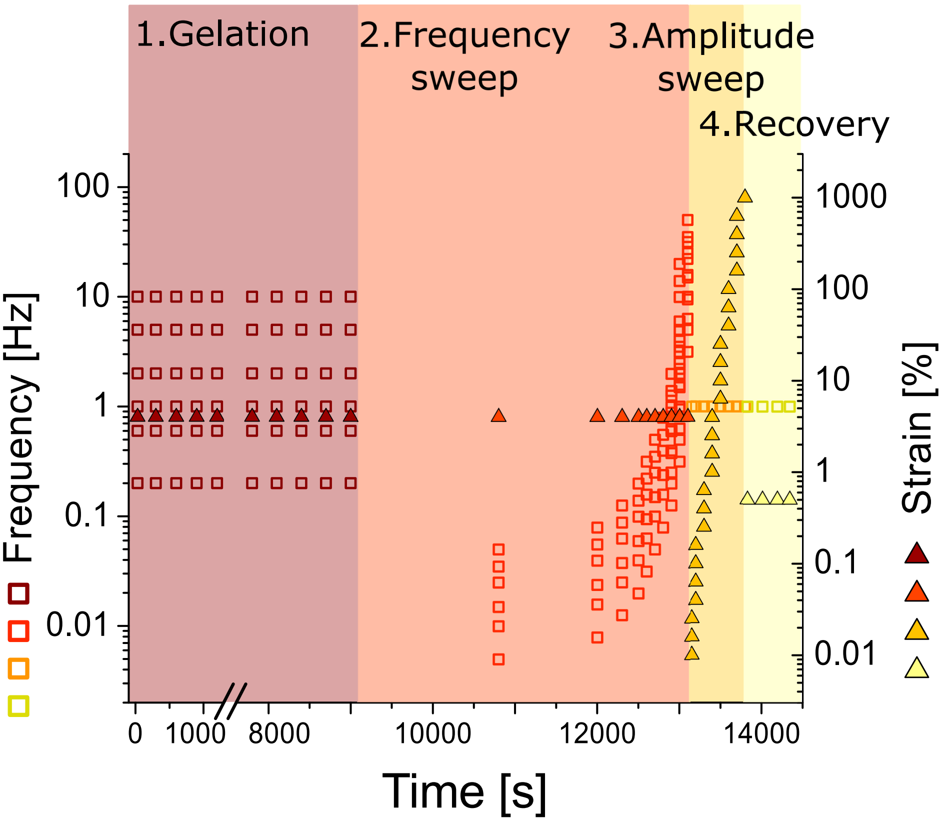

Figure 6.1 *Illustration of the measuring sequence for the oscillatory rheometry of the emulsion gels, detailed in the Methods part. Frequency (open squares) and strain amplitude (filled triangles) of the oscillatory shear vary with time in the 4 steps of the measurement. At the time $t = 0\,\mathrm{s}$, the glucono δ-lactone was added to the sols.*

increased ($\gamma_0 = 0.01 \ldots 1000\,\%$) at fixed frequency ($f = 1\,\mathrm{Hz}$). It is assumed that because of the low amplitude used during the frequency sweep, the structure of the gel was not modified.

4. Small-amplitude oscillations to see if there is recovery of elasticity at rest after the breaking of the structure: a constant signal was applied over time ($\gamma_0 = 0.5\,\%$ and $f = 1\,\mathrm{Hz}$)

For each sample, 3 measurements were performed and the values were averaged.

6.2.4 Laser scanning confocal microscopy

The gels were imaged using laser scanning confocal microscopy, here a setup based on LSM 780 microscope on inverted Axio observer (Zeiss).

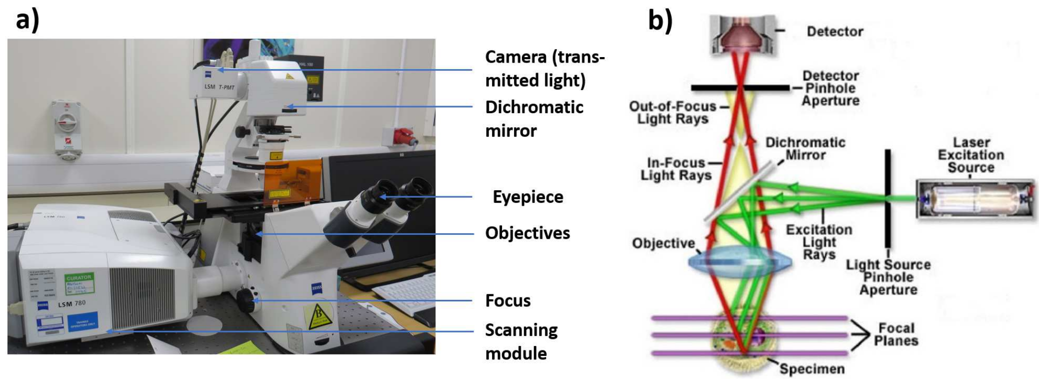
a)
Camera (trans-mitted light)
Dichromatic mirror
Eyepiece
Objectives
Focus
Scanning module
b)
Detector
Detector Pinhole Aperture
Out-of-Focus Light Rays
Dichromatic Mirror
Laser Excitation Source
In-Focus Light Rays
Objective
Excitation Light Rays
Light Source Pinhole Aperture
Focal Planes
Specimen

Figure 6.2 *Illustration of laser scanning confocal microscopy: (a) Setup of the confocal microscope used in this study (LSM 780 with inverted Axio observer, Zeiss), (b) Principal light pathways in confocal microscopy (reproduced from Ref. [15]).*

This fluorescence microscopy technique, illustrated in Figure 6.2, is based upon point-by-point scanning of the sample in the focal plan by a laser beam. The image is then reconstructed pixel-by-pixel by collecting the emitted fluorescence. Confocal microscopy is a useful tool to elucidate the microstructure of colloidal systems and has been extensively used to that purpose in the last three decades [155].

The main advantage of confocal microscopy is the spatial filtering, using a pinhole in front of the detector, which allows removal of the out-of-focus light. The thickness of the optical “slice” is adjusted by changing the aperture of the pinhole. In practice, this gives the ability to image within the sample without further sample preparation, and the associated risks of modification. By carrying out a series of measurements on several consecutive optical slices, a 3D image of the sample can be reconstructed, despite a significantly lower resolution on the z-axis.

Multi-component systems are conveniently imaged by confocal microscopy using several channels to measure the emitted fluorescence at different ranges of wavelengths. Several lasers can also be used to induce fluorescence over a wide range of emission wavelengths. Because the lasers are powerful, it is important in the imaging protocol to keep the exposure time low enough that little local heating is induced upon scanning.

Whilst some natural tissues present autofluorescence, it is common to add fluorophores in samples to label specifically their different components.

Fluorescent dyes

A wide range of commercial fluorescent dyes is available to label different components, depending on specific molecular interactions or hydrophobicity. The choice of fluorophores is important in the imaging protocol to ensure the accuracy of the measurements.

A much-used dye for emulsions is Nile Blue. Indeed, this fluorophore dyes proteins efficiently, and contains traces of an associated dye, Nile Red, which dyes apolar phases such as oil. However, Nile Blue and Nile Red present an overlap of the two absorption and emission spectra, as well as a strong dependence of their spectra with the environment, which make them not ideal for an accurate imaging of the gelation process.

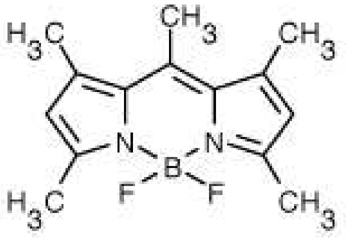

Figure 6.3 *Molecular structure of Bodipy 493/503*

Instead, in this study, Rhodamine B (Sigma Aldrich) and Bodipy 493/503 (Molecular Probes) were identified as a more appropriate pair of dyes. Indeed, Rhodamine B gives satisfying results in labelling acid-induced sodium caseinate gels [10]. In addition, Bodipy 493/503 makes a good tracer for oil thanks to its non-polar structure and its narrow spectra, both in excitation and in emission. Its blue colour is also far away from the red of Rhodamine B.

Protocol for imaging of gels

The gels were prepared in advance in imaging chambers (CoverWell, diameter x thickness 20 mm × 1.7 mm, Grace Bio-Labs) so they could be examined without the modifications of the structure that inevitably occur when the samples are squeezed or scooped out. Because the gelation is not instantaneous, the following preparation protocol was carried out on the day before the imaging.

Thus, Rhodamine B (dissolved in water at 0.01 %, for protein suspensions and protein-stabilised emulsions) and Bodipy 493/503 (dissolved in ethanol at 0.001 %, only for protein-stabilised emulsions) were added to the sols, respectively at ≈ 90 ppm and ≈ 15 ppm.

For each concentration and type of gel, a 3 g sol sample was prepared and mixed with the desired amount of fluorescent dyes first, and then with the appropriate amount of glucono δ-lactone quickly dissolved in a droplet of water (as described in Chapter 3). After mixing, the imaging chamber was filled with the suspension and sealed with a glass coverslip. It was then deposited in a small beaker that was placed in a water bath set at 35 °C and left to gel overnight. Finally the imaging chamber was left to equilibrate at room temperature before being examined with a LSM 780 (Zeiss) confocal microscope.

6.2.5 Rheo-imaging

Simultaneous rheological and microscopical measurements can be performed on viscoelastic materials using rheo-imaging. The setup is illustrated in Figure 6.4 and is the combination of a rheometer head with a confocal microscope. The sample is imaged through a glass slide that replaces the rheometer plate, at a point shifted from the centre of the measuring tool. A more detailed description of a similar device can be found elsewhere [156].

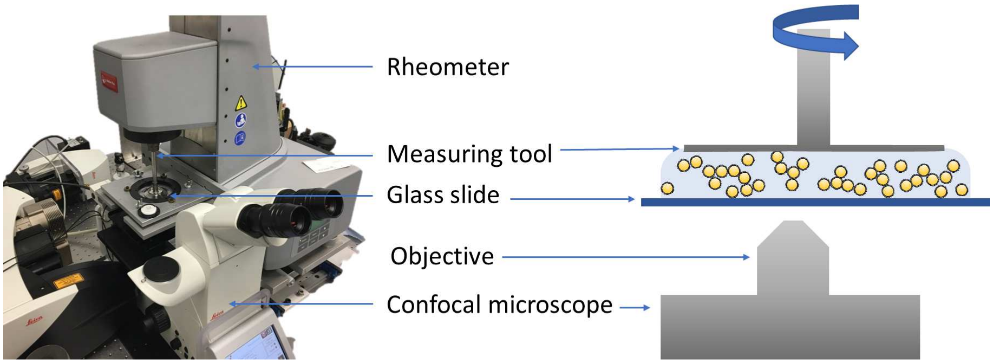

Figure 6.4 *Experimental setup for rheo-imaging. Assembly of a rheometer (MCR 502, Anton Paar) and a fast-imaging confocal microscope (DMI8-CS, Leica). The cartoon represents the measurement zone: the sample is deposited between a circular glass slide and a rheometer tool, here a plate geometry (PP25, smooth).*

The use of this setup allows the imaging of samples under shear and the

Table 6.1 *Experimental details for the rheo-imaging of protein and droplet gels*

Parameter	Protein gel	Droplet gel
Concentration	$c = 1.4\,\%$(wt)	$c = 5\,\%$(wt)
Volume fraction	$\phi_{eff,prot} = 9.8\,\%$	$\phi_{eff,drop} = 9.0\,\%$
Glucono δ-lactone	0.18 g gdl/g protein	0.075 g gdl/ g droplet
Objective	20x/0.75 dry	20x/0.75 dry
Laser	552 nm	552 nm
Rhodamine B	≈ 90 ppm	≈ 90 ppm
Bodipy 493/503	0	≈ 15 ppm
Rheometer tool	PP25/S	PP25/S
Gap	500 µm	500 µm
3D stack size	57 frames	30 frames
Time for 3D stack	44 s	13 s
Delay between 3D stacks	120 s	60 s

correlation of their microstructure changes with their viscoelastic behaviour. Here, a rough sand blasted top plate of diameter 25 mm was chosen as measuring tool to prevent slip, while the bottom plate was necessarily a glass slide with no roughness. Silicon oil was deposited around the edges of the rheometer tool to avoid evaporation of water during the measurement.

The exact configurations used for the different samples are described in Table 6.1.

The rheo-imaging setup presented here allowed the imaging of the gelation process of the suspensions. Indeed, the sols were mixed with glucono δ-lactone and immediately placed on the glass slide used as the rheometer plate. Oscillatory rheometry and 4D imaging (3D stacks imaged at a different points in time) could be performed simultaneously, and the fast scanning unit of the Leica microscope provided a good temporal resolution, as the scanning time for a frame of 1024×1024 pixels was 0.8 s.

6.2.6 Image analysis

The image analysis of 2D micrographs obtained using either a standard confocal microscope or a rheo-imaging setup is performed using the image processing software ImageJ [157].

The Fast Fourier Transform (FFT) analysis is applied to the image after Hanning windowing. The image in the Fourier space is then radially averaged to obtain the spectrum $I(q)$. In the case of rheo-imaging sequences, the structure factor $S(q)$ at time t is calculated by dividing this quantity by the spectrum of the suspension $I(q, t = 0)$, obtained by averaging 3 spectra of images captured before the gelation occurs, so $S(q, t) = I(q, t)/I(q, t = 0)$. The wave vector q represents a spatial frequency, it is a function of the distance from the centre in the Fourier space and of the image size, and is expressed in μm^{-1}.

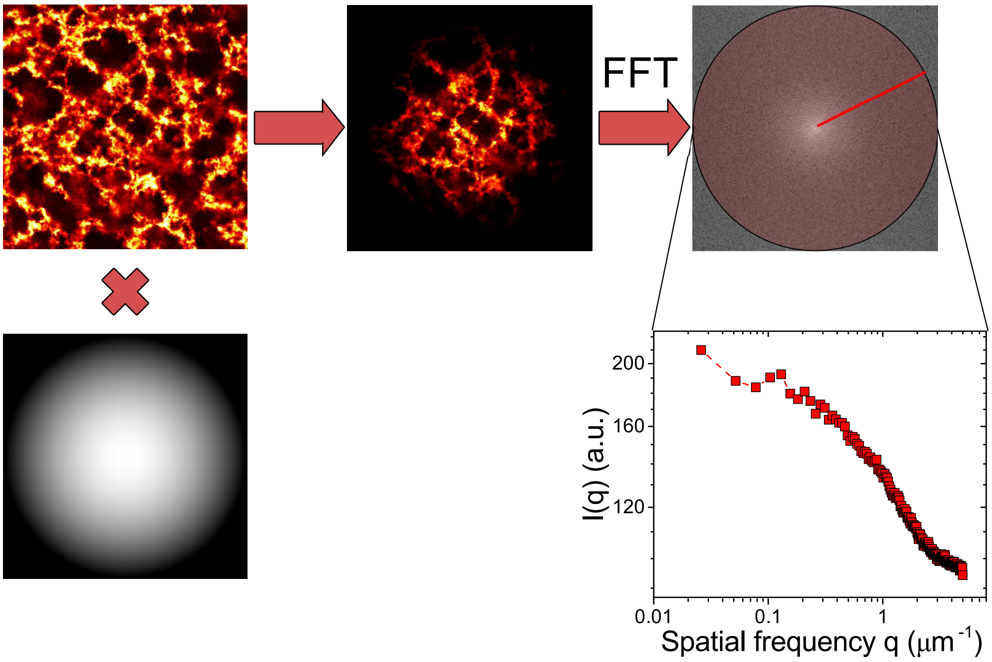

Figure 6.5 *Protocol for the Fast Fourier Transform of a micrograph. The image is multiplied by a Hanning window of the same size before the FFT is calculated. The spectrum $I(q)$ is obtained using the plugin Radial Profile to perform a radial average of the Fourier transform.*

The variations of both $I(q)$ and $S(q, t)$ can be described by several parameters. The determination of the two parameters chosen in this study, the position of the shoulder q_c and peak height, is illustrated in Figure 6.6. The position of the shoulder is chosen as critical wave vector because it can be estimated in a reproducible way by fitting the power law decrease of the peak, as opposed to the top of the peak that is slightly flattened.

It has to be noted that the resolution of confocal microscopy (limited to $\approx 200\,\text{nm}$ by light diffraction) does not allow imaging of the single protein aggregates, or single droplets. Instead, the range of wave vectors q accessible by this imaging technique corresponds to the structure over a few colloidal particles, and is thus

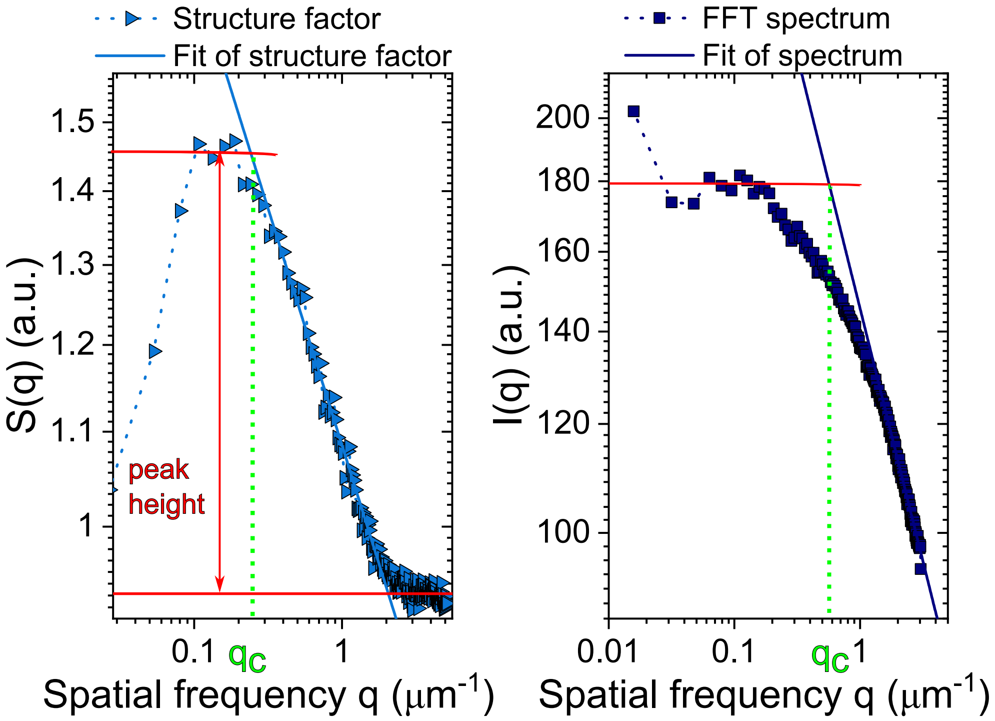

Figure 6.6 *Illustration of the quantifications of the gel microstructure and extraction of the parameters from the Fast Fourier Transform analysis. The decrease of the structure factor $S(q)$ (left) and FFT spectrum $I(q)$ (right) is first fitted by a power law, linear in double logarithmic scale. Its intersection with the plateau defines the critical spatial frequency q_c. The distance between the plateau at low and high frequency (red arrow) marks the peak height.*

more suitable for the description of colloidal aggregation and gelation than for the supramolecular structure of the particles. The latter would require to use neutron or X-ray scattering.

6.3 Formation of protein and droplet gels: kinetics of gelation

When glucono δ-lactone is added to aqueous solutions such as suspensions of proteins and of protein-stabilised droplets, it is progressively hydrolysed in gluconic acid, thus decreasing the pH, as presented in Chapter 3. This, in turn, destabilises the protein, whether adsorbed at the oil/water interface or in suspension, and causes aggregation of the colloidal species. Here we focus on the gelation of sodium caseinate and of caseinate-stabilised droplets, and we study the structure formation and the subsequent emergence of viscoelasticity.

6.3.1 Gelation and microstructure coarsening

The gelation of a suspension of colloidal particles such as sodium caseinate and caseinate-stabilised droplets consists of the aggregation of particles into fractal clusters that, under certain conditions, form ultimately a gel structure [20, 77, 78]. Although the small size of the particles used here, presented in Chapter 4, is lower than the resolution limit of confocal microscopy, the rheo-imaging technique, presented in Figure 6.4, makes possible the observation of the structure formation that occurs inside the sample during gelation. Because the confocal microscope is coupled with a rheometer, the technique also gives access to the viscoelastic properties of the sample at any point in time. It is thus possible to correlate rheology and microstructure during gelation.

Rheo-imaging during gelation of a protein suspension

The rheo-imaging study of the gelation of a semi-dilute suspension ($\phi_{eff,prot} = 9.8\,\%$) of sodium caseinate at room temperature is presented in Figure 6.7. For clarity, only a few stages of the gelation were selected here, and the snapshots were taken at a fixed depth in the sample (at 10 µm from the bottom coverslide). These results can be discussed following the chronology of gelation.

First, as noted previously, the hydrolysis of glucono δ-lactone is progressive, so initially the pH is above the isoelectric point of sodium caseinate, and there is little to no aggregation of the naturally-occurring protein assemblies. Here, the first micrograph shows that the sample is homogeneous at the scale of observation. Macroscopically, the sample still behaves as a liquid, as will be detailed later, so it is likely that the values of viscoelasticity and their increase at this stage are related to measurement uncertainties.

As the pH drops, as can be observed in micrographs 2 and 3, a dark protein-depleted aqueous phase and a bright protein-rich phase appear, and this phase separation shows that extensive aggregation of the protein takes place. This stage corresponds to a pH close to the isoelectric point, at which the electrostatic repulsion between proteins fades away and attraction dominates the interpacticle interactions. At this stage, the viscoelasticity is low as the aggregates can still

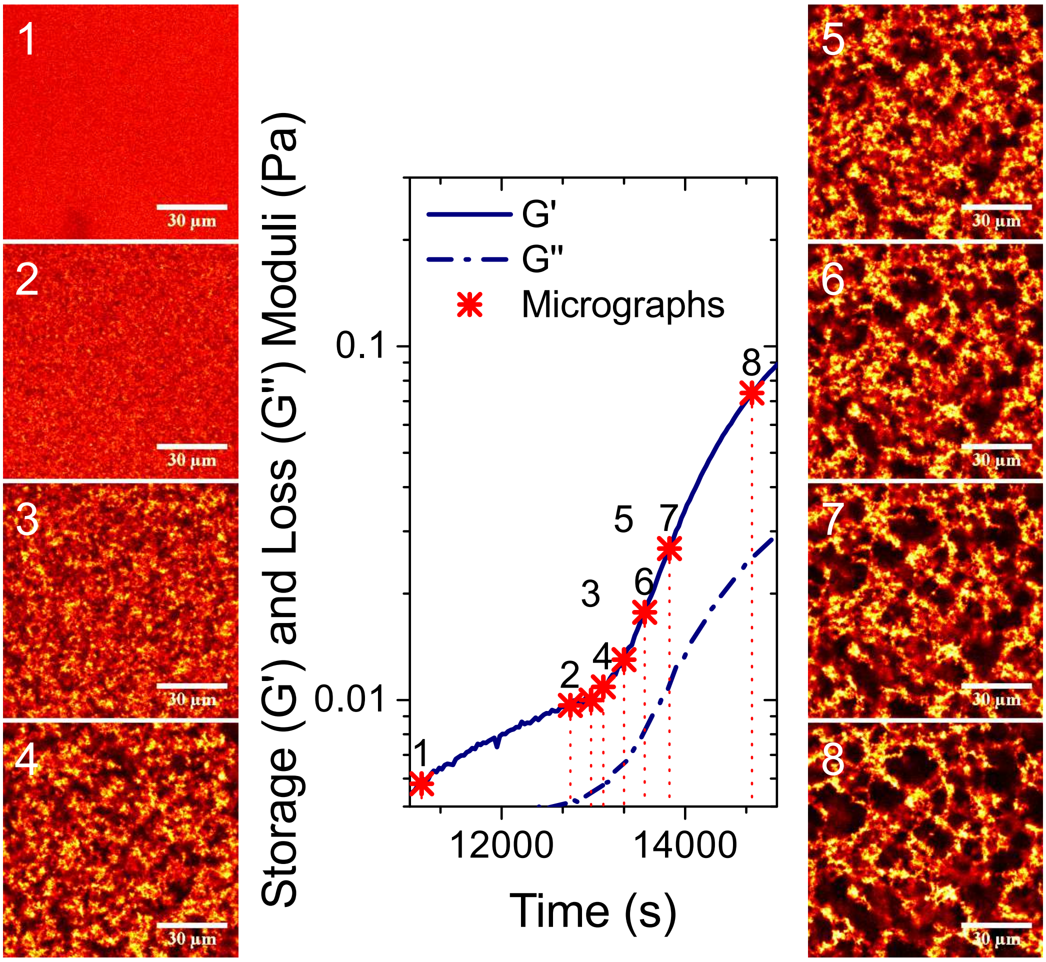

Figure 6.7 *Confocal micrographs of acid-induced gelation of a suspension of sodium caseinate* ($\phi_{eff,prot} = 9.8\,\%$) *at room temperature, and emergence of viscoelasticity.*
Sodium caseinate is labelled by adding Rhodamine B in the suspension before gelation. Each frame is taken at $10\,\mu\mathrm{m}$ *above the glass slide and at different stages of gelation, and is numbered from top to bottom and left to right: (1)* $t = t_0 = 11 \times 10^3\,\mathrm{s}$ *after addition of glucono* δ*-lactone. , (2)* $t = t_0 + 1620\,\mathrm{s}$, *(3)* $t = t_0 + 1845\,\mathrm{s}$, *(4)* $t = t_0 + 1980\,\mathrm{s}$, *(5)* $t = t_0 + 2205\,\mathrm{s}$, *(6)* $t = t_0 + 2430\,\mathrm{s}$, *(7)* $t = t_0 + 2700\,\mathrm{s}$, *(8)* $t = t_0 + 3600\,\mathrm{s}$. *The length of the scale bar represents* $30\,\mu\mathrm{m}$*.*
The storage (G', solid line) and loss (G", dashed line) corresponding to the micrographs are indicated on the gelation plot (red stars).

diffuse freely in the suspension. But, as the clusters keep growing, they soon become interconnected, as can be observed in micrograph 4. The formation of a space-filling network marks the onset of the rise in viscoelasticity, as the system reaches the gelation point.

As soon as a network is formed, both storage (G') and loss (G'') moduli increase sharply, as can be noted on the rheological response. Micrograph 5 represents the gel just after percolation of the network, and the following images are mostly similar to it. The main difference that appears is a progressive widening of the pores and narrowing of the protein strands. This seems to indicate that the initial network forms a very soft solid, and that the viscoelastic properties of the gel mostly arises from the reorganisation of the proteins within this network and its subsequent coarsening.

These results are consistent with the model of gelation envisioned as a kinetically arrested structure due to the crowding of fractal clusters [158]. Indeed, at the onset of viscoelasticity, the gel appears to be formed of interconnected clusters, and its mechanical properties are linked to their open structure. Over the next 20 min however, the clusters seem to be significantly modified as they become denser and smaller, and leave more space for the pores, while the general pattern of the network stays identical. These changes are probably responsible for the rise of the storage and loss moduli. A similar coarsening was obtained for rennet-induced casein gels [123].

In addition, the large dependence of viscoelasticity on the ageing of the network demonstrates that the correlation of confocal micrographs of different gels with their rheological properties requires great caution. The results presented here show the rheology of a given gel is more related to its structure at the mesoscale (dozens of particles) than to the topology of the network. Indeed, pictures that seem overall similar relate to very different values for the viscoelasticity of the gel. Instead, it is necessary to examine the micrographs in detail and to study the time evolution at a smaller length scale, corresponding to individual strands of colloidal particles. Other observation techniques would thus be needed to fully relate structure of the network (over a wide range of lengthscales) and rheology [159].

Rheo-imaging during gelation of a droplet suspension

Similarly to protein, the gelation of a protein-stabilised droplet suspension ($\phi_{eff,drop} = 9.0\,\%$) at room temperature can be studied using the rheo-imaging setup, and is presented in Figure 6.8. The quality of the rheology measurement could be improved but it is assumed here that the gelation behaviour is representative of the general behaviour of gelling droplets.

The micrographs presented here are significantly more heterogeneous, at the scale of the image, than in Figure 6.7 for proteins. Indeed, from frame 2 to 7 the bottom right of the image appears significantly different from the rest of the image. It seems that the gelation is not occurring homogeneously but rather following a front that is spreading here from bottom right to top left. This anisotropy is markedly dissimilar to the gelation of sodium caseinate, where a rather uniform cluster growth was observed until percolation.

In addition, if coarsening of the image is observed in frames 1 to 5, consistent with the protein case, the mechanisms leading to the reinforcement of the network appears to be different. Indeed, a careful observation of the frames between 6 and 8, including those not presented here, seems to indicate that when the network is formed, in the first stage, there are a significant amount of droplets forming small aggregates in the pores. These small-sized clusters then appear to either stick to the network, that is already formed, or to flow out of the field of view. This phenomenon is distinct from the jamming of clusters of similar sizes in the case of proteins, although both lead to an increase in storage and loss moduli.

Finally, at longer times after formation of the network, no deswelling of the gel strands can be observed. Instead, over 30 min after frame 8, the only visible change is the small-amplitude motion of the dangling strands in the network. This could be related to a different structure of the clusters at a smaller size scale, as droplet clusters may not reorganise as much as protein clusters. It may also be due to internal rigidity of the droplets as opposed to the softness of the proteins.

In order to explain theses difference in mechanisms leading to the formation of gels in the case of sodium caseinate and of caseinate-stabilised droplets, two main discrepancies can be accounted for. First, the size of the elementary particles differs by an order of magnitude, as shown in Chapter 4. This results in a difference in their mobility, that may play a part in the formation of gels. In

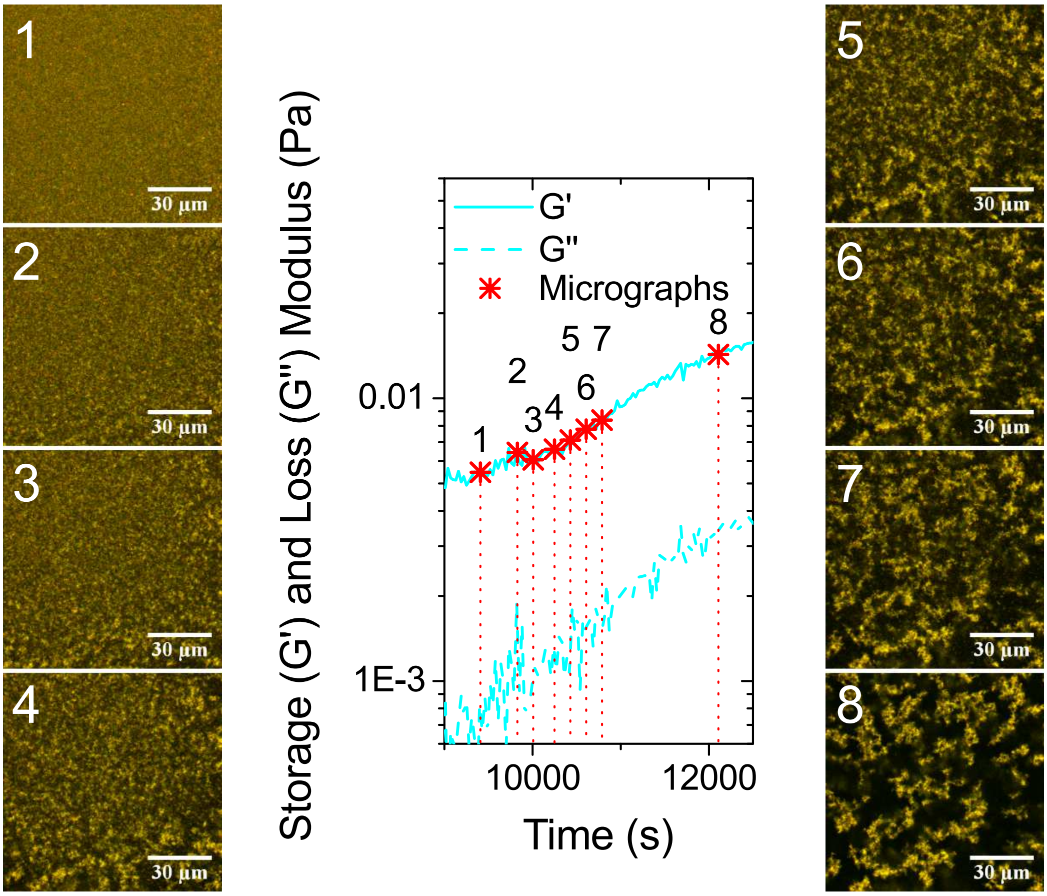

Figure 6.8 *Confocal micrographs of acid-induced gelation of a suspension of caseinate-stabilised nanosized oil droplets ($\phi_{eff,drop} = 9.0\,\%$) at room temperature, and emergence of viscoelasticity.*
Sodium caseinate is labelled using Rhodamine B, and oil using Bodipy 493/503, both were added in the suspension before gelation. Each frame is taken at $10\,\mu\text{m}$ *above the glass slide and at different stages of gelation, and is numbered from top to bottom and left to right: (1)* $t = t_0 = 9.4 \times 10^3\,\text{s}$ *after addition of glucono δ-lactone, (2)* $t = t_0 + 420\,\text{s}$ *, (3)* $t = t_0 + 600\,\text{s}$ *, (4)* $t = t_0 + 840\,\text{s}$ *, (5)* $t = t_0 + 1020\,\text{s}$ *, (6)* $t = t_0 + 1200\,\text{s}$ *, (7)* $t = t_0 + 1380\,\text{s}$ *, (8)* $t = t_0 + 2700\,\text{s}$ *. The length of the scale bar represents* $30\,\mu\text{m}$.
The storage (G', solid line) and loss (G", dashed line) corresponding to the micrographs are indicated on the gelation plot (red stars).

addition, there may be differences in the interparticle potential linked to the different supramolecular structures of these components. Little is known indeed about the difference in “stickiness” of sodium caseinate that is in suspension or adsorbed at an oil/water interface, at its isoelectric point.

Further work would be required to elucidate the exact source of this discrepancy, as the data presented here are not sufficient to fully explain it. Studying the gelation of different droplet sizes, or changing the temperature, could help identify the effect of the size of the elementary particles. In addition, looking at the gelation of other systems, such as hard spheres, of similar sizes, would allow pinpointing differences arising from the structure of the particles. Computer simulations would also be a relevant tool to investigate the effect of softness and mobility on gelation, while keeping constant all other variables, such as particle interactions.

Quantification of the formation of micro-structure during gelation

It is possible to further study the micrographs presented in Figure 6.7 and 6.8 by performing a Fast Fourier Transform (FFT) analysis on the images, as described earlier. The FFT spectra thus obtained are shown in Figure 6.9 (a). Their aspect is very similar to the structure factors obtained during the fractal aggregation of clusters of polystyrene spheres [160], where the mechanisms were related to a spinodal decomposition [161].

As can be seen, for both protein and droplet suspensions, the gelation and consequent emergence of microstructure is marked by the appearance of a peak in the Fourier space. This peak can be characterised by its height, and by its shoulder position q_C, as illustrated in Figure 6.6. The latter is defined as the intersection between the oblique asymptote at high q and the peak horizontal asymptote, and corresponds, in the real space, to the characteristic lengthscale $L_C = 2\pi/q_C$ of the structure. Characteristic lengthscales and peak heights for gelation of protein and droplet suspension can be found in Figure 6.9 (b).The FFT analysis thus allows quantification of the development of microstructure discussed previously.

A common feature of the gelation of protein and droplet suspensions is the formation of the fractal structure and the emergence of heterogeneity, as the strands become brighter and the protein-depleted pores darken. As can be

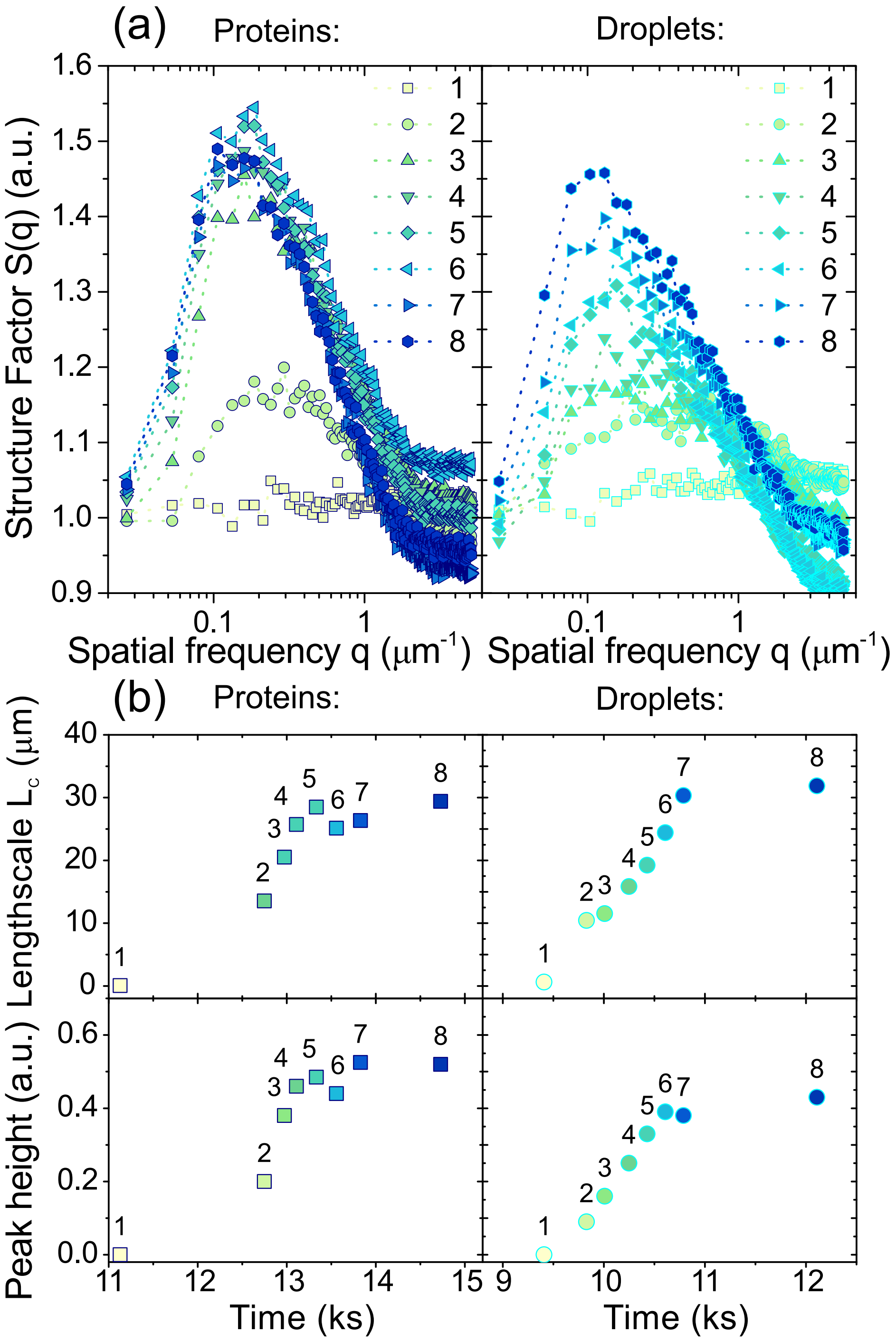

Figure 6.9 *Fast Fourier Transform analysis of the confocal micrographs of gelation of a suspension of sodium caseinate (left, $\phi_{eff,prot} = 9.8\,\%$, presented in Figure 6.7) of a suspension of caseinate-stabilised droplets (right, $\phi_{eff,drop} = 9.0\,\%$, presented in Figure 6.8).*
(a) Structure factors $S(q)$ of each micrograph are plotted versus the spatial frequency q.
(b) Characteristic lengthscales L_C (top) and peak heights (bottom) extracted from the structure factors $S(q)$ are plotted versus the gelation time t.

observes in Figure 6.9 (b), this transition appears in the FFT analysis as the progressive increase of the peak height and characteristic lengthscale L_C.

The two types of suspensions also present a similar characteristic lengthscale of the final gel. Indeed, the FFT analysis gives $L_{C,f} = 32\,\mu\mathrm{m}$ for droplets and $L_{C,f} = 29\,\mu\mathrm{m}$ for proteins. The aspect of the gels will be further discussed in Section 6.4.

In contrast, some differences between the samples can also be quantified with this technique. To start with, the spectra of the micrographs corresponding to the gelation of proteins present more narrow and higher peaks than for the droplets. This is related to the images being more homogeneous, because of an apparent uniform gelation.

In addition, the increase in size of the microstructural features is much faster for proteins than for droplets. Indeed, after aggregation starts, the proteins reach 75 % of the final L_C in less than 400 s, while it takes 800 s for aggregating droplets to reach 75 % $L_{C,f}$. In terms of the micrographs, this is reflected by the presence of a structure similar to those of the final protein gel from the fourth frame. Considering the small variation of the pH on this timescale, this may be related to the different aggregation mechanisms of the two colloidal suspensions.

To conclude, the FFT analysis provides a quantification of the microstructure over time that is consistent with the qualitative comments made from the observation of the confocal images. The acid-induced gelation of protein suspension appears to be significantly different, both qualitatively and quantitatively, from the gelation of protein-coated droplets. It is believed that these observations, made on dilute suspensions gelled at ambient temperatures, can be generalised to all the gels studied here, prepared at 35 °C, and characterised mostly by their rheological behaviour. More generally, the gelation behaviour of these two suspensions present the signature low-q signal of the diffusion-limited cluster aggregation (DLCA) regime of colloidal gelation [77, 160, 162].

It has to be noted, however, that for both of these rheo-imaging measurements, the moduli obtained by using a plate-plate geometry are much lower than those obtained with concentric cylinders (Couette cell). Indeed, for droplets the final storage modulus G' should be around 3 Pa, and for proteins $G' = 2\,\mathrm{Pa}$, as will be seen in Figure 6.13. The gelation times are also twice as long as for the gels that will be presented in Figure 6.11. There are two possible sources for the discrepancy: first, the gelation here occurs at ambient temperature (22 °C) rather than at 35 °C for the following gels. It has been shown that the gelation temperature plays an important role on the final properties of sodium caseinate gels [122]. Secondly, it is possible that the confinement of the gel in a thin layer may result in a gel with different properties. Finally, there may be wall slip at the bottom plate, as it is made of glass.

6.3.2 Development of mechanical properties

To study more in detail the dramatic changes of the mechanical properties occurring in the sample during the sol/gel transition, it is useful to carry out a more thorough rheological study of the gelation of protein and droplet suspensions at several volume fractions. Here, the oscillatory rheometry is performed using a Couette geometry and the results correspond to the first stage of the sequence presented in Figure 6.1 at the frequency $f = 1\,\mathrm{Hz}$.

Examples of gelation curves for concentrated samples ($\phi_{eff} = 0.53$) of protein and of pure droplets can be found in Figure 6.10. Their shape is representative of the gelation curves for all samples studied here, on a wide range of volume fractions ($\phi_{eff} = 0.09 \ldots 0.90$). For clarity, both are shifted so that gelation occurs at the same time.

As can be observed, for the two types of samples, there is a rapid rise of both storage and loss moduli simultaneously at the gelation time t_{gel}. The shape of this increase is very reproducible over the 3 repetitions of the same sample, as can be seen from the low width of the shaded area representing the error after averaging. It occurs faster for droplets than for proteins, which may indicate that the reorganisation of the network described previously is easier for protein-stabilised droplets than for proteins at a given volume fractions.

The protein gel has a higher phase angle, meaning that the viscous contribution relative to the elastic contribution is 1.4 times higher for the protein gel than for the droplet gel. The behaviour of the protein gel is thus more shifted towards that of a viscous liquid, and this is another indication that the protein gel is more able to reorganise than the droplet gel. Interestingly, this characteristic is time-dependent and the discrepancy between both systems increases with time. For each system, there is also a decrease of the phase angle with time, which goes in the direction of a reinforcement of the elastic aspect of the gels with time.

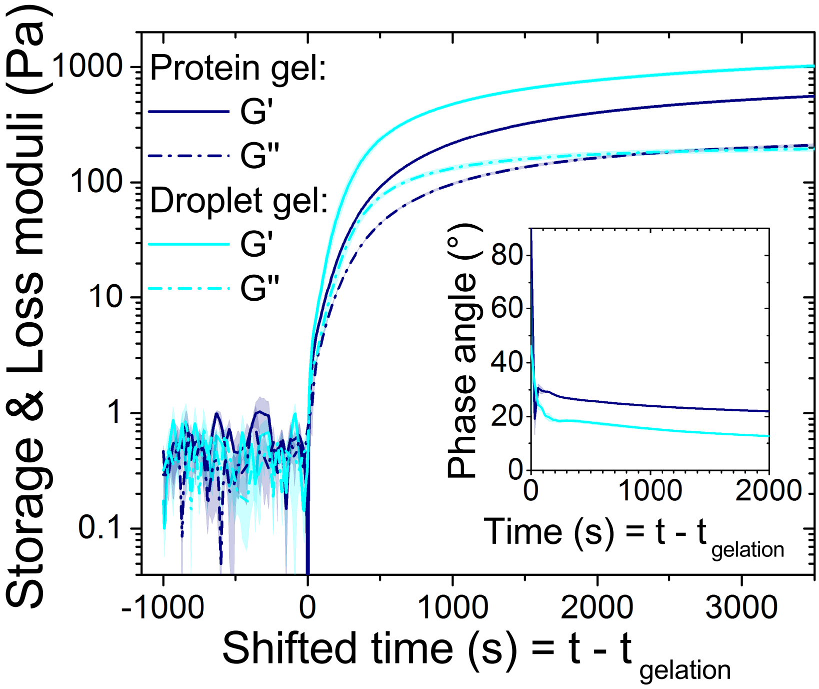

Figure 6.10 *Comparison between acid-induced gelation behaviour of protein suspensions ($\phi_{eff,prot} = 53\,\%$ sodium caseinate, in navy blue) and protein stabilised droplets ($\phi_{eff,drop} = 53\,\%$ caseinate-stabilised oil droplets, in cyan) at $35\,°\mathrm{C}$.*
Storage (G', continuous line) and loss (G'', dotted line) moduli were averaged on the existing data, and the coloured area represents the error after averaging. The inset represents the variation of the phase angle δ after gelation.
All are plotted as function of the shifted time $t' = t - t_{gel}$. Small-oscillatory measurements at $1\,\mathrm{Hz}$.

In addition, it is interesting to consider the gelation time t_{gel}, which is the time after addition of glucono δ-lactone for the sol-gel transition to occur. Because the cross-over between storage and loss modulus does not appear clearly in the gelation curves, an arbitrary criterion was chosen to determine the gel state, and the gelation time t_{gel} was defined as:

$$\begin{cases} G'(t) \leq 1Pa & \text{for } t \leq t_{gel} \\ G'(t) \geq 1Pa & \text{for } t \geq t_{gel} \end{cases}$$

This criterion makes it possible to estimate t_{gel} required to reach the sol-gel transition of suspensions of proteins and of protein-stabilised droplets at different volume fractions ϕ_{eff}. These values are shown in Figure 6.11. By contrast with the shape of the gelation curve, t_{gel} presents small variations upon repetition of the experiment, which may be due to changes in pH decrease between samples.

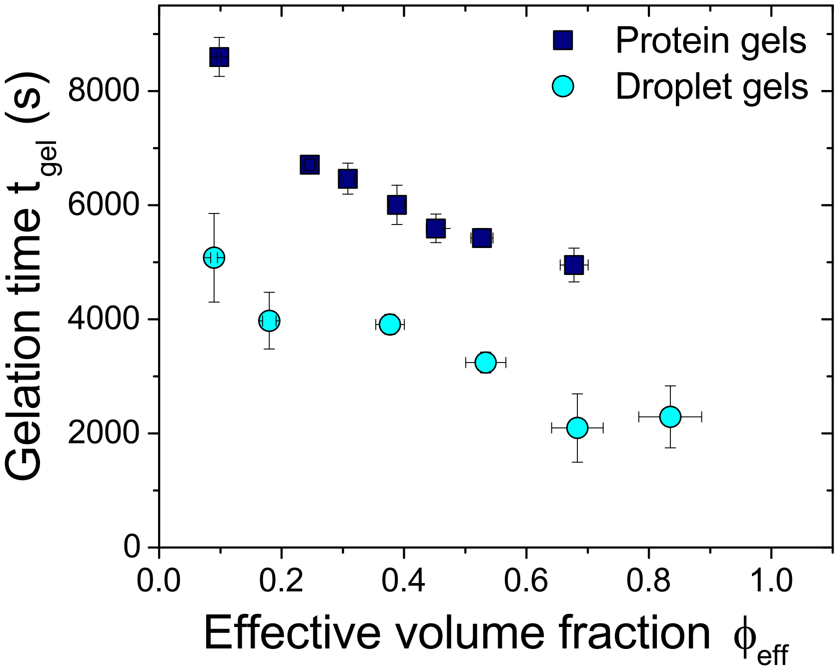

Figure 6.11 *Gelation times t_{gel} of protein (squares, navy blue) and droplet (circles, cyan) suspensions, at 35 °C, after addition of glucono δ-lactone, as a function of the volume fraction ϕ_{eff}. The error bars represent the standard deviation of data for each sample. Each gel is prepared using a fixed gdl:protein ratio, as decribed in Chapter 3.*

Inspection of Figure 6.11 indicates first that the gelation time t_{gel} drops with the volume fraction ϕ_{eff}, which is in good correspondence with a previous study on acid-induced caseinate gels [127]. Considering the short timescale identified for the aggregation process in the previous section, this decay may be related to a faster acidification for concentrated samples, because a fixed glucono δ-lactone:protein ratio is used to prepare the gels.

In addition, it appears here that this trend is also valid for the gelation of protein-coated droplets, although their gelation time is consistently 30% to 50% smaller than for pure proteins. Again, it is likely that this dissimilarity is related to a discrepancy in acidification kinetics rather than in aggregation mechanisms. This may be due to the different amounts of glucono δ-lactone used to prepare the types of samples in order to reach a similar final pH, as detailed in Chapter 3.

Thus, the rheological characterisation of the acid-induced gelation shows significant differences between protein assemblies and droplets. Indeed, droplet suspensions appear to have shorter gelation times and a sharper increase in viscoelasticity than protein suspensions. The difference in gelation time is probably related to the change of hydrolysis rate of glucono δ-lactone in complex media, as there are possibly specific molecular interactions and buffer effects. The increase in viscoelasticity on the other hand may be due to the discrepancy in gelation mechanisms observed with the rheo-imaging technique. Indeed, it appeared that the gel structure, once formed, does not present major visible changes with time in the case of droplet gels, while there is significant reorganisation of the protein gel to form thicker strands. These measurements were however performed on relatively short timescales, so it is important to consider the evolution of the gels at longer times.

6.3.3 After gelation: is there an end point?

By definition of the colloidal gelation, gels are dynamically arrested networks rather than structures at equilibrium [77, 163]. It is thus not surprising to observe a slow increase in storage and loss moduli in Figure 6.10, after the initial rapid emergence of viscoelasticity. Indeed, over a few thousand seconds here, the gelation curves for both protein and droplet gels do not display a plateau but a gradual rise of G' and G'', a behaviour that is consistent over the range of concentrations studied in the following.

This is consistent with the literature on caseinate gels and caseinate-stabilised emulsion gels [120], where such increase was shown to last over 24 h [127]. It has to be noted that for acid-induced gels, this behaviour depends strongly on the choice of final pH. Indeed, here the system was chosen to plateau at the isoelectric point. If the pH was to be further decreased, positive charges would appear at the surface of caseinate particles leading to a release from the gel structure and a decrease in viscoelasticity, as shown in Figure 2.13 (B) [11]. Instead, the toughening of the caseinate gels with ageing observed here has been attributed to significant rearrangements occurring in the gel microstructure [114, 122, 164].

These rearrangements can be understood by considering colloidal gelation on a standard system. Fluctuations in the interparticle interactions mean that the reversible bonds can be broken and reformed [77]. Simulation studies have shown that rearrangements follow a complex cooperative process driven by the minimisation of internal stresses in the network [163, 165]. The experimental study of the ageing of a nanoparticle gel showed that such a gel develops more compact regions and also becomes more heterogeneous, resulting in a structure with an increased storage modulus [166]. Here, we see that these results also apply to more complex systems, such as protein and emulsion gels.

This strengthening of gels upon ageing can, however, limit drawing comparisons between different gels. In order to avoid this limitation, and to consider gels at a similar stage of ageing, the viscoelasticity of the gels is compared in the following at a fixed $t' = t - t_{gel}$. Arbitrarily, $t' = 2500\,\mathrm{sec}$ was chosen, as a trade-off between ageing time and reachability by the slowest gelling systems. Because of the sequential measurements of the gel properties, as presented in Figure 6.1, the frequency dependence and the high-shear behaviour of the gels were measured at a fixed t rather than a fixed t' so not all gels present the same ageing. However, the effect of the rearrangement on these rheological properties is assumed to be negligible in order to make possible the comparison between gels of different nature and concentration.

To conclude on the gelation of these systems, differences were found in the kinetics both of microstructure formation and of rheology between protein gels and droplet gels. A significant challenge is to decorrelate the gelation kinetics from the rate of acidification, in order to identify the intrinsic contribution of the colloidal particles to these discrepancies. An estimation of the aggregation rate during the entire gelation process would in theory allow drawing a more precise picture of the gelation. This could be achieved by NMR [167] or by measuring the amount of unadsorbed proteins over time [11]. In the following sections, the rheology and microstructure of the gels are studied by considering them as static structures, but it is essential to keep in mind that there is an important kinetic component to these properties, and that the gels are modified upon ageing.

6.4 Micro-structure of gels: colloidal species and volume fraction

Confocal microscopy is a commonly used technique to observe the structure of colloidal gels at the micron scale [155, 168, 169] that makes possible the comparison of this structure for gels of different composition and volume fraction. Casein and sodium caseinate gels have been imaged in other studies [10, 11, 76, 123, 125, 154]. Their fractal structure has been highlighted,and it has been found to be dependent on the pH, ageing time and addition of other components. However, the influence of their volume fraction on their structure is yet to be studied. In addition, caseinate-stabilised emulsion gels have been shown to present a similar structure [152], but its change with volume fraction is equally unknown.

Here we compare the microstructure of gels that were prepared by acidifying suspensions of either sodium caseinate or pure caseinate-stabilised droplets, at different concentrations. As described in Section 6.2.4, the gels were imaged a long time after gelation, and considered to be in an approximated equilibrium. The imaging was thus performed over the three spatial dimensions, by contrast with the gelation results described previously that were based on four-dimensional measurements because the changes of the 3D structure with time were measured. The image analysis was performed as described in Figure 6.5, but because the suspension was not imaged before gelation, the spectrum $I(q)$ could not be normalised by $I(q, t = 0)$, leading to a decreased precision in the determination of the peak.

The micrographs of caseinate and droplet gels, together with their characteristic lengthscale L_C, determined by the position of the peak on the spectrum $I(q)$ as described in Figure 6.6, are presented in Figure 6.12. The gels of the two components appear to form similar gels over the range of volume fraction studied here.

First, the micrographs are similar for protein and droplet gels, especially at lower volume fraction. Indeed, in both cases, the fractal structure typical of colloidal gels is present, with interconnected particle aggregates (in colour) separated by water-filled pores (in black). At high concentrations, these networks are denser in particles, with the pores of the droplet gels appearing to be smaller than for the protein gels.

In addition, the characteristic lengthscales L_C are of the same order of magnitude for the two components, and their values range between 5 µm and 20 µm for all the gels presented here. Because the features picked up by the Fast Fourier Transform are probably a combination of the size of the aggregates and the size of the pores, the variation of L_C as a function of the volume fraction cannot be interpreted in details. This is reflected by the discrepancy of L_C for two different micrographs

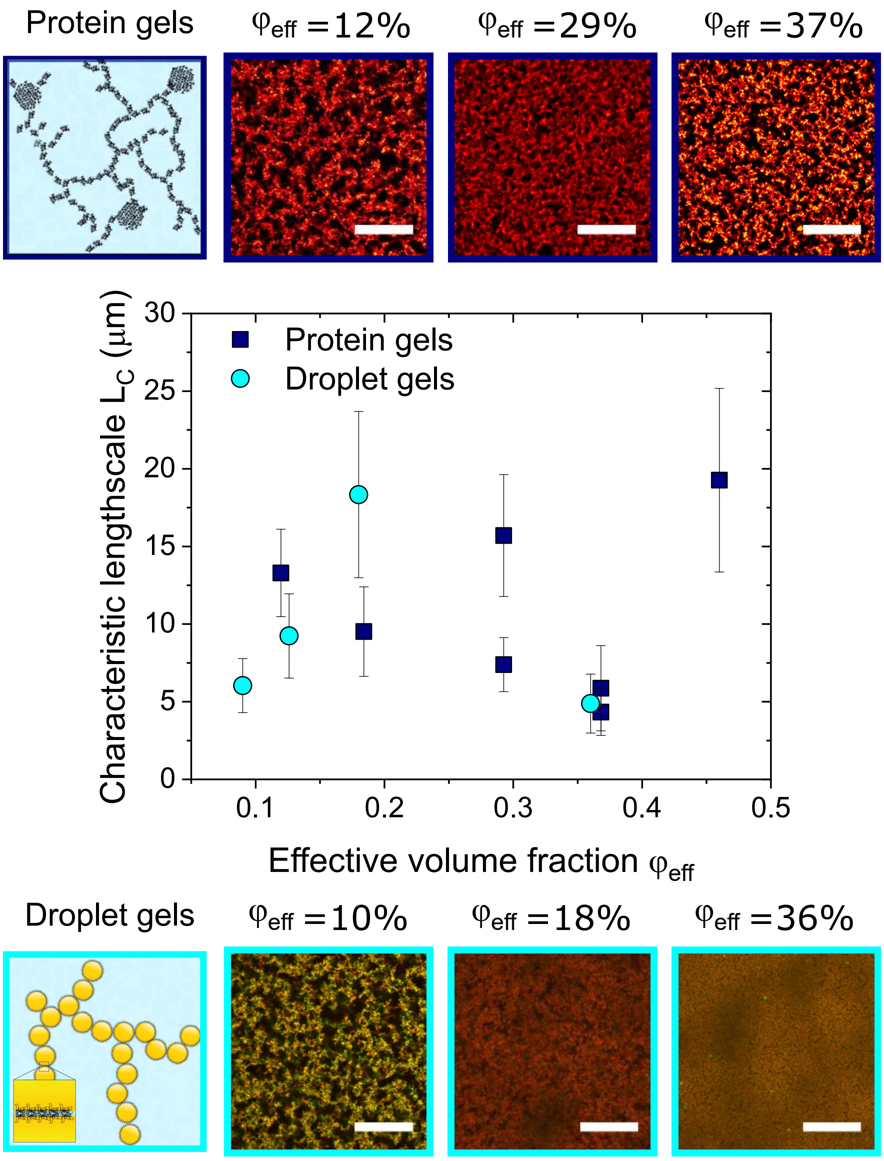

Figure 6.12 *Micrographs ($100\,\mu m \times 100\,\mu m$) of aged acid-induced gels formed from suspensions of: (top) sodium caseinate, and of (bottom) caseinate-stabilised droplets, at different volume fractions ϕ_{eff}. The scale bars are $30\,\mu m$ long.*
The graph presents the characteristic lengthscale L_C of the gels, as a function of the volume fraction ϕ_{eff}, for caseinate gels (squares, navy blue) and caseinate-stabilised droplet gels (circles, cyan).
For each point, L_C was obtained by performing a FFT of one micrograph and extracting the position of the peak in the spectrum $I(q)$, as described in Figure 6.5. The inaccuracy of this determination is indicated by the error bar. When two points are presented for one concentration, they correspond to different micrographs of similar samples.

of the same protein gel at $\phi_{eff} = 30\,\%$. It is however expected that the mesh size decreases with increasing volume fraction, as has been observed numerically for colloidal gels at a lower range of volume fractions ($\phi = 2.5\,\%$ to $\phi = 10\,\%$) [163]. In the framework of the fractal theory, this decrease in lengthscale with the volume fraction can be understood as a decrease in the cluster size required to reach a volume-spanning network.

Finally, it has to be noted that the gel structures presented here are less open than for the gelation sequence presented in Figures 6.7 and 6.8, for which $L_C \approx 30\,\mu\text{m}$. This is most likely due to the different gelation conditions. Indeed, the gelation sequences were performed at room temperature ($\approx 21\,°\text{C}$), while here the gels were prepared at 35 °C and then imaged at room temperature. This is in good agreement with previous studies on casein gels, where the gels prepared at lower temperatures presented larger pores [123].

We can thus conclude that the observation of gels of proteins and droplets using confocal microscopy allows comparison of the micro-structure of gels of different composition. The fractal structure of the gels and the presence of interconnected networks of pores and of particle clusters make their quantification difficult. Here, the FFT was chosen to determine a characteristic length scale L_C of the networks, that appeared to be in the same order of magnitude for all the micrographs presented. In addition, it may be possible to extract other features from the images, such as the size distribution of the pores, the fractal dimension and the connectivity of the network. This information could possibly bring a deeper understanding of the structure of protein and droplet gels, but would require higher quality confocal micrographs, as any pre-treatment of the image may induce a bias. The fractal dimension for example, despite being clearly defined in theory, has been shown to poorly describe casein gels [10, 123].

6.5 Rheology of gels: comparison of droplet gels and protein gels

In addition to the gelation, and the micro-structure consequently formed, it is interesting to compare the rheology of gels made of pure sodium caseinate and of pure caseinate-stabilised droplets. Indeed, the characterisation of the mechanical properties of single-component gels will allow elucidation of the contributions of each species in emulsion gels, composed of un-adsorbed proteins and droplets. In the previous sections, it was shown that these systems gel in a similar fashion and have a very comparable structure, despite the discrepancy in size and softness of their primary particles. Here we will see that the rheological properties also present similarities when the gels are described by their volume fractions.

It is important to emphasise that protein and droplet gels can be compared to each other by using the effective volume fraction ϕ_{eff} as the scaling parameter. As presented in Chapter 5, ϕ_{eff} represents the volume occupied by the particles in the sample, and is calculated by multiplying the concentration with a parameter k_0 derived by approximating protein aggregates and protein-stabilised droplets to model hard spheres when in semi-dilute suspensions. It is assumed that this scaling holds for the description of acid-induced gels, regardless of the modifications that are likely to happen at the protein scale upon change in pH.

As described in Figure 6.1, several rheological parameters were measured for each of the gels prepared, and are discussed in the following. The viscoelastic moduli, G' and G'', are first compared at fixed frequency, strain and time after gelation for gels of different compositions. Then the dependences of G' and G'' with the frequency and strain amplitude are presented. Finally, the recovery of the gels after large strain is considered.

6.5.1 Linear viscoelasticity of gels

As mentioned previously, the colloidal gels do not reach an equilibrium state, but go through rearrangement of their network upon ageing. To compare the viscoelasticity of the gels at similar ageing time, the storage and loss moduli G' and G'' were measured at 2500 s after gelation. For both gels of protein-stabilised droplets and of proteins, the influence of the effective volume fraction was studied, and both behaviours were compared.

The elastic modulus G' and the loss modulus G'' of the two types of gels at 1 Hz are presented in Figure 6.13 as functions of their effective volume fraction ϕ_{eff}. The phase angle $\delta = arctan(G''/G')$, indicating the viscoelastic character of the gels, is found to be relatively constant for each sort of gels, with $\delta_{prot} = 21°$ and $\delta_{drop} = 13°$. The higher phase angle found for protein gels indicates that their behaviour is slightly shifted towards the viscous materials on the spectrum of viscoelastic materials.

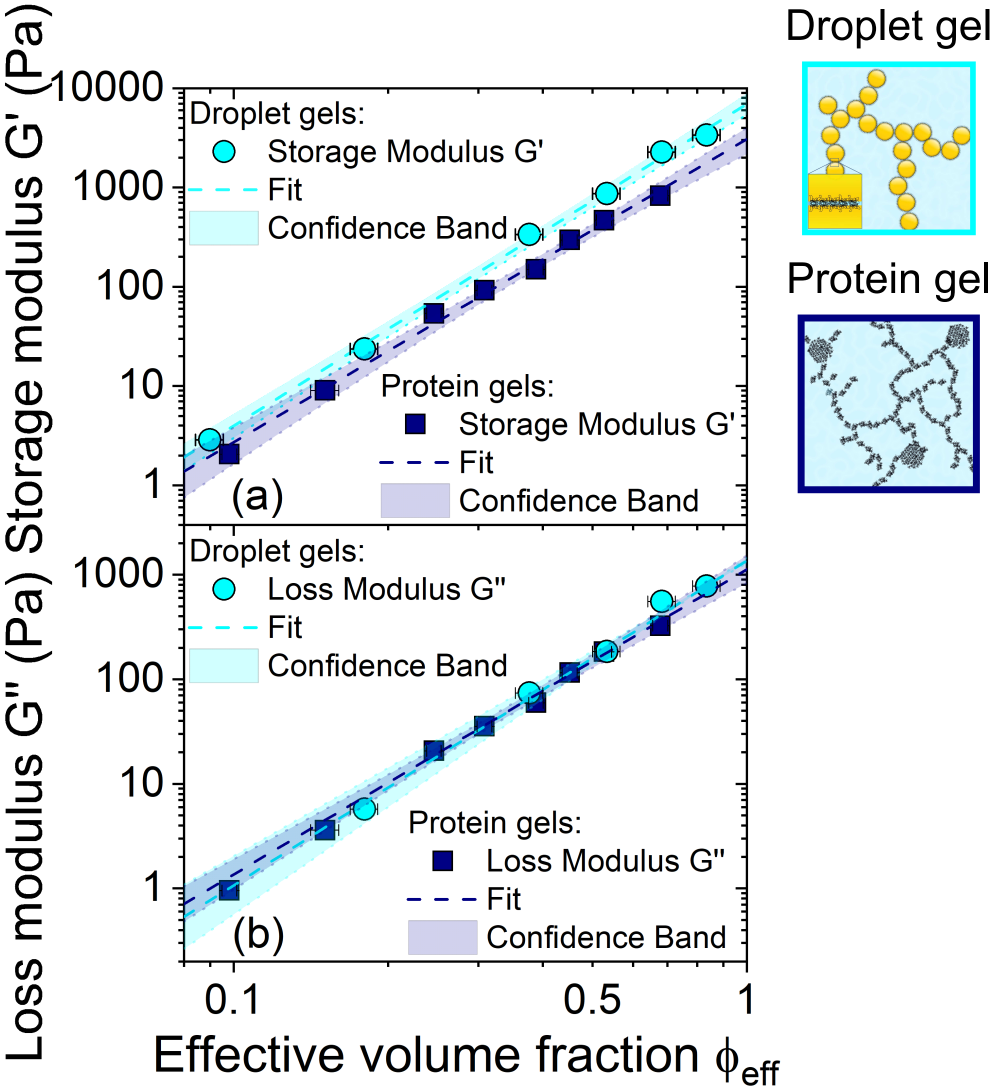

Figure 6.13 *Storage (G', (a)) and loss (G'', (b)) moduli at 1 Hz of protein-stabilised droplet gels (circles, cyan) and of protein gels (squares, navy blue) as functions of the effective volume fraction of the gel (scaling derived in Section 5.3.2).*
A fit (Equation 6.1) of each type of system was performed and the model (parameters listed in Table 6.2) as well as the 95 % confidence band are displayed on each graph.
The horizontal error bars arise from error propagation upon calculation of the volume fraction, while the vertical error bars are smaller than the data points, so not diplayed here.

It appears in Figure 6.13 that sodium caseinate and sodium caseinate-stabilised droplets form gels of very similar viscoelasticity when scaled by the volume fraction. This shows that protein-stabilised droplets in emulsion gels do not act only as fillers but actively contribute to the network and are even able to form networks of their own that are slightly stronger, at a given volume fraction, than pure proteins.

Power-law increase with volume fraction

The variations of both storage G' and loss G'' moduli as functions of effective volume fraction can be described as a power law for the two types of gels:

$$G(\phi_{eff}) = G_{0,\phi} \times \phi_{eff}^{\alpha} \tag{6.1}$$

Where $G_{0,\phi}$ is the pre-factor of the power-law and the exponent α can be interpreted using the theory of fractal gels, as discussed in the next section. The values found by fitting $G'(\phi_{eff})$ and $G''(\phi_{eff})$ with Equation 6.1 are summarised in Table 6.2.

Table 6.2 *Parameters for Equation 6.1 to fit viscoelasticity of gels at* 1 Hz *displayed in Figure 6.13*

Gel type	Storage modulus G'		Loss modulus G''	
	$G'_{0,\phi}$	α	$G''_{0,\phi}$	α
Droplet gels	6.93 kPa	3.24 ± 0.07	1.37 kPa	3.11 ± 0.09
Protein gels	(3.1 ± 0.4) kPa	3.05 ± 0.11	1.11 kPa	2.91 ± 0.11

This power-law dependence of the viscoelasticity of sodium caseinate gels is in good correspondence with previous studies on casein gels [76, 79, 121, 127, 154] and particle gels [170, 171]. The value of the exponent for sodium caseinate varies significantly with the experimental conditions, like temperature and ageing time, as it is was found to vary from $\alpha = 2.57$ [127] to $\alpha = 4.6$ [79], a precise comparison of the value found here with the literature may thus not be relevant.

In addition, the similar behaviour observed for gels made of protein-stabilised droplets proves that these systems display comparable mechanical properties to caseinate gels. No data is available on the rheological properties of acid-induced droplet gels, but it is expected that the similarity underlined here is a consequence of the scaling of the samples by their volume fraction. Indeed, if the moduli were plotted as functions of the weight concentration, the two power laws would be shifted horizontally, and the moduli of a protein gel would be almost two orders of magnitude higher than the moduli of a droplet gel at the same concentration. If the protein concentration was instead chosen to describe the droplet system, as proteins are only roughly 10 % of the weight of the droplets, then the droplet gels would seem in appearance much stiffer than the protein gel [120]. Here we argue that there is actually little difference between the two types of gels, provided that the comparison is drawn between samples at the same volume fraction.

This result corroborates the observations made for the micro-structure, and confirms that the volume fraction scaling is a relevant approximation to study colloidal gels. Indeed, if the gels were compared using their weight concentration, the discrepancy in volume fraction could be mistaken for an intrinsic difference between protein and emulsion gels. Despite its definition being non-trivial for complex colloidal particles, the volume fraction is thus an essential parameter that reveals the similarity between protein gels and droplet gels.

It has to be noted that the power law dependence of the elastic modulus G' is a common feature of fractal colloidal gels, as previously observed experimentally and numerically [78]. Consequently, the results displayed in Table 6.2 can be examined in light of the theory developed for such systems.

Comparison with fractal gel theory

As presented in Chapter 2, the viscoelasticity of a colloidal gel is closely related to its fractal structure. In particular, the storage modulus G' is a direct consequence of the presence of a stress-bearing network within the material. The behaviour of G' with the volume fraction of particles ϕ can thus be linked to the way the elementary particles are arranged, described by the fractal dimension D_f. In this framework, the exponent α of the power law presented in Figure 6.13 is expressed [20, 171]:

$$\alpha = \frac{3 + D_b}{3 - D_f} \tag{6.2}$$

Where the bond dimension D_b reflects the fractal dimension of the gel backbone.

For gels formed by attractive particles in the dilute regime, the gelation most likely occurs by diffusion-limited cluster aggregation (DLCA), and in that case the stress-bearing backbone is relatively linear, yielding a bond dimension of $D_b \approx 1.1$. If this approximation is applied to the protein and droplet gels, the fractal dimension of such networks is found to be $D_f = 3 - (3 + D_b)/\alpha \approx 1.7$. This value is in good correspondence with previous results for DLCA particle gels [171, 172], which seems to indicate that the formation of protein gels follow this mechanism. The detailed nature and energy profile of interparticle interaction involved in sodium caseinate aggregation is not known, but this result seems to correspond with a strong Van der Waals attraction when the proteins are at their isoelectric point.

However, it has to be noted that the behaviour of G' with ϕ is only a proxy for determining the fractal dimension, and is greatly limited by the wide range of concentrations explored here. Indeed, if a DLCA regime is expected for gels formed from semi-dilute suspensions ($\phi_{eff} \approx 10\,\%$), the mechanisms are likely to be different for gels at $\phi_{eff} \approx 70\,\%$, in which particle crowding will play an important part in the structure formation, and the the fractal dimension may differ. To further explore the fractal nature of casein gels, a careful characterisation of the gel micro-structure at each concentration would be required. Because confocal imaging has limitations, as pointed out previously, this characterisation could possibly be achieved by using neutron scattering techniques.

In addition to the exponent α, the pre-factor of the power law $G'_{0,\phi}$ can also be discussed in the theoretical framework of colloidal gels. Droplet gels appear to form slightly stiffer gels when scaled by the volume fraction, as $G'_{0,\phi,drop} \approx 2 \times G'_{0,\phi,prot}$. An explanation for this difference could be the discrepancy in size of the particles, or a difference in bond topology between protein assemblies and protein-stabilised droplets. Indeed, a difference in bond strength may appear depending on the contact area between bonded droplets, which is unknown. This point can be studied in more detail if the droplet size is changed, and will thus be further developed in Chapter 8.

The study of the gel moduli as a function of their composition, described both by the nature of the elementary particles and by their volume fraction, offers thus some information on the mechanical properties of caseinate and emulsion gels. The behaviour of the two types of gel is very similar and reminiscent of those of more model colloidal gels and confirms their fractal nature. In addition to this static view of protein and emulsion gels, it is important to compare their dynamic properties.

6.5.2 Frequency dependence of gels

The moduli of the newly formed gels were then measured over a wide range of frequency. This measurement of the frequency dependence enables probing of the dynamics of the gels. Because these are solids, this aspect is limited to fluctuations inside their structure, for example rearrangement of the particle bonds, relaxation of the stress bearing strands, or motion of non-stress bearing strands like dangling chains.

Comparison of the frequency dependence of protein gels and droplet gels

In order to compare similar gels of proteins and of protein-stabilised droplets, gels of equal volume fraction ($\phi_{eff} = 0.53$) are displayed in Figure 6.14.

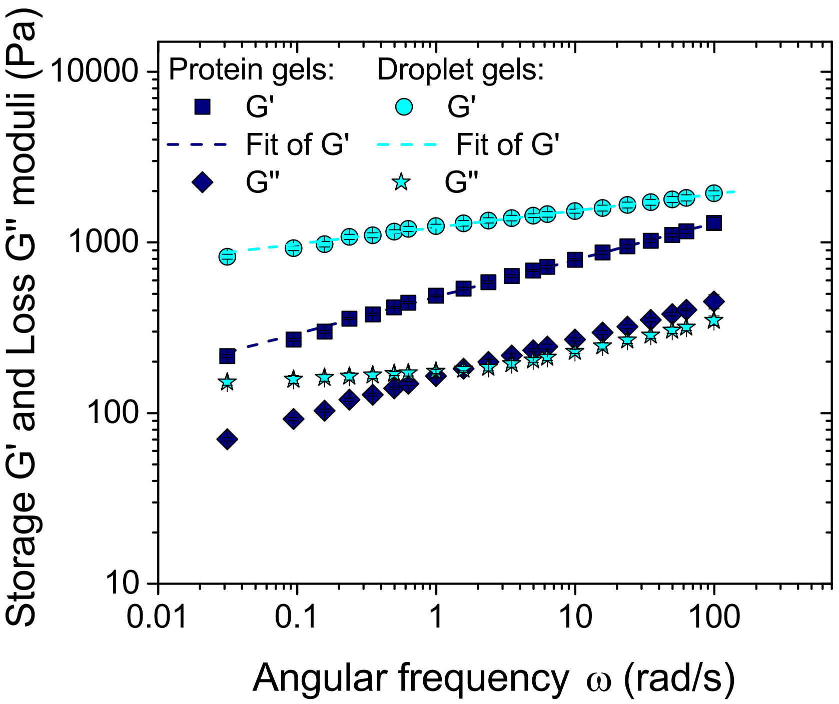

Figure 6.14 *Comparison of the frequency dependence for protein gels (sodium caseinate: $\phi_{eff} = 53\,\%$, in navy blue) and droplet gels (caseinate-stabilised oil droplets: $\phi_{eff} = 53\,\%$, in cyan).*
Storage modulus G' and loss modulus G'' are represented as functions of the angular frequency ω.
G' was fitted with a power law for both types of samples, and the fitting parameters can be found in Table 6.3.

As can be observed, the protein gel displays a higher dependence on frequency than the droplet gel, as both storage and loss moduli increase faster with the angular frequency. The non-monotonic behaviour of the loss modulus G'' for droplets gels may be an indication of a relaxation of droplet networks, that would be absent for protein gels in this range of frequency, but an extended spectrum would be required to definitely identify a possible peak.

Furthermore, the behaviour of the storage modulus G' can be modelled by a power law for both protein and droplet gels:

$$G' = G'_{0,\omega} \left(\frac{\omega}{\omega_\beta} \right)^\beta \tag{6.3}$$

Where $G'_{0,\omega}$ and β are two empirical parameters to be determined, and $\omega_\beta = 1.00\,\mathrm{rad \cdot s^{-1}}$ is used for dimensional purposes. The values of the empirical parameters for the frequency dependence of the gels displayed in Figure 6.14 can be found in Table 6.3.

Table 6.3 *Frequency dependence of gels: parameters for Equation 6.3 to fit the viscoelasticity of gels displayed in Figure 6.14*

Gel type	$G'_{0,\omega}$	β
Protein gels	0.5 kPa	0.22
Droplet gels	1.2 kPa	0.10

The value of the exponent β for caseinate gels is slightly higher than in previous studies. Indeed, for acid-induced casein gels at 30 °C, β was measured to be 0.15 [79, 120, 127], the discrepancy may come from different values of pH of the gels, which was shown to have a strong influence on the frequency dependence of such systems [120].

No comparable data could be found for the frequency dependence of gels made of pure protein-stabilised droplets, but the comparison between protein gels and gels of mixtures of proteins and droplets appears to be system-dependent. On one hand, the exponent β was found to be identical for acid-induced gels of caseinate emulsions and for caseinate gels, i.e. 0.15 [120]. On the other hand, for heat-set gels and emulsion gels prepared with β-lactoglobulin, the slope β is three times higher for protein gels than for emulsion gels [129]. This discrepancy is believed to result from the nature of the bonds between particles in these two types of gels: heat-set gels form more transient bonds than acid-induced gels, making thus for more mobile structures.

Influence of volume fraction on the frequency dependence of gels

This analysis of the frequency dependence can be extended to gels at all volume fractions. The empirical model in Equation 6.3 was thus applied to the gels of droplets and proteins at different volume fractions, and the resulting value of the power law exponent is displayed in Figure 6.15.

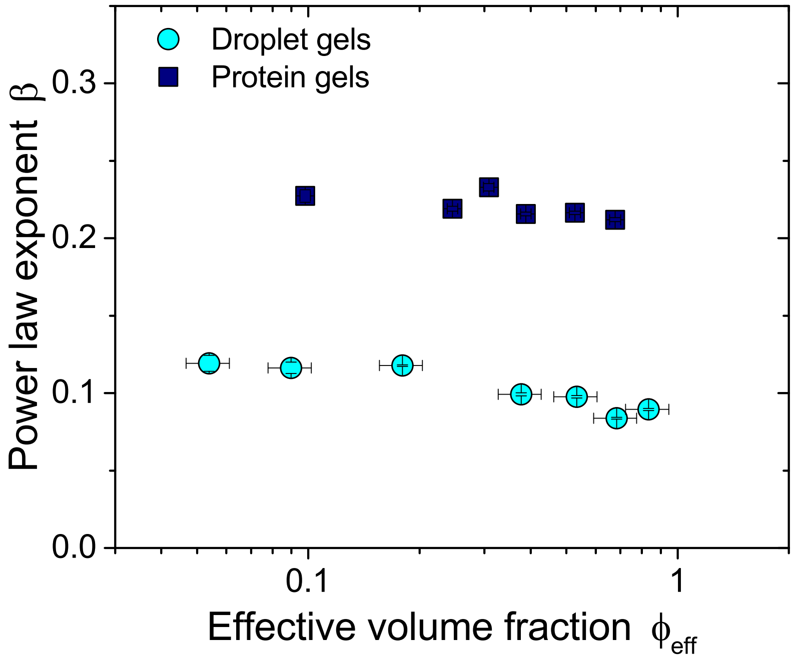

Figure 6.15 *Comparison of frequency dependence for protein gels (squares, navy blue) and protein stabilised droplets (circles, cyan): power-law exponent* β*, obtained by fitting* $G' = f(\omega)$ *with Equation 6.14, as a function of the effective volume fraction* ϕ_{eff}*.*

As can be observed, the difference in dynamic behaviour between protein gels and droplet gels is consistent over the range of volume fractions explored here. This seems to indicate that caseinate gels have more internal fluctuations than droplet gels, which may be a reflection of the more pronounced rearrangement of protein gels observed by rheo-imaging during gelation.

Furthermore, there is little influence of the volume fraction on the variation of the elasticity of the gels with the frequency. This indicates that over the range of concentrations studied, the dynamical behaviour of the gels is the same. By contrast, the viscosity of the suspensions increases dramatically over the same range of volume fraction, as discussed in Chapter 5. The negligible variations of the frequency dependence of the gels seem to indicate that there is no change in regime due to the crowding of the colloidal particles at the solid state, and the gels formed by proteins and droplets suspensions are similar in that respect.

In addition, as can be seen in Figure 6.14, the variations of the loss modulus G'' with the frequency ω differ between protein and droplet gels. This is better visualised by looking at the phase angle of the gels. The peculiar phase angle behaviour of droplet gels as a function of the frequency is presented in Figure 6.16 and is characterised by a drop around $2\,\mathrm{rad}\cdot\mathrm{s}^{-1}$ followed by an increase at higher frequency. In contrast, the phase angle of all the protein gels studied is constant with frequency. The physical nature of this behaviour is not known but it represents an additional significant difference in the frequency dependence of droplet gels compared to protein gels.

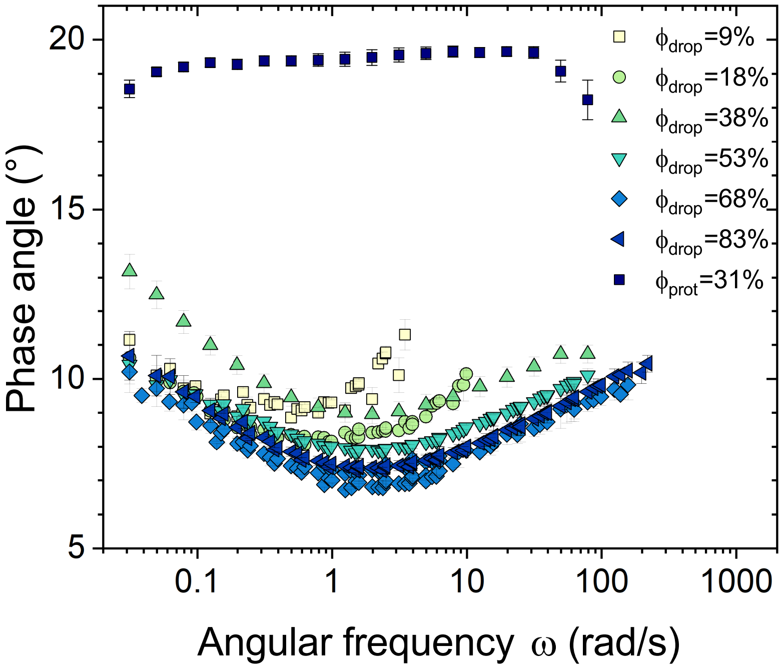

Figure 6.16 *Variation of the phase angle with the angular frequency ω for droplet gels at several effective volume fractions $\phi_{eff,drop}$. The behaviour of one protein gel ($\phi_{eff,prot} = 31\,\%$, squares, in navy blue) is presented to illustrate the absence of variations in this type of samples.*

These results for colloidal gels can be compared with another sort of arrested state of colloidal particles, such as glasses of soft colloids. For such systems, it was observed that at moderately high volume fraction, the glasses display a slow increase in elastic modulus G' with the frequency, associated with some mobility of the particles in a state of entropic glass. By contrast, at higher volume fraction, the particles are completely jammed and G' is constant over the range of frequency explored [52]. The fact that this frequency-independent regime is not reached here seems to indicate that the acid induced gels studied are quite dynamic, rather than completely arrested, and that this more the case for protein gels than for droplet gels.

6.5.3 Strain dependence of gels

The oscillatory strain sweep performed on the protein and droplet gels after formation and frequency sweep, as shown in Figure 6.1 allows the study of the variations of the storage modulus with the amplitude of the strain oscillation. The typical strain behaviour of the gel is represented in Figure 6.17.

As can be seen, both types of gels present at first a linear response to small-amplitude oscillations. But as the amplitude of the strain increases, a change in behaviour marks the end of the linear regime, which ends when the critical strain γ_c is reached. The applied stress at that point is defined as the critical stress σ_c. On the samples presented here, the linear regime is followed by an increase in normalised storage modulus G'/G'_0 when larger shear amplitudes are applied. This phenomenon is known as strain stiffening and will be detailed in the next section. Finally, upon further increase of the strain and stress, the gel structure breaks and its elasticity drops. The maximum stress borne by the gel is written σ_m and the corresponding maximum strain is γ_m.

This visual analysis of the strain response can be performed on the gels of proteins and protein-stabilised droplets at different concentrations. The parameters thus found are presented in Figure 6.18.

In terms of shear amplitude γ, the protein gels display a consistently higher critical strain γ_c indicating a slightly longer linear viscoelasticity regime than for droplet gels. This difference is smaller than the one observed between heat-set β-lactoglobulin gels and emulsion gels [129]. In addition, the maximum strain γ_m is close for the two types of gels, so $(\gamma_m - \gamma_c)_{drop} < (\gamma_m - \gamma_c)_{prot}$, indicating that the non-linear regime is less extended for droplet gels than for protein gels.

Furthermore, the dependence on the volume fraction is different whether the

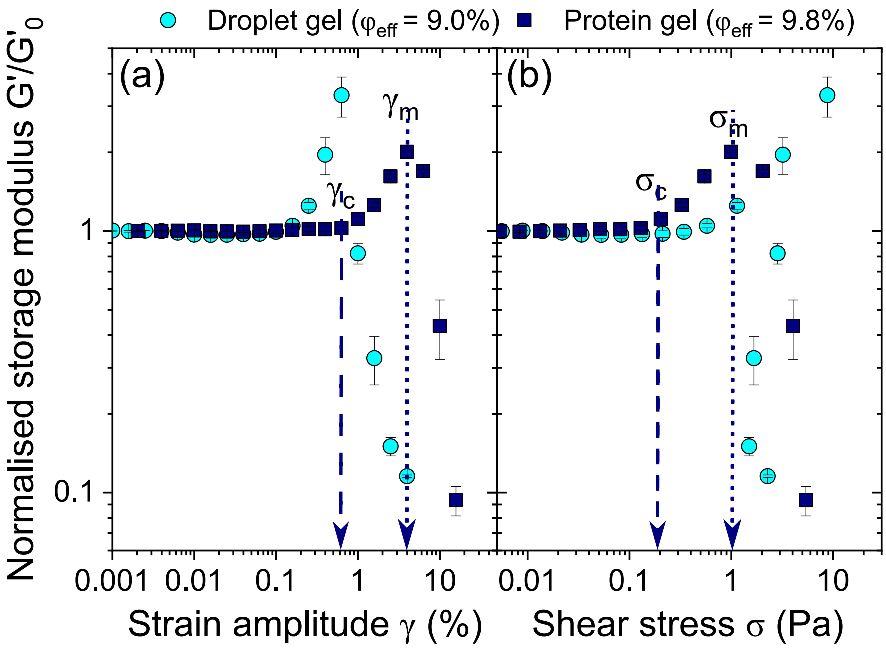

Figure 6.17 *Oscillatory strain sweep of protein ($\phi_{eff,prot} = 9.8\,\%$, squares, navy blue) and protein-stabilised droplet ($\phi_{eff,drop} = 9.0\,\%$, circles, in cyan) gels. Normalised storage modulus G'/G'_0 of the gels as a function of (a) the shear strain amplitude γ (in %), and (b) the shear stress amplitude σ (in Pa).*

The changes in regime are described by the critical and maximum strain (γ_c and γ_m) in (a), as well as critical and maximum stress (σ_c and σ_m) in (b), and their determination illustrated for the protein gel by the dashed and dotted lines.

Beyond γ_m and σ_m, the samples fracture irreversibly so the measurement is not reliable.

Each curve is an average of 3 measurements, after normalisation by the storage modulus in linear regime G'_0. The error bars represent the standard error upon averaging.

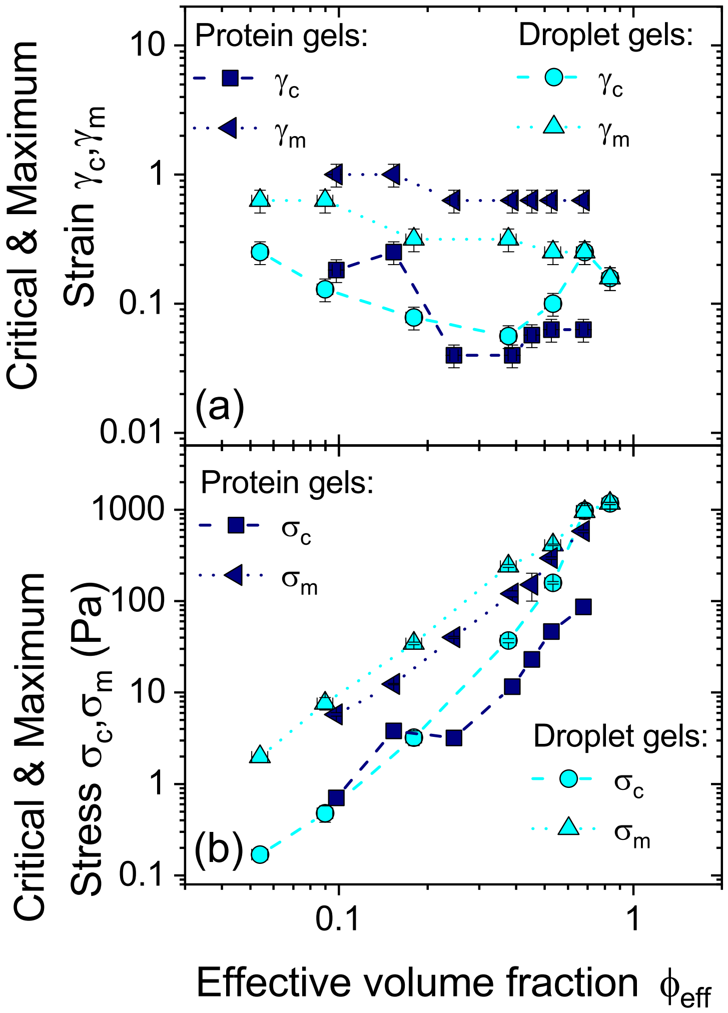

Figure 6.18 *Parameters for the strain dependence of protein gels (navy blue) and protein-stabilised droplet gels (cyan). (a) Critical strain γ_c and maximum strain γ_m, and (b) Critical stress σ_c and maximum stress σ_m (Pa) as a function of the effective volume fraction ϕ_{eff} in protein and in droplets.*
The parameters are extracted as illustrated in Figure after averaging the curves for 3 measurements of gels prepared in a similar fashion. The error bars represent the accuracy of this procedure.

chosen parameter is strain γ or stress σ. Indeed, the variations of the critical and maximum strain with the volume fractions are relatively small. On the other hand, the values of the critical and maximum shear stresses increase considerably for the two types of gels. This result indicates that the networks can bear more pressure as they become denser in particles but their deformation is limited by their microstructure over the range of volume fractions.

The discussion of the parameters presented in Figure 6.18 thus allow further characterisation of protein and droplet gels. The critical values for strain and shear stress amplitudes γ_c and σ_c can also be used to normalise the strain responses of the gels in order to better visualise and compare the strain stiffening displayed across the range of concentrations studied.

Strain stiffening

The presence of strain stiffening for multiple gels makes relevant the comparison of the different strain responses of the material with the one presented in Figure 6.17. In order to highlight the difference, the strain amplitude at each concentration is divided by its critical value γ_c, found in Figure 6.18. The resulting curves are displayed in Figure 6.19.

As can be seen, the nature of the non-linear regime varies with the type of gel formed and its volume fraction in proteins or droplets. The behaviour of gels at each concentration range can be discussed separately.

First, for gels prepared with suspensions of moderately low volume fraction of both proteins and protein-stabilised droplets, corresponding to the lighter colours in Figure 6.19, the storage modulus of the gel increases for $\gamma > \gamma_c$ and then decreases upon reaching γ_m. It can be noted that the strain stiffening is more pronounced for the droplet gels and is present on a wider range of volume fraction. Yet, as described in Chapter 2, it was shown that strain stiffening corresponds to a stress redistribution in the structural heterogeneities within the network [81, 84]. This result may thus indicate that the proteins form gels that are overall more homogeneous than the droplet gels at low volume fraction, possibly because of the more extensive rearrangements occurring in protein networks, as pointed out previously.

In addition, the concentrated samples of protein gels show a slight softening in the non-linear regime, over one order of magnitude of strain amplitude, before fracture

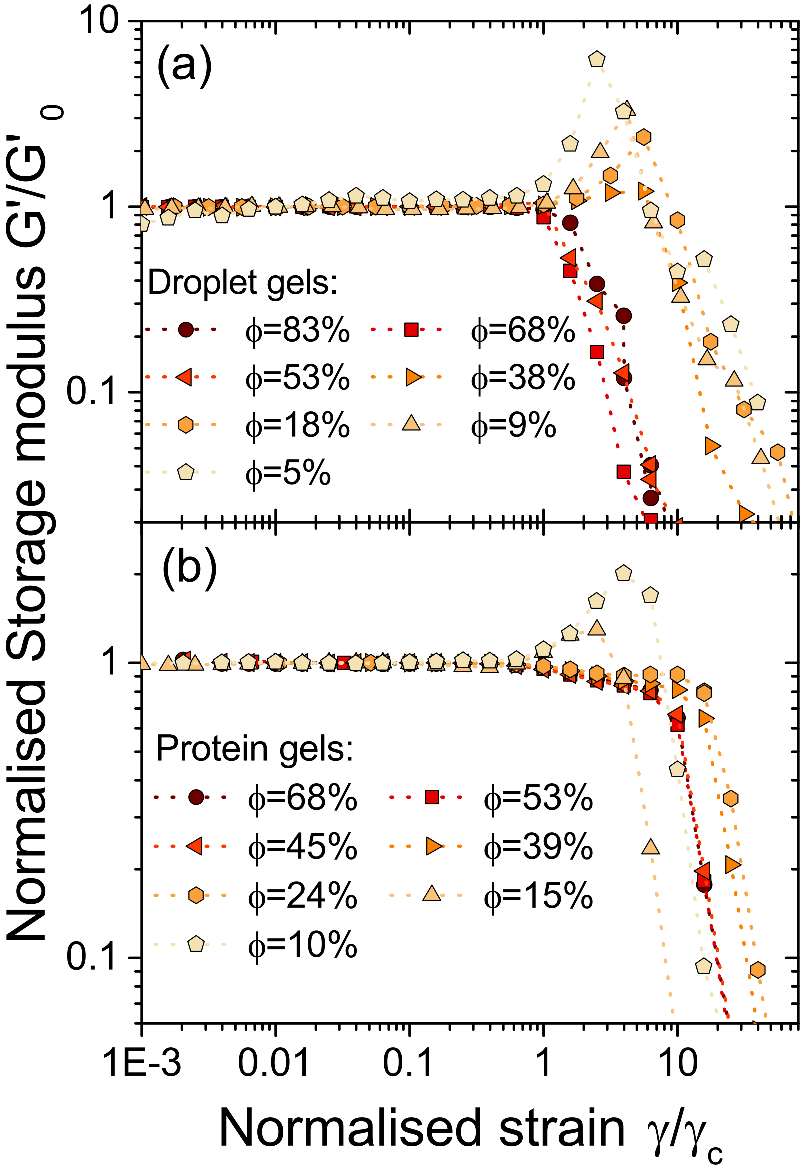

Figure 6.19 *Storage modulus G' normalised by its value in the linear regime G'_0 as a function of the oscillatory strain amplitude γ normalised by its value at the onset of the non-linear regime γ_c.(a) Sodium caseinate-stabilised droplet gels at several volume fractions ϕ , (b) Sodium caseinate gels at several volume fractions ϕ.*
Each curve is the average of 3 measurements, but for clarity the error bars are not represented here.

of the material. This effect is absent in the droplet gels, where concentrated gels break at the end of the linear regime. This difference in the stress-bearing behaviour of concentrated gels may also arise from structural differences between the networks. Indeed, it seems that the breakage of some bonds in the dense protein gels is not critical to the elasticity of the overall network. On the other hand, for the dense droplet gels, the immediate drop in elasticity seems to indicate that the integrity of the whole structure is degraded upon application of a critical shear stress σ_c.

Finally, a common feature to all the protein and droplet gels is the fracture of the material at very high shear, indicated by the drop in their elasticity.

6.5.4 Irreversible fracture of gels

After measuring the strain dependence of the gels, small-amplitude oscillations were performed to characterise the recovery of the systems, following the sequence illustrated in Figure 6.1. The recovery of protein and droplet gels at $\phi_{eff} \approx 10\,\%$ and $\phi_{eff} \approx 53\,\%$ is displayed in Figure 6.20.

As can be seen, the recovery is small compared to the value of the storage modulus in linear regime G'_0 for most of the gels considered. The elasticity presents a small increase soon after the large oscillations are stopped, but this increase slows down after around 2 min. The final elasticity is far from its initial value, indicating that the gels probably fracture irreversibly at high strains. In this scenario, it is possible that the measured value of the moduli lacks relevance as the gel is macroscopically heterogeneous.

This behaviour seems to indicate a brittle fracture of protein and droplet gels, and this result is in good correspondence with previous studies on caseinate gels [120, 124, 128]. It is in theory possible for the samples to form a solid again, as they are still at their isoelectric point, so they present an attractive potential. However, the applied high shear is not sufficient to recover a situation where individual droplets or protein aggregates can move freely. Instead, the structure of the fractured gel is probably made of partially connected clusters with little mobility. This situation is not advantageous to forming new bonds in order to recover a percolated network, and thus the viscoelasticity stays low.

Finally, this brittle fracture demonstrates that the elasticity of protein and droplet

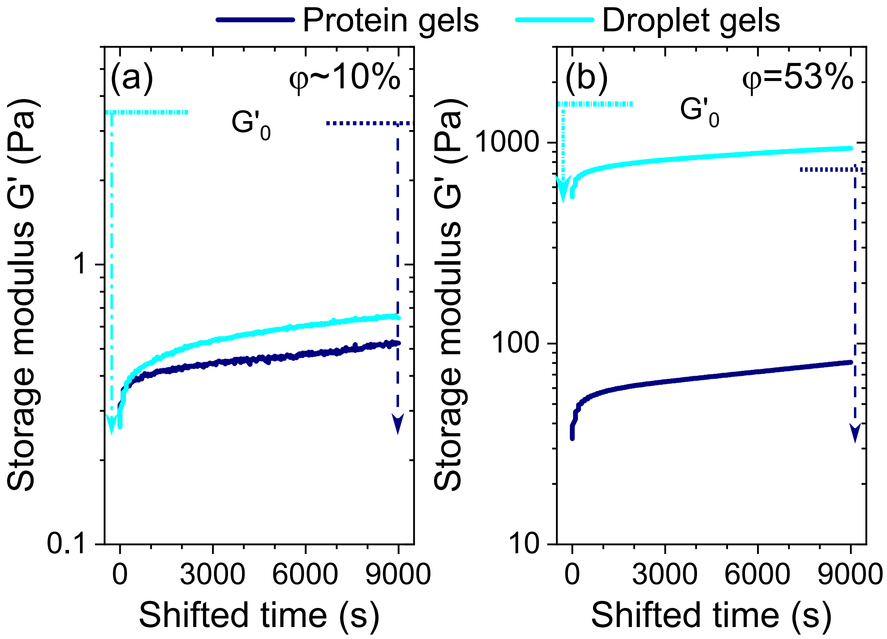

Figure 6.20 *Recovery of protein gels (navy blue) and protein-stabilised droplet gels (cyan) after application of large-amplitude oscillatory shear. The storage modulus* G' *(*Pa*) measured by small-amplitude oscillations is represented as a function of time* t *(*s*), starting immediately after shearing the sample. The storage modulus in linear regime* G'_0 *and the drop upon fracture for protein gels and droplets gels are represented by the sets of horizontal lines and arrows.*
(a) Recovery of gels at low concentration: protein gel at $\phi_{eff} \approx 9\,\%$ *and droplet gel at* $\phi_{eff} \approx 9.8\,\%$*. (b) Recovery of gels at high concentration: protein gel and droplet gel at* $\phi_{eff} \approx 53\,\%$*.*

gels arises from attractive forces rather than from jamming of the particles, as confirmed by the flow behaviour of the concentrated suspensions, presented in Chapter 5. Indeed colloidal glasses, for which the solid nature comes from entropic repulsions and jamming, present a power-law decrease of viscoelasticity and yielding when sheared with high-amplitude oscillations, and then recover their storage and loss moduli when at rest [52].

The full sequence of rheological measurement presented in Figure 6.1 thus allows a thorough characterisation of protein and droplet gels by their gelation, moduli after gelation, frequency dependence and linear viscoelasticity. As the two types of gels are made with colloidal particles of different nature, their behaviour was characterised over a wide range of volume fraction, in order to discriminate the intrinsic differences between the gels from the variations arising from their particle density.

6.6 Conclusion

It was found here that both protein and droplet suspensions gel in a similar way to DLCA colloidal gels. Their gelation presents minor differences in the development of the microstructure and in the kinetics. A further understanding of the gelation of these systems could be achieved by decorrelating the hydrolysis rate of glucono δ-lactone from the actual gelation kinetics, by measuring the aggregation state in the sample, directly [167] or indirectly [11].

In addition, the fractal nature of the two types of gel was confirmed by the visualisation of their microstructure. The densification of the network upon increase of the volume fraction was also characterised. The quantification of the microstructure by FFT, despite being imprecise, showed that the feature size for all gels is in the range of 5 µm to 20 µm. Alternative analysis of the pores or the fractality may require better-quality images.

Finally, the rheological behaviour of protein gels and droplet gels was characterised. Here again, these behaviours could be compared to results for model colloidal gels. Some discrepancies between the two systems seem to indicate that this theoretical framework may not be sufficient for an entirely accurate description, and some system-specific characteristics, such as a possible change in protein structure upon adsorption, may have to be taken into account. It is believed that upon emulsification, the single proteins adsorb at the surface of the droplets, anchoring the hydrophobic parts of their chains in the oil. This means that droplets and protein aggregates may have a different stickiness. Neutron scattering would be a good starting point for developing a deeper knowledge of the protein conformation when adsorbed and un-adsorbed.

These characterisations of the gelation behaviour, microstructure and rheological properties of pure protein and pure droplet gels can also be used to develop a better understanding of emulsion gels. In Chapter 7, mixtures of known composition are studied using the properties of the individual components to identify their contributions to the overall behaviour of the mixtures.

Chapter 7

Gelation and rheology of gels of mixtures of proteins and droplets

In this Chapter, I study emulsion gels considering them as gels containing a mixture of protein-coated droplets and un-adsorbed proteins. I thus use the characterisation of the pure gels performed in Chapter 6. The gels of mixtures are obtained by acidifying the suspensions presented in Chapter 5, as detailed in Chapter 3.

I first use the rheo-imaging technique introduced in Chapter 6 to examine the acid-induced gelation of an emulsion. I find that the gelation process presents some morphological features found for pure gels of both proteins and of droplets in Chapter 6.

I then present the relevant parameters to describe the bi-dimensional range of composition of the emulsion gels. Because of the morphology of the gels, and especially the aggregation of primary colloidal species into aggregates and strands, I argue that the parameters chosen to describe the emulsion gels must be different than for emulsions in suspension.

Using these parameters, I next study the rheological properties of the wide range of emulsion gels. I find that the moduli are mostly determined by the total volume fraction of the components, but can be slightly adjusted by changing their ratio. The frequency dependence, on the other hand, appears to only depend on the relative proportions of droplets and proteins.

Finally, I explore the classic, but approximate, view of emulsion gels as a rubbery matrix of protein gel filled with droplets. I show that the reinforcement effect of the fillers does not depend on the density of the matrix. More surprisingly, I find that the same results are obtained by interchanging the components and considering the reinforcement of a droplet gel matrix filled with proteins. I conclude that a more integrated approach than the classic view of filled gels allows a better comprehension of their rheological properties.

7.1 Introduction

Many food products are colloidal gels, as pointed out in Chapter 6, but in many cases, like yoghurt, they are not pure gels of one colloidal species, but they are complex mixtures in which several components may interact to form a viscoelastic solid. In this chapter, this complexity is accounted for by studying the gels made of protein-stabilised droplets and proteins.

These gels are commonly called emulsion gels, because they are formed by destabilising an emulsion, which causes particle clustering and eventually percolation of a network. However, the term *emulsion* only implies the presence of droplets and covers a wide range of compositions, as pointed out in Chapter 5. The suspension could indeed contain mostly protein-stabilised droplets, or instead only a few droplets in a concentrated suspension of un-adsorbed proteins.

The composition of the emulsion gels is however important. Indeed, it was shown previously that the presence of un-adsorbed proteins in the aqueous phase after emulsification of the oil phase could affect significantly the viscosity of emulsions, and it has to be expected that the same is true regarding the viscoelasticity of emulsion gels. Here attention is focused on characterising the rheological properties of these systems as a function of the composition.

The rheological behaviour of protein-stabilised emulsion gels has been studied in the past, but the focus was mostly on characterising the influence of the droplet content of these soft solids [9, 16, 120, 173]. It was found that an increase in droplet content resulted in a rise of the viscoelastic modulus, and a decrease of its frequency dependence. These results could not be satisfyingly explained by the existing model developed for bitumen suspensions classically used for emulsion gels [16, 174].

Here, it is hypothesised that this model is not sufficient for protein-stabilised emulsion gels, because it is based on the idea that the droplets act as fillers in a matrix of protein gel. Such a framework considers the matrix as homogeneous at the scale of the fillers, which does not correspond with the confocal imaging results on caseinate gels presented in Chapter 6. Instead, here the droplets are not only much smaller than the pore size of the protein gels, but they can also form gels in the absence of non-adsorbed proteins.

An important part of the present study on emulsion gels is thus to frame the problem in a different way, that takes into account the fractal structure of protein gels and thus the relevance of the colloidal gel framework to study gels of mixtures. This allows a wider vision of these systems and a characterisation of the influence of their composition on their mechanical properties.

In order to do so, the gelation of an emulsion gel is first characterised by using the rheo-imaging technique presented in the previous chapter. A relevant framework to describe emulsion gels is then carefully discussed. This description is later applied to the analysis of the rheological properties of these soft solids. Finally, the need to change the paradigm of emulsion gels is emphasised, and a transition from the image of filled gels to those of colloidal gels with intermediate composition between pure protein gels and pure droplet gels is suggested.

7.2 Materials & Methods

Mixtures were prepared as detailed in Chapter 3, and the list of their compositions are shown in Table 3.2.

Rheology measurements were performed after addition of glucono δ-lactone as a slow acidifier, and the preparation and measurement sequence have been detailed in Chapter 6.

7.2.1 Rheo-imaging

The rheo-imaging technique was used as presented in Chapter 6 on a gel of mixtures. The exact configuration of the setup and the details of the sample are summarised in Table 7.1.

Table 7.1 *Experimental details for the rheo-imaging of emulsion gels.*

Parameter	Emulsion gel
Concentration	$c = 1\,\%$(wt) of proteins and $c = 2.4\,\%$(wt) of droplets
Volume fraction	$\phi_{eff,prot} = 7.6\,\%$ and $\phi_{eff,drop} = 4.3\,\%$
Glucono δ-lactone	0.18 g gdl/g protein and 0.075 g gdl/ g droplet
Objective	20x/0.75 dry
Laser	552 nm
Rhodamine B	1.2×10^2 µL / g protein
Bodipy 493/503	41 µL / g droplet
Rheometer tool	PP25/S (parallel plates 25 mm diameter, sand blasted)
Gap	400 µm
3D stack size	30 frames
Time for a 3D stack	13 s (50 µm)
Delay between 3D stacks	60 s

7.3 Gelation of emulsion gels: a rheo-imaging study

The rheo-imaging technique can be used to characterise the gelation of emulsions, similarly to the gelation of suspensions of pure droplets (Figure 6.8) and of pure protein (Figure 6.7), as detailed in Chapter 6. The micrographs of a gelling suspension of droplets and proteins, and the corresponding increase in viscoelasticity, are presented in Figure 7.1.

As can be observed, the gelation of the emulsion follows the same steps as for the pure suspensions. First, for almost 3 h, the progressive acidification causes little modification in the appearance and rheology of the suspension. But from Frames 2 to 4, the particles start aggregating into growing clusters and this transition goes together with an increase in storage and loss moduli G' and G''. Then, at Frame 5, these clusters percolate into a space-spanning network, and there is a cross-over between loss and storage modulus at what can be defined as the gelation point. Finally, from Frames 6 to 8, the changes in microstructure consist mostly in shrinking of the network strands, probably because of their densification. As for pure protein networks, this early ageing of the network seems to considerably contribute to the its increase in elasticity.

This gelation behaviour shows that, similarly to the gels of pure suspensions,

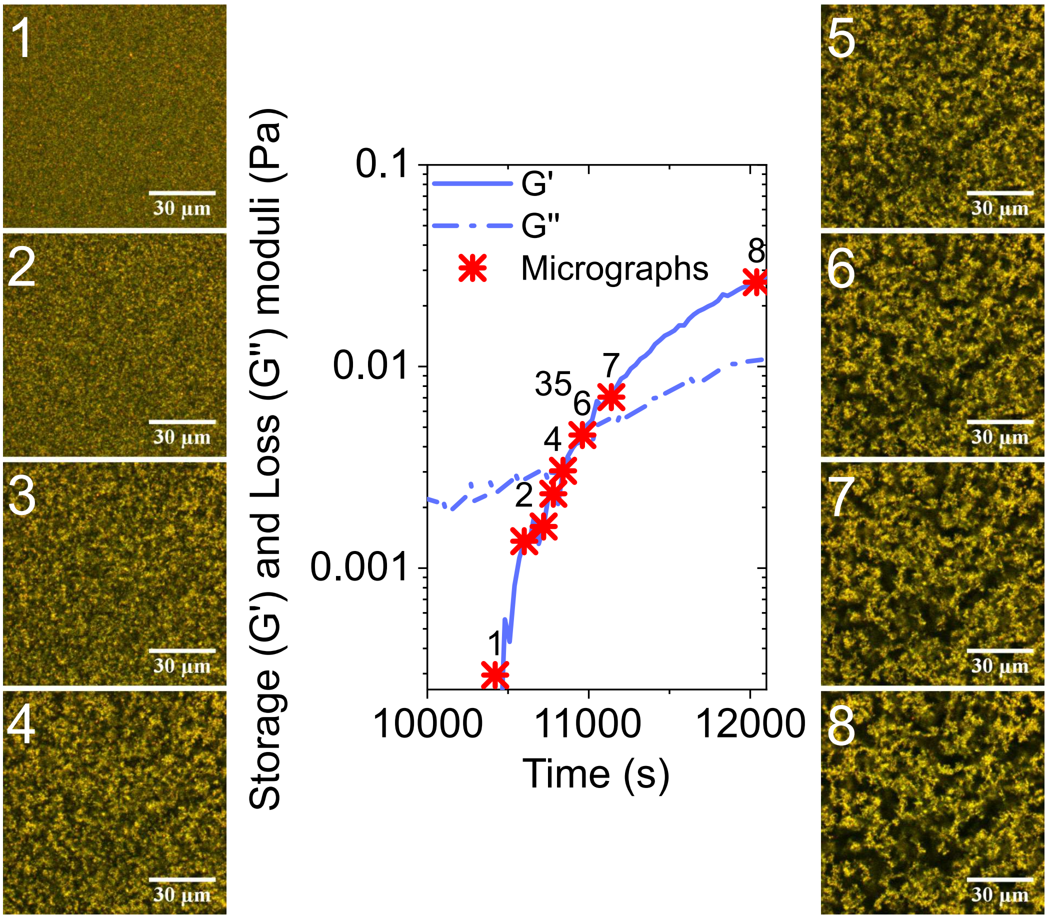

Figure 7.1 *Confocal micrographs of the acid-induced gelation of a suspension containing sodium caseinate ($\phi_{eff,prot} = 7.6\,\%$) and caseinate-stabilised droplets ($\phi_{eff,drop} = 4.3\,\%$) at room temperature, and emergence of viscoelasticity.*

Sodium caseinate and oil are labelled by adding Rhodamine B (red) and Bodipy 493/503 (green) in the suspension before gelation. Each frame is taken at $10\,\mu\mathrm{m}$ *above the glass slide and at different stages of gelation, and is numbered from top to bottom and left to right: (1)* $t = t_0 = 10.4 \times 10^3\,\mathrm{s}$ *after addition of glucono δ-lactone, (2)* $t = t_0 + 180\,\mathrm{s}$, *(3)* $t = t_0 + 300\,\mathrm{s}$, *(4)* $t = t_0 + 360\,\mathrm{s}$, *(5)* $t = t_0 + 420\,\mathrm{s}$, *(6)* $t = t_0 + 540\,\mathrm{s}$, *(7)* $t = t_0 + 720\,\mathrm{s}$, *(8)* $t = t_0 + 1620\,\mathrm{s}$. *The length of the scale bar represents* $30\,\mu\mathrm{m}$.

The storage (G', solid line) and loss (G", dashed line) corresponding to the micrographs are indicated on the gelation plot (red stars).

the formation of emulsion gels can be modeled by a diffusion-limited cluster aggregation (DLCA) and the final structure is a fractal network of interconnected micron-sized clusters. Interestingly, the end of the gelation presents the two signature behaviours that were identified for the pure gels, namely the shrinking strands of the protein gels and the mobile dangling chains of the protein gels.

In addition, the development of the microstructure can be quantified using a Fast Fourier Transform (FFT) analysis, as illustrated in Figures 6.5 and 6.6. The structure factors and parameters obtained from the application of this protocol to the micrographs of Figure 7.1 are presented in Figure 7.2.

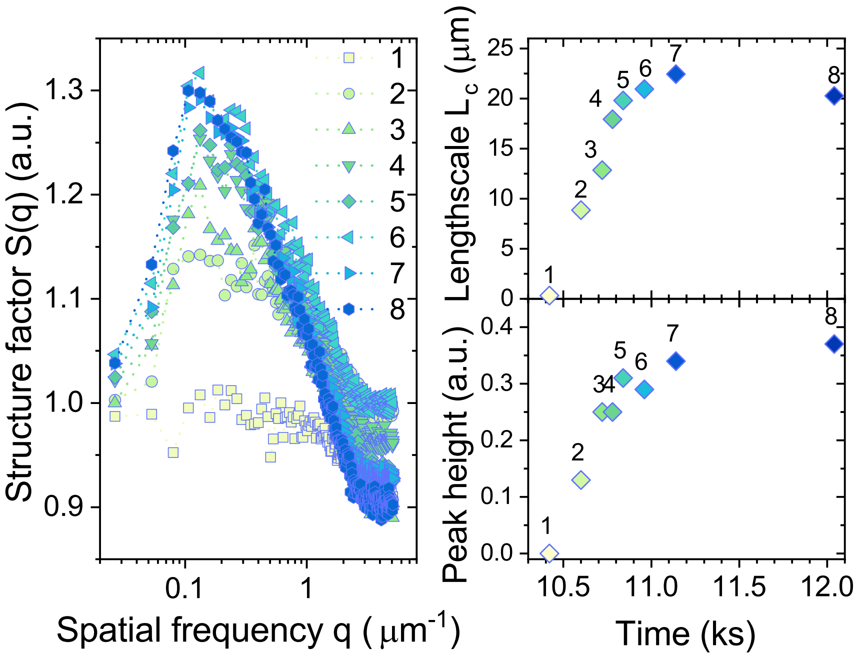

Figure 7.2 *Fast Fourier Transform analysis of the confocal micrographs of gelation of a suspension of sodium caseinate and of caseinate-stabilised droplets (presented in Figure 7.1).*
(Left) Structure factors $S(q)$ of each micrograph are plotted versus the spatial frequency q.
(Right) Characteristic lengthscales L_C (top) and peak heights (bottom) extracted from the structure factors $S(q)$ are plotted versus the gelation time t.

As previously, the structure formation appears, in terms of structure factor $S(q)$, as a peak increasing in amplitude and narrowing with time. This appears clearly when the typical lengthscale L_c and peak height are presented as a function of time. Both parameters increase sharply at the beginning of the sol-gel transition and then plateau.

Most importantly, the gelation seems to be simultaneous for the two components of the mixture, and no distinction can be made between proteins and droplets on the final structure at the scale of the micrographs. Indeed, the images coming from the fluorescence of the oil and of the protein are similar, as demonstrated by the yellow colour of the network because of the overlap of the green and red images. This apparent homogeneity forms the basis of the framework developed here for the emulsion gels, seen here not as droplet-filled protein gels but as composite networks where the two components play an equal role.

7.4 Description of gels of mixtures: a change of the composition parameters for a new framework

A more thorough study of emulsion gels requires exploration of the full range of composition of these systems. The parameters used to describe this composition range, however, are not mere mathematical tools but a core part of the framework applied to the problem of the study of mixtures. It is thus essential to reflect on the choice of the parameters in conjunction with the nature of the system.

In the suspensions of emulsion described and studied in Chapter 5, the two components contribute distinctively to the viscosity of the mixture, mostly because of their size discrepancy. Indeed, the smaller un-adsorbed proteins form a viscous continuous phase, modifying the hydrodynamic interactions between the droplets and increasing the overall viscosity of the mixture. It is thus convenient to think of mixtures as ternary suspensions, with un-adsorbed proteins, droplets and water playing distinct roles.

However, in the case of emulsion gels, the contribution of un-adsorbed proteins and droplets may be less clear. Indeed, the two components form fractal gels of similar rheological properties and microstructures, as presented in Chapter 6. Rheological and microstructural features of colloidal gels are best understood when the length-scale considered is of the strands of particles, and gels are thus examined at a much larger scale than of the single particles [20, 81, 84, 165]. At this length-scale, it can be assumed that the discrepancy in size and structure of the protein aggregates and protein-stabilised droplets is not as critical as for emulsions in suspensions. Thus, for gels made of mixtures of proteins and droplets, the hypothesis leading this work is that there is little distinction between droplets and un-adsorbed proteins in the way each contributes to the properties of the gel of mixture. Instead, it is important to relate the emulsion gels to the pure gels of proteins and droplets.

The study of gels made of both proteins and droplets therefore requires a different description of these systems than for suspensions. Indeed, the focus of the new framework has to be changed from the individual content of each component in the mixture $\phi_{eff,prot}$ and $\phi_{eff,drop}$ to the total content $\phi_{eff,tot} = \phi_{eff,prot} + \phi_{eff,drop}$ and their relative amounts, described here as $\phi_{eff,drop}/(\phi_{eff,prot} + \phi_{eff,drop})$. This change of variable is illustrated in Figure 7.3.

These parameters make the distinction between gels that are similar to protein gels and gels that are closer to droplet gels, as well as between sparse gels and very dense gels. The change of variables presented in Figure 7.3 thus allows more meaningful discussion of the properties of gels containing both proteins and protein-coated droplets.

It should be noted that this framework was previously introduced in Chapter 5 to improve the visualisation of the viscosity of emulsions. By contrast, it is here an essential ingredient for the analysis of the rheology of emulsion gels that sets a certain vision of these systems. The relevance of this choice will be discussed later in light of another framework commonly used for emulsion gels.

7.5 Rheology of gels of mixtures

The observation of the gelation of an emulsion is instructive, but a general understanding of the properties of emulsion gels can only be built on the exploration of their bi-dimensional composition range. Indeed, such a study allows discrimination of the rheological properties arising from the particle content of the gel, from those related to the composition of the mixture.

7.5.1 Viscoelastic properties: decoupling of total volume fraction and composition

Here, the rheological properties of the samples, whose compositions are presented in Figure 7.3, were measured using the protocol shown in Figure 6.1. The storage

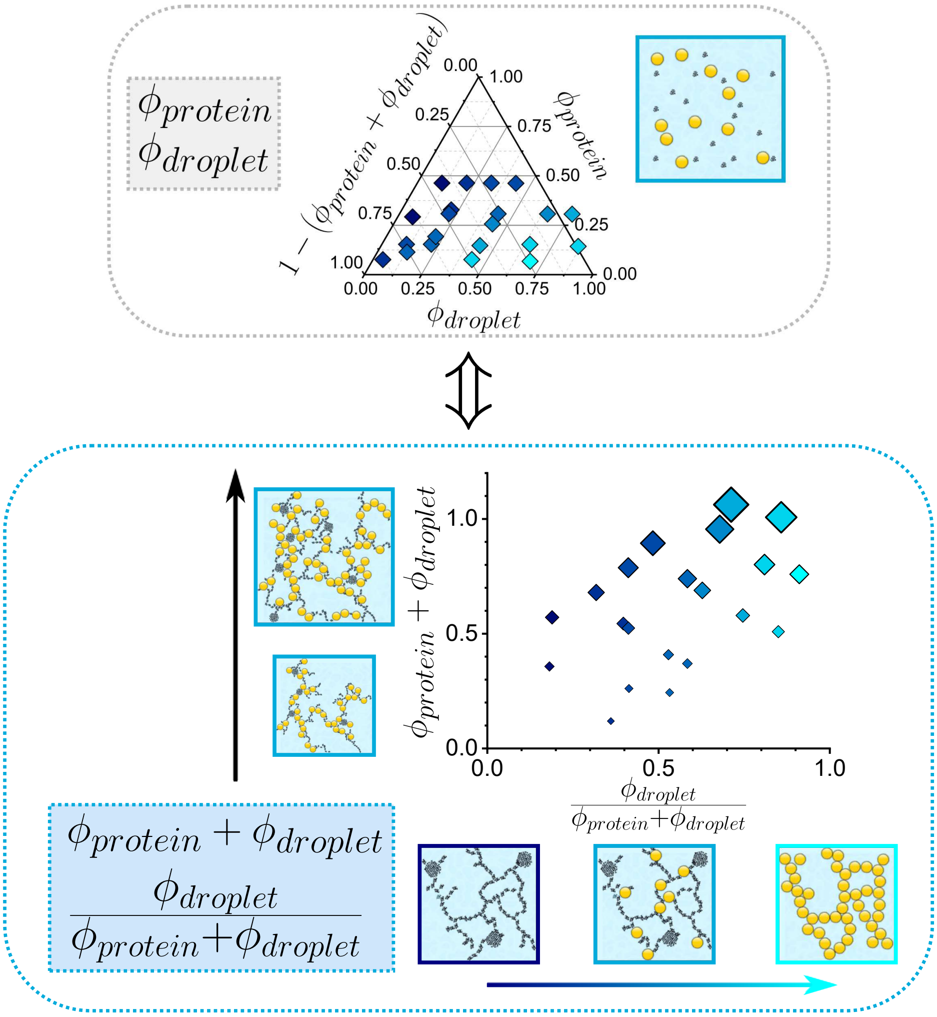

Figure 7.3 *From emulsions in suspensions to emulsion gels: a change of variables for the description of mixtures. Emulsion gels are better described by their total volume fraction* $\phi_{eff,prot}+\phi_{eff,drop}$ *(coded by the size of symbols), and by the ratio of droplets over the total volume fraction* $\phi_{eff,drop}/(\phi_{eff,prot}+\phi_{eff,drop})$ *(colour-coded as introduced in Chapter 5).*

and loss moduli of emulsion gels at t_{gel}+2500 s can be compared with the moduli of the gels of pure components presented in Figure 6.13. These results are displayed in Figure 7.4.

As can be seen, the moduli of the emulsion gels are of the same order of magnitude than for the pure protein or droplet gels and they follow the same trend with the volume fraction. The elastic and viscous aspects of the network are thus mainly determined by the total effective volume fraction $\phi_{eff,droplet} + \phi_{eff,protein}$, and only moderately by the composition. This result demonstrates that the use of the effective volume fraction developed for suspensions of pure components in Section 5.3.2 is also relevant for the description of emulsion gels, despite the approximations used.

In addition, small variations in the viscoelastic properties of emulsion gel samples with similar volume fractions but different compositions seem to imply that the nature of the elementary particles forming the network must be taken into account for a more detailed description. Two approaches for the analysis of the storage moduli, shown in Figure 7.4, are therefore suggested here to emphasise the influence of the composition and the reinforcement of the gels.

Influence of the composition

For the purpose of assessing the role of the composition of the mixtures in the strength of the gels formed by their destabilisation, it is useful to subtract the power law dependence with the volume fraction identified in Equation 6.1 for pure gels. This normalisation by the total effective volume fraction can be achieved by dividing the storage modulus of the mixture $G'^{\,exp}_{mixture}$ by the modulus expected for a protein gel of identical volume fraction:

$$\frac{G'^{\,exp}_{mixture}}{G'^{\,model}_{protein}(\phi_{protein} + \phi_{droplet})} \tag{7.1}$$

Where $G'^{\,model}_{protein}$ designates the modulus of a hypothetical protein gel, containing the same total volume fraction $\phi_{protein} + \phi_{droplet}$ as the mixture, and calculated using the model developed in Chapter 6, described by Equation 6.1 with the values of Table 6.2.

In other words, the normalisation in Equation 7.1 can be seen as the estimation of the distance from the model for protein gels, for which the navy blue line

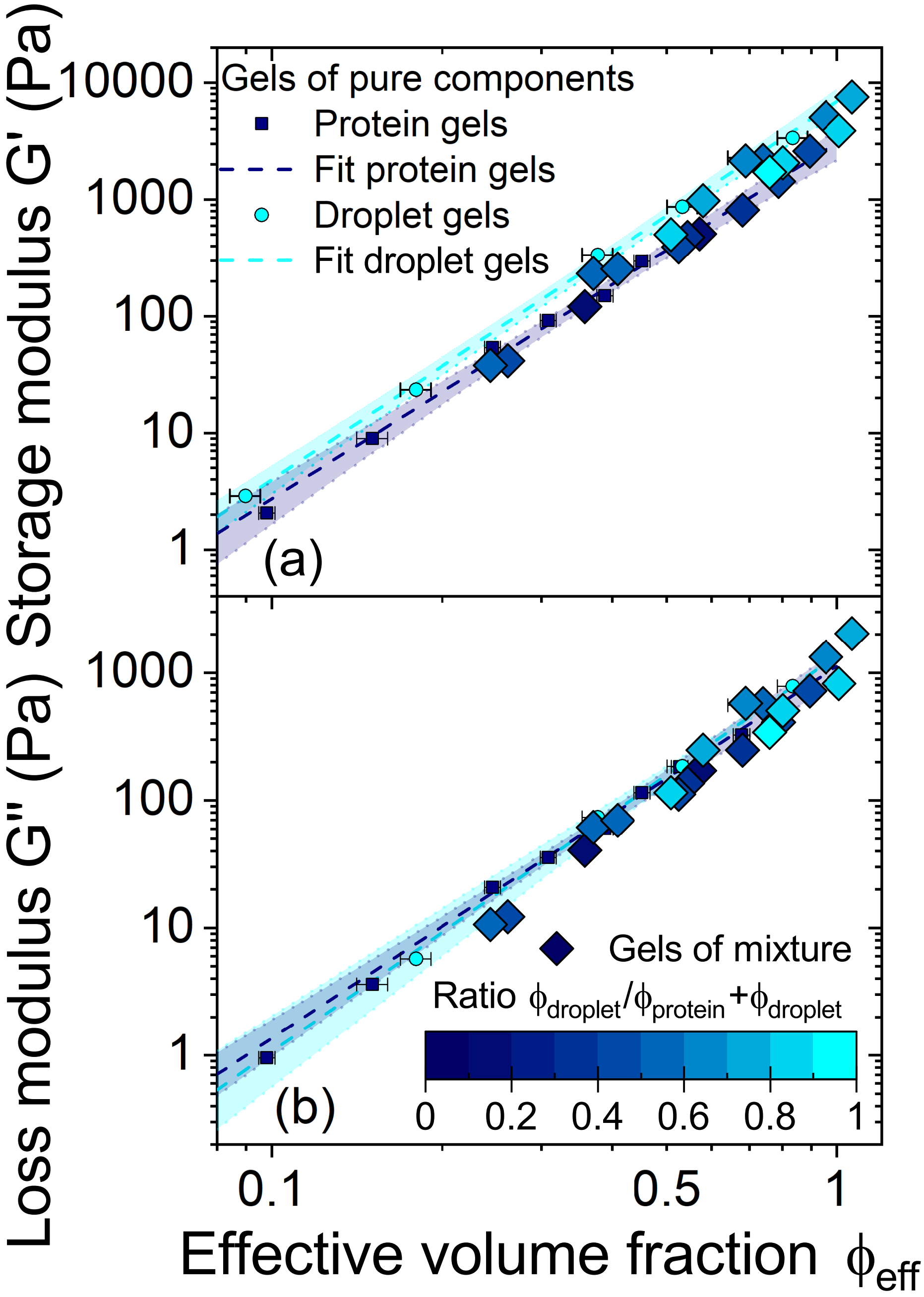

Figure 7.4 *Storage (G', (a)) and loss (G'', (b)) moduli at 1 Hz of protein-stabilised droplet gels (circles, cyan), of protein gels (squares, navy blue), and of gels of mixtures (diamonds, colour-coded), as functions of the effective volume fraction of the gel (respectively $\phi_{eff,drop}$, $\phi_{eff,prot}$ and $\phi_{eff,prot} + \phi_{eff,drop}$, scaling derived in Section 5.3.2).*
A fit (Equation 6.1) was performed for each system and the model (parameters listed in Table 6.2) as well as the 95 % confidence band are displayed on each graph.
The horizontal error bars arise from error propagation upon calculation of the volume fraction, while the vertical error bars are smaller than the data points, so not diplayed here.

in Figure 7.4 is used as baseline. Schematically, this can be represented as the change in gel strength in a network of fixed volume fraction when some proteins are substituted by droplets. The change thus defined is shown in Figure 7.5 as a function of the composition, described by the ratio $\phi_{eff,drop}/(\phi_{eff,prot} + \phi_{eff,drop})$.

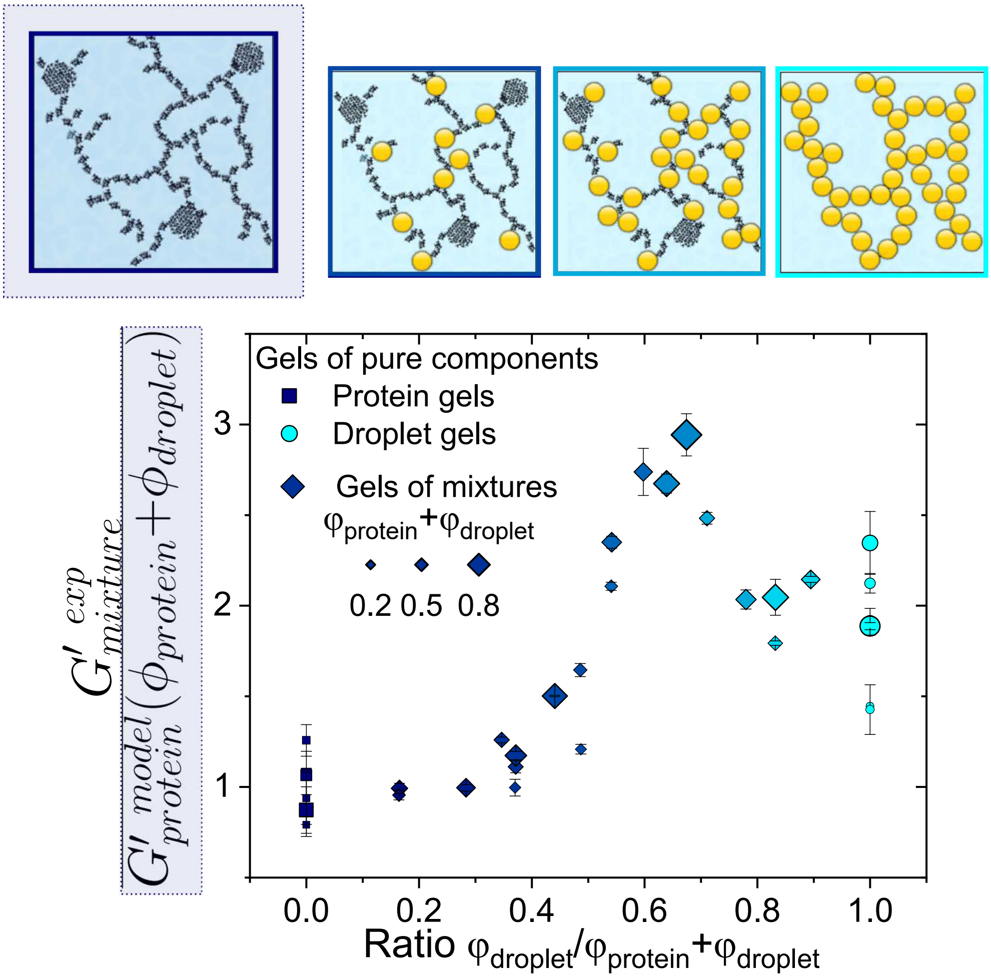

Figure 7.5 *Storage modulus normalised by the effect of the volume fraction* $G'^{\,exp}_{mixture}/G'^{\,model}_{protein}(\phi_{protein} + \phi_{droplet})$ *as a function of the relative amount of the composition* $\phi_{eff,drop}/(\phi_{eff,prot} + \phi_{eff,drop})$. *The size of the data points indicates the total volume fraction* $\phi_{eff,tot} = \phi_{eff,drop} + \phi_{eff,prot}$. *This graph represents the same samples of gels of mixtures than shown in Figure 7.4.*

As can be seen, there is a non-linear variation of the strength of the networks between the boundaries represented by pure gels of proteins and droplets. First, gels with less than $\phi_{eff,drop}/(\phi_{eff,prot} + \phi_{eff,drop}) \leq 40\,\%$, *i.e.* less than 40 % droplets in their solid content, present the same storage modulus than equivalent protein gels. When more proteins are substituted by droplets and $\phi_{eff,drop}/(\phi_{eff,prot}+\phi_{eff,drop})$ increases, the stength of the emulsion gels grows and reaches a maximum at $\phi_{eff,drop}/(\phi_{eff,prot} + \phi_{eff,drop}) \approx 70\,\%$, where its value is 3 times higher than pure protein gels, and 1.5 times higher than pure droplet gels. Finally, when even more droplets replace proteins, the strength of the mixture gel decreases slightly and plateau from $\phi_{eff,drop}/(\phi_{eff,prot} + \phi_{eff,drop}) \approx 80\,\%$ at the same level than pure droplet gels.

In addition, this non-linear behaviour of the mixtures as a function of the composition does apparently not depend on the total volume fraction, indicated by the size of the data points in Figure 7.5. Such a result seems to imply that the two compositional parameters of the framework introduced earlier can be decoupled, and their contribution to the properties of the mixtures can be analysed separately.

Finally, a consequence of this decoupling and of the characterisation of the influence of the ratio of components is the ability to predict the storage modulus of an emulsion gel of known composition. Indeed, a rough estimation of its strength can first be calculated from Equation 6.1 with the values of Table 6.2 for a protein gel. It is then corrected for the composition of the mixture by using the results in Figure 7.5.

7.5.2 Frequency dependence of emulsion gels

Similarly to the pure protein and droplet gels, the frequency dependence of emulsion gels was measured after gelation, following the protocol presented in Figure 6.1. The dependence of the storage modulus of emulsion gels on frequency can also be modelled by a power law $G' = G'_{0,\omega} \times \omega^{\beta}$, as in Equation 6.3. The exponent β, which describes the dynamic behaviour of the networks, is estimated for each emulsion gel of the bi-dimensional range shown in Figure 7.3 and presented as a function of the composition in Figure 7.6.

This representation allows the observation of a continuous transition of the frequency dependence between that of droplet gels ($\phi_{eff,drop}/(\phi_{eff,prot} + \phi_{eff,drop}) = 0$) and of protein gels ($\phi_{eff,drop}/(\phi_{eff,prot} + \phi_{eff,drop}) = 1$). Indeed, the frequency dependence of mixtures presents some variations with the total volume fraction, represented by the size of the data points, but varies overall between $\beta_{droplet} \approx 0.1$ and $\beta_{protein} \approx 0.2$ as the proportion of protein increases in the mixture. This is in good correspondence with previous studies in which a decrease in frequency dependence was observed upon addition of casein-coated droplets in a casein gel

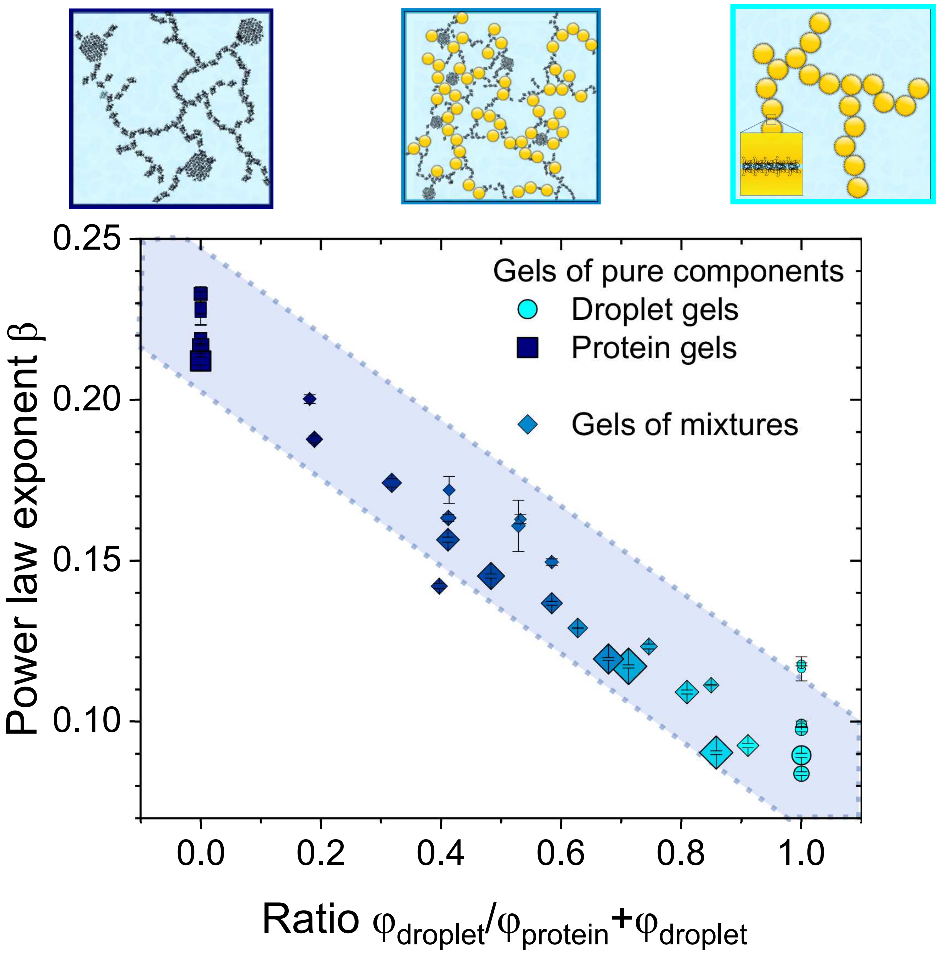

Figure 7.6 *Comparison of frequency dependence for gels of mixtures (diamonds, colour-coded), of protein stabilised droplets (circles, in cyan) and of protein (squares, in dark blue): power-law exponent* β*, obtained by fitting* $G' = f(\omega)$ *with Equation 6.14, as a function of the ratio* $\phi_{eff,drop}/(\phi_{eff,prot} + \phi_{eff,drop})$*. The size of the data points indicates the total volume fraction* $\phi_{eff,tot} = \phi_{eff,drop} + \phi_{eff,prot}$*. The shaded area is a guide for the eye.*

[16].

Therefore, it seems that the difference in dynamics between droplets and proteins is reflected linearly in the mixtures as a function of their composition. This result reinforces the hypothesis that emulsion gels are composite networks that are best described as intermediary between protein gels and droplet gels.

7.6 Change in paradigm for the description of emulsion gels

The results discussed so far are based on the description of emulsion gels as colloidal gels of total volume fraction $\phi_{eff,prot} + \phi_{eff,drop}$ and for which the composition indicates how similar they are to pure gels of droplets and of proteins, as described previously. However, in the literature, these systems are more commonly studied in a material engineering framework, in which protein-stabilised droplets act as fillers in a protein matrix [9, 16, 173]. It is interesting to compare these two approaches, filled gel and intermediate colloidal gel, and the results arising from them.

7.6.1 Classical approach: emulsion gels as a filled matrix

As detailed in Chapter 2, emulsion gels have been studied in the past by borrowing the theoretical framework developed for the effect of fillers on the mechanical properties of composite materials such as bitumen [174]. In these works, the droplets in the emulsion were considered to be similar to fillers and thus to reinforce the matrix of protein gel [16].

However, it has also been observed that this theory did not accurately predict the increase in elastic modulus upon addition of droplets in emulsion gels [16, 173]. This model has since then been improved by considering the clustering of the droplets, but its validity is still limited to a relatively small range of matrix stiffness and of filler content [175].

Here, the focus is on the description of the reinforcement of a caseinate-stabilised emulsion gel using the filler effect approach. As discussed in the previous section, the way the problem is framed can appreciably affect the conclusions, so close attention is paid to the choice of the parameters.

Reinforcement of gels by fillers: symmetry of components

Emulsion gels can be considered either as protein gel matrixes filled with droplets, or the other way round. In this framework, it is interesting to look at the change in rheological properties of the matrix gel upon addition of fillers. The presence of attractive van der Waals interactions between protein-stabilised droplets and proteins when gelation occurs indicates that the addition of filler probably has a reinforcing effect [16].

This reinforcing effect of the component arbitrarily chosen as filler, droplets for example, on the strength of the matrix of the other component, here the protein gel, can mathematically be expressed by the ratio of storage moduli between mixture and matrix:

$$\frac{G'^{\,exp}_{mixture}}{G'^{\,model}_{protein}(\phi_{protein})} \tag{7.2}$$

Where $G'^{\,exp}_{mixture}$ is the experimental storage modulus of the mixture, as presented in Figure 7.4. In addition, $G'^{\,model}_{protein}$ designates the modulus of a hypothetical protein gel, containing the same volume fraction of protein $\phi_{protein}$ as the mixture, and calculated using the model developed in Chapter 6, described by Equation 6.1 with the values of Table 6.2.

Reciprocally, if any emulsion gel is seen as a protein-filled droplet gel matrix, then the reinforcing role of the proteins can be expressed by $G'^{\,exp}_{mixture}/G'^{\,model}_{droplet}(\phi_{droplet})$, where the storage modulus of the matrix $G'^{\,model}_{droplet}(\phi_{droplet})$ is also calculated using the values of Table 6.2 in Equation 6.1.

The two scenarios, droplet-filled protein gels and protein-filled droplet gels, are used for the analysis of the gels of mixtures presented in Figure 7.4, and the reinforcement in both cases is shown in Figure 7.7. It is represented as a function of the proportion of droplets in the mixture, rather than the volume fraction of droplets, in order to balance the concentration of the matrix.

As can be seen, there is a collapse of the reinforcing effects for matrixes of different volume fraction in a single mastercurve in both cases. For the two scenarios, the elastic modulus is doubled when the amount of filler added is 11 % of the matrix volume fraction (*i.e.* $\phi_{filler}/(\phi_{filler} + \phi_{matrix}) = 0.2$), and grows ten-fold when the amount of filler is equal to the volume fraction of the matrix (*i.e.*

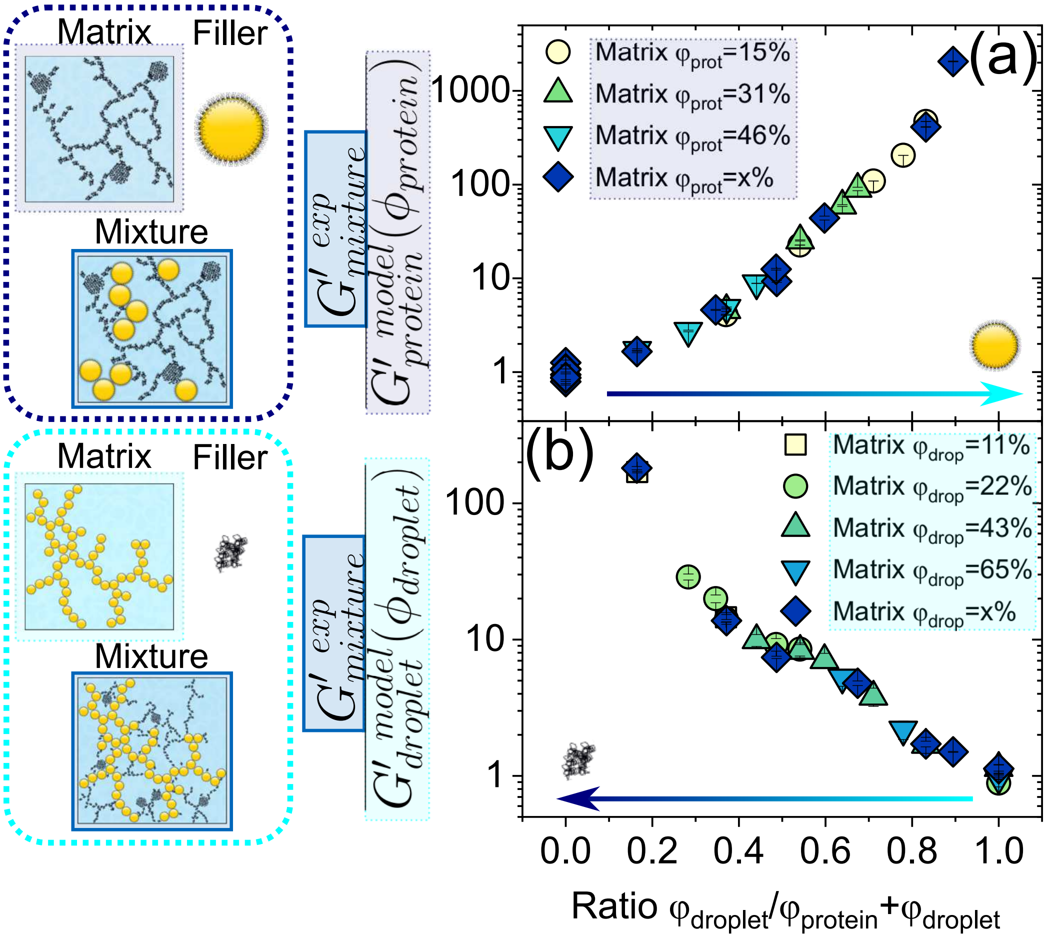

Figure 7.7 *Reinforcement of a protein gel upon addition of droplets* $G'^{\,exp}_{mixture}/G'^{\,model}_{protein}(\phi_{protein})$ *(top, from left to right), and of a droplet gel upon addition of proteins* $G'^{\,exp}_{mixture}/G'^{\,model}_{droplet}(\phi_{droplet})$ *(bottom, from right to left) as a function of the relative amount of droplet added* $\phi_{eff,drop}/(\phi_{eff,prot}+\phi_{eff,drop})$. $\phi = x\%$ *indicates samples of miscellaneous concentrations. The two graphs represent the same samples of gels of mixtures, as shown in Figure 7.4, but differ by the arbitrary role of the components: the proteins form the matrix in the top graph while they are the fillers in the bottom graph, and vice-versa for the droplets.*

$\phi_{filler}/(\phi_{filler} + \phi_{matrix}) = 0.5$. The increase in storage modulus as a function of the relative amount of fillers is thus independent of the density of the matrix.

This invariability is probably related to the fractal nature of the colloidal gels studied here. Indeed, for all the gels of mixtures, the matrix, whether protein gel or droplet gel, is a fractal gel with a heterogeneous structure, as illustrated in Figure 6.12. For the fillers to significantly reinforce this structure, they must contribute to the network as much as the particles forming the matrix gel and their amount has thus to be calculated relative to the matrix density rather than in absolute terms, in which case the master curve does not appear.

Furthermore, each scenario of pair matrix/filler gives a similar result, which seems to indicate that protein-coated droplets and un-adsorbed proteins have a symmetric contribution to the viscoelasticity of the gels of their mixtures. The ability of the two components to form a gel of their own, as shown in Chapter 6, may be the source of this specificity of protein-stabilised emulsion gels. In that regard, the established approach of emulsion gels as droplet-filled protein gels does not reflect the complex structure of these systems. Instead of matrix and fillers, it may thus be more appropriate to consider emulsion gels as fractal composite networks made of both proteins and droplets.

7.6.2 New approach: intermediate behaviour of gels of mixtures

On the other hand, the results shown previously converge to form an emerging picture of protein-stabilised emulsion gel as intermediate between droplet and protein gels. Indeed, it was shown that:

- The rheo-imaging technique revealed that the gelation of an emulsion gel presents both the shrinking of the strands at early ageing observed for protein gels, and the visible dangling of end chains observed for droplet gels.
- The storage modulus is mostly determined by the total volume fraction of the emulsion gel $\phi_{eff,prot} + \phi_{eff,drop}$. Furthermore, when the strength of the emulsion gels is scaled in order to account for the variations in volume fraction, it varies continuously between the behaviour of pure protein gels and pure droplet gels.

- Similarly, the frequency dependence varies continuously between the behaviour of protein gels and droplet gels, linearly with the composition ratio $\phi_{eff,drop}/(\phi_{eff,prot} + \phi_{eff,drop})$.

It should also be noted that these behaviours are consistent over the bi-dimensional composition range of emulsion gels explored in this study, as presented in Figure 7.3.

Finally, even the filled matrix approach used in the previous section yields results that seem to reinforce the image of emulsion gel as intermediate colloidal gels. Indeed, the mastercurve obtained for the reinforcing effect of fillers as a function of their amount relative to the density of the matrix is yet another indication that the total volume fraction is more important that the absolute amount of fillers. In addition, the symmetric role of the components may reinforce the idea of composite networks, where the stress-bearing strands are formed by the proteins and protein-stabilised droplets alike.

7.6.3 Changing framework for the study of emulsion gels

Modeling protein-stabilised emulsion gels as simple filled gels presents several conceptual limitations, namely the existence of pure droplet gels and the increase in volume fraction upon addition of fillers. For those to be taken into account, the way the problem is framed has to be changed.

First, the focus on droplets as fillers ignores the fact that they can form a stress-bearing network of their own, and not only large clusters, as demonstrated in Chapter 6. This aspect is mentioned in some studies, but not taken into account for the analysis of the rheological behaviour [9].

Furthermore, the idea that the matrix is not changed by the addition of fillers is only valid if this viscoelastic solid is homogeneous at the length scale of the droplets. This is not the case for caseinate gels, as observed in Chapter 6. Instead, the droplets are much smaller than the pores of the structure, and the increase of volume fraction caused by their addition must thus be considered.

These two points justify the approach of emulsion gels as intermediate colloidal gels, as well as the choice of the parameters describing their composition. Indeed, the existence of pure droplet gels makes it necessary to evaluate how similar the gel of mixture is to the pure gels using the composition ratio $\phi_{eff,drop}/(\phi_{eff,prot} +$

$\phi_{eff,drop}$). In addition, the heterogeneous structure of protein gels calls for the use of the total volume fraction $\phi_{eff,prot} + \phi_{eff,drop}$.

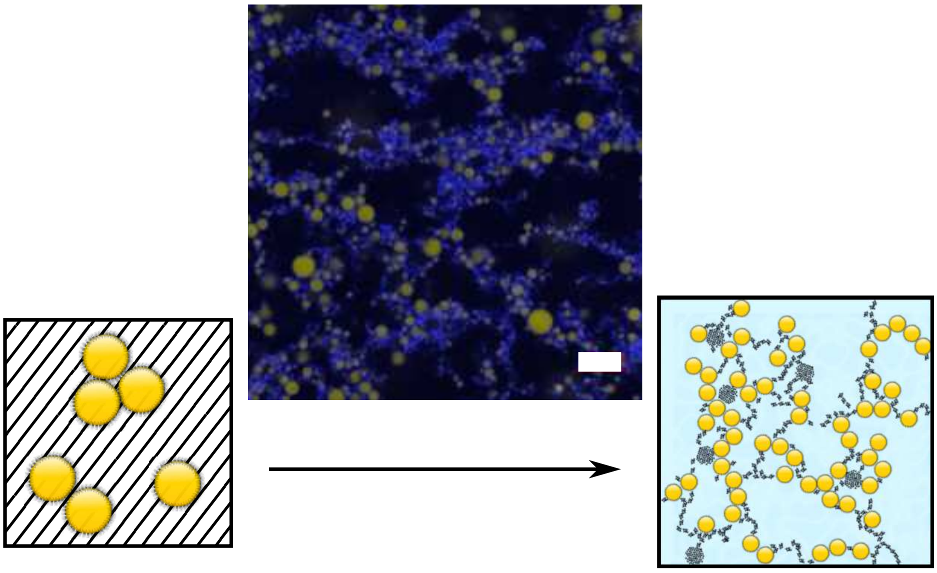

Figure 7.8 *From droplet-filled protein gel matrix to composite gel: changing paradigm for the study of protein-stabilised emulsion gels.*
The cartoon on the left is inspired from the existing literature on emulsion gels and present emulsion gels as a matrix of protein gel (lines) containing droplets that act as fillers [16].
Motivated by the heterogeneous structure of the emulsion gel (centre, confocal microscopy image, scale bar 10 µm*, oil dyed in yellow and proteins in blue), a novel approach was developed.*
The cartoon on the right represents the new paradigm, in which emulsion gels are envisioned as composite colloidal gels with an intermediate behaviour between pure protein gels and pure droplet gels.

This change in framework is illustrated in Figure 7.8, and visually justified by the microscopic observation of an emulsion gel containing droplets large enough to be imaged individually.

As noted previously, the chosen framework affects the results yielded by the analysis. Here the description of emulsion gels as intermediate colloidal gels opens the road for a similar semi-predictive approach to that developed for suspensions of mixtures in Chapter 5.

Indeed, the study of emulsion gels of any composition could be performed in two steps. First, pure gels of the two components are characterised over a wide range of volume fraction, in what could be described as a calibration step. Then, using the quantification of the variation in the intermediate zone between the two limit systems, the properties of any gel of mixture can be calculated using their composition.

Finally, the choice of this framework to study the properties of emulsion gels and the possibility of estimating those for mixtures of any composition, after calibration of the system, could offer a model for the formulation of emulsion gels of fine-tuned rheology. Such an analytical approach to formulation would present the advantage of identifying a small range of possible composition to reach the required mechanical properties, rather than using a more common “trial and error” process.

7.7 Conclusion

In this chapter, the properties of gels containing both protein-stabilised droplets and proteins were studied. They were found to be best described as colloidal gels with an intermediate behaviour between those of pure gels of droplets and pure gels of proteins, characterised in Chapter 6.

The importance of the choice of the parameters to describe emulsion gels was first discussed. Based on qualitative arguments on the structure of colloidal gels, the composition of these systems was thus defined by their total volume fraction $\phi_{eff,prot} + \phi_{eff,drop}$ and composition ratio $\phi_{eff,drop}/(\phi_{eff,prot} + \phi_{eff,drop})$. These parameters could be calculated by using the viscosity scaling presented in Chapter 5.

The analysis of the rheological properties of emulsion gels in this framework confirmed the relevance of this choice. Indeed, the storage modulus and frequency dependence variations with the composition of the emulsion gels appeared to be in good correspondence with the literature on colloidal gels, and to be close to the results found for pure protein gels and droplet gels. Notably, the decoupling of total volume fraction and relative composition for the rheological properties justifies *a posteriori* the choice of parameters.

In addition, this framework is at odds with the approach commonly used for emulsion gels, namely droplet fillers in a matrix of protein gels. The main criticisms presented here are that the filler approach does not take into account the inhomogeneity of the matrix nor the change in volume fraction induced by the addition of droplets. Although this approach makes possible the quantification of the reinforcement of gels, it is thought to limits the analysis. As famously said by Box, "all models are wrong, [but] some are useful" [176], so I argue here that a more careful choice of parameters in the model allows a better, and thus more useful, description of the actual system.

More generally, mixture systems are not commonly studied in academic research, despite being ubiquitous in industrial products. Here a simple framework for thinking about emulsion gels is suggested. In this, they are first deconstructed into their components, protein-stabilised drolets and unadsorbed proteins, and then compared to these primary systems. This approach may be valid for a larger range of ternary mixtures in which two components play a similar role in building up the viscoelasticity, while the solvent plays none.

Chapter 8

Influence of the droplet size on the rheology of droplet emulsions and gels

In this Chapter, I study the changes in the rheological properties of suspensions and gels of droplets when the droplet size is increased. To that aim, I prepare larger droplets than the ones used in Chapters 5, 6 and 7 using a similar protocol, and I proceed to the same characterisation work.

First, I present the properties of these droplets prepared as detailed in Chapter 3. The different size distribution leads to a larger concentration of the droplet stock.

Then, I focus on the viscosity behaviour of droplet suspensions when the droplet size is changed. Hardly any difference is observed in the zero-shear viscosity when the effective volume fraction scaling is used, but there is some discrepancy in the non-Newtonian behaviour of the most concentrated suspensions.

Finally, I prepare acid-induced gels of droplets and I study the rheological properties of these gels. I show that the influence of the droplet size is more or less marked depending on the property studied.

8.1 Introduction

In the previous chapters, I have pointed out the similarities and differences between the rheological properties of protein-coated droplets and of self-assembling protein aggregates, whether they are in suspension or trapped in a gel structure. The size of these soft colloidal particles is one of the striking differences between them, and it is thus interesting to change the dimensions of the droplets to identify for which rheological properties the particle size is a relevant parameter.

In addition, there is a practical interest in determining the influence of the droplet size on the rheology of droplet suspensions and gels. Indeed, in commercial emulsions the droplet size is strongly dependent on the formulation and the emulsification process. When discussing the properties of emulsions and emulsion gels, it is thus important to know how they are affected by the droplet size, and on which size range the results are valid.

Despite the theoretical and industrial relevance of this topic, only few studies have tackled the influence of droplet size on the viscosity of emulsions. Some work on surfactant-stabilised emulsions with micron-sized droplets has been performed and showed that the influence of the droplet size on the viscosity only becomes visible at high volume fractions, and that this parameter also plays a role on the shear-thinning of the emulsions [70].

Furthermore, there is also a lack of consensus on the effect of the size of the droplets on the rheology of emulsion gels, if these are modelled by fractal colloidal gels, as in Chapter 6. Indeed, some argue that the gel modulus depends on the particle size [170], while others see in the fractal aggregation theory a much bigger influence of the size of clusters, rather than of individual particles [79]. It is important to remember that the acid-induced droplet gels prepared here differ from emulsion glasses, in which the viscoelasticity of the jammed droplets does depend on the droplet size [71].

Here, the rheological properties of pure suspensions of droplets are first compared for two different droplet sizes. The gelation of these suspensions is then performed and the influence of the droplet size on the rheological properties of the two types of droplet gels is then studied.

8.2 Materials & Methods

8.2.1 Preparation of the large droplets

In addition to the droplets described in the previous chapters, some larger droplets were produced using a high-pressure homogeniser, as detailed in Chapter 3.

For convenience, the droplets of radius $R_h = (110 \pm 49)\,\mathrm{nm}$ used previously are designated as small droplets in this chapter, while the droplets prepared using the homogeniser are designated as large droplets, and their size distribution is presented in the next section.

8.2.2 Rheological measurements

The viscosity results presented in Section 8.4 were performed as described in Chapter 5. The flow curves were measured for each sample.

The suspensions were then gelled in-situ in a rheometer to study the gel properties presented in Section 8.5, as described in Chapter 3. The amount of glucono δ-lactone was determined empirically to reach a final pH of ≈ 4.5, and was found to follow the weight ratio $\frac{glucono\ \delta-lactone}{droplet} = 0.009$. This is around one order of magnitude lower than for the smaller droplets used in the previous chapters, but the reason for this discrepancy is not clear.

The measurements were then performed described in Chapter 6, following the sequence shown in Figure 6.1. For each concentration of large droplets, this protocol was performed on only one sample, rather than repeated three times as in the previous chapters. There is thus a possible lack of accuracy in the results presented here, and no error bars could be calculated for some rheological results.

8.3 Characterisation of the large droplets

After preparation of the larger droplets using a homogeniser, it was important to estimate their concentration and size, in order to draw comparisons with the smaller droplets characterised in Chapter 4.

8.3.1 Concentration of the droplet suspensions

The droplets were separated by centrifugation from the unadsorbed proteins, which were present in solution after emulsification. This fractionation resulted in a dense layer of large droplets used as a stock to prepare different concentrations of droplet suspensions.

The concentration of this stock of large droplets was estimated by drying the paste in a vacuum oven and measuring the weight loss, as described in Chapter 4. Using Equation 4.3 with the moisture content, the concentration was found to be $c_{stock,\ large} = 0.62\,\mathrm{g \cdot mL^{-1}}$. This is larger than for the stock of small droplets, for which $c_{stock,\ large} = 0.52\,\mathrm{g \cdot mL^{-1}}$.

In addition, the density of the stock was measured by filling a 7 mL vial with paste and weighting it, as described in Chapter 4. The density of the stock of large droplets was found to be $\rho_{stock,\ large} = 0.962\,\mathrm{g \cdot mL^{-1}}$. This value is intermediate between the density of the oil and the one of the small droplets, as $\rho_{oil} = 0.956\,\mathrm{g \cdot mL^{-1}} < \rho_{stock,\ large} < \rho_{stock,\ small} = 0.987\,\mathrm{g \cdot mL^{-1}}$.

The droplets formed using a homogeniser present thus slightly different concentrations and densities to the droplets prepared using the microfluidiser. The concentrations of the droplet suspensions were then estimated using the characterisation of the droplet stock presented here.

8.3.2 Size distributions of the large droplets

The size distribution of the droplets prepared using a homogeniser was measured and compared to the small droplets, as presented in Figure 8.1.

The distributions given by both the Mastersizer, providing the optical cross-section D_{opt}, and by DLS, providing the hydrodynamic size D_h, can be averaged. When the volume percentage is used to weight the sizes, the volume average D_{43} is obtained.

Here, the droplets prepared with a homogeniser yield the following average radii $R_{43,opt} = (210 \pm 105)\,\mathrm{nm}$ and $R_{43,h} = (450 \pm 815)\,\mathrm{nm}$. These values have to be compared with those measured for the droplets prepared using a microfluidiser, for which $(65 \pm 31)\,\mathrm{nm}$ and $(110 \pm 50)\,\mathrm{nm}$ respectively. The homogeniser thus makes it possible to produce droplets that are around 3 times larger than the

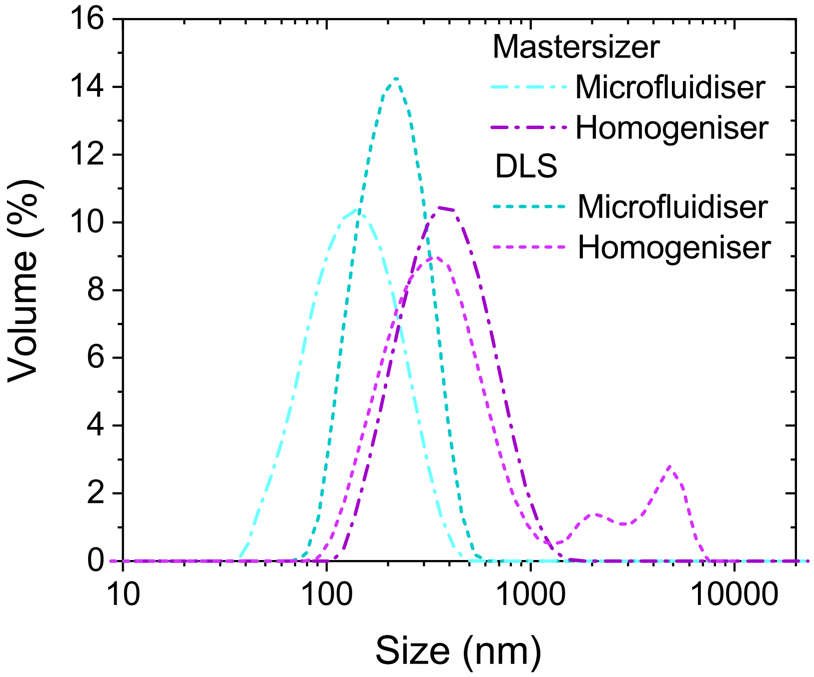

Figure 8.1 *Size distributions of the droplets prepared using a microfluidiser (blue, as presented in Chapter 4) and a homogeniser (purple). The volume-weighted distributions were measured using a Mastersizer (dash-dot line) and a Zetasizer (DLS, short-dashed line).*

droplets presented in the previous chapters.

As can be observed, DLS measurements on the homogenised droplets reveal a significant tail of droplets with a radius $R_h > 500\,\mathrm{nm}$. It is possible that these large droplets, which are less visible in the intensity-weighted distribution, and thus present only in a small amount, are the trace of a valve malfunction in the homogeniser.

In the following, the droplets are designated by their hydrodynamic radius R_h measured via DLS rather than by the equipment used to prepare them.

8.3.3 Increasing the size of the droplets changes their structure

The results presented in this section illustrate the change in the droplet properties when increasing the radius. Indeed, as the droplet becomes larger, the surface:volume ratio becomes smaller, and the contribution of the layer of adsorbed proteins to the droplet structure becomes smaller, both in terms of mass and in terms of size. This explains why larger droplets are less dense than the small ones, and that the peak values of the optical cross-section and the hydrodynamic radius distributions are more similar.

It is also expected that the softness of the droplets, as discussed in Chapter 5, depends on their size [177]. Two aspects of the softness vary in opposite directions with the size of the droplets. On one hand, the internal pressure in the droplet, arising from the surface tension, varies as $1/R$ and thus decreases in larger droplets. The oil core is thus less rigid for larger droplets. On the other hand, the soft layer of adsorbed proteins is a smaller portion of the total size of the droplets, so the reach of its softness is shortened for larger droplets.

In the following work on the viscosity of droplet suspensions and on the viscoelasticity of droplet gels, these changes with respect to the droplets studied in the previous chapters have to be taken into account, in addition to the increase in size.

8.4 Influence of the droplet size on the viscosity of suspensions

Similarly to Chapter 5, the viscosity of pure suspensions of large droplets was characterised over a wide range of concentrations. The flow curves of the Newtonian suspensions are presented in Figure 8.2, and the non-Newtonian behaviour of the most concentrated samples will be discussed in Section 8.4.3.

The variation of the viscosity in the semi-dilute regime could first be used to estimate the volume fraction occupied by the droplets.

8.4.1 Estimation of the volume fraction

As described in Section 5.3.2, the equation for the viscosity of semi-dilute colloidal suspensions developed by Batchelor [29] (Equation 2.3) can be used to fit the relative viscosity of suspensions of large droplets, as shown in Figure 8.3.

By asuming that the droplets behave as hard spheres in the semi-dilute regime, the effective volume fraction of the suspensions ϕ_{eff} can thus be estimated as a

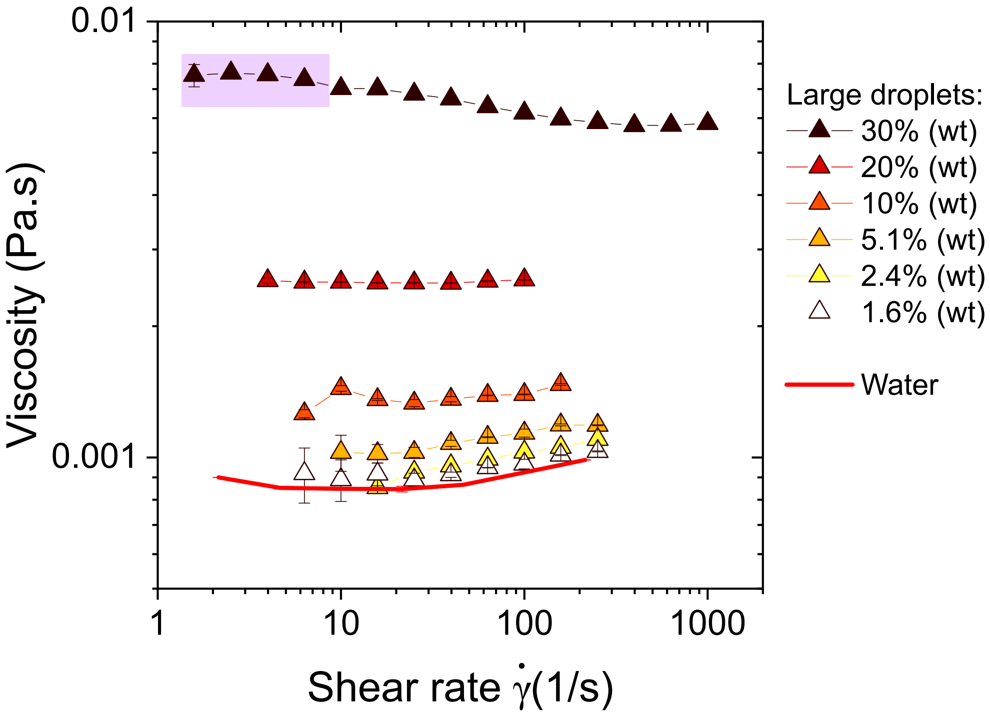

Figure 8.2 *Flow curves of sodium caseinate-stabilised droplets (R_h = $(450 \pm 815)\,\mathrm{nm}$) at several concentrations. These curves are the average of 3 measurements, and the error bars indicate the reproducibility. For the shear thinning samples, only the zero-shear viscosity η_0 is considered, as indicated by the shaded area. A more thorough study of their behaviour is presented in Section 8.4.3.*

function of their concentration c: $\phi_{eff,largedrop} = k_{0,\ large\ drop} \times c$. Here, it is found that $k_{0,\ large\ drop} = (1.71 \pm 0.05)\,\mathrm{g} \cdot \mathrm{mL}^{-1}$.

This value is lower than for smaller droplets, for which $k_{0,drop} = (2.2 \pm 0.1)\,\mathrm{g} \cdot \mathrm{mL}^{-1}$. This difference can be attributed to a relatively lower contribution of the protein layer to the volume of the droplets, as the dimension of the oil core increased, as discussed previously.

In the following, the composition of the suspensions of large droplets is thus described by their effective volume fraction $\phi_{eff,\ large\ drop} = 1.71 \times c$. As for the smaller droplets, this definition is an extension of the hard-sphere approximation in semi-dilute regime, and may thus break down at high concentrations.

8.4.2 Viscosity model for suspensions of large droplets

Once the composition of the suspensions is scaled by the effective volume fraction, it is possible to study the viscosity behaviour of the emulsions over a wider range

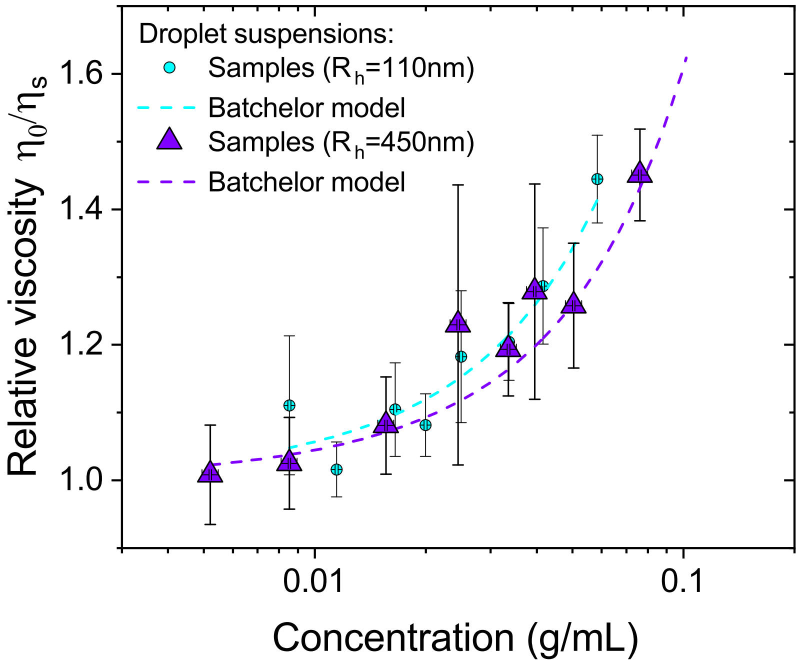

Figure 8.3 *Relative viscosity of sodium caseinate-stabilised droplets of radii* $R_h = (110 \pm 49)\,\mathrm{nm}$ *(circles, cyan, as presented in Chapter 6) and* $R_h = (450 \pm 815)\,\mathrm{nm}$ *(triangles, purple) as a function of the concentration. The lines denote Batchelor model for hard spheres in the dilute regime, Equation 2.3. The error bars represent the standard error upon averaging the viscosity plateau for the three measurements.*

of concentrations by measuring the flow curves of these samples. Similarly to the smaller droplets, most of the samples display a Newtonian behaviour, *i.e.* their viscosity is not dependent on the shear rate. For the most concentrated samples, which present shear-thinning at higher shear rates, as detailed in the next section, the zero-shear viscosity η_0 at the low-shear plateau is used. Figure 8.4 presents the relative zero-shear viscosity η_0/η_s of suspensions of large droplets, where η_s is the viscosity of pure water, as a function of their effective volume fraction ϕ_{eff}.

As can be seen, the viscosity behaviour is similar to model hard sphere, with an exponential divergence of the viscosity at a maximum volume fraction ϕ_m. As in Chapter 5, this behaviour can conveniently be fitted with the theoretical model developed by Quemada for model hard sphere suspensions: $\eta_0/\eta_s = (1 - \phi/\phi_m)^{-2}$ (described previously as Equation 2.4). When this model is used to describe the viscosity of suspensions of large droplets, the volume fraction at which the viscosity diverges is found to be $\phi_m = 0.75 \pm 0.03$.

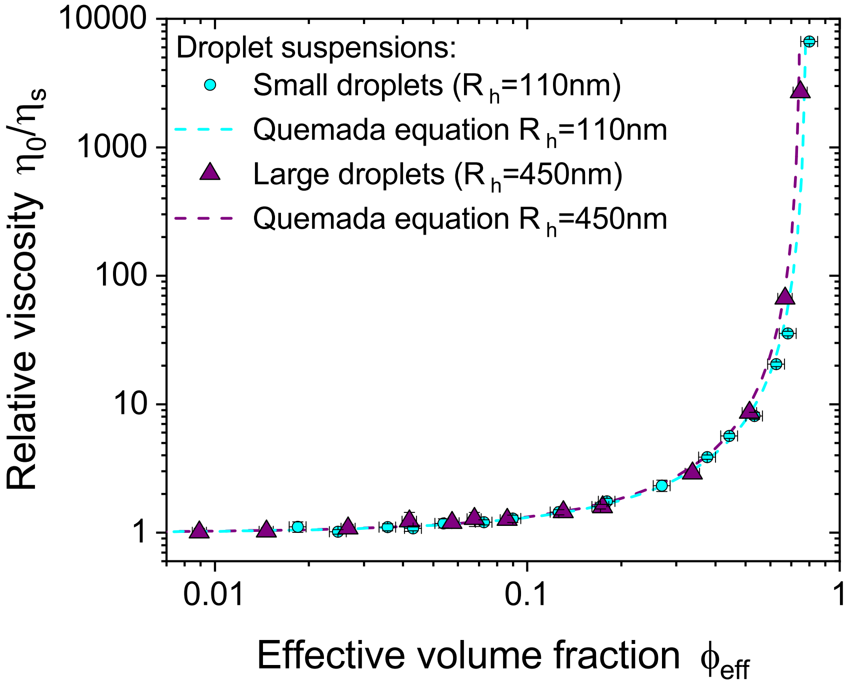

Figure 8.4 *Relative viscosity of sodium caseinate-stabilised large droplets ($R_h = (450 \pm 815)\,\mathrm{nm}$, triangles, purple) and small droplets ($R_h = (110 \pm 49)\,\mathrm{nm}$, circles, cyan, as presented in Chapter 5) as a function of the effective volume fraction ϕ_{eff}. The dashed lines denote Quemada equation for hard spheres, Equation 2.4 for large droplets ($R_h = (450 \pm 815)\,\mathrm{nm}$, purple, with $\phi_m = 75\,\%$) and small droplets ($R_h = (110 \pm 49)\,\mathrm{nm}$, purple, with $\phi_m = 79\,\%$, as presented in Chapter 5).*

Both the behaviour and the numerical value of ϕ_m are very similar to those identified in Chapter 5 for suspensions of small droplets. This is in good agreement with previous studies on caseinate-stabilised emulsions, where the jamming transition of micron-sized droplets appeared to be independent of their radius [119]. However, it does not correspond to the results for surfactant-stabilised emulsions, for which a change of viscosity with the droplet size at high concentration was observed [70].

The maximum volume fraction can furthermore be related to the size distribution of the droplets by estimating the random close packing efficiency of a polydisperse hard sphere suspension [41, 42]. Here, the size distribution obtained using DLS presented in Figure 8.1 was used to estimate the random close-packing volume fraction ϕ_{rcp} with the `spherepack1d` software [43], and it was found that $\phi_{rcp,\ large\ drop} = 0.72$. Because the large droplets are more polydisperse than the small droplets prepared with a microfluidiser, this value is larger than the result for small droplets, for which $\phi_{rcp,\ small\ drop} = 0.68$. The random close packing volume fraction is thus a better approximation of ϕ_m for the large droplets than for the small ones.

8.4.3 Non-Newtonian suspensions and shear-thinning

As mentioned previously, most of the suspensions of large droplets prepared here display a constant viscosity as a function of the shear rate, *i.e.* a Newtonian behaviour. However, at $\phi = 0.51$ and at higher concentrations, the flow curves show a decrease in viscosity of the suspension upon increasing shear rate and shear stress σ, as shown in Figure 8.5. This phenomenon is called shear thinning, as described in previous studies [35, 36] and Chapter 5.

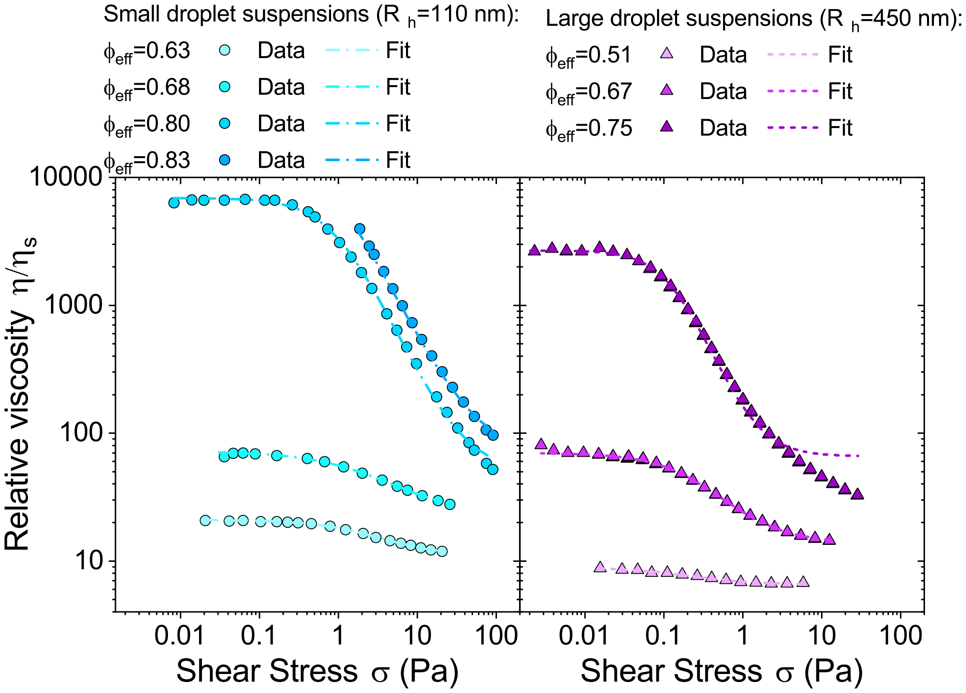

Figure 8.5 *Flow curves of shear-thinning samples, fitted using Equation 2.7. The relative viscosity* η/η_s *is plotted as a function of the shear stress* σ.
Left (circles): Concentrated suspensions of pure small oil droplets ($R_h = (110 \pm 49)$ nm*) at effective volume fractions* $\phi_{eff,drop}$ *of* 0.63, 0.68, 0.80 *and* 0.83, *from Figure 5.14.*
Right (triangles): Concentrated suspensions of pure large oil droplets ($R_h = (450 \pm 815)$ nm*) at effective volume fractions* $\phi_{eff,large\ drop}$ *of* 0.51, 0.67 *and* 0.75.

As can be seen on Figure 8.5, the onset of shear thinning occurs at a lower volume fraction for the large droplets than for the small droplets. Furthermore, at a given volume fraction, the extent of shear thinning is larger when the droplet size increases. This result is in good correspondence with previous studies on the effect of droplet size on the rheology of emulsions [69, 70].

The shear thinning behaviour, and more specifically the variation of the relative viscosity η/η_s with the shear stress can be modelled by Equation 2.7. As presented in Figure 8.5, this model fits the flow curves with a good accuracy, and thus makes possible to estimate the critical shear stress σ_c that needs to be applied to the suspension for the viscosity to decrease. It is interesting to compare this parameter for different suspensions. Figure 8.6 (a) presents the critical shear stress σ_c of suspensions of small and large droplets, as well as of protein suspensions.

As can be noted the critical shear stress $\sigma_c \sim 0.1\,\mathrm{Pa}$ for large droplets while $\sigma_c \sim 1\,\mathrm{Pa}$ for small droplets, they thus differ of one order of magnitude for the droplets of different sizes. As presented in Chapter 5, a certain extent of size dependency is expected, as shear-thinning is a result of the competition of the size-related Brownian motion with the applied shear. In order to account for the difference in radius, the dimensionless reduced critical shear stress $\sigma_{r,c}$ can be calculated using Equation 5.14.

The values of the reduced critical shear stress $\sigma_{r,c}$ for the different droplet and protein suspensions are presented in Figure 8.6 (b). Here the mean value of the hydrodynamic radius is used to normalise the critical shear stress for each colloidal species, and the width of the distribution is used to calculate the error bar. As can be seen, the discrepancy of critical shear stress σ_c does not fade completely when reduced for the large droplets, in contrast to the small droplets and proteins, as detailed in Chapter 5.

This is probably related to the polydispersity of the large droplets, as presented in Figure 8.1. Indeed, if the radius at the centre of the main peak of the distribution is used to normalise the critical shear stress, *i.e.* if $R_{h,\ large\ drop} = 200\,\mathrm{nm}$, then $\sigma_{r,c} \sim 1$ for the large droplets. In that case, both sizes of droplets and the proteins present a similar value of $\sigma_{r,c}$. For a polydisperse emulsion, the size of the smaller droplets is thus the important parameter to describe the critical stress at which shear thinning occurs, as noted in previous studies [69].

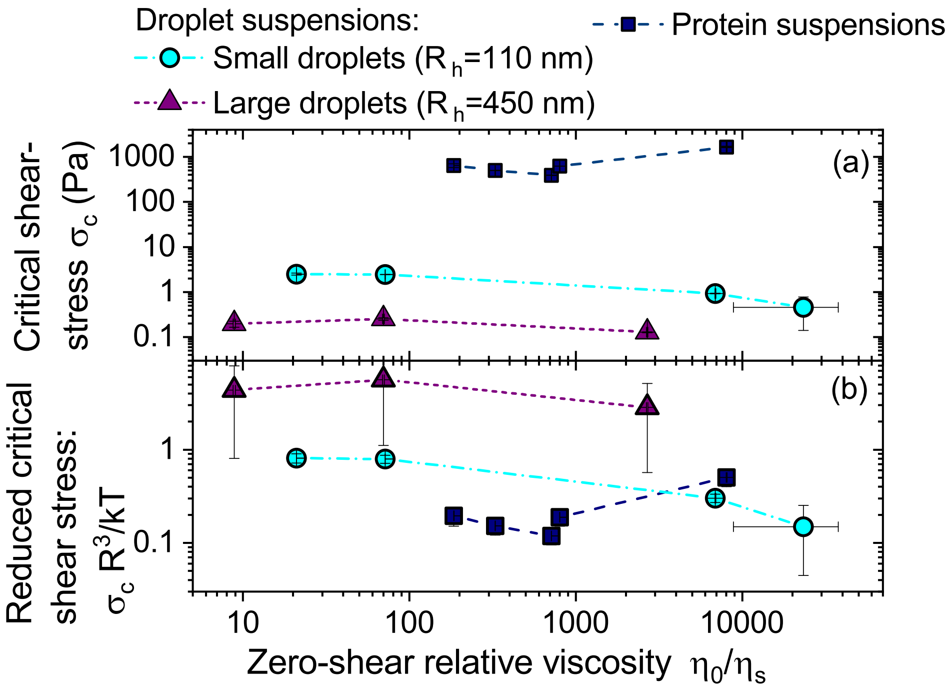

Figure 8.6 *Shear thinning behaviour of concentrated suspensions of sodium-caseinate stabilised droplets of different sizes:* $R_h = (110 \pm 49)\,\mathrm{nm}$ *(circles, cyan) and* $R_h = (450 \pm 815)\,\mathrm{nm}$ *(triangles, purple), and of sodium caseinate (squares, navy).*
(a) Critical shear stress σ_c *as a function of the zero-shear relative viscosity* η_0/η_s *for several concentrated suspensions.* σ_c *and* η_0 *were estimated by fitting the flow curves flow curves in Figure 5.14 and 8.5 with Equation 2.7.*
(b) Reduced critical shear stress $\sigma_{r,c}$*, calculated using Equation 5.14, as a function of the zero-shear relative viscosity* η_0/η_s*.*
The error bars indicate the uncertainty of the fitting parameters, and the lines are indicated as guide for the eye. The data for the small droplet and the protein suspensions are from Figure 5.16.

8.4.4 Conclusion on the effect of droplet size on the rheological behaviour of suspensions of droplets

In this section, the viscosity of emulsions of two different droplet sizes was studied over a wide range of concentrations. Indeed, the rheological behaviour of small and large droplets, both submicron, was compared in semi-dilute regime and concentrated regime, the latter presenting some shear thinning. The results are summarised in Table 8.1.

The effective volume fraction was first defined as a function of the concentration by approximating the viscosity in the semi-dilute regime, and the proportionality

Table 8.1 *Summary table: Influence of the size of droplets on the rheological properties of droplet suspensions*

Parameter	Small droplets	Large droplets
Emulsification	Microfluidiser	Homogeniser
Mean hydrodynamic radius $R_{43,h}$	(110 ± 50) nm	(450 ± 815) nm
Mean optical radius $R_{43,opt}$	(65 ± 30) nm	(210 ± 105) nm
Voluminosity k_0 $(\mathrm{g \cdot mL^{-1}})$	2.2 ± 0.1	1.71 ± 0.05
Concentration of stock c_{stock} $(\mathrm{g \cdot mL^{-1}})$	0.52	0.62
Density of stock ρ_{stock} $(\mathrm{g \cdot mL^{-1}})$	0.987	0.962
Maximum volume fraction ϕ_m	0.79 ± 0.02	0.75 ± 0.03
Random close-packing ϕ_{rcp}	0.68	0.72
Critical shear stress σ_c	~ 1	~ 0.1

factor was determined for the larger droplets. It was shown that this factor decreases slightly when the droplet size is increased.

The zero-shear viscosity was then studied over the whole range of concentrations, from semi-dilute to jammed suspensions. When the scaling by the effective volume fraction was used, the variations of viscosity appeared to be very similar for the two different sizes of droplets.

Finally, the most concentrated suspensions prepared here present some shear-thinning behaviour, that was compared for the two sizes of droplets and the proteins. This behaviour appeared to present some variations at a given volume fraction, which indicates that a similar zero-shear viscosity does not equate to a similar rheological behaviour of the suspensions of droplets. More specifically, the value of the critical shear stress is different for the two droplet sizes, but this discrepancy can fade away if the reduced critical shear stress is calculated using the mean size of the smallest droplets of the size distribution rather than the distribution average.

8.5 Influence of the droplet size on the rheology of emulsion gels

Similarly to the gels of small droplets presented in Chapter 6, the emulsions prepared in this Chapter can be destabilised by slow acidification and can therefore form fractal gels. Although the size-dependence of the rheology of such gels is of practical interest, there have been very few studies on this topic.

First, for fractal colloidal gels, there does not seem to be an agreement on the effect of the particle radius R on the mechanical properties. Indeed, some studies showed that the yield stress of colloidal gels scales with R^{-m}, with m between 2 and 3, and that this scaling also holds for the storage modulus G' [170]. Others indicate that the particle radius does not influence the mechanical properties [79].

In addition, regarding sodium-caseinate stabilised emulsions, a study was performed on jammed glasses. In that case, it was shown that smaller droplets make stronger glasses, with a factor 10 increase of the storage modulus for a droplet size decreased by a factor 6 [119].

8.5.1 Linear viscoelasticity of the droplet gels

The suspensions of droplets could then be turned into soft solids by using a slow acidifier, as described in Chapter 3. This sol-gel transition was performed in the cup of a rheometer, thus making it possible to measure the changes in viscoelasticity of the samples. Similarly to the gels made of small droplets, as shown previously in Figure 6.10, the gels of large droplets present a sharp increase of storage and loss moduli upon gelation, followed by a slower increase upon ageing. As before, for a given sample, storage and loss moduli were measured 2500 s after gelation.

In Chapter 6, it was shown that the moduli of caseinate gels and caseinate-coated droplet gels, at a given volume fraction, have very similar values of storage and loss moduli. This is despite the difference in radii of the two colloidal particles, namely protein aggregates and droplets. Here, it is interesting to compare the moduli of the acid-induced gels of larger droplets with these results, as presented in Figure 8.7.

As can be seen, both the storage and the loss moduli of gels formed of large droplets display a similar dependence on the effective volume fraction ϕ_{eff}, that can be modelled by a power law, as in Equation 6.1. The parameters resulting from these fits are shown in Table 8.2.

The moduli for the large droplet gels are in the same region than for the small droplet gels, despite being slightly lower. More precisely, at high concentrations, storage and loss moduli are almost equal at a given volume fraction, hence the very similar values of $G'_{0,\phi}$ and $G''_{0,\phi}$. But the variations of both moduli with

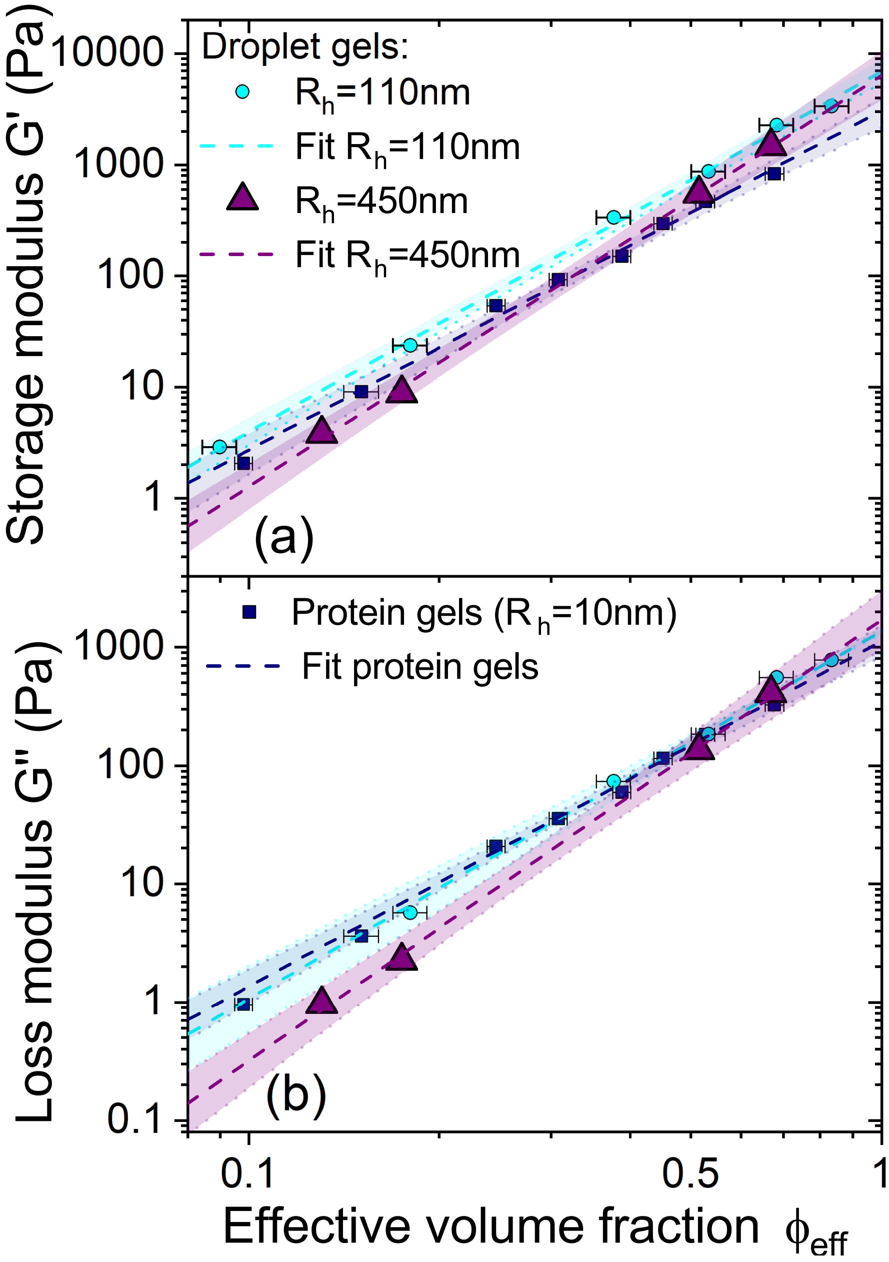

Figure 8.7 *Storage (G', (a)) and loss (G'', (b)) moduli at* 1 Hz *of protein gels (square, navy blue, from Chapter 6) and of gels of protein-stabilised droplet of radii* $R_h = (110 \pm 49)\,\mathrm{nm}$ *(circle, cyan, from Chapter 6) and* $R_h = (450 \pm 815)\,\mathrm{nm}$ *(triangle, purple) as functions of the effective volume fraction of the gel.*
A fit of each type of system was performed using Equation 6.1, and the models (with the parameters listed in Table 8.2) as well as the 95 % *confidence bands are displayed on each graph.*

Table 8.2 *Parameters used to fit the viscoelasticity of gels at* 1 Hz *displayed in Figure 8.7 with Equation 6.1.*

Gel type	Storage modulus G'		Loss modulus G''	
	$G'_{0,\phi}$	α	$G''_{0,\phi}$	α
Protein gels	(3.10 ± 0.04) kPa	3.0 ± 0.1	1.11 kPa	2.9 ± 0.1
Small droplet gels	6.93 kPa	3.24 ± 0.07	1.37 kPa	3.11 ± 0.09
Large droplet gels	6.31 kPa	3.70 ± 0.08	1.70 kPa	3.7 ± 0.1

the volume fraction are larger for the large droplets than for the small droplets, specifically 3.7 rather than 3.2, meaning that at low concentrations the moduli of the large droplet gels are lower than for lower droplet sizes.

It thus seems that for dense gels of droplets, the viscoelastic properties are very similar, but there is a larger difference for more sparse networks at low concentrations. More data points would be required to assess whether the linear fit is a good approximation or if there are two regimes of viscoelasticity over the range of concentration of the droplet gels.

8.5.2 Frequency dependence of the droplet gels

In addition to the influence of the droplet size on the linear viscoelasticity, it is interesting to study the frequency dependence of the two types of droplet gels. This could be achieved by measuring the viscoelasticity over a wide range of frequency, as illustrated in Figure 6.1.

The storage G' and loss G'' moduli of the gels as functions of the angular frequency are presented in Figure 8.8. The comparison between a gel of small droplets, one of large droplets and a protein gel is drawn by fixing the effective volume fraction at $\phi_{eff} \approx 50\,\%$, *i.e.* in the intermediate range of the concentrations used in this study. These curves are representative of the differences between all the samples prepared here.

As can be seen, the frequency dependence of the storage G' and loss G'' moduli for the two sizes of droplets is very similar, as emphasised by the significantly different behaviour of the protein gel. Indeed, the loss modulus G'' presents the same variation, namely an initial plateau followed by a linear at higher frequencies, for the gels made of droplets, in contrast with the power law behaviour of the protein gel. If this non-monotonic variation hints at the relaxation of the droplet networks at frequencies lower than explored here, as suggested in Chapter 6, then

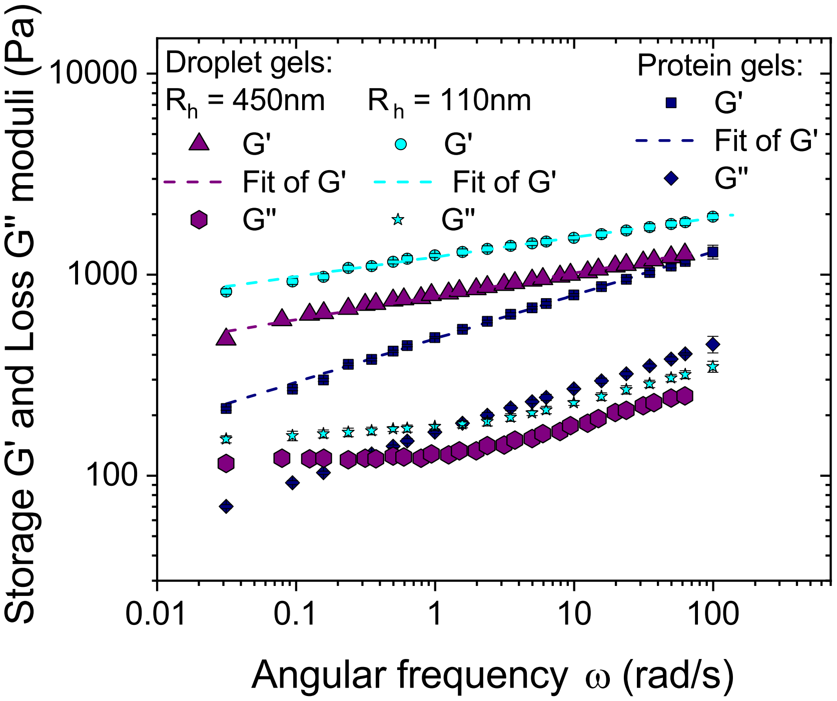

Figure 8.8 *Comparison of the frequency dependence of a gel of small droplets ($R_h = (110 \pm 49)\,\mathrm{nm}$, $\phi_{eff} = 53\,\%$, in cyan), a gel of large droplets ($R_h = (450 \pm 815)\,\mathrm{nm}$, $\phi_{eff} = 51\,\%$, in purple), and a protein gel ($\phi_{eff} = 53\,\%$, in navy blue).*
Storage modulus G' and loss modulus G'' are represented as functions of the angular frequency ω.
G' was fitted with a power law for both types of samples.

it is possible that it occurs around the same frequency for both gels.

In addition, for all the gels presented in Figure 8.8, the storage modulus can be modelled by a power law, as expressed previously by Equation 6.3. By extension, this model can also be applied to the gels formed with suspensions of large droplets at any concentration. The exponent of the power law β is an indication of the frequency-dependence and is presented as a function of the effective volume fraction ϕ_{eff} in Figure 8.9.

It appears that the exponent for the frequency dependence is very similar for the two droplet gels, with $\beta_{droplet} \sim 0.1$, while for protein gels $\beta_{protein} \sim 0.2$. This seems to indicate that the value of this exponent is a signature of the type of colloidal particles used rather than of their size. This is in good correspondence with the results obtained for gels of mixtures of proteins and droplets, where the exponent $\beta_{mixture}$ varied continuously between 0.1 and 0.2 as a function of the

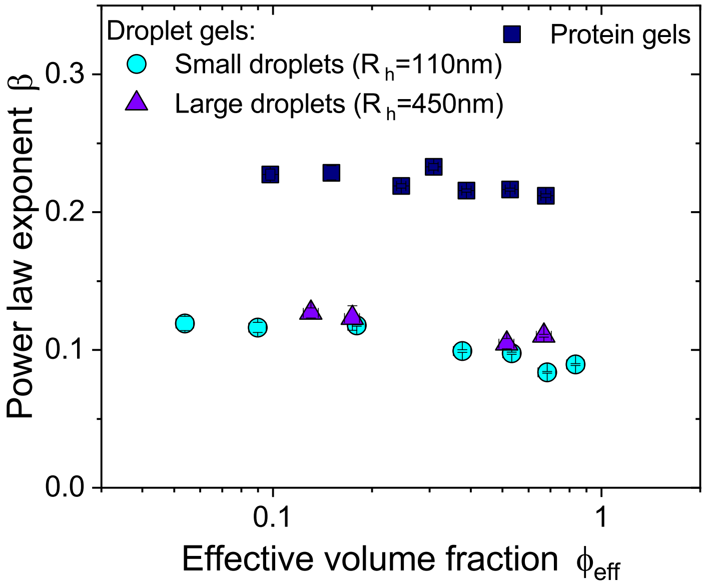

Figure 8.9 *Modelling of the frequency dependence of gels of small droplets ($R_h = (110 \pm 49)\,\mathrm{nm}$, circles, in cyan), gels of large droplets ($R_h = (450 \pm 815)\,\mathrm{nm}$, triangles, in purple), and protein gels (squares, in navy blue): power-law exponent β, obtained by fitting $G' = f(\omega)$ with Equation 6.14, as a function of the effective volume fraction ϕ_{eff}.*

composition of the samples, as shown in Figure 7.6.

8.5.3 Strain dependence and non-linear viscoelasticity

Finally, the non-linear behaviour of the droplet gels could be studied as a function of the droplet size. A strain sweep of the gels was thus performed, as shown previously in Figure 6.1. For the gels of large droplets, the typical strain behaviour of the gel represented previously in Figure 6.17 was also obtained. The same normalisation of the strain curve using G'_0 and γ_c was thus applied for an improved visualisation of the strain dependence at different volume fractions, as shown in Figure 8.10. The values used for γ_c are displayed in Table 8.3.

As can be seen, the non-linear regime is similar to the one observed for gels of small droplets in Figure 6.17. Indeed, for moderately concentrated samples, an increase of the storage modulus G' is observed beyond the linear regime, *i.e.* for $\gamma > \gamma_c$. This strain hardening can be compared for samples of similar

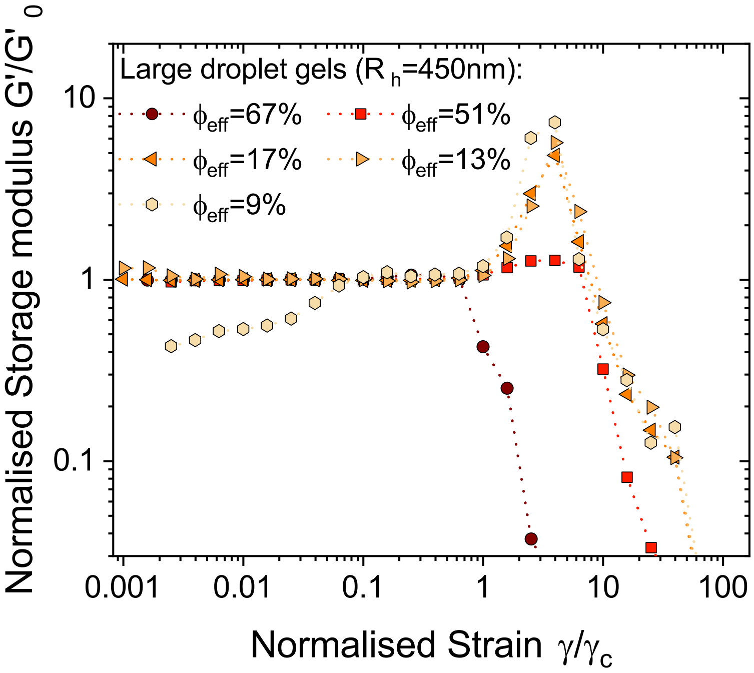

Figure 8.10 *Storage modulus G' normalised by its value in the linear regime G'_0 as a function of the oscillatory strain amplitude γ normalised by its value at the onset of the non-linear regime γ_c: Sodium caseinate-stabilised large droplet gels ($R_h = (450 \pm 815)\,\mathrm{nm}$) at several effective volume fractions ϕ_{eff}.*

Table 8.3 *Parameters for normalising the strain dependence displayed in Figure 8.10*

Volume fraction ϕ_{eff}	Critical strain γ_c
9%	15.9%
13%	10%
17%	10%
51%	6.3%
13%	6.3%

volume fractions made of small droplets, large droplets and proteins, as shown in Figure 8.11.

It appears that the strain hardening is more pronounced for gels of larger droplets, both at low and high volume fraction. This may be related to an increasing inhomogeneity of the gel with the droplet size, as the strands of the network become thicker. This heterogeneity allows in turn more stress redistribution at high strain, with almost a ten-fold increase of the storage modulus relative to the linear regime.

This result seems to indicate that the size of the colloidal particles play a role in the structure of the fractal gels, and more specifically on its level of heterogeneity. Indeed, in Chapter 6, it was observed that the protein gels present consistently less strain hardening than the small droplet gels, and the naturally-occurring protein aggregates are ten times smaller than the droplets. The larger strain hardening obtained for larger droplets thus reinforces the hypothesis that the size of the primary particles is an important factor for the heterogeneity of fractal colloidal gels.

Going back to Figure 8.11, if the strain is further increased, the sharp decrease of storage modulus marks the irreversible yielding of the gel structure as strands are suddenly broken, thus leading to the structural collapse of the material.

8.5.4 Summary of the effect of the droplet size on the rheological behaviour of emulsion gels

To conclude this section, the influence of the droplet size on the rheological properties of pure droplet gels was studied. This effect was shown to be dependent on the mechanical property of interest. The main numerical results for the two sizes of droplets studied are summarised in Table 8.4.

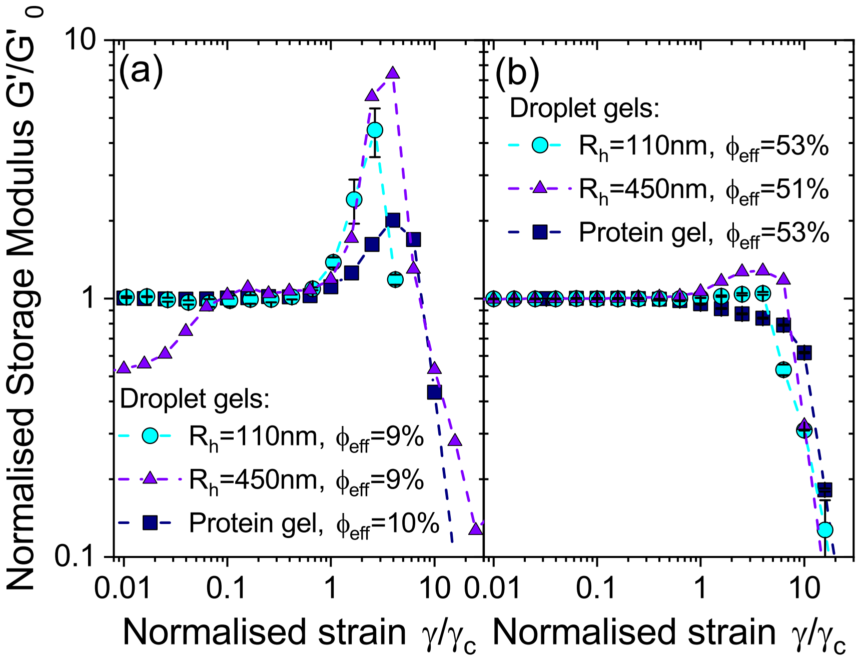

Figure 8.11 *Strain hardening of gels of small droplets ($R_h = (110 \pm 49)\,\mathrm{nm}$, circles, in cyan), gels of large droplets ($R_h = (450 \pm 815)\,\mathrm{nm}$,triangles, in purple), and protein gels (squares, in navy blue).*
Storage modulus G' normalised by its value in the linear regime G'_0 as a function of the oscillatory strain amplitude γ normalised by its value at the onset of the non-linear regime γ_c for: (a) Gels of low volume fraction ($\phi_{eff} \approx 10\,\%$), and (b) gels of high volume fraction ($\phi_{eff} \approx 50\,\%$).

First, for the linear viscoelasticity, the same power-law behaviour was identified for the storage and loss moduli for gels of two different droplet sizes. The exponent is however larger for gels made with larger droplets, showing that their viscoelasticity is more dependent on their volume fraction

Then, in terms of frequency dependence, no difference was observed between gels made of the two droplet sizes. Indeed, over the whole range of volume fraction, the variation of their storage modulus with frequency can also be modelled by a power law, and the exponent is almost equal for all the droplet gels studied, in contrast with the higher exponent for protein gels. This seems to indicate that the dynamic properties of these gels are not influenced by the size of the colloidal particles, but by other aspects that were not identified.

Finally, beyond the linear strain regime, a similar strain hardening effect was observed for the two types of droplet gels. This increase in storage modulus

Table 8.4 *Summary table: Influence of the size of droplets on the rheological properties of droplet gels*

Parameter	Small droplets	Large droplets
Emulsification	Microfluidiser	Homogeniser
Mean hydrodynamic radius $R_{43,h}$	$(110 \pm 50)\,\mathrm{nm}$	$(450 \pm 815)\,\mathrm{nm}$
Storage modulus exponent $\alpha_{G'}$	3.24 ± 0.07	3.70 ± 0.08
Storage modulus pre-factor $G'_{0,\phi}$	$6.93\,\mathrm{kPa}$	$6.31\,\mathrm{kPa}$
Loss modulus exponent $\alpha_{G''}$	3.11 ± 0.09	3.7 ± 0.1
Loss modulus pre-factor $G''_{0,\phi}$	$1.37\,\mathrm{kPa}$	$1.70\,\mathrm{kPa}$
Frequency dependence exponent β	0.10 ± 0.01	0.11 ± 0.01
G'/G'_0 at strain γ_m and $\phi_{eff} = 9\,\%$	4.5 ± 0.5	7.5

at high strain was slightly larger for the large droplets than for the small droplets, which was also larger than for protein gels. Thus, there may be a direct dependence of this effect to the size of the colloidal particle, *via* the strand thickness.

8.6 Conclusion

In this chapter, the influence of the droplet size on the rheological properties of droplet suspensions and droplet gels was studied. It was found that there are only minor differences between the two sizes of droplets studied here.

For the droplet suspensions first, once the composition of the samples was scaled by the effective volume fraction, the viscosity behaviour was very similar at both droplet sizes. Some differences could be observed in the shear thinning behaviour of the most concentrated suspensions, as the critical shear stress required for the samples to decrease in viscosity decreased as the droplet size increased.

Furthermore, the two types of droplet gels displayed a similar scaling of their viscoelastic moduli with the volume fraction, but slightly different parameters. The frequency dependence appeared to be almost identical for the two sizes of droplets, while for the non-linear behaviour the strain hardening of the gels with larger droplets was moderately more marked than for gels of smaller droplets.

Finally, it would be interesting to explore a wider range of droplet sizes in order to study more thoroughly the influence of the droplet size on the rheology of emulsions and emulsion gels. This is however experimentally challenging. Indeed, in general as the droplet size is increased, so is the polydispersity, and it becomes necessary to discriminate the effect of each parameter. In addition, larger droplets may present some creaming, so the matching of the densities of the continuous phase and of the droplets would be required, which may in turn change the adsorbtion of the proteins at the interface.

Chapter 9

Conclusion and outlook

In this thesis, I have investigated the rheological properties and the microstructure of protein-stabilised emulsions and emulsion gels. More specifically, I have studied the influence of the composition of these systems on their properties.

By using a soft colloidal framework, the viscosity of pure suspensions of proteins and of droplets was modelled as a function of their content in colloidal particles, expressed as the effective volume fraction. This confirmed that the use of this framework is relevant for these systems. It also allowed the development of a semi-empirical model for predicting the viscosity of mixtures of these two components, provided that their composition is known.

The formation of soft acid-induced gels was investigated for both pure suspensions. Gelation was observed using a rheo-imaging setup, and some characteristic features were identified for the protein gel and for the droplet gel. This technique also enabled relating the microstructure of the gels to their rheological properties. More specifically, a delay was observed between the coarsening of the microstructure during gelation and the emergence of the viscoelasticity. This result raises questions about the source of the viscoelasticity of fractal networks, and requires further investigation, both experimental and computational, to be fully understood. Future work on this topic should include refining the rheo-imaging measurement to prevent wall slip, and increasing the range of lengthscales at which the microstructure is observed.

The rheological properties of the pure protein gels and the droplet gels were characterised as a function of their concentration, scaled again by the effective volume fraction derived from viscosities of the dilute suspensions. It was found that, for the two types of gels, the rheological features correspond to those of fractal colloidal networks. These could thus be modelled by power laws, that appeared to be remarkably similar for protein gels and droplet gels. Because gels of pure droplets have not previously been investigated, this study comparing the two types of gels is the first of its kind, and it makes evident that they are more similar than previously thought. This result can be applied to the formulation of edible emulsion gels, like yogurt, as it shows that, for some aspects of the texture, fat can be entirely replaced by proteins.

A wide range of gels containing proteins and droplets were prepared by gelling mixtures of these two components. The imaging of the gelation of a mixed emulsion gel revealed the presence of the features identified for both types of pure gels. The study of the rheological properties also showed that the emulsion gels, even if they are mixtures, can be described by the model of fractal colloidal gels. And the variation of the properties with composition suggests that the classical framework of droplet-filled protein gels fails to provide a comprehensive explanation for the viscoelasticity of protein-stabilised emulsion gels. Instead, it appears that these systems are better described as composite colloidal gels, with properties that vary between those of pure protein gels and those of pure droplet gels. This study thus provides an innovative paradigm for future studies of emulsion gels that contain both droplets and un-adsorbed proteins.

The results regarding the influence of composition on the rheological properties of mixtures of proteins and droplets, gelled or not, are promising because they open a path to new paradigms for a knowledge-based approach to formulation. In many industries, the manufacturing of complex fluids is usually based on trial and error: the development and improvement of products go through multiple and varied attempts until a satisfactory result is obtained. A transition towards a predictive approach would result in the savings of time and resources. This study is a small step towards such a transition, but further work is required. It was shown here that the frameworks for the mixtures are different for emulsions and emulsion gels, so the range of application of each of the paradigms could be explored. Future studies should thus focus on the application of the frameworks developed here to other systems, for example to systems containing different soft colloidal particles like polyelectrolyte microgels or star polymers.

Appendix A

Error propagation theory

The error bars indicated in the figures indicates the uncertainty of the measurements and/or the calculations, and are calculated using the error propagation theory that we shortly describe here. More information can be found in Ref. [178].

The uncertainty of each quantity is calculated from the uncertainty of its variables, assuming that these are independents. In practice, if the quantity R is calculated as a function of quantities X, Y, $Z\ldots$ - assumed to be independent - and if each one of those presents an uncertainty δX, δY, $\delta Z\ldots$; then the uncertainty δR can be written:

If we calculate a quantity R as a function of the quantities X, Y, Z, $\ldots$ and each one presents an uncertainty δX, δY, δZ, $\ldots$, then the uncertainty δR can be written:

$$\delta R = \sqrt{\left(\frac{\partial R}{\partial X} \times \delta X\right)^2 + \left(\frac{\partial R}{\partial Y} \times \delta Y\right)^2 + \left(\frac{\partial R}{\partial Z} \times \delta Z\right)^2 + ...} \tag{A.1}$$

In this thesis, the calculations for the uncertainty were performed for each quantity calculated, using either the uncertainties derived previously, or the standard errors obtained from the fitting procedure or from the calculation of the mean value. The resulting uncertainty is not a standard error in the strict statistical definition, but it gives a satisfactory estimation of the reliability of the numerical results among an arrow of data points. It is only displayed where it is larger than the symbol for the data point.

Bibliography

[1] M. Roullet, P. S. Clegg, and W. J. Frith. Viscosity of protein-stabilized emulsions: Contributions of components and development of a semipredictive model. *Journal of Rheology*, 63(1):179–190, 2019. ISSN 0148-6055 1520-8516. doi: 10.1122/1.5062837.

[2] Anton Paar GmbH. Basics of rheology, 2010. URL `https://wiki.anton-paar.com/en/basics-of-rheology/`.

[3] D. Vlassopoulos and M. Cloitre. Tunable rheology of dense soft deformable colloids. *Current Opinion in Colloid AND Interface Science*, 19(6):561–574, 2014. ISSN 1359-0294. doi: 10.1016/j.cocis.2014.09.007. URL `<GotoISI>://WOS:000347766000008`.

[4] G. M. Conley, P. Aebischer, S. Nojd, P. Schurtenberger, and F. Scheffold. Jamming and overpacking fuzzy microgels: Deformation, interpenetration, and compression. *Sci Adv*, 3(10):e1700969, 2017. ISSN 2375-2548 (Electronic) 2375-2548 (Linking). doi: 10.1126/sciadv.1700969. URL `https://www.ncbi.nlm.nih.gov/pubmed/29062888`.

[5] D. Quemada. Rheology of concentrated disperse systems and minimum energy dissipation principle, i. *Rheol. Acta*, 16:82–94, 1977.

[6] M. M. Robins and D. J. Hibberd. *Emulsion Flocculation and Creaming*, book section 4, pages 115–144. Royal Society of Chemistry, 1998. doi: 10.1039/9781847551474-00115.

[7] L. D. Gelb, A. L. Graham, A. M. Mertz, and P. H. Koenig. On the permeability of colloidal gels. *Physics of Fluids*, 31(2), 2019. ISSN 1070-6631 1089-7666. doi: 10.1063/1.5054596.

[8] H. Murata. *Rheology - Theory and application to biomaterials.* InTech, 2012. doi: 10.5772/48393. URL `http://www.intechopen.com/books/howtoreference/polymerization/rheology-theory-and-application-to-biomaterialshttps://cdn.intechopen.com/pdfs-wm/38909.pdf`.

[9] E. Dickinson. Emulsion gels: The structuring of soft solids with protein-stabilized oil droplets. *Food Hydrocolloids*, 28(1):224–241, 2012. ISSN

0268-005x. doi: 10.1016/j.foodhyd.2011.12.017. URL `<GotoISI>://WOS:000299951300026`.

[10] L. A. Pugnaloni, L. Matia-Merino, and E. Dickinson. Microstructure of acid-induced caseinate gels containing sucrose: quantification from confocal microscopy and image analysis. *Colloids Surf B Biointerfaces*, 42(3-4):211–7, 2005. ISSN 0927-7765 (Print) 0927-7765 (Linking). doi: 10.1016/j.colsurfb.2005.03.002. URL `https://www.ncbi.nlm.nih.gov/pubmed/15893221`.

[11] M. Leocmach, M. Nespoulous, S. Manneville, and T. Gibaud. Hierarchical wrinkling in a confined permeable biogel. *Sci Adv*, 1(9):e1500608, 2015. ISSN 2375-2548 (Print) 2375-2548 (Linking). doi: 10.1126/sciadv.1500608. URL `https://www.ncbi.nlm.nih.gov/pubmed/26601296`.

[12] Beckman Coulter. User's manual: Tabletop ultracentrifuge rotors and tubes, 2003.

[13] L. Øgendal. *Light Scattering Demystified: Theory and Practice.* Lecture notes for PhD course. University of Copenhagen, 2012.

[14] Postnova Ltd. Fff principles, Retrieved on 31/10/2018 2018. URL `http://s2.postnova.com/tl_files/postnova/content/products/images/FFF%20Systems/FFF_Principle_2014.png`.

[15] Nikon Instruments Inc. Microscopy u, 2018. URL `https://www.microscopyu.com/techniques/confocal/introductory-confocal-concepts`.

[16] T. van Vliet. Rheological properties of filled gels. influence of filler matrix interaction. *Colloid and Polymer Science*, 266:518–524, 1988.

[17] E. Dickinson. Food colloids research: historical perspective and outlook. *Adv Colloid Interface Sci*, 165(1):7–13, 2011. ISSN 1873-3727 (Electronic) 0001-8686 (Linking). doi: 10.1016/j.cis.2010.05.007. URL `https://www.ncbi.nlm.nih.gov/pubmed/20566190`.

[18] R. Mezzenga, P. Schurtenberger, A. Burbidge, and M. Michel. Understanding foods as soft materials. *Nat Mater*, 4(10):729–40, 2005. ISSN 1476-1122 (Print) 1476-1122 (Linking). doi: 10.1038/nmat1496. URL `https://www.ncbi.nlm.nih.gov/pubmed/16195765`.

[19] B.P. Binks. *Emulsions - Recent Advances in Understanding*, book section 1, pages 1–55. Royal Society of Chemistry, 2006. ISBN 978-0-85404-439-9. doi: 10.1039/9781847551474.

[20] E. Del Gado, D. Fiocco, G. Foffi, S. Manley, V. Trappe, and A. Zaccone. *Colloidal gelation*, book section 14. John Wiley and Sons, 2016.

[21] L.G. Phillips, D.M. Whitehead, and J. Kinsella. *Emulsions*, book section 7, pages 153–169. Academic Press, 1994. ISBN 978-0-12-554360-6.

[22] L.G. Phillips, D.M. Whitehead, and J. Kinsella. *Protein Gelation*, book section 9, pages 179–204. Academic Press, 1994. ISBN 978-0-12-554360-6.

[23] E. Dickinson. Structure formation in casein-based gels, foams, and emulsions. *Colloids and Surfaces a-Physicochemical and Engineering Aspects*, 288(1-3):3–11, 2006. ISSN 0927-7757. doi: 10.1016/j.colsurfa.2006.01.012. URL `<GotoISI>://WOS:000240613200002`.

[24] C. W. Macosko. *Rheology : Principles, Measurements, and applications*. Advances in interfacial engineering series. VCH Publishers, 1994. ISBN 1-56081-579-5.

[25] S. R. Nagel. Experimental soft-matter science. *Reviews of Modern Physics*, 89(2), 2017. ISSN 0034-6861 1539-0756. doi: 10.1103/RevModPhys.89.025002.

[26] W. B. Russel, D. A. Saville, and W. R. Schowalter. *Colloidal Dispersions*. Cambridge monographs on mechanics. Cambridge University Press, Cambridge, 1989. ISBN 9780511608810. doi: 10.1017/cbo9780511608810.

[27] S. A. Faroughi and C. Huber. A generalized equation for rheology of emulsions and suspensions of deformable particles subjected to simple shear at low reynolds number. *Rheologica Acta*, 54(2):85–108, 2014. ISSN 0035-4511 1435-1528. doi: 10.1007/s00397-014-0825-8.

[28] A. Einstein. Berichtigung zu meiner arbeit: Eine neue bestimmung der moleküldimensionen. *Annalen der Physik*, 339(3):591–592, 1911. ISSN 00033804 15213889. doi: 10.1002/andp.19113390313. URL `https://onlinelibrary.wiley.com/doi/abs/10.1002/andp.19113390313`.

[29] G. K. Batchelor. The effect of brownian motion on the bulk stress in a suspension of spherical particles. *Journal of Fluid Mechanics*, 83(01):97–117, 1977. ISSN 0022-1120 1469-7645. doi: 10.1017/s0022112077001062.

[30] M. Mooney. The viscosity of a concentrated suspension of spherical particles. *Journal of Colloid Science*, 6(2):162–170, 1951. doi: Doi10.1016/0095-8522(51)90036-0. URL `<GotoISI>://WOS:A1951UJ16900007`.

[31] I. M. Krieger. Rheology of monodisperse latices. *Adv Colloid Interface Sci*, 3(2):111–136, 1972.

[32] J. F. Brady. Rheological behavior of concentrated colloidal suspensions. *J Chem Phys*, 99(1):567–581, 1993.

[33] C. I. Mendoza and I. Santamaria-Holek. The rheology of hard sphere suspensions at arbitrary volume fractions: An improved differential viscosity model. *J Chem Phys*, 130(4):044904, 2009. ISSN 1089-7690 (Electronic) 0021-9606 (Linking). doi: 10.1063/1.3063120. URL `https://www.ncbi.nlm.nih.gov/pubmed/19191410`.

[34] B. J. Ackerson. Shear induced order and shear processing of model hard sphere suspensions. *Journal of Rheology*, 34(4):553–590, 1990. ISSN 0148-6055 1520-8516. doi: 10.1122/1.550096.

[35] C. G. de Kruif, E. M. F. van Iersel, A. Vrij, and W. B. Russel. Hard sphere colloidal dispersions: Viscosity as a function of shear rate and volume fraction. *The Journal of Chemical Physics*, 83(9):4717–4725, 1985. ISSN 0021-9606 1089-7690. doi: 10.1063/1.448997.

[36] M. E. Helgeson, N. J. Wagner, and D. Vlassopoulos. Viscoelasticity and shear melting of colloidal star polymer glasses. *Journal of Rheology*, 51(2): 297–316, 2007. ISSN 0148-6055. doi: 10.1122/1.2433935. URL `<GotoISI>://WOS:000244941500008`.

[37] M. M. Cross. Rheology of non-newtonian fluids - a new flow equation for pseudoplastic systems. *Journal of Colloid Science*, 20(5):417–AND, 1965. doi: Doi10.1016/0095-8522(65)90022-X. URL `<GotoISI>://WOS:A19656634000003`.

[38] M. M. Cross. Kinetic interpretation of non-newtonian flow. *Journal of Colloid and Interface Science*, 33(1):30–AND, 1970. ISSN 0021-9797. doi: Doi10.1016/0021-9797(70)90068-8. URL `<GotoISI>://WOS:A1970G254100005`.

[39] M. E. Woods and I. M. Krieger. Rheological studies on dispersions of uniform colloidal spheres: I. aqueous dispersions in steady shear flow. *Journal of Colloid and Interface Science*, 34(1):91–99, 1970.

[40] W. J. Frith, J. Mewis, and T. A. Strivens. Rheology of concentrated suspensions - experimental investigations. *Powder Technology*, 51(1):27–34, 1987. ISSN 0032-5910. doi: Doi10.1016/0032-5910(87)80037-2. URL `<GotoISI>://WOS:A1987H621600004`.

[41] H. M. Shewan and J. R. Stokes. Analytically predicting the viscosity of hard sphere suspensions from the particle size distribution. *Journal of Non-Newtonian Fluid Mechanics*, 222:72–81, 2015. ISSN 0377-0257. doi: 10.1016/j.jnnfm.2014.09.002. URL `<GotoISI>://WOS:000357906400009`.

[42] R. S. Farr and R. D. Groot. Close packing density of polydisperse hard spheres. *J Chem Phys*, 131(24):244104, 2009. ISSN 1089-7690 (Electronic) 0021-9606 (Linking). doi: 10.1063/1.3276799. URL `https://www.ncbi.nlm.nih.gov/pubmed/20059051`.

[43] R. S. Farr. spherepack1d, 2012. URL `https://sourceforge.net/projects/spherepack1d/`.

[44] S. Pednekar, J. H. Chun, and J. F. Morris. Bidisperse and polydisperse suspension rheology at large solid fraction. *Journal of Rheology*, 62(2):513–526, 2018. ISSN 0148-6055. doi: 10.1122/1.5011353. URL `<GotoISI>://WOS:000427032600010`.

[45] P. M. Mwasame, N. J. Wagner, and A. N. Beris. Modeling the effects of polydispersity on the viscosity of noncolloidal hard sphere suspensions. *Journal of Rheology*, 60(2):225–240, 2016. ISSN 0148-6055 1520-8516. doi: 10.1122/1.4938048.

[46] C. I. Mendoza. A simple semiempirical model for the effective viscosity of multicomponent suspensions. *Rheologica Acta*, 56(5):487–499, 2017. ISSN 0035-4511. doi: 10.1007/s00397-017-1011-6. URL `<GotoISI>://WOS:000399884300006`.

[47] P. M. Mwasame, N. J. Wagner, and A. N. Beris. Modeling the viscosity of polydisperse suspensions: Improvements in prediction of limiting behavior. *Physics of Fluids*, 28(6):061701, 2016. ISSN 1070-6631. doi: Artn06170110.1063/1.4953407. URL `<GotoISI>://WOS:000379040200001`.

[48] S. Adams, W. J. Frith, and J. R. Stokes. Influence of particle modulus on the rheological properties of agar microgel suspensions. *Journal of Rheology*, 48(6):1195–1213, 2004. ISSN 0148-6055. doi: 10.1122/1.1773782. URL `<GotoISI>://WOS:000225243000002`.

[49] H. M. Shewan and J. R. Stokes. Viscosity of soft spherical micro-hydrogel suspensions. *J Colloid Interface Sci*, 442:75–81, 2015. ISSN 1095-7103 (Electronic) 0021-9797 (Linking). doi: 10.1016/j.jcis.2014.11.064. URL `https://www.ncbi.nlm.nih.gov/pubmed/25521552`.

[50] M. Cloitre, R. Borrega, F. Monti, and L. Leibler. Structure and flow of polyelectrolyte microgels: from suspensions to glasses. *Comptes Rendus Physique*, 4(2):221–230, 2003. ISSN 1631-0705. doi: 10.1016/S1631-0705(03)00046-X. URL `<GotoISI>://WOS:000183582800003`.

[51] B. H. Tan, K. C. Tam, Y. C. Lam, and C. B. Tan. Microstructure and rheological properties of ph-responsive core–shell particles. *Polymer*, 46(23):10066–10076, 2005. ISSN 00323861. doi: 10.1016/j.polymer.2005.08.007.

[52] C. Pellet and M. Cloitre. The glass and jamming transitions of soft polyelectrolyte microgel suspensions. *Soft Matter*, 12(16):3710–20, 2016. ISSN 1744-6848 (Electronic) 1744-683X (Linking). doi: 10.1039/c5sm03001c. URL `https://www.ncbi.nlm.nih.gov/pubmed/26984383`.

[53] J. Roovers. Concentration-dependence of the relative viscosity of star polymers. *Macromolecules*, 27(19):5359–5364, 1994. ISSN 0024-9297. doi: DOI10.1021/ma00097a015. URL `<GotoISI>://WOS:A1994PG44900015`.

[54] R. G. Winkler, D. A. Fedosov, and G. Gompper. Dynamical and rheological properties of soft colloid suspensions. *Current Opinion in Colloid AND Interface Science*, 19(6):594–610, 2014. ISSN 1359-0294. doi: 10.1016/j.cocis.2014.09.005. URL `<GotoISI>://WOS:000347766000011`.

[55] F. A. M. Leermakers, J. C. Eriksson, and H. Lyklema. *Association Colloids and their Equilibrium Modelling*, volume Volume 5, book section 4, pages 4.1–4.123. Academic Press, Cambridge, Massachusetts, 2005. ISBN 1874-5679. doi: https://doi.org/10.1016/S1874-5679(05)80008-X. URL `https://www.sciencedirect.com/science/article/pii/S187456790580008X`.

[56] C. Leverrier, G. Almeida, P. Menut, and G. Cuvelier. Design of model apple cells suspensions: Rheological properties and impact of the continuous phase. *Food Biophysics*, 12(3):383–396, 2017. ISSN 1557-1858. doi: 10.1007/s11483-017-9494-3. URL `<GotoISI>://WOS:000407379100012`.

[57] N. Koumakis, A. Pamvouxoglou, A. S. Poulos, and G. Petekidis. Direct comparison of the rheology of model hard and soft particle glasses. *Soft Matter*, 8(15):4271–4284, 2012. ISSN 1744-683x. doi: 10.1039/c2sm07113d. URL `<GotoISI>://WOS:000301801100028`.

[58] A. K. Doukas, C. N. Likos, and P. Ziherl. Structure formation in soft nanocolloids: liquid-drop model. *Soft Matter*, 14(16):3063–3072, 2018. ISSN 1744-6848 (Electronic) 1744-683X (Linking). doi: 10.1039/c8sm00293b. URL `https://www.ncbi.nlm.nih.gov/pubmed/29663000`.

[59] H. Senff, W. Richtering, C. Norhausen, A. Weiss, and M. Ballauff. Rheology of a temperature sensitive core-shell latex. *Langmuir*, 15(1):102–106, 1999. ISSN 0743-7463. doi: DOI10.1021/la980979q. URL `<GotoISI>://WOS:000077982800017`.

[60] B. H. Tan and K. C. Tam. Review on the dynamics and micro-structure of ph-responsive nano-colloidal systems. *Adv Colloid Interface Sci*, 136(1-2):25–44, 2008. ISSN 0001-8686 (Print) 0001-8686 (Linking). doi: 10.1016/j.cis.2007.07.002. URL `https://www.ncbi.nlm.nih.gov/pubmed/17707760`.

[61] R. Borrega, M. Cloitre, I. Betremieux, B. Ernst, and L. Leibler. Concentration dependence of the low-shear viscosity of polyelectrolyte micro-networks: From hard spheres to soft microgels. *Europhysics Letters*, 47(6):729–735, 1999. ISSN 0295-5075. doi: DOI10.1209/epl/i1999-00451-1. URL `<GotoISI>://WOS:000082702700014`.

[62] T. J. Weyer and A. R. Denton. Concentration-dependent swelling and structure of ionic microgels: simulation and theory of a coarse-grained model. *Soft Matter*, 14(22):4530–4540, 2018. ISSN 1744-6848 (Electronic) 1744-683X (Linking). doi: 10.1039/c8sm00799c. URL `https://www.ncbi.nlm.nih.gov/pubmed/29796467`.

[63] D. Farrer and A. Lips. On the self-assembly of sodium caseinate. *International Dairy Journal*, 9(3-6):281–286, 1999. ISSN 0958-6946. doi: Doi10.1016/S0958-6946(99)00075-8. URL `<GotoISI>://WOS:000082012600021`.

[64] D. Vlassopoulos, G. Fytas, S. Pispas, and N. Hadjichristidis. Spherical polymeric brushes viewed as soft colloidal particles: zero-shear viscosity. *Physica B-Condensed Matter*, 296(1-3):184–189, 2001. ISSN 0921-4526. doi: Doi10.1016/S0921-4526(00)00798-5. URL `<GotoISI>://WOS:000167877900029`.

[65] M. Boulet, M. Britten, and M. Lamarche. Voluminosity of some food proteins in aqueous diepersions at various ph and ionic strengths. *Food Hydrocolloids*, 12:433–441, 1998. doi: https://doi.org/10.1016/S0268-005X(98)00009-5.

[66] C. I. Mendoza. Model for the shear viscosity of suspensions of star polymers and other soft particles. *Macromolecular Chemistry and Physics*, 214(5):599–604, 2013. ISSN 1022-1352. doi: 10.1002/macp.201200551. URL `<GotoISI>://WOS:000315523300009`.

[67] P. Walstra. *Emulsions*, volume Volume 5, book section 8, pages 8.1–8.94. Academic Press, 2005. ISBN 1874-5679. doi: https://doi.org/10.1016/S1874-5679(05)80012-1. URL `https://www.sciencedirect.com/science/article/pii/S1874567905800121`.

[68] P. Walstra and I. Smulders. *Making Emulsions and Foams: An Overview A2 - Dickinson, E*, pages 367–381. Woodhead Publishing, 2004. ISBN 978-1-85573-783-9. doi: https://doi.org/10.1533/9781845698263.6.367. URL `https://www.sciencedirect.com/science/article/pii/B9781855737839500333`.

[69] Y. Otsubo and R. K. Prudhomme. Effect of drop size distribution on the flow behavior of oil-in-water emulsions. *Rheologica Acta*, 33(4):303–306, 1994. ISSN 0035-4511. doi: Doi10.1007/Bf00366956. URL `<GotoISI>://WOS:A1994PE63300006`.

[70] R. Pal. Shear viscosity behavior of emulsions of two immiscible liquids. *J Colloid Interface Sci*, 225(2):359–366, 2000. ISSN 1095-7103 (Electronic) 0021-9797 (Linking). doi: 10.1006/jcis.2000.6776. URL `https://www.ncbi.nlm.nih.gov/pubmed/11254273`.

[71] F. Scheffold, F. Cardinaux, and T. G. Mason. Linear and nonlinear rheology of dense emulsions across the glass and the jamming regimes. *J Phys Condens Matter*, 25(50):502101, 2013. ISSN 1361-648X (Electronic) 0953-8984 (Linking). doi: 10.1088/0953-8984/25/50/502101. URL `https://www.ncbi.nlm.nih.gov/pubmed/24222446`.

[72] Jian Ping Gong. Why are double network hydrogels so tough? *Soft Matter*, 6(12), 2010. ISSN 1744-683X 1744-6848. doi: 10.1039/b924290b.

[73] Costantino Creton. 50th anniversary perspective: Networks and gels: Soft but dynamic and tough. *Macromolecules*, 50(21):8297–8316, 2017. ISSN 0024-9297 1520-5835. doi: 10.1021/acs.macromol.7b01698.

[74] International Union of Pure Division and Applied Chemistry. Polymer. Compendium of polymer terminology and nomenclature : Iupac recommendations 2008, 2009. URL `http://dx.doi.org/10.1039/9781847559425`.

[75] E. van der Linden and E. A. Foegeding. *Gelation: Principles, Models and Applications to Proteins*, book section 2, pages 29–91. Academic Press, 2009. ISBN 978-0-12-374195-0.

[76] P. Walstra, T. van Vliet, and L.G.B. Bremer. *On the fractal nature of particle gels*, pages 369–382. Royal Society of Chemistry, 1991. doi: 10.1533/9781845698331.369.

[77] E. Zaccarelli. Colloidal gels: equilibrium and non-equilibrium routes. *Journal of Physics-Condensed Matter*, 19(32), 2007. ISSN 0953-8984. doi: Artn32310110.1088/0953-8984/19/32/323101. URL `<GotoISI>://WOS:000248185800004`.

[78] T. van Vliet. *Structure and rheology of gels formed by aggregated protein particles*, pages 367–377. Elsevier, 2000. ISBN 978-0-444-50178-3.

[79] L. G. B. Bremer, B. H. Bijsterbosch, R. Schrijvers, T. van Vliet, and P. Walstra. On the fractal nature of the structure of acid casein gels. *Colloids and Surfaces*, 51:159–170, 1990. ISSN 0166-6622. doi: Doi10.1016/0166-6622(90)80139-U. URL `<GotoISI>://WOS:A1990EL41200013`.

[80] S. Aime, L. Cipelletti, and L. Ramos. Power law viscoelasticity of a fractal colloidal gel. *Journal of Rheology*, 62(6):1429–1441, 2018. ISSN 0148-6055. doi: 10.1122/1.5025622. URL `<GotoISI>://WOS:000449684700010`.

[81] J. Colombo and E. Del Gado. Stress localization, stiffening, and yielding in a model colloidal gel. *Journal of Rheology*, 58(5):1089–1116, 2014. ISSN 0148-6055. doi: 10.1122/1.4882021. URL `<GotoISI>://WOS:000342206200002`.

[82] Mehdi Bouzid and Emanuela Del Gado. *Mechanics of Soft Gels: Linear and Nonlinear Response*, book section Chapter 129-1, pages 1–29. 2018. ISBN 978-3-319-50257-1 978-3-319-50257-1. doi: 10.1007/978-3-319-50257-1_129-1.

[83] E. Dickinson. Structure and rheology of colloidal particle gels: insight from computer simulation. *Adv Colloid Interface Sci*, 199-200:114–27, 2013. ISSN 1873-3727 (Electronic) 0001-8686 (Linking). doi: 10.1016/j.cis.2013.07.002. URL `https://www.ncbi.nlm.nih.gov/pubmed/23916723`.

[84] M. Bouzid and E. Del Gado. Network topology in soft gels: Hardening and softening materials. *Langmuir*, 34(3):773–781, 2018. ISSN 1520-5827 (Electronic) 0743-7463 (Linking). doi: 10.1021/acs.langmuir.7b02944. URL `https://www.ncbi.nlm.nih.gov/pubmed/28977748`.

[85] E. Dickinson. Flocculation of protein-stabilized oil-in-water emulsions. *Colloids Surf B Biointerfaces*, 81(1):130–40, 2010. ISSN 1873-4367 (Electronic) 0927-7765 (Linking). doi: 10.1016/j.colsurfb.2010.06.033. URL `https://www.ncbi.nlm.nih.gov/pubmed/20667698`.

[86] G. Heinrich, M. Kluppel, and T. A. Vilgis. Reinforcement of elastomers. *Current Opinion in Solid State and Materials Science*, 6:195–203, 2002.

[87] J. S. Chen and E. Dickinson. Effect of surface character of filler particles on rheology of heat-set whey protein emulsion gels. *Colloids and Surfaces B-Biointerfaces*, 12(3-6):373–381, 1999. ISSN 0927-7765. doi: Doi10.1016/S0927-7765(98)00091-5. URL `<GotoISI>://WOS:000078554200026`.

[88] G. O. Phillips and P. A. Williams. *Introduction to food proteins*, pages 1–12. Food Science, Technology and Nutrition. Woodhead Publishing, 2011. doi: 10.1533/9780857093639.1.

[89] A.V. Finkelstein and O.B. Ptitsyn. Introduction. In A.V. Finkelstein; O.B. Ptitsyn, editor, *Protein physics, A course of lectures*, Soft Condensed Matter, Complex Fluids and Biomaterials, serial 1, pages 3–11. Academic Press, Amsterdam, 2002. doi: 10.1016/B978-012256781-0/50000-7.

[90] H. Frauenfelder. *Tertiary structure of proteins.* Biological and Medical Physics, Biomedical Engineering. Springer New York, 2010. ISBN 1618-7210 2197-5647. doi: 10.1007/978-1-4419-1044-8.

[91] L.G. Phillips, D.M. Whitehead, and J. Kinsella. *Protein Stability*, book section 2, pages 25–61. Academic Press, 1994.

[92] R. Mezzenga and P. Fischer. The self-assembly, aggregation and phase transitions of food protein systems in one, two and three dimensions. *Rep Prog Phys*, 76(4):046601, 2013. ISSN 1361-6633 (Electronic) 0034-4885 (Linking). doi: 10.1088/0034-4885/76/4/046601. URL `https://www.ncbi.nlm.nih.gov/pubmed/23455715`.

[93] E. Dickinson and G. Stainsby. *Emulsion stability*, book section 1, pages 1–44. Elsevier Applied Science, 1988. ISBN 1-85166-200-6.

[94] W. Norde, J. Buijs, and H. Lyklema. *Adsorption Of Globular Proteins*, volume Volume 5, book section 3, pages 3.1–3.59. Academic Press, Cambridge, Massachusetts, 2005. ISBN 1874-5679. doi: https://doi.org/10.1016/S1874-5679(05)80007-8. URL `https://www.sciencedirect.com/science/article/pii/S1874567905800078`.

[95] J. L. Zhai, L. Day, M. I. Aguilar, and T. J. Wooster. Protein folding at emulsion oil/water interfaces. *Current Opinion in Colloid AND Interface Science*, 18(4):257–271, 2013. ISSN 1359-0294. doi: 10.1016/j.cocis.2013.03.002. URL `<GotoISI>://WOS:000321406600003`.

[96] D. S. Horne. Protein-stabilized emulsions. *Current Opinion in Colloid AND Interface Science*, 1(6):752–758, 1996. ISSN 1359-0294. URL `<GotoISI>://WOS:A1996WB77100007`.

[97] K. Koczo, A. D. Nikolov, D. T. Wasan, R. P. Borwankar, and A. Gonsalves. Layering of sodium caseinate submicelles in thin liquid films - a new stability mechanism for food dispersions. *Journal of Colloid and Interface Science*, 178(2):694–702, 1996. ISSN 0021-9797. doi: DOI10.1006/jcis.1996.0167. URL `<GotoISI>://WOS:A1996UF03200035`.

[98] M. Srinivasan, H. Singh, and P. A. Munro. Adsorption behaviour of sodium and calcium caseinates in oil-in-water emulsions. *International Dairy Journal*, 9(3-6):337–341, 1999. ISSN 0958-6946. doi: Doi10.1016/S0958-6946(99)00084-9. URL `<GotoISI>://WOS:000082012600030`.

[99] F. Spyropoulos, E.A.K. Heuer, T.B. Mills, and S. Bakalis. *Protein-stabilised emulsions and rheological aspects of structure and mouthfeel*, book section 9, pages 193–2018. Wiley-Blackwell, Hoboken, New Jersey, 2010.

[100] P. J. Wilde, A. R. Mackie, M. J. Ridout, F. A. Husband, G. K. Moates, and M. M. Robins. *Role of Protein-Stabilized Interfaces on the Microstructure and Rheology of Oil-in-Water Emulsions*, pages 385–397. Royal Society of Chemistry, 2007. doi: 10.1039/9781847557698-00383.

[101] E. Dickinson, G. Stainsby, and L. Wilson. An adsorption effect on the gel strength of dilute gelatin-stabilized oil-in-water emulsions. *Colloid and Polymer Science*, 263(11):933–934, 1985. ISSN 0303-402x. doi: Doi10.1007/Bf01469632. URL `<GotoISI>://WOS:A1985AWM1100011`.

[102] E. Tornberg, A. Olsson, and K. Persson. *The structural and interfacial properties of food proteins in relation to thei function in emulsions*, pages 279–359. Marcel Dekker, 3 edition, 1997.

[103] Jr. Farrell, H. M., P. X. Qi, E. M. Brown, P. H. Cooke, M. H. Tunick, E. D. Wickham, and J. J. Unruh. Molten globule structures in milk proteins: implications for potential new structure-function relationships. *J Dairy Sci*, 85(3):459–71, 2002. ISSN 0022-0302 (Print) 0022-0302 (Linking). doi: 10.3168/jds.S0022-0302(02)74096-4. URL `https://www.ncbi.nlm.nih.gov/pubmed/11949847`.

[104] A. Bouchoux, P. E. Cayemitte, J. Jardin, G. Gesan-Guiziou, and B. Cabane. Casein micelle dispersions under osmotic stress. *Biophys J*, 96(2):693–706, 2009. ISSN 1542-0086 (Electronic) 0006-3495 (Linking). doi: 10.1016/j.bpj.2008.10.006. URL `https://www.ncbi.nlm.nih.gov/pubmed/19167314`.

[105] T. Huppertz, I. Gazi, H. Luyten, H. Nieuwenhuijse, A. Alting, and E. Schokker. Hydration of casein micelles and caseinates: Implications for casein micelle structure. *International Dairy Journal*, 74:1–11, 2017. ISSN 0958-6946. doi: 10.1016/j.idairyj.2017.03.006. URL `<GotoISI>://WOS:000410669000001`.

[106] C. G. De Kruif and C. Holt. *Casein Micelle Structure, Functions and Interactions*, book section Chapter 5, pages 233–276. 2003. ISBN 978-0-306-47271-8 978-1-4419-8602-3. doi: 10.1007/978-1-4419-8602-3_5.

[107] H. M. Farrell, E. L. Malin, E. M. Brown, and P. X. Qi. Casein micelle structure: What can be learned from milk synthesis and structural biology? *Current Opinion in Colloid and Interface Science*, 11(2-3):135–147, 2006. ISSN 13590294. doi: 10.1016/j.cocis.2005.11.005.

[108] D. G. Dalgleish and A. J. R. Law. Sodium caseinates - composition and properties of different preparations. *Journal of the Society of Dairy Technology*, 41(1):1–4, 1988. ISSN 0037-9840. URL `<GotoISI>://WOS:A1988M190100001`.

[109] J. A. Lucey, M. Srinivasan, H. Singh, and P. A. Munro. Characterization of commercial and experimental sodium caseinates by multiangle laser light scattering and size-exclusion chromatography. *J Agric Food Chem*, 48(5): 1610–6, 2000. ISSN 0021-8561 (Print) 0021-8561 (Linking). URL `https://www.ncbi.nlm.nih.gov/pubmed/10820067`.

[110] A. Pitkowski, D. Durand, and T. Nicolai. Structure and dynamical mechanical properties of suspensions of sodium caseinate. *J Colloid Interface Sci*, 326(1):96–102, 2008. ISSN 1095-7103 (Electronic) 0021-9797 (Linking). doi: 10.1016/j.jcis.2008.07.003. URL `https://www.ncbi.nlm.nih.gov/pubmed/18674776`.

[111] A. HadjSadok, A. Pitkowski, T. Nicolai, L. Benyahia, and N. Moulai-Mostefa. Characterisation of sodium caseinate as a function of ionic strength, ph and temperature using static and dynamic light scattering. *Food Hydrocolloids*, 22(8):1460–1466, 2008. ISSN 0268-005x. doi: 10.1016/j.foodhyd.2007.09.002. URL `<GotoISI>://WOS:000257638300005`.

[112] A. Smialowska, L. Matia-Merino, B. Ingham, and A. J. Carr. Effect of calcium on the aggregation behaviour of caseinates. *Colloids and Surfaces a-Physicochemical and Engineering Aspects*, 522:113–123, 2017. ISSN 0927-7757. doi: 10.1016/j.colsurfa.2017.02.074. URL `<GotoISI>://WOS:000404491600013`.

[113] E. Dickinson. Caseins in emulsions: interfacial properties and interactions. *International Dairy Journal*, 9(3-6):305–312, 1999. ISSN 0958-6946. doi: Doi10.1016/S0958-6946(99)00079-5. URL `<GotoISI>://WOS:000082012600025`.

[114] E. Dickinson. Milk protein interfacial layers and the relationship to emulsion stability and rheology. *Colloids Surf B Biointerfaces*, 20(3): 197–210, 2001. ISSN 1873-4367 (Electronic) 0927-7765 (Linking). URL `https://www.ncbi.nlm.nih.gov/pubmed/11172975`.

[115] D. E. Graham and M. C. Phillips. Proteins at liquid interfaces ii adsorption isotherms. *Journal of Colloid and Interface Science*, 70(3):415–426, 1979. ISSN 00219797. doi: 10.1016/0021-9797(79)90049-3.

[116] Y. Mine. *Adsorption Behaviour of Caseinate in Oil-in-Water Emulsions: A Nuclear Magnetic Resonance Approach*, pages 229–235. Woodhead Publishing, 2004. ISBN 978-1-85573-783-9. doi: https://doi.org/10.1533/9781845698263.4.229. URL `https://www.sciencedirect.com/science/article/pii/B9781855737839500205`.

[117] M. Srinivasan, H. Singh, and P. A. Munro. Sodium caseinate-stabilized emulsions: Factors affecting coverage and composition of surface proteins. *Journal of Agricultural and Food Chemistry*, 44(12):3807–3811, 1996. ISSN 0021-8561. doi: DOI10.1021/jf960135h. URL `<GotoISI>://WOS:A1996VZ01000017`.

[118] E. Dickinson and M. Golding. Rheology of sodium caseinate stabilized oil-in-water emulsions. *J Colloid Interface Sci*, 191(1):166–76, 1997. ISSN 1095-7103 (Electronic) 0021-9797 (Linking). URL `https://www.ncbi.nlm.nih.gov/pubmed/9241217`.

[119] L. Bressy, P. Hebraud, V. Schmitt, and J. Bibette. Rheology of emulsions stabilized by solid interfaces. *Langmuir*, 19(3):598–604, 2003. ISSN 0743-7463. doi: 10.1021/la0264466. URL `<GotoISI>://WOS:000180737100020`.

[120] J. S. Chen, E. Dickinson, and M. Edwards. Rheology of acid-induced sodium caseinate stabilized emulsion gels. *Journal of Texture Studies*, 30 (4):377–396, 1999. ISSN 0022-4901. doi: DOI10.1111/j.1745-4603.1999.tb00226.x. URL `<GotoISI>://WOS:000084327500002`.

[121] M. Mellema, J. H. J. van Opheusden, and T. van Vliet. Categorization of rheological scaling models for particle gels applied to casein gels. *Journal of Rheology*, 46(1):11–29, 2002. ISSN 0148-6055. doi: Doi10.1122/1.1423311. URL `<GotoISI>://WOS:000174333200002`.

[122] K. P. Takeuchi and R. L. Cunha. Influence of ageing time on sodium caseinate gelation induced by glucono-delta-lactone at different temperatures. *Dairy Science AND Technology*, 88(6):667–681, 2008. ISSN 1958-5586. doi: 10.1051/dst:2008031. URL `<GotoISI>://WOS:000261976800005`.

[123] M. Mellema, J. W. M. Heesakkers, J. H. J. van Opheusden, and T. van Vliet. Structure and scaling behavior of aging rennet-induced casein gels examined by confocal microscopy and permeametry. *Langmuir*, 16(17):6847–6854, 2000. ISSN 0743-7463. doi: DOI10.1021/la000135i. URL `<GotoISI>://WOS:000088816000015`.

[124] B. Saint-Michel, T. Gibaud, and S. Manneville. Predicting and assessing rupture in protein gels under oscillatory shear. *Soft Matter*, 13(14):

2643–2653, 2017. ISSN 1744-6848 (Electronic) 1744-683X (Linking). doi: 10.1039/c7sm00064b. URL `https://www.ncbi.nlm.nih.gov/pubmed/28327777`.

[125] T. Moschakis, B. S. Murray, and E. Dickinson. On the kinetics of acid sodium caseinate gelation using particle tracking to probe the microrheology. *J Colloid Interface Sci*, 345(2):278–85, 2010. ISSN 1095-7103 (Electronic) 0021-9797 (Linking). doi: 10.1016/j.jcis.2010.02.005. URL `https://www.ncbi.nlm.nih.gov/pubmed/20223466`.

[126] A. L. M. Braga, M. Menossi, and R. L. Cunha. The effect of the glucono-delta-lactone/caseinate ratio on sodium caseinate gelation. *International Dairy Journal*, 16(5):389–398, 2006. ISSN 0958-6946. doi: 10.1016/j.idairyj.2005.06.001. URL `<GotoISI>://WOS:000235089700001`.

[127] H. G. M. Ruis, P. Venema, and E. van der Linden. Relation between ph-induced stickiness and gelation behaviour of sodium caseinate aggregates as determined by light scattering and rheology. *Food Hydrocolloids*, 21(4):545–554, 2007. ISSN 0268-005x. doi: 10.1016/j.foodhyd.2006.06.004. URL `<GotoISI>://WOS:000244024700006`.

[128] M. Leocmach, C. Perge, T. Divoux, and S. Manneville. Creep and fracture of a protein gel under stress. *Phys Rev Lett*, 113(3):038303, 2014. ISSN 1079-7114 (Electronic) 0031-9007 (Linking). doi: 10.1103/PhysRevLett.113.038303. URL `https://www.ncbi.nlm.nih.gov/pubmed/25083668`.

[129] E. Dickinson and Y. Yamamoto. Rheology of milk protein gels and protein-stabilized emulsion gels cross-linked with transglutaminase. *Journal of Agricultural and Food Chemistry*, 44(6):1371–1377, 1996. ISSN 0021-8561. doi: DOI10.1021/jf950705y. URL `<GotoISI>://WOS:A1996UT20800003`.

[130] G. Doxastakis and P. Sherman. The interaction of sodium caseinate with monoglyceride and diglyceride at the oil-water interface and its effect on interfacial rheological properties. *Colloid and Polymer Science*, 264(3):254–259, 1986. ISSN 0303-402x. doi: Doi10.1007/Bf01414962. URL `<GotoISI>://WOS:A1986A624800010`.

[131] Sigma Aldrich. Safety data sheet: Glyceryl trioctanoate, 2012.

[132] H. Zhao, P. H. Brown, and P. Schuck. On the distribution of protein refractive index increments. *Biophys J*, 100(9):2309–17, 2011. ISSN 1542-0086 (Electronic) 0006-3495 (Linking). doi: 10.1016/j.bpj.2011.03.004. URL `https://www.ncbi.nlm.nih.gov/pubmed/21539801`.

[133] P. Myllarinen, J. Buchert, and K. Autio. Effect of transglutaminase on rheological properties and microstructure of chemically acidified sodium caseinate gels. *International Dairy Journal*, 17(7):800–807, 2007. ISSN 0958-6946. doi: 10.1016/j.idairyj.2005.10.031. URL `<GotoISI>://WOS:000245972600010`.

[134] F.-X. Schmid. *Biological Macromolecules: UV-visible Spectrophotometry.* 2001. doi: doi:10.1038/npg.els.0003142. URL `https://onlinelibrary.wiley.com/doi/abs/10.1038/npg.els.0003142`.

[135] J. Babul and E. Stellwagen. Measurement of protein concentration with interferences optics. *Anal Biochem*, 28(1):216–21, 1969. ISSN 0003-2697 (Print) 0003-2697 (Linking). doi: https://doi.org/10.1016/0003-2697(69)90172-9. URL `https://www.ncbi.nlm.nih.gov/pubmed/5781411`.

[136] D. Piovesan, F. Tabaro, I. Micetic, M. Necci, F. Quaglia, C. J. Oldfield, M. C. Aspromonte, N. E. Davey, R. Davidovic, Z. Dosztanyi, A. Elofsson, A. Gasparini, A. Hatos, A. V. Kajava, L. Kalmar, E. Leonardi, T. Lazar, S. Macedo-Ribeiro, M. Macossay-Castillo, A. Meszaros, G. Minervini, N. Murvai, J. Pujols, D. B. Roche, E. Salladini, E. Schad, A. Schramm, B. Szabo, A. Tantos, F. Tonello, K. D. Tsirigos, N. Veljkovic, S. Ventura, W. Vranken, P. Warholm, V. N. Uversky, A. K. Dunker, S. Longhi, P. Tompa, and S. C. Tosatto. Disprot 7.0: a major update of the database of disordered proteins. *Nucleic Acids Res*, 45(D1):D219–D227, 2017. ISSN 1362-4962 (Electronic) 0305-1048 (Linking). doi: 10.1093/nar/gkw1056. URL `https://www.ncbi.nlm.nih.gov/pubmed/27899601`.

[137] T. G. Mason, J. N. Wilking, K. Meleson, C. B. Chang, and S. M. Graves. Nanoemulsions: formation, structure, and physical properties. *Journal of Physics-Condensed Matter*, 18(41):R635–R666, 2006. ISSN 0953-8984. doi: 10.1088/0953-8984/18/41/R01. URL `<GotoISI>://WOS:000241277900005`.

[138] R. Piazza, S. Buzzaccaro, E. Secchi, and A. Parola. What buoyancy really is. a generalized archimedes' principle for sedimentation and ultracentrifugation. *Soft Matter*, 8:7112–7115, 2012. doi: 10.1039/c2sm26120k.

[139] K. Busch, C. M. Soukoulis, and E. N. Economou. Transport and scattering mean free paths of classical waves. *Phys Rev B Condens Matter*, 50(1):93–98, 1994. ISSN 0163-1829 (Print) 0163-1829 (Linking). URL `https://www.ncbi.nlm.nih.gov/pubmed/9974517`.

[140] S. Graves, K. Meleson, J. Wilking, M. Y. Lin, and T. G. Mason. Structure of concentrated nanoemulsions. *J Chem Phys*, 122(13):134703, 2005. ISSN 0021-9606 (Print) 0021-9606 (Linking). doi: 10.1063/1.1874952. URL `https://www.ncbi.nlm.nih.gov/pubmed/15847485`.

[141] D. G. Dalgleish, S. J. West, and F. R. Hallett. The characterization of small emulsion droplets made from milk proteins and triglyceride oil. *Colloids and Surfaces a-Physicochemical and Engineering Aspects*, 123:145–153, 1997. ISSN 0927-7757. doi: Doi10.1016/S0927-7757(97)03783-7. URL `<GotoISI>://WOS:A1997XG19000015`.

[142] P. S. Sarangapani, S. D. Hudson, K. B. Migler, and J. A. Pathak. The limitations of an exclusively colloidal view of protein solution hydrodynamics and rheology. *Biophys J*, 105(10):2418–26, 2013. ISSN 1542-0086 (Electronic) 0006-3495 (Linking). doi: 10.1016/j.bpj.2013.10.012. URL `https://www.ncbi.nlm.nih.gov/pubmed/24268154`.

[143] P. S. Sarangapani, S. D. Hudson, R. L. Jones, J. F. Douglas, and J. A. Pathak. Critical examination of the colloidal particle model of globular proteins. *Biophys J*, 108(3):724–37, 2015. ISSN 1542-0086 (Electronic) 0006-3495 (Linking). doi: 10.1016/j.bpj.2014.11.3483. URL `https://www.ncbi.nlm.nih.gov/pubmed/25650939`.

[144] M. L. Huggins. The viscosity of dilute solutions of long-chain molecules iv dependence on concentration. In *Buffalo Meeting of the American Chemical Society*, 1942.

[145] C. E. Brunchi, S. Morariu, and M. Bercea. Intrinsic viscosity and conformational parameters of xanthan in aqueous solutions: salt addition effect. *Colloids Surf B Biointerfaces*, 122:512–519, 2014. ISSN 1873-4367 (Electronic) 0927-7765 (Linking). doi: 10.1016/j.colsurfb.2014.07.023. URL `https://www.ncbi.nlm.nih.gov/pubmed/25108480`.

[146] M. V. S. Rao. Viscosity of dilute to moderately concentrated polymer-solutions. *Polymer*, 34(3):592–596, 1993. ISSN 0032-3861. doi: Doi10.1016/0032-3861(93)90555-O. URL `<GotoISI>://WOS:A1993KM38800022`.

[147] D. V. Brooksbank, C. M. Davidson, D. S. Horne, and J. Leaver. Influence of electrostatic interactions on beta-casein layers adsorbed on polystyrene latices. *Journal of the Chemical Society-Faraday Transactions*, 89(18): 3419–3425, 1993. ISSN 0956-5000. doi: DOI10.1039/ft9938903419. URL `<GotoISI>://WOS:A1993LY83800014`.

[148] F. A. Husband and P. J. Wilde. The effects of caseinate submicelles and lecithin on the thin film drainage and behavior of commercial caseinate. *J Colloid Interface Sci*, 205(2):316–322, 1998. ISSN 1095-7103 (Electronic) 0021-9797 (Linking). doi: 10.1006/jcis.1998.5622. URL `https://www.ncbi.nlm.nih.gov/pubmed/9735194`.

[149] S. M. Loveday, M. A. Rao, L. K. Creamer, and H. Singh. Rheological behavior of high-concentration sodium caseinate dispersions. *J Food Sci*, 75(2):N30–5, 2010. ISSN 1750-3841 (Electronic) 0022-1147 (Linking). doi: 10.1111/j.1750-3841.2009.01493.x. URL `https://www.ncbi.nlm.nih.gov/pubmed/20492251`.

[150] B. M. Erwin, M. Cloitre, M. Gauthier, and D. Vlassopoulos. Dynamics and rheology of colloidal star polymers. *Soft Matter*, 6(12):2825–2833, 2010. ISSN 1744-683x. doi: 10.1039/b926526k. URL `<GotoISI>://WOS:000278587900030`.

[151] J. Bibette. Depletion interactions and fractionated crystallization for polydisperse emulsion purification. *Journal of Colloid and Interface Science*, 147(2):474–478, 1991. ISSN 0021-9797. doi: Doi10.1016/0021-9797(91)90181-7. URL `<GotoISI>://WOS:A1991GR43000021`.

[152] E. Dickinson, S. J. Radford, and M. Golding. Stability and rheology of emulsions containing sodium caseinate: combined effects of ionic calcium and non-ionic surfactant. *Food Hydrocolloids*, 17(2):211–220, 2003. ISSN 0268-005x. doi: PiiS0268-005x(02)00055-3Doi10.1016/S0268-005x(02)00055-3. URL `<GotoISI>://WOS:000181072000010`.

[153] R. J. Farris. Prediction of the viscosity of multimodal suspensions from unimodal viscosity data. *Transactions of the Society of Rheology*, 12(2):281–301, 1968. ISSN 0038-0032. doi: 10.1122/1.549109.

[154] N. Mahmoudi and A. Stradner. Making food protein gels via an arrested spinodal decomposition. *J Phys Chem B*, 119(50):15522–9, 2015. ISSN 1520-5207 (Electronic) 1520-5207 (Linking). doi: 10.1021/acs.jpcb.5b08864. URL `https://www.ncbi.nlm.nih.gov/pubmed/26595592`.

[155] V. Prasad, D. Semwogerere, and E. R. Weeks. Confocal microscopy of colloids. *Journal of Physics-Condensed Matter*, 19(11):113102, 2007. ISSN 0953-8984. doi: Artn11310210.1088/0953-8984/19/11/113102. URL `<GotoISI>://WOS:000245650700003`.

[156] S. K. Dutta, A. Mbi, R. C. Arevalo, and D. L. Blair. Development of a confocal rheometer for soft and biological materials. *Rev Sci Instrum*, 84(6):063702, 2013. ISSN 1089-7623 (Electronic) 0034-6748 (Linking). doi: 10.1063/1.4810015. URL `https://www.ncbi.nlm.nih.gov/pubmed/23822347`.

[157] W.S. Rasband. Imagej, 1997-2016. URL `http://imagej.nih.gov/ij/`.

[158] P. N. Segre, V. Prasad, A. B. Schofield, and D. A. Weitz. Glasslike kinetic arrest at the colloidal-gelation transition. *Phys Rev Lett*, 86(26 Pt 1):6042–5, 2001. ISSN 0031-9007 (Print) 0031-9007 (Linking). doi: 10.1103/PhysRevLett.86.6042. URL `https://www.ncbi.nlm.nih.gov/pubmed/11415424`.

[159] W. C. K. Poon and M. D. Haw. Mesoscopic structure formation in colloidal aggregation and gelation. *Advances in Colloid and Interface Science*, 73:71–126, 1997. ISSN 0001-8686. doi: Doi10.1016/S0001-8686(97)90003-8. URL `<GotoISI>://WOS:A1997YJ69100003`.

[160] M. Carpineti and M. Giglio. Spinodal-type dynamics in fractal aggregation of colloidal clusters. *Phys Rev Lett*, 68(22):3327–3330, 1992. ISSN 1079-7114 (Electronic) 0031-9007 (Linking). doi: 10.1103/PhysRevLett.68.3327. URL `https://www.ncbi.nlm.nih.gov/pubmed/10045674`.

[161] L. C. Hsiao and P. S. Doyle. Celebrating soft matter's 10th anniversary: Sequential phase transitions in thermoresponsive nanoemulsions. *Soft Matter*, 11(43):8426–31, 2015. ISSN 1744-6848 (Electronic) 1744-683X (Linking). doi: 10.1039/c5sm01581b. URL `https://www.ncbi.nlm.nih.gov/pubmed/26367251`.

[162] F. Sciortino and P. Tartaglia. Structure factor scaling during irreversible cluster-cluster aggregation. *Phys Rev Lett*, 74(2):282–285, 1995. ISSN 1079-7114 (Electronic) 0031-9007 (Linking). doi: 10.1103/PhysRevLett.74.282. URL `https://www.ncbi.nlm.nih.gov/pubmed/10058349`.

[163] J. Colombo and E. Del Gado. Self-assembly and cooperative dynamics of a model colloidal gel network. *Soft Matter*, 10(22):4003–15, 2014. ISSN 1744-6848 (Electronic) 1744-683X (Linking). doi: 10.1039/c4sm00219a. URL `https://www.ncbi.nlm.nih.gov/pubmed/24737066`.

[164] Ton van Vliet, Katja Grolle, Pieter Walstra, and John A. Lucey. *Rearrangements in Acid-Induced Casein Gels during and after Gel Formation*, pages 335–345. Woodhead Publishing, 2004. ISBN 978-1-85573-783-9. doi: https://doi.org/10.1533/9781845698263.5.335. URL `https://www.sciencedirect.com/science/article/pii/B9781855737839500308`.

[165] J. Colombo, A. Widmer-Cooper, and E. Del Gado. Microscopic picture of cooperative processes in restructuring gel networks. *Phys Rev Lett*, 110(19):198301, 2013. ISSN 1079-7114 (Electronic) 0031-9007 (Linking). doi: 10.1103/PhysRevLett.110.198301. URL `https://www.ncbi.nlm.nih.gov/pubmed/23705744`.

[166] L. Cipelletti, S. Manley, R. C. Ball, and D. A. Weitz. Universal aging features in the restructuring of fractal colloidal gels. *Phys Rev Lett*, 84 (10):2275–8, 2000. ISSN 0031-9007 (Print) 0031-9007 (Linking). doi: 10.1103/PhysRevLett.84.2275. URL `https://www.ncbi.nlm.nih.gov/pubmed/11017262`.

[167] E. R. Cross, S. Sproules, R. Schweins, E. R. Draper, and D. J. Adams. Controlled tuning of the properties in optoelectronic self-sorted gels. *J Am Chem Soc*, 140(28):8667–8670, 2018. ISSN 1520-5126 (Electronic) 0002-7863 (Linking). doi: 10.1021/jacs.8b05359. URL `https://www.ncbi.nlm.nih.gov/pubmed/29944359`.

[168] A. D. Dinsmore, E. R. Weeks, V. Prasad, A. C. Levitt, and D. A. Weitz. Three-dimensional confocal microscopy of colloids. *Appl Opt*, 40(24):4152–9, 2001. ISSN 1559-128X (Print) 1559-128X (Linking). URL `https://www.ncbi.nlm.nih.gov/pubmed/18360451`.

[169] A. Stradner, H. Sedgwick, F. Cardinaux, W. C. Poon, S. U. Egelhaaf, and P. Schurtenberger. Equilibrium cluster formation in concentrated protein solutions and colloids. *Nature*, 432(7016):492–5, 2004. ISSN 1476-4687 (Electronic) 0028-0836 (Linking). doi: 10.1038/nature03109. URL `https://www.ncbi.nlm.nih.gov/pubmed/15565151`.

[170] R. Buscall, P. D. A. Mills, J. W. Goodwin, and D. W. Lawson. Scaling behavior of the rheology of aggregate networks formed from colloidal particles. *Journal of the Chemical Society-Faraday Transactions I*, 84(12): 4249–4260, 1988. ISSN 0300-9599. doi: DOI10.1039/f19888404249. URL `<GotoISI>://WOS:A1988T169500005`.

[171] A. H. Krall and D. A. Weitz. Internal dynamics and elasticity of fractal colloidal gels. *Physical Review Letters*, 80(4):778–781, 1998. ISSN 0031-9007. doi: DOI10.1103/PhysRevLett.80.778. URL `<GotoISI>://WOS:000071717100034`.

[172] D. Asnaghi, M. Carpineti, M. Giglio, and M. Sozzi. Coagulation kinetics and aggregate morphology in the intermediate regimes between diffusion-limited and reaction-limited cluster aggregation. *Physical Review A*, 45(2): 1018–1023, 1992. ISSN 1050-2947. doi: DOI10.1103/PhysRevA.45.1018. URL `<GotoISI>://WOS:A1992HB01900053`.

[173] P. Rosa, G. Sala, T. Van Vliet, and F. Van De Velde. Cold gelation of whey protein emulsions. *Journal of Texture Studies*, 37(5):516–537, 2006. ISSN 0022-4901. doi: DOI10.1111/j.1745-4603.2006.00066.x. URL `<GotoISI>://WOS:000240741800004`.

[174] C. van der Poel. On the rheology of concentrated dispersions. *Rheol Acta*, pages 198–205, 1958.

[175] L. Oliver, L. Berndsen, G. A. van Aken, and E. Scholten. Influence of droplet clustering on the rheological properties of emulsion-filled gels. *Food Hydrocolloids*, 50:74–83, 2015. ISSN 0268005X. doi: 10.1016/j.foodhyd.2015.04.001.

[176] G. E. P. Box. *Robustness in the Strategy of Scientific Model Building*, pages 201–236. Academic Press, 1979. ISBN 978-0-12-438150-6. doi: https://doi.org/10.1016/B978-0-12-438150-6.50018-2. URL `http://www.sciencedirect.com/science/article/pii/B9780124381506500182`.

[177] E. Dickinson. *Rheology of Emulsions :The Relationship to Structure and Stability*, book section 5, pages 145–174. Royal Society of Chemistry, 1998. doi: 10.1039/9781847551474-00145.

[178] P. Fornasini. *The uncertainty in physical measurements an introduction to data analysis in the physics laboratory.* Data analysis in the physics laboratory. New York : Springer, New York, 2008.